OPTIMIZATION OF INTERFACIAL BONDING AT METAL CASE-ADHESIVE AND ADHESIVE-EPDM INSULATION INTERFACES THROUGH SURFACE TREATMENTS FOR ROCKET MOTOR APPLICATIONS

A THESIS SUBMITTED TO
THE GRADUATE SCHOOL OF NATURAL AND APPLIED SCIENCES
OF
MIDDLE EAST TECHNICAL UNIVERSITY

BY

NEHİR KAHRAMAN

IN PARTIAL FULFILLMENT OF THE REQUIREMENTS
FOR
THE DEGREE OF MASTER OF SCIENCE
IN
POLYMER SCIENCE AND TECHNOLOGY

JANUARY 2026

Approval of the thesis:

OPTIMIZATION OF INTERFACIAL BONDING AT METAL CASE-ADHESIVE AND ADHESIVE-EPDM INSULATION INTERFACES THROUGH SURFACE TREATMENTS FOR ROCKET MOTOR APPLICATIONS

submitted by **NEHİR KAHRAMAN** in partial fulfillment of the requirements for the degree of **Master of Science** i**n Polymer Science and Technology, Middle East Technical University** by,

Prof. Dr. Naci Emre Altun
Dean, **Graduate School of Natural and Applied Sciences** _____

Prof. Dr. Necati Özkan
Head of the Department, **Polymer Science and Technology** _____

Prof. Dr. Necati Özkan
Supervisor, **Polymer Science and Technology, METU** _____

Dr. Yasemin Altun
Co-Supervisor, **Roketsan** _____

Examining Committee Members:

Prof. Dr. Cevdet Kaynak
Metallurgical and Materials Engineering, METU _____

Prof. Dr. Necati Özkan
Polymer Science and Technology, METU _____

Assist. Prof. Dr. Cengiz Uzun
Chemistry, Hacettepe University _____

Date: 22.01.2026

I hereby declare that all information in this document has been obtained and presented in accordance with academic rules and ethical conduct. I also declare that, as required by these rules and conduct, I have fully cited and referenced all material and results that are not original to this work.

Name Last name : Nehir Kahraman

Signature :

ABSTRACT

OPTIMIZATION OF INTERFACIAL BONDING AT METAL CASE-ADHESIVE AND ADHESIVE-EPDM INSULATION INTERFACES THROUGH SURFACE TREATMENTS FOR ROCKET MOTOR APPLICATIONS

Kahraman, Nehir
Master of Science, Polymer Science and Technology
Supervisor: Prof. Dr. Necati Özkan
Co-Supervisor: Dr. Yasemin Altun

January 2026, 170 pages

Elastomer-metal bonding systems are critical in the defense and aerospace industry because they operate under high mechanical loads and challenging environmental conditions. Creating a reliable bond is critical for maintaining structural integrity and ensuring service safety. Although these bonding systems are commonly utilized in insulation applications, bonding EPDM with adhesives poses serious challenges due to its low surface energy and complex surface chemistry. Existing literature focuses primarily on vulcanization-based or primer-assisted approaches; however, the quantitative effect of surface cleanliness on adhesive-based EPDM-metal bonding has not been sufficiently addressed.

In this study, the adhesion behavior of EPDM rubber bonded to steel substrates using epoxy-based structural adhesives was investigated. The research evaluates the effects of surface roughness, surface cleanliness, mechanical roughening methods of EPDM, and atmospheric plasma application. The metal-adhesive interface was isolated through metal-to-metal bonding experiments, while the EPDM-adhesive interface was enhanced by mechanical roughening and plasma treatments. Adhesion

performance was evaluated through tensile and shear tests, followed by failure mode analysis.

The results indicated that the primary interface limiting bond strength was the EPDM-adhesive interface, not the metal-to-adhesive interface. Metal-to-metal experiments showed that optimum surface conditions correspond to Ra 4–8 μm and 0–50 RFU cleanliness. Mechanical roughening of EPDM surfaces resulted in bond strength increases of up to 154%, while atmospheric plasma application provided an additional strength increase of up to 54%, especially under shear loads. This study presents a quantitative and systematic surface preparation approach focusing on the EPDM interface for optimizing EPDM-metal bonding systems.

Keywords: Adhesive bonding, Elastomer–metal bonding, Interface optimization, Surface cleanliness, Surface roughness.

ÖZ

ROKET MOTORU UYGULAMALARI İÇİN YÜZEY İŞLEMLERİ İLE METAL GÖVDE–YAPIŞTIRICI VE YAPIŞTIRICI–EPDM YALITIM ARAYÜZLERİNDEKİ YAPIŞMANIN OPTİMİZASYONU

Kahraman, Nehir
Yüksek Lisans, Polimer Bilim ve Teknolojisi
Tez Yöneticisi: Prof. Dr. Necati Özkan
Ortak Tez Yöneticisi: Dr. Yasemin Altun

Ocak 2026, 170 sayfa

Elastomer-metal yapıştırma sistemleri, yüksek mekanik yükler ve zorlu çevresel koşullar altında çalışmaları nedeniyle savunma ve havacılık sektörlerinde kritik öneme sahiptir. Yapısal bütünlüğün korunması ve hizmet güvenliğinin sağlanması için güvenilir bir bağ oluşturulması hayati önem taşır. Bu yapışma sistemleri yalıtım uygulamalarında yaygın olarak kullanılsa da düşük yüzey enerjisi ve karmaşık yüzey kimyası nedeniyle EPDM'in yapıştırıcılarla birleştirilmesi ciddi zorluklar teşkil etmektedir. Mevcut literatür temel olarak vulkanizasyon esaslı veya astar destekli yaklaşımlara odaklanmaktadır, ancak yüzey temizliğinin yapıştırıcı esaslı EPDM-metal yapışma sistemi üzerindeki nicel etkisi yeterince ele alınmamıştır.

Bu çalışmada, epoksi esaslı yapısal yapıştırıcılar kullanılarak çelik substratlara yapıştırılan EPDM kauçuğun yapışma davranışı incelenmiştir. Araştırma kapsamında; yüzey pürüzlülüğü, yüzey temizliği, EPDM'nin mekanik pürüzlendirme yöntemleri ve atmosferik plazma uygulamasının etkileri değerlendirilmiştir. Metal–yapıştırıcı arayüzü yüzey pürüzlülüğü ve temizlik parametreleri üzerinden optimize edilirken; EPDM–yapıştırıcı arayüzü mekanik

pürüzlendirme ve plazma işlemleri ile optimize edilmiştir. Yapışma performansı, çekme ve kayma testleri ile değerlendirilmiş ve hasar modları analiz edilmiştir.

Sonuçlar, yapışma mukavemetini sınırlayan birincil arayüzün metal-yapıştırıcı arayüzü değil, EPDM-yapıştırıcı arayüzü olduğunu göstermiştir. Metal-metal deneyleri, optimum yüzey koşullarının Ra 4–8 μm pürüzlülük ve 0–50 RFU temizlik değerlerine karşılık geldiğini ortaya koymuştur. EPDM yüzeylerinin mekanik olarak pürüzlendirilmesi yapışma mukavemetinde %154'e varan artışlar sağlarken, atmosferik plazma uygulaması özellikle kayma yükleri altında %54'e kadar ek bir mukavemet artışı sağlamıştır. Bu çalışma, EPDM-metal yapışma sistemlerini optimize etmek için EPDM arayüzüne odaklanan nicel ve sistematik bir yüzey hazırlama yaklaşımı sunmaktadır.

Anahtar Kelimeler: Yapıştırıcı ile bağlanma, Elastomer–metal yapıştırma, Arayüz optimizasyonu, Yüzey temizliği, Yüzey pürüzlülüğü.

To my beloved grandmother…

ACKNOWLEDGMENTS

I express my sincere gratitude to my supervisor, Prof. Dr. Necati Özkan, for his invaluable knowledge, guidance, and patience throughout this study. It has been a privilege to be his student. His thoughtful feedback and critical approach have been highly influential in shaping my academic development.

I also thank my thesis committee members, Prof. Dr. Necati Özkan, Prof. Dr. Cevdet Kaynak, and Assist. Prof. Dr. Cengiz Uzun, for their valuable time and constructive suggestions, which significantly improved the quality of this work. I am grateful to Dr. Yasemin Altun for her role as co-advisor and her contributions.

Special thanks to Roketsan for supporting my master's studies and providing the opportunity to conduct this research. I am grateful to Hakan Der for defining the scope of this study and for his valuable technical guidance. I thank Alpercan Kurdaş, Nedim Çağlıyan, and Akın Güler for production planning support and technical coordination; Berk Polat and Durmuş Deniz Doğan for assistance during experimental tests; and Nihat Özer Uçar for his contributions in SEM/EDS analysis. I also thank Tarık Bostan and Duran Ülsü for their technical support during the experimental stages.

I would also like to thank Onur Aydın, Melisa Yücel, Elif Tanrıverdi, Buse Yatar, Beyza Kaya, Melike Kafaoğlu, Necla Nur Halhallı, Ecem Kacar, Tuğba Horuz and Tolga Horuz for their constant support, patience, and encouragement throughout this journey. Their understanding, and unwavering belief in me, along with their timely reminders that I was not alone, made even the most challenging moments more manageable. Their presence turned a demanding process into a more meaningful experience.

Finally, I thank my family for their unconditional love and endless support. Their belief in me and the sacrifices they made have been instrumental in bringing me to where I am today. Without them, this journey would not have been possible.

TABLE OF CONTENTS

ABSTRACT v

ÖZ vii

ACKNOWLEDGMENTS x

TABLE OF CONTENTS xii

LIST OF TABLES xvi

LIST OF FIGURES xvi

LIST OF ABBREVIATIONS xxix

LIST OF SYMBOLS xxxi

CHAPTERS

1 INTRODUCTION 1

1.1 Solid Rocket Motor 1

1.1.1 Motor Case 2

1.1.2 Propellant 3

1.1.3 Liner 3

1.1.4 Insulation 3

1.1.5 Adhesive or Primer Systems 4

1.1.6 Igniter 4

1.1.7 Nozzle Assembly 5

1.2 Importance of Adhesion between Motor Case and Insulation 5

1.3 Adhesive Bonding 6

1.3.1 Adhesion Mechanisms 7

1.3.2 Failure Modes 12

1.4 Surface Preparation 14
1.4.1 Mechanical Surface Preparation and Measurement Methods 15
1.4.2 Chemical Surface Preparation Methods 17
1.4.3 Physicochemical Surface Preparation Methods 19
1.5 Aim and Motivation of The Study 20
2 LITERATURE REVIEW 23
2.1 The Effect of Surface Roughness of Materials on Adhesion Strength ... 23
2.2 Effect of Surface Contamination of Materials on Adhesion Strength 30
2.3 Effect of Surface Activation of Materials on Adhesion Strength 34
3 EXPERIMENTAL WORK 39
3.1 Materials 40
3.1.1 AISI 4140 Steel 40
3.1.2 Ethylene Propylene Diene Monomer (EPDM) 40
3.1.3 Araldite® 2011 41
3.1.4 3M™ Scotch-Weld™ DP-490 42
3.2 Preparation and Characterization Instruments 43
3.2.1 Sandblasting Equipment 43
3.2.2 Universal Testing Machine 44
3.2.3 Surface Cleanliness Measurement Device (SITA Cleanospector) . 44
3.2.4 Surface Roughness Measurement Device (MAHR Marsurf PS10) 45
3.2.5 Cold Plasma Treatment Device (PiezoBrush® PZ3) 46
3.2.6 Scanning Electron Microscopy (Thermo Scientific Phenom XL) .. 47
3.3 Investigation of the Effect of Metal Surface Preparation Parameters on EPDM-Metal Bond Strength 49

3.4 Evaluation of Metal-Adhesive Interface Through Metal-Metal Bonding Experiments 57
3.5 Investigation of the Effects of Different EPDM Surface Roughening Methods on the EPDM-Adhesive Interface 59
3.6 Investigation of EPDM Surface Activation and Time Effect via Plasma Application 60
4 RESULTS AND DISCUSSION 63
4.1 The Effect of Metal Surface Roughness and Cleanliness Level on EPDM-Metal Bond Strength 63
4.2 Evaluation of Metal-Adhesive Interface with Metal-Metal Shear Tests 70
4.3 The Effect of EPDM Surface Roughening Methods on the EPDM-Adhesive Interface 78
4.4 Investigation of EPDM Surface Activation and Time Effect with Plasma Application 88
4.5 Evaluation of Adhesion Behaviors Based on Wetting and Mechanical Interlocking Mechanisms 92
4.6 Mechanical and Interfacial Evaluation of the Difference Between Tensile and Shear Test Results in EPDM-Metal Bonding Systems 95
5 CONCLUSION 97
6 FINAL REMARKS and FUTURE WORK 101
REFERENCES 103
APPENDICES
A. Roughness and Cleanliness Measurements of Samples and Test Results 111
B. Tensile Test and Shear Test Coupon Images and Failure Modes 119
C. Summary of Failure Modes 163
D. SEM and EDS Analysis of EPDM Surface 167

E. SEM and EDS Analysis of Metal Surface 170

LIST OF TABLES

TABLES

Table 1.1 Bond / Interaction Types and Approximate Energies (Ebnesajjad, 2013).9
Table 2.1 Shear Strength with respect to Surface Roughness Value of Aluminum Adherends Joints (Ghumatkar et al., 2016) 23
Table 2.2 Shear Strength with respect to Surface Roughness Value of Mild Steel Adherends Joints (Ghumatkar et al., 2016) 24
Table 2.3 Experimental Surface Roughness Ra and Rz Depending on the Mechanical Treatment (Spaggiari and Dragoni, 2013) 27
Table 2.4 Stress-Strain Values of Tensile Specimens (T1→Cleaned Surface, ... 32
Table 2.5 Element Content in Atomic Percent of the Untreated and Plasma Treated NBR and EPDM Rubbers (Moraes et al., 2007) 34
Table 3.1 Surface Preparation Matrix for Rubber-Metal Bonding 54
Table 4.1 EDS Analysis of Metal with Medium Roughness (2-4 μm) 76
Table 4.2 EDS Analysis of Metal with High Roughness (4-8 μm) 77
Table 4.3 EDS Analysis of Unroughened EPDM 85
Table 4.4 EDS Analysis of EPDM Roughened with Peel Ply 86
Table 4.5 EDS Analysis of EPDM Roughened with Sandpaper 87
Table A. 1 Rubber-Metal Bonding Roughness and Cleanliness Measurement and Tensile Test Results (DP490) 111
Table A. 2 Rubber-Metal Bonding Roughness and Cleanliness Measurement and Tensile Test Results (Araldite 2011) 112
Table A. 3 Rubber-Metal Bonding Roughness and Cleanliness Measurement and Shear Test Results (DP490) 113
Table A. 4 Rubber-Metal Bonding Roughness and Cleanliness Measurement and Shear Test Results (Araldite 2011) 114

Table A. 5 Metal-Metal Bonding Roughness and Cleanliness Measurement and Shear Test Results (DP490) 115
Table A. 6 Metal-Metal Bonding Roughness and Cleanliness Measurement and Shear Test Results (Araldite 2011) 116
Table A. 7 Rubber-Metal Bonding with Different Roughness Methods Tensile Test Results 117
Table A. 8 Rubber-Metal Bonding with Different Roughness Methods Shear Test Results 117
Table A. 9 Rubber-Metal Bonding with Different Plasma Treatment Time Tensile Test Results 118
Table A. 10 Rubber-Metal Bonding with Different Plasma Treatment Time Shear Test Results 118
Table C. 1 Failure Mode Analysis for Part I 163
Table C. 2 Failure Mode Analysis for Part II 164
Table C. 3 Failure Mode Analysis for Part III 165
Table C. 4 Failure Mode Analysis for Part IV 166

LIST OF FIGURES

FIGURES

Figure 1.1 Components of Solid Rocket Motor Case (Purdue University, n.d.)..... 1
Figure 1.2 Cross Section of a Solid Rocket Motor (Debnath et al., 2018)..... 2
Figure 1.3 Illustration of Mechanical Interlocking Theory (Clearfield et al., 1991). 8
Figure 1.4 a) Poor Wetting b) Good Wetting (Lee et al., 2009)..... 10
Figure 1.5 Illustration of Wetting Level According to Contact Angle (Giridhar et al., 2017)..... 12
Figure 1.6 Failure Modes in Adhesion (Omairey et al., 2021)..... 13
Figure 2.1 Uncontaminated Peel Test (Cohesive Failure) (Moreira et al., 2022) ... 31
Figure 2.2 Peel Test with 10 Sprays (Mixed Failure) (Moreira et al., 2022) 31
Figure 2.3 Peel Test with 10 sprays (Mixed Failure) (Moreira et al., 2022)..... 32
Figure 2.4 Microscopic Morphology of Uncleaned Surfaces, (a)(b) particles, (c)(d) chips, (e)(f) fibers (Zhao et al., 2021) 33
Figure 2.5 Microscopic Morphology of Cleaned Substrate Surfaces (Zhao et al., 2021)..... 33
Figure 2.6 Contact Angle and Polar Surface Tension (mJ/m^2) of Untreated NBR and EPDM Rubber and Plasma Treated EPDM Rubber (Moraes et al., 2007) 34
Figure 3.1 Araldite® 2011 Adhesive (Henkel, 2023) 42
Figure 3.2 3M™ Scotch-Weld™ DP-490 (3M, 2022)..... 43
Figure 3.3 Universal Testing Machine 44
Figure 3.4 SITA Cleanospector (SITA Messtechnik GmbH, 2021) 45
Figure 3.5 MAHR MarSurf PS10 (Mahr GmbH, 2021) 46
Figure 3.6 PiezoBrush® PZ3 (Relyon Plasma, 2022)..... 47
Figure 3.7 Thermo Scientific Phenom XL (Thermo Fisher Scientific, 2021) and Agar Sputter Coater..... 48

Figure 3.8 Surface Roughness Measurements with Marsurf PS10 49
Figure 3.9 Non-sandblasted Surfaces (<1 μm) 50
Figure 3.10 Samples with Low Surface Roughness (1-2 μm) 50
Figure 3.11 Samples with Moderate Surface Roughness (2-4 μm) 51
Figure 3.12 Samples with High Surface Roughness (4-8 μm) 51
Figure 3.13 Cleaning of Samples with MEK by Using the Immersion Method 52
Figure 3.14 Surface Contamination Process with Mobil Vactra Oil No. 2 52
Figure 3.15 Surface Cleaning Measurement with Sita Cleanospector 53
Figure 3.16 Preparing a Tensile Test Specimens with DP490 and Araldite 2011 .. 55
Figure 3.17 Tensile Test Specimens Curing Under Pressure 55
Figure 3.18 Shear Test Specimens Curing Under Pressure 56
Figure 3.19 Geometrical Details and Dimensions of the Tensile and Shear Test Specimens 56
Figure 3.20 Non-sandblasted Surfaces (<1 μm) 57
Figure 3.21 Samples with Low Surface Roughness (1-2 μm) 57
Figure 3.22 Samples with Moderate Surface Roughness (2-4 μm) 58
Figure 3.23 Samples with High Surface Roughness (4-8 μm) 58
Figure 3.24 Shear Test Coupons for Clean Surface → 40, Modaretely Contaminated Surface → 51, Highly Contaminated Surface →41 59
Figure 3.25 a) Smooth Surface b) Roughened with Peel Ply c) Roughened with Sandpaper 60
Figure 3.26 EPDM Plasma Treatment 61
Figure 4.1 The Mean Tensile Strength as a Function of Surface Roughness for DP490 64
Figure 4.2 The Mean Tensile Strength as a Function of Surface Roughness for Araldite 2011 65
Figure 4.3 The Mean Shear Strength as a Function of Surface Roughness for DP490 66
Figure 4.4 The Mean Shear Strength as a Function of Surface Roughness for Araldite 2011 67

Figure 4.5 2-4 μm, 0-50 RFU, DP490, Adhesive Failure 68
Figure 4.6 2-4 μm, 0-50 RFU, Araldite 2011, Adhesive Failure 68
Figure 4.7 1-2 μm, 0-50 RFU, DP490, Cohesive Failure in EPDM, DP490 69
Figure 4.8 1-2 μm, 0-50 RFU, DP490, Cohesive Failure in EPDM, Araldite 201169
Figure 4.9 The Mean Shear Strength as a Function of Surface Roughness for DP490 (Metal-Metal Bonding)..... 70
Figure 4.10 Metal-Metal Bonding, Shear Test, DP490, 2-4 μm, 0-50 RFU, Cohesive Failure in Adhesive..... 72
Figure 4.11 The Mean Shear Strength as a Function of Surface Roughness for Araldite 2011 (Metal-Metal Bonding)..... 72
Figure 4.12 4-8 μm, 0-50 RFU, Adhesive Failure, Araldite 2011 73
Figure 4.13 SEM Image of Smooth Metal Surface (<1 μm)..... 75
Figure 4.14 SEM Image of Metal with Low Roughness (1-2 μm) 75
Figure 4.15 SEM Image of Metal with Medium Roughness (2-4 μm) 76
Figure 4.16 SEM Image of Metal with High Roughness (4-8 μm)..... 77
Figure 4.17 The Mean Tensile Strength vs EPDM Roughness Method for DP490 79
Figure 4.18 The Mean Tensile Strength vs EPDM Roughness Method for Araldite 2011 80
Figure 4.19 The Mean Shear Strength vs EPDM Roughness Method for DP490 .. 81
Figure 4.20 The Mean Shear Strength vs EPDM Roughness Method for Araldite 2011 82
Figure 4.21 SEM Image of Unroughened EPDM 84
Figure 4.22 SEM Image of EPDM Roughened with Peel Ply 85
Figure 4.23 SEM Image of EPDM Roughened with Sandpaper..... 86
Figure 4.24 The Mean Tensile Strength vs Plasma Treatment Time for DP490 89
Figure 4.25 The Mean Tensile Strength vs Plasma Treatment Time for Araldite 2011 89
Figure 4.26 The Mean Shear Strength vs Plasma Treatment Time for DP490..... 90
Figure 4.27 The Mean Shear Strength vs Plasma Treatment Time for Araldite 2011 91

Figure 5.1 Schematic Illustration of the Experimental Strategy Adopted in the Study to Investigate and Optimize Rubber–Metal Adhesion 97
Figure 6.1 Schematic Cross-section of the Solid Rocket Motor Assembly 101
Figure B. 1 Rubber-Metal Bonding, Tensile Test, DP490, Non-blasted, 0-50 RFU, Adhesive Failure 119
Figure B. 2 Rubber-Metal Bonding, Tensile Test, DP490, Non-blasted, 50-200 RFU, Adhesive Failure 119
Figure B. 3 Rubber-Metal Bonding, Tensile Test, DP490, Non-blasted, 300-750 RFU, Adhesive Failure 119
Figure B. 4 Rubber-Metal Bonding, Tensile Test, DP490, 1-2 μm, 0-50 RFU, Adhesive Failure 120
Figure B. 5 Rubber-Metal Bonding, Tensile Test, DP490, 1-2 μm, 50-200 RFU, Mixed Failure 120
Figure B. 6 Rubber-Metal Bonding, Tensile Test, DP490, 1-2 μm, 300-750 RFU, Mixed Failure 120
Figure B. 7 Rubber-Metal Bonding, Tensile Test, DP490, 2-4 μm, 0-50 RFU, Adhesive Failure 121
Figure B. 8 Rubber-Metal Bonding, Tensile Test, DP490, 2-4 μm, 50-200 RFU, Adhesive Failure 121
Figure B. 9 Rubber-Metal Bonding, Tensile Test, DP490, 2-4 μm, 300-750 RFU, Adhesive Failure 121
Figure B. 10 Rubber-Metal Bonding, Tensile Test, DP490, 4-8 μm, 0-50 RFU, Adhesive Failure 122
Figure B. 11 Rubber-Metal Bonding, Tensile Test, DP490, 4-8 μm, 50-200 RFU, Adhesive Failure 122
Figure B. 12 Rubber-Metal Bonding, Tensile Test, DP490, 4-8 μm, 300-750 RFU, Adhesive Failure 122

Figure B. 13 Rubber-Metal Bonding, Tensile Test, Araldite 2011, Non-blasted, 0-50 RFU, Adhesive Failure 123
Figure B. 14 Rubber-Metal Bonding, Tensile Test, Araldite 2011, Non-blasted, 50-200 RFU, Adhesive Failure 123
Figure B. 15 Rubber-Metal Bonding, Tensile Test, Araldite 2011, Non-blasted, 300-750 RFU, Adhesive Failure 123
Figure B. 16 Rubber-Metal Bonding, Tensile Test, Araldite 2011, 1-2 µm, 0-50 RFU, Adhesive Failure 124
Figure B. 17 Rubber-Metal Bonding, Tensile Test, Araldite 2011, 1-2 µm, 50-200 RFU, Adhesive Failure 124
Figure B. 18 Rubber-Metal Bonding, Tensile Test, Araldite 2011, 1-2 µm, 300-750 RFU, Adhesive Failure 124
Figure B. 19 Rubber-Metal Bonding, Tensile Test, Araldite 2011, 2-4 µm, 0-50 RFU, Adhesive Failure 125
Figure B. 20 Rubber-Metal Bonding, Tensile Test, Araldite 2011, 2-4 µm, 50-200 RFU, Adhesive Failure 125
Figure B. 21 Rubber-Metal Bonding, Tensile Test, Araldite 2011, 2-4 µm, 300-750 RFU, Adhesive Failure 125
Figure B. 22 Rubber-Metal Bonding, Tensile Test, Araldite 2011, 4-8 µm, 0-50 RFU, Adhesive Failure 126
Figure B. 23 Rubber-Metal Bonding, Tensile Test, Araldite 2011, 4-8 µm, 50-200 RFU, Adhesive Failure 126
Figure B. 24 Rubber-Metal Bonding, Tensile Test, Araldite 2011, 4-8 µm, 300-750 RFU, Adhesive Failure 126
Figure B. 25 Rubber-Metal Bonding, Shear Test, DP490, Non-blasted, 0-50 RFU, Adhesive Failure 127
Figure B. 26 Rubber-Metal Bonding, Shear Test, DP490, Non-blasted, 50-200 RFU, Cohesive Failure in EPDM 127
Figure B. 27 Rubber-Metal Bonding, Shear Test, DP490, Non-blasted, 300-750 RFU, Adhesive Failure 128

Figure B. 28 Rubber-Metal Bonding, Shear Test, DP490, 1-2 μm, 0-50 RFU, Cohesive Failure in EPDM 128
Figure B. 29 Rubber-Metal Bonding, Shear Test, DP490, 1-2 μm, 50-200 RFU, Cohesive Failure in EPDM 129
Figure B. 30 Rubber-Metal Bonding, Shear Test, DP490, 1-2 μm, 300-750 RFU, Cohesive Failure in EPDM 129
Figure B. 31 Rubber-Metal Bonding, Shear Test, DP490, 2-4 μm, 0-50 RFU, Mixed Failure 130
Figure B. 32 Rubber-Metal Bonding, Shear Test, DP490, 2-4 μm, 50-200 RFU, Cohesive Failure in EPDM 130
Figure B. 33 Rubber-Metal Bonding, Shear Test, DP490, 2-4 μm, 300-750 RFU, Mixed Failure 131
Figure B. 34 Rubber-Metal Bonding, Shear Test, DP490, 4-8 μm, 0-50 RFU, Mixed Failure 131
Figure B. 35 Rubber-Metal Bonding, Shear Test, DP490, 4-8 μm, 50-200 RFU, Mixed Failure 132
Figure B. 36 Rubber-Metal Bonding, Shear Test, DP490, 4-8 μm, 300-750 RFU, Mixed Failure 132
Figure B. 37 Rubber-Metal Bonding, Shear Test, Araldite 2011, Non-blasted, 0-50 RFU, Adhesive Failure 133
Figure B. 38 Rubber-Metal Bonding, Shear Test, Araldite 2011, Non-blasted, 50-200 RFU, Adhesive Failure 133
Figure B. 39 Rubber-Metal Bonding, Shear Test, Araldite 2011, Non-blasted, 300-750 RFU, Adhesive Failure 134
Figure B. 40 Rubber-Metal Bonding, Shear Test, Araldite 2011, 1-2 μm, 0-50 RFU, Cohesive Failure in EPDM 134
Figure B. 41 Rubber-Metal Bonding, Shear Test, Araldite 2011, 1-2 μm, 50-200 RFU, Cohesive Failure in EPDM 135
Figure B. 42 Rubber-Metal Bonding, Shear Test, Araldite 2011, 1-2 μm, 300-750 RFU, Cohesive Failure in EPDM 135

Figure B. 43 Rubber-Metal Bonding, Shear Test, Araldite 2011, 2-4 µm, 0-50 RFU, Adhesive Failure....136
Figure B. 44 Rubber-Metal Bonding, Shear Test, Araldite 2011, 2-4 µm, 50-200 RFU, Adhesive Failure....136
Figure B. 45 Rubber-Metal Bonding, Shear Test, Araldite 2011, 2-4 µm, 300-750 RFU, Adhesive Failure....137
Figure B. 46 Rubber-Metal Bonding, Shear Test, Araldite 2011, 4-8 µm, 0-50 RFU, Adhesive Failure....137
Figure B. 47 Rubber-Metal Bonding, Shear Test, Araldite 2011, 4-8 µm, 50-200 RFU, Adhesive Failure....138
Figure B. 48 Rubber-Metal Bonding, Shear Test, Araldite 2011, 4-8 µm, 300-750 RFU, Adhesive Failure....138
Figure B. 49 Metal-Metal Bonding, Shear Test, DP490, Non-blasted, 0-50 RFU, Adhesive Failure....139
Figure B. 50 Metal-Metal Bonding, Shear Test, DP490, Non-blasted, 50-200 RFU, Adhesive Failure....139
Figure B. 51 Metal-Metal Bonding, Shear Test, DP490, Non-blasted, 300-750 RFU, Adhesive Failure....140
Figure B. 52 Metal-Metal Bonding, Shear Test, DP490, 1-2 µm, 0-50 RFU, Cohesive Failure in Adhesive....140
Figure B. 53 Metal-Metal Bonding, Shear Test, DP490, 1-2 µm, 50-200 RFU, Cohesive Failure in Adhesive....141
Figure B. 54 Metal-Metal Bonding, Shear Test, DP490, 1-2 µm, 300-750 RFU, Cohesive Failure in Adhesive....141
Figure B. 55 Metal-Metal Bonding, Shear Test, DP490, 2-4 µm, 0-50 RFU, Cohesive Failure in Adhesive....142
Figure B. 56 Metal-Metal Bonding, Shear Test, DP490, 2-4 µm, 50-200 RFU, Cohesive Failure in Adhesive....142
Figure B. 57 Metal-Metal Bonding, Shear Test, DP490, 2-4 µm, 300-750 RFU, Cohesive Failure in Adhesive....143

Figure B. 58 Metal-Metal Bonding, Shear Test, DP490, 4-8 µm, 0-50 RFU, Substrate Failure 143
Figure B. 59 Metal-Metal Bonding, Shear Test, DP490, 4-8 µm, 50-200 RFU, Adhesive Failure 144
Figure B. 60 Metal-Metal Bonding, Shear Test, DP490, 4-8 µm, 300-750 RFU, Cohesive Failure in Adhesive 144
Figure B. 61 Metal-Metal Bonding, Shear Test, Araldite 2011, Non-blasted, 0-50 RFU, Adhesive Failure 145
Figure B. 62 Metal-Metal Bonding, Shear Test, Araldite 2011, Non-blasted, 50-200 RFU, Adhesive Failure 145
Figure B. 63 Metal-Metal Bonding, Shear Test, Araldite 2011, Non-blasted, 300-750 RFU, Adhesive Failure 146
Figure B. 64 Metal-Metal Bonding, Shear Test, Araldite 2011, 1-2 µm, 0-50 RFU, Adhesive Failure 146
Figure B. 65 Metal-Metal Bonding, Shear Test, Araldite 2011, 1-2 µm, 50-200 RFU, Adhesive Failure 147
Figure B. 66 Metal-Metal Bonding, Shear Test, Araldite 2011, 1-2 µm, 300-750 RFU, Adhesive Failure 147
Figure B. 67 Metal-Metal Bonding, Shear Test, Araldite 2011, 2-4 µm, 0-50 RFU, Adhesive Failure 148
Figure B. 68 Metal-Metal Bonding, Shear Test, Araldite 2011, 2-4 µm, 50-200 RFU, Adhesive Failure 148
Figure B. 69 Metal-Metal Bonding, Shear Test, Araldite 2011, 2-4 µm, 300-750 RFU, Adhesive Failure 149
Figure B. 70 Metal-Metal Bonding, Shear Test, Araldite 2011, 4-8 µm, 0-50 RFU, Adhesive Failure 149
Figure B. 71 Metal-Metal Bonding, Shear Test, Araldite 2011, 4-8 µm, 50-200 RFU, Lack of Adhesive 150
Figure B. 72 Metal-Metal Bonding, Shear Test, Araldite 2011, 4-8 µm, 300-750 RFU, Adhesive Failure 150

Figure B. 73 Rubber-Metal Bonding, Tensile Test, DP490, 4-8 µm, Smooth EPDM, Adhesive Failure....151
Figure B. 74 Rubber-Metal Bonding, Tensile Test, DP490, 4-8 µm, EPDM Roughened with Sandpaper, Adhesive Failure....151
Figure B. 75 Rubber-Metal Bonding, Tensile Test, DP490, 4-8 µm, EPDM Roughened with Peel Ply, Adhesive Failure....152
Figure B. 76 Rubber-Metal Bonding, Tensile Test, Araldite 2011, 4-8 µm, Smooth EPDM, Adhesive Failure....152
Figure B. 77 Rubber-Metal Bonding, Tensile Test, Araldite 2011, 4-8 µm, EPDM Roughened with Sandpaper, Adhesive Failure....153
Figure B. 78 Rubber-Metal Bonding, Tensile Test, Araldite 2011, 4-8 µm, EPDM Roughened with Peel Ply, Adhesive Failure....153
Figure B. 79 Rubber-Metal Bonding, Shear Test, DP490, 4-8 µm, Smooth EPDM, Adhesive Failure....154
Figure B. 80 Rubber-Metal Bonding, Shear Test, DP490, 4-8 µm, EPDM Roughened with Sandpaper, Adhesive Failure....154
Figure B. 81 Rubber-Metal Bonding, Shear Test, DP490, 4-8 µm, EPDM Roughened with Peel Ply, Adhesive Failure....155
Figure B. 82 Rubber-Metal Bonding, Shear Test, Araldite 2011, 4-8 µm, Smooth EPDM, Adhesive Failure....155
Figure B. 83 Rubber-Metal Bonding, Shear Test, Araldite 2011, 4-8 µm, EPDM Roughened with Sandpaper, Adhesive Failure....156
Figure B. 84 Rubber-Metal Bonding, Shear Test, Araldite 2011, 4-8 µm, EPDM Roughened with Peel Ply, Adhesive Failure....156
Figure B. 85 Rubber-Metal Bonding, Tensile Test, DP490, 4-8 µm, EPDM Roughened with Sandpaper, EPDM Without Plasma, Mixed Failure....157
Figure B. 86 Rubber-Metal Bonding, Tensile Test, DP490, 4-8 µm, EPDM Roughened with Sandpaper, 30 s Plasma Treatment, Mixed Failure....157
Figure B. 87 Rubber-Metal Bonding, Tensile Test, DP490, 4-8 µm, EPDM Roughened with Sandpaper, 60 s Plasma Treatment, Mixed Failure....158

Figure B. 88 Rubber-Metal Bonding, Tensile Test, Araldite 2011, 4-8 µm, EPDM Roughened with Sandpaper, EPDM without Plasma, Adhesive Failure 158
Figure B. 89 Rubber-Metal Bonding, Tensile Test, Araldite 2011, 4-8 µm, EPDM Roughened with Sandpaper, 30 s Plasma Treatment, Cohesive Failure in EPDM 159
Figure B. 90 Rubber-Metal Bonding, Tensile Test, Araldite 2011, 4-8 µm, EPDM Roughened with Sandpaper, 60 s Plasma Treatment, Cohesive Failure in EPDM 159
Figure B. 91 Rubber-Metal Bonding, Shear Test, DP490, 4-8 µm, EPDM Roughened with Sandpaper, EPDM Without Plasma, Mixed Failure 160
Figure B. 92 Rubber-Metal Bonding, Shear Test, DP490, 4-8 µm, EPDM Roughened with Sandpaper, 15 s Plasma Treatment, Mixed Failure 160
Figure B. 93 Rubber-Metal Bonding, Shear Test, DP490, 4-8 µm, EPDM Roughened with Sandpaper, 30 s Plasma Treatment, Cohesive Failure in EPDM..... 161
Figure B. 94 Rubber-Metal Bonding, Shear Test, Araldite 2011, 4-8 µm, EPDM Roughened with Sandpaper, EPDM without Plasma, Adhesive Failure 161
Figure B. 95 Rubber-Metal Bonding, Shear Test, Araldite 2011, 4-8 µm, EPDM Roughened with Sandpaper, 15 s Plasma Treatment, Adhesive Failure 162
Figure B. 96 Rubber-Metal Bonding, Shear Test, DP490, 4-8 µm, EPDM Roughened with Sandpaper, 30 s Plasma Treatment, Cohesive Failure in EPDM..... 162
Figure D. 1 SEM Image of Smooth EPDM 167
Figure D. 2 X-ray Intensity (counts) vs. X-ray Energy (keV) of Smooth EPDM Surface 167
Figure D. 3 SEM Image of EPDM Roughened with Sandpaper 168
Figure D. 4 X-ray Intensity (counts) vs. X-ray Energy (keV) of EPDM Surface Roughened with Sandpaper 168
Figure D. 5 SEM Image of EPDM Roughened with Peel Ply 169

Figure D. 6 X-ray Intensity (counts) vs. X-ray Energy (keV) of EPDM Surface Roughened with Peel Ply.....169
Figure E. 1 SEM Image of Metal with Medium Roughness (2-4 μm).....170
Figure E. 2 X-ray Intensity (counts) vs. X-ray Energy (keV) of Metal Surface with Medium Roughness (2-4 μm).....170

LIST OF ABBREVIATIONS

ABBREVIATIONS

AFM Atomic Force Microscopy

AP Ammonium Perchlorate

ASTM American Society for Testing and Materials

$BKNO_3$ Boron Potassium Nitrate

DMA Dynamic Mechanical Analysis

DSC Differential Scanning Calorimetry

EDS Energy Dispersive Spectroscopy

EDX Energy Dispersive X-ray Spectroscopy

EPDM Ethylene Propylene Diene Monomer

HTPB Hydroxyl-Terminated Polybutadiene

PSA Pressure-Sensitive Adhesive

RFU Relative Fluorescence Unit

SEM Scanning Electron Microscopy

SLS Single-Lap Shear

SRM Solid Rocket Motor

TVC Thrust Vector Control

UV Ultraviolet

WBL Weak Boundary Layer

WLI White Light Interferometry

XPS X-ray Photoelectron Spectroscopy

LIST OF SYMBOLS

SYMBOLS

°C Degree Celsius

Δ Change / Difference

ε Strain

θ Contact Angle

μm Micrometer

MPa Megapascal

N Newton

Ra Arithmetic Mean Surface Roughness

Rz Average Maximum Height of the Profile

σ Stress

s Second

Tg Glass Transition Temperature

γ Surface Energy

CHAPTER 1

INTRODUCTION

1.1 Solid Rocket Motor

Solid rocket motors (SRM) are widely used in the defense industry, space launch systems, and short-range weapon systems due to their high energy density and structural simplicity (Sutton & Biblarz, 2017). These motors consist of various functional subsystems, and each component has a direct impact on the overall performance, safety, and thrust efficiency of the motor. Solid rocket motors can be examined under seven main components: motor case, propellant, insulation, liner, adhesive/primer system, igniter, and the nozzle system that directs the thrust (Humble, Henry, & Larson, 1995).

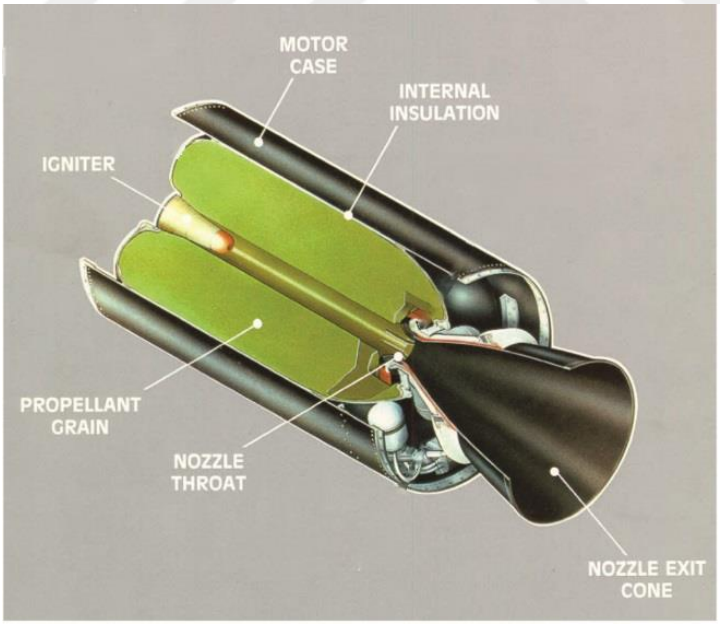


Figure 1.1 Components of Solid Rocket Motor Case (Purdue University, n.d.)

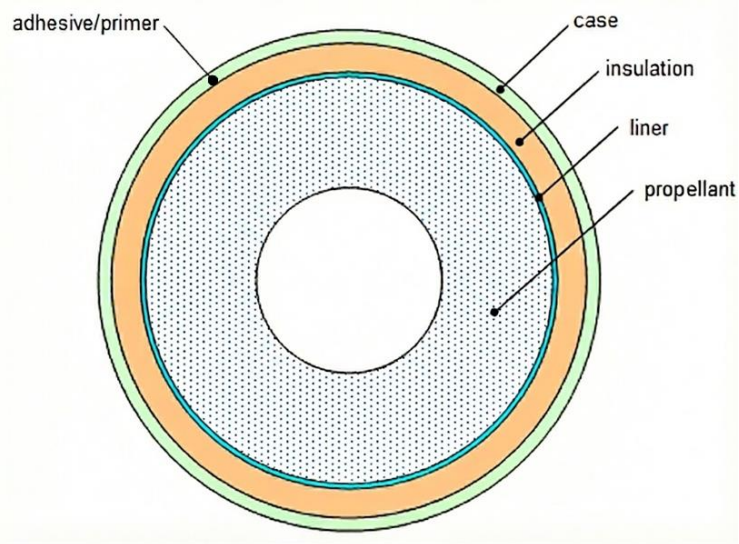


Figure 1.2 Cross Section of a Solid Rocket Motor (Debnath et al., 2018)

1.1.1 Motor Case

The motor casing, which forms the outer structure of a solid propellant rocket motor, provides structural integrity by resisting all internal pressures and mechanical loads. The casing also contains other components such as the propellant, insulation, liner, and nozzle. High pressures, ranging from 3–20 MPa, are generated within the engine during combustion, and this pressure requires the casing to be highly resistant to elastic and plastic deformation. Therefore, motor casings are typically manufactured using high-strength steel alloys (e.g., AISI 4130 or 4140), aluminum composite tubes, or carbon fiber-reinforced epoxy composite materials (Sutton & Biblarz, 2017). Material selection is determined by the optimization of the mission profile and cost parameters. Composite structures are preferred, especially in space applications where weight is critical, while steel casings are widely used in the defense industry.

1.1.2 Propellant

The propellant, which is the energy source of a solid propellant motor, is a compound system that includes fuel, oxidizer, and additives. Composite solid propellants are generally favored, and in these systems, HTPB (Hydroxyl-Terminated Polybutadiene) is used as propellant, ammonium perchlorate (AP) as an oxidizer, and aluminum powder to increase the combustion temperature. This combination is frequently molded into the proper geometry by casting it in a mold. Grain geometry (star, tubular, finocyl, etc.) has a direct impact on burn rate and thrust profile (Yang, Brill & Ren, 2000). The physical structure and chemical stability of the propellant determine the engine's performance and safety. Air voids and crack formation within the grain must be carefully monitored to achieve uniform combustion and crack management.

1.1.3 Liner

The liner is an adhesive interface layer located between the propellant and the inner surface of the motor. Its primary function is to ensure that the propellant block adheres homogeneously, durably and without void to the insulation or motor case. It also serves to seal micropores and prevents moisture, gas, or chemical migration (Culick, 2001). Liner systems are usually produced from epoxy, HTPB, or phenolic resin-based prepolymers and are cured after application. To prevent debonding under post-combustion stresses, the liner material must be chemically compatible with both the insulation layer and the propellant load.

1.1.4 Insulation

The insulation layer is a thick intermediate layer that protects the motor case from the damaging effects of high temperatures while also limiting the transfer of thermal energy to the casing. As temperatures in the combustion chamber can reach 3000 K,

the insulation material must be resistant to both heat and particle erosion. Commonly used materials for this purpose include EPDM rubber, silicone elastomers, glass fiber-reinforced phenolic composites, and carbon-filled ablation materials. The insulation can be vulcanized directly to the inner casing surface or bonded with adhesive systems. In engines with a high risk of erosion, ablation behavior and material thickness are specifically analyzed (Elashker et al., 2023).

1.1.5 Adhesive or Primer Systems

In solid propellant rocket motors, specially developed adhesive or primer systems are used at the interface to ensure permanent and durable bonding of elastomer-based materials directly to the metal body. These methods increase the metal's surface energy, which allows for chemical and physical bonding with the elastomer. The adhesives utilized are often epoxy, phenolic resin, or isocyanate-based systems, with the primer layer serving as a low-viscosity substrate to improve adhesive adhesion. The adhesive/primer layer has to maintain its adhesion quality, especially over the engine's shelf life (5-20 years), and minimize cracking or separation at the interface due to differential thermal expansion between the elastomer and metal. Therefore, thermomechanical compatibility is a critical parameter not only for initial adhesion but also for long-term durability (Ebnesajjad, 2013; Kinloch, 1987).

1.1.6 Igniter

The igniter is the component that initiates the controlled and safe combustion of solid propellant. It is typically located at the front end of the motor and is triggered by a pyrotechnic mixture, an electrical resistance element, or a pressure-activated mechanism. The purpose of the igniter system is to ensure simultaneous and central ignition of the propellant charge across all combustion surfaces. Since a failed ignition can lead to rocket failure or structural damage, igniter systems must have very high reliability. Commonly used pyrotechnic materials include boron-

potassium nitrate ($BKNO_3$) or zirconium-based compounds (NASA SP-8051, 1971).

1.1.7 Nozzle Assembly

The nozzle is a critical component that generates thrust by directing the high-pressure, high-temperature gases formed in the combustion chamber into the external environment at high speed. It typically has a Laval-type converging-diverging geometry and enables the gases to reach the speed of sound (Mach 1) at the throat and supersonic speeds (Mach > 3) at the exit. Because the throat is subjected to extreme thermal and mechanical loads, materials such as graphite, tungsten, carbon-carbon composite, or ceramic materials protected by ablation are typically used (Huzel & Huang, 1992). In some advanced rocket motors, thrust vector control (TVC) systems provide steering capability to the nozzle by providing maneuverability. The exit cone width determines the maximum thrust and specific impulse.

1.2 Importance of Adhesion between Motor Case and Insulation

In rockets used in the defense industry, strong adhesion between the motor case and the insulation material is critical for the integrity and safety of the system. Since rocket cases operate under high temperatures, pressures and mechanical loads, weak adhesion at this interface can lead to serious failures, especially during combustion (Zhou et al., 2015). In areas where adhesion is insufficient, hot gases formed during combustion can leak into the interface, progress under the insulation layer, and directly contact the metal surface (Guo & Zhang, 2015). Exposure of the metal tube surface to high temperatures can result in deformation, oxidation, and structural failures.

Good adhesion between the motor case and the insulation material must also tolerate thermal expansion differences. The case and insulation material expand at different

rates during rocket motor operation; this has been simulated as interface mismatch in cohesive zone models (Zhou et al., 2015). The adhesion strength must be able to absorb these differences. Therefore, adhesives used to optimize adhesion properties must be high-temperature resistant, elastic, and have high adhesion strength.

As a result, good adhesion of insulation materials used in rocket motors in the defense industry to the motor case is a basic requirement for safe, efficient, and long-term operation of the rocket. Achieving this bond strength is made possible by correct adhesive selection, appropriate surface preparation, and optimum bonding parameters (adhesion time, temperature, humidity, surface roughness etc.) These principles are clearly emphasized in the literature (Zhou et al., 2015; Guo & Zhang, 2015).

1.3 Adhesive Bonding

Adhesive bonding is a technique in which two surfaces are joined by adhesive material. An adhesive is any substance that can cause permanent or semi-permanent bonding between surfaces. Adhesives are usually applied in liquid, paste, or film form and develop an enduring bond between the materials after curing or hardening. Most adhesives are polymer-based and their formulation contains base materials like epoxy, polyurethane, or acrylic. The bonding between surfaces is based on different mechanisms, such as chemical bonding, mechanical interlocking, and physical interactions like van der Waals bonds (Kinloch, 1987).

The adhesive bonding process is based on two basic forces: adhesion and cohesion. Adhesion is the ability of the adhesive to adhere to the substrate or surface to which it is applied; this can be achieved by physical forces, such as van der Waals, by chemical bonding, like covalent or hydrogen bonds, or by mechanical interlocking. Cohesion, on the other hand, is defined as the internal strength of the adhesive or its ability to stay intact without breaking (Kinloch, 1987).

A variety of adhesives have been developed based on their chemical composition and applications. Examples include epoxies, which are two-component systems with excellent strength and chemical resistance in structural applications; polyurethanes, which are flexible and offer impact resistance; acrylics, which cure rapidly and offer good adhesion to metals and plastics; cyanoacrylates, which bond rapidly on small areas with good strength; and silicones for high-temperature and high-humidity environments (Ebnesajjad, 2013).

1.3.1 Adhesion Mechanisms

In technical literature, the roles of mechanical interlocking (mechanical adhesion), diffusion, adsorption, surface reactions (chemical bonding), wettability and electrostatic forces in the formation of adhesion between dissimilar material pairs are frequently discussed. However, it is often not possible to attribute adhesive bonding to a single mechanism. In a given adhesive system, adhesion usually occurs through a combination of these mechanisms. The level of contribution of each mechanism varies depending on the system used.

1.3.1.1 Mechanical Interlocking

Although the surface of a material may appear shiny and smooth, at the microscopic level it is filled with countless structural defects such as voids, craters, pits, holes, pores, cracks, scratches, and deep grooves. In addition to the existing defects, the surface is treated to increase its roughness. This intervention can be carried out by mechanical processes like sandblasting or grinding, physical processes like plasma, flame, or corona discharge, or chemical processes such as wet abrasion and dissolution of the components (Wypych, 2018).

Mechanical theory states that adhesion occurs when the adhesive penetrates the pores, voids, and other irregularities of the substrates. During this procedure, the adhesive displaces trapped air at the interface. Therefore, the penetration of the

adhesive into these rough areas causes the two surfaces to interlock. This mechanical interlock between the adhesive and the bonded surfaces contributes significantly to the bond strength. A fundamental assumption of this theory is that adhesives generally adhere better to porous and abraded surfaces than to smooth surfaces (Ebnesajjad, 2013).

However, since good adhesion can also be achieved between smooth surfaces, this theory does not apply in all cases. The increase in adhesive strength after surface abrasion may result from multiple factors, including not only mechanical interlocking but also the formation of a clean surface, the formation of a highly reactive surface, or an increase in the contact surface area. Although mechanical abrasion makes the surface rougher, it is thought that changes in the physical and chemical properties of the surface to be bonded increase the adhesion strength (Wypych, 2018).

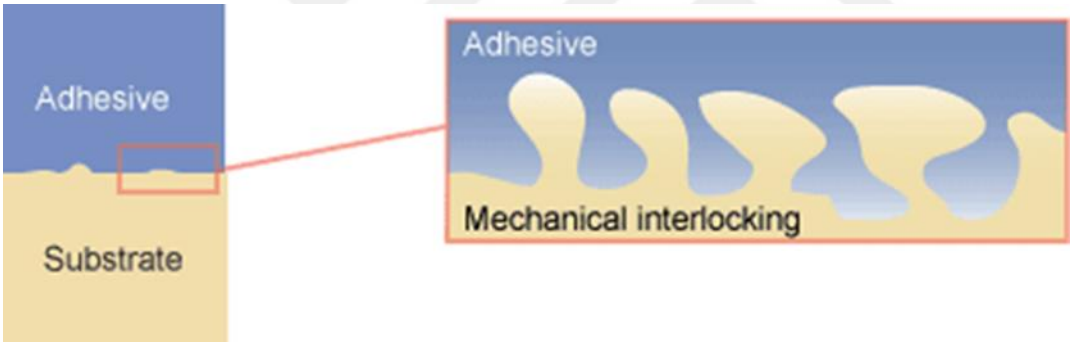


Figure 1.3 Illustration of Mechanical Interlocking Theory (Clearfield et al., 1991)

1.3.1.2 Chemical Bonding

The chemical mechanism attributes the adhesive bond formation directly to chemical forces operating at the surface interface. Consequently, all interactions such as covalent, ionic, and hydrogen bonds between adhesive and adherends, are far stronger than weaker dispersion forces. (Bond / Interaction Types and Approximate Energies are given in Table 1.1.)

Broadly, the bonding and interactions between the molecules include four general types of interactions: covalent bonds, hydrogen bonds, van der Waals forces, and acid-base interactions. The actual chemical composition at the interface determines the specific nature of each type of interaction for any adhesive bond. Covalent and ionic bonds, as included in Table 1.1, are examples of chemical bonding, providing substantially higher bond strength relative to secondary forces. Secondary valence bonds, on the other hand, rely on much weaker physical forces; hydrogen bonds are a common example of such bonds. These latter, weaker bonds are relatively more significant for polar group-containing materials, such as those containing carboxylic acid groups, as opposed to apolar materials like polyolefins. Chemical forces between the adhesive and the bonded surfaces are not necessarily the only interactions; contributions from other adhesion mechanisms can take place, such as mechanical interlocking, diffusion, or electrostatic mechanisms (Ebnesajjad, 2013).

Table 1.1 Bond / Interaction Types and Approximate Energies (Ebnesajjad, 2013)

Bond / Interaction Types	***Example***	***Approximate Energies (kJ/mole)***	***Relative Strength***
Covalent	C–C	150-1000	Strongest
Ion–ion	$Na^+ \cdots Cl^-$	400-4000 (in vacuum) 100-300 (in water)	Very strong
Ion–dipole	$Na^+ \cdots CF_3\ H$	50 -200	Strong
Hydrogen bonding	$H_2\ O \cdots H_2\ O$	10-40	Moderate
Dipole–dipole	$CF_3\ H \cdots CF_3\ H$	5-25	Weak
London dispersion	$CF_4 \cdots CF_4$	0.5-8	Weakest

1.3.1.3 Wetting Theory

This theory proposes that bonding is established through the molecular contact between two materials, resulting in the development of interfacial surface forces.

The initial and most crucial step in bond formation is the creation of these interfacial forces between the adhesive and the substrate. The continuous process of maintaining intimate contact between these two components is termed as wetting.

For an adhesive to effectively wet a solid surface, its surface tension must be lower than the solid surface's critical surface tension. (A Figure 1.4 is used to illustrate the difference between poor and good wetting as an adhesive spread across a surface). Optimal wetting occurs when the adhesive flows easily, penetrating and completely filling the microscopic pits and cavities on the substrate's surface. Conversely, poor wetting happens when the adhesive merely bridges over these surface irregularities. This bridging drastically reduces the actual contact area between the two materials, with the overall bond strength reduced correspondingly. When complete wetting is not possible, defects appear at the interface and seriously weaken the bond strength that results. Therefore, the condition of full wetting is essential for achieving the maximum possible bond strength.

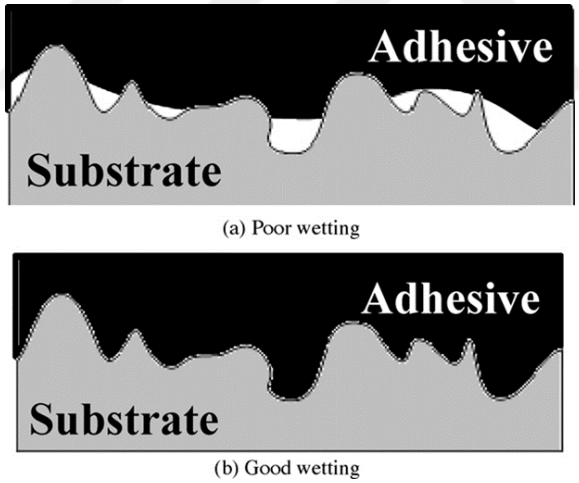


Figure 1.4 a) Poor Wetting b) Good Wetting (Lee et al., 2009)

Most organic adhesives are inherently capable of easily wetting metal surfaces. However, many solid organic substrates possess surface tensions lower than those of commonly employed adhesives. To ensure good wetting, the adhesive's surface tension must be lower than the critical surface tension of the substrate being bonded.

This principle partly accounts for why organic adhesives like epoxy demonstrate excellent adhesion to metals, yet often exhibit poor adhesion to untreated polymer substrates such as polyethylene, polypropylene, and fluoroplastics (Petrie, 2007).

1.3.1.3.1 Surface Energy

Surface energy is a thermodynamic property arising from the higher free energy of atoms or molecules on the surface of a material over their bonded states inside the interior. Solids with high surface energy are thermodynamically more supportive of the formation of new bonds on their surfaces and the spreading (wetting) of liquids onto these surfaces. From the perspective of adhesion science, surface energy is an important parameter for an adhesive to provide adequate wetting of the substrate. Low wetting would reduce the actual area of contact between the adhesive and the surface to result in weak interfacial bonds and poor adhesion performance. (Kinloch, 1987).

The contact angle, θ, represents the spreading behavior of a liquid on a solid surface. It is the angle that the liquid droplet makes with the surface. Young's equation defines it as:

$$\gamma_{SV} = \gamma_{SL} + \gamma_{LV}\cos\theta$$

$\gamma_{SV} = \text{solid} - \text{vapor surface energy}$

$\gamma_{SL} = \text{solid} - \text{liquid surface energy}$

$\gamma_{LV} = \text{liquid surface tension}$

A contact angle less than 90° means that the liquid wets the surface well, offering a larger effective contact area for bond formation. On the other hand, if the contact angle is high (θ > 90°), it indicates low surface energy and limited spread of the adhesive on the surface. This is very typical for low-surface energy elastomers (<25

mN/m) such as EPDM, which represents one of the major reasons for adhesion problems (Ebnesajjad, 2013).

For adhesion to take place, the adhesive must wet the surface completely; that is, the liquid adhesive must come into close molecular contact with the solid surface. Thus, surface energy and contact angle are the two important parameters for assessing the efficacy of substrate surface preparation. The methods generally used for increasing surface energy involve increasing the number of polar functional groups on the surface or altering the roughness. An increase in surface energy by this technique has a corresponding decrease in contact angle, hence better wetting and stronger mechanical-chemical interfacial bonds (Mittal, 2013).

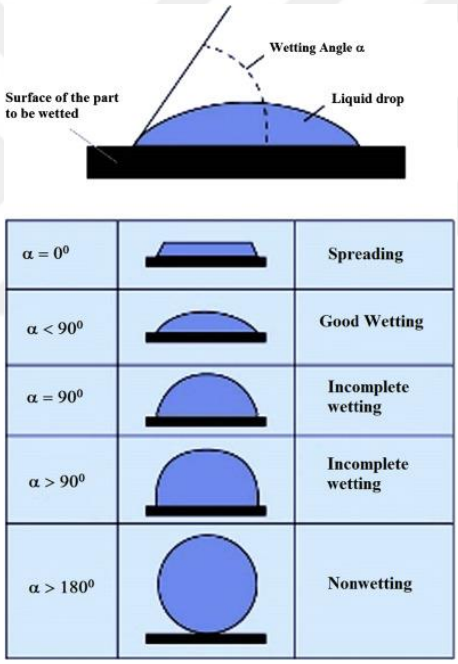


Figure 1.5 Illustration of Wetting Level According to Contact Angle (Giridhar et al., 2017)

1.3.2 Failure Modes

Figure 1.6 shows failure modes in adhesion. When a hypothetical adhesive bond is subjected to a tensile load applied perpendicular to the joint, different failure types

may occur. The surfaces on which failure originates are collectively called the locus of failure (Omairey et al., 2021).

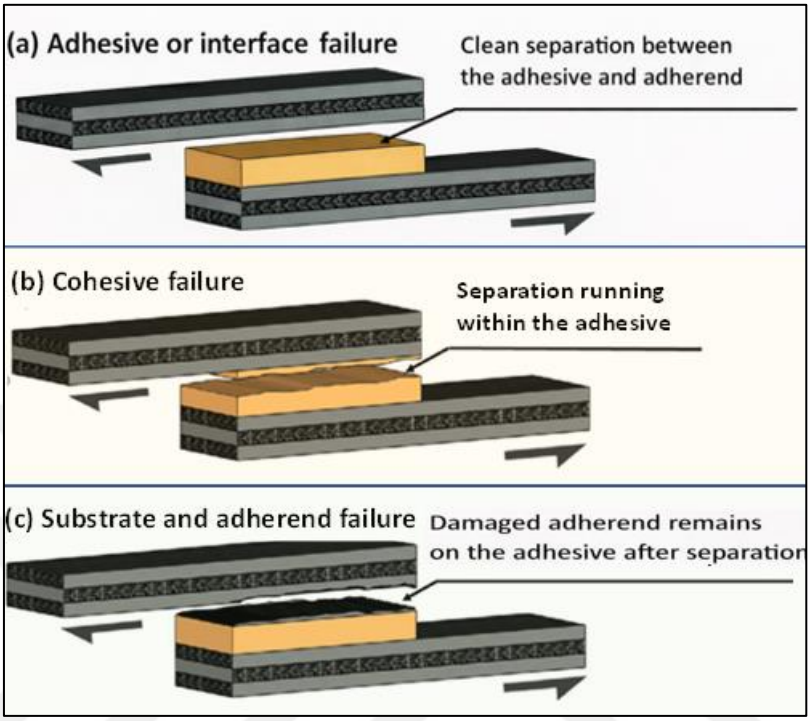


Figure 1.6 Failure Modes in Adhesion (Omairey et al., 2021)

If the separation occurs between the adhesive layer and one of the adherend surfaces, it is called adhesive failure. On the other hand, if the failure occurs completely within the adhesive layer, such that both joined surfaces are still covered with adhesive, it is referred to as cohesive failure. In some instances, the adhesive bond is strong enough that the failure takes place within the bulk of the adherend material itself, away from the adhesive interface. In this case, it is called cohesive failure in the adherend. Substrate failure occurs when failure takes place within the bonded material itself, independently of the adhesive and interface. This failure mode indicates that the mechanical strength of the interface bond and adhesive exceeds the substrate strength, thus demonstrating a high degree of optimization of the bonding system. Mixed failure represents transitional states where both adhesive and cohesive failure zones are observed simultaneously on the same bond surface and

occurs in systems where bond strength is balanced between interface interaction and material cohesive strength (Ebnesajjad, 2013; Baldan, 2012; da Silva et al., 2011).

Cohesive failures, whether they occur within the adhesive or the adherend material are generally the preferred mode of failure, as this implies that the joint has successfully reached the maximum load-bearing capacity of the weakest material within the assembly. Ideally, the failure mode should be %100 cohesive failure within the adhesive layer (Baldan, 2012; da Silva et al., 2011).

The mode of failure should not be used as the only criterion for assessing the usefulness of an adhesive joint. Although some adhesive-substrate combinations may exhibit adhesive failure, they may exhibit higher strength than when the same joint is cohesionally failed with a weaker adhesive. Therefore, the ultimate strength of a joint is a more important evaluation criterion than the mode of failure. Nevertheless, mode of failure analysis can be an extremely useful tool in determining whether failure is due to a weak boundary layer or insufficient surface preparation (Omairey et al., 2021; Spaggiari & Dragoni, 2013).

1.4 Surface Preparation

In adhesive bonding technologies, the nature of the interfacial interactions between the adhesive and the substrate has significant effects on the bonding process. When bonding different types of materials, such as metals and rubbers, it is critical to remove layers that hinder adhesion, such as oxides, oils, and vulcanization residues, often known as the "Weak Boundary Layer" (WBL). These weak layers limit bond strength and cause adhesive failure modes, which often occur between the adhesive and the bonding surface (Baldan 2004). As a result, surface preparation is more than just a preliminary step; it is one of the most important variables influencing bonding success and neglect that leads in joints with low bond strength, discontinuity, and poor resistance to environmental factors. Surface preparation techniques are divided into three categories, with the aim of promoting mechanical

interlocking, increasing surface energy, and the formation of chemical functional groups.

1.4.1 Mechanical Surface Preparation and Measurement Methods

Mechanical methods modify the surface's topography to create macro and micro roughness that allows adhesive penetration. According to mechanical interlocking theory, this method increases actual surface area, hence improving load transfer capacity. These procedures physically remove impurities from the surface, such as oxide layers and mold-releasing agents.

1.4.1.1 Sandpapering

One of the most popular mechanical techniques for rubber and metal surfaces is sandpapering, which produces macro-scale roughness by creating peaks and valleys that enable the adhesive adhere to the surface. This process exposes fresh metal surfaces and increases surface free energy for metals by breaking the passive oxide layer. Sandpapering rubber materials eliminates the oxidized outer layer and blooming products that remain on the surface after vulcanization. The viscosity of the adhesive and the optimal level of roughness are closely associated; too much roughness could result in air gaps by preventing the adhesive from fully wetting the surface (Baldan, 2004).

1.4.1.2 Grit Blasting

The principle behind grit blasting is to use a high-pressure air stream to collide abrasive particles (such as steel balls, silica, or alumina) with the surface. Compared to sandpapering, this technique produces a significantly more uniform and isotropic surface topography for metals. The surface area increases logarithmically, which improves thermodynamic wetting capability. Sandblasting can also locally increase

the mechanical resistance of the surface by creating work hardening on the metal surface. In rubber materials, the sandblasting process is more complex; at room temperature, the elastic structure of the rubber dampens the energy of the impacting particles and makes abrasion more difficult. Therefore, cryogenic sandblasting methods, where the surface is lowered below the glass transition temperature (Tg), or more aggressive particles are often preferred for rubbers. The aim is to create large anchor points for the adhesive by breaking down the amorphous structure on the rubber surface (Critchlow & Brewis, 1996).

1.4.1.3 Texture Transfer via Peel Ply

This method, unique to rubber and composite materials, is a technique integrated into the curing (vulcanization) process. Before the rubber compound is placed into the mold, fabrics made of nylon or polyester with a specific texture, known as peel ply, are placed on its surface. Under pressure and heat, the rubber replicates the texture of this fabric exactly. Once curing is complete, the fabric is peeled off the surface. The biggest advantage of this method is that, unlike sandpapering or sandblasting, it produces a clean, chemically fresh, and patterned surface without creating micro-cracks or thermal degradation in the polymer chains. This textured surface provides an ideal mechanical locking area for the adhesive and minimizes the risk of contamination (Adams & Wake, 1984; Kanerva & Saarela, 2013).

1.4.1.4 Roughness Measurement Methods

Accurate and reliable measurement of surface roughness in bonding processes is crucial for both quality control and the improvement of surface preparation procedures. One of the most commonly used methods for measuring surface roughness is contact profilometers. These devices evaluate surface roughness based on parameters such as Ra and Rz. The measurement process is based on a diamond-tipped probe scanning the surface at a specific speed and force. The most important

advantage of contact profilometers is that they offer fast and repeatable measurements. Thanks to these features, they are widely preferred in various applications due to their ease of use and reliability. However, the contact measurement principle carries the risk of surface damage, especially on soft, thin, and delicate surfaces. In such cases, using alternative measurement methods that do not require direct contact with the surface is a more appropriate approach. In this context, non-contact optical profilometry techniques such as white light interferometry (WLI) and confocal microscopy stand out. These methods allow for the high-precision determination of three-dimensional topographic structures on the surface without physical contact with the surface. For smaller scales, such as when surface roughness needs to be evaluated at the nanometer level, Atomic Force Microscopy (AFM) is used. AFM is a preferred method for examining delicate surfaces such as thin films, polymers, and biomaterials, allowing for the simultaneous evaluation of surface morphology as well as parameters such as surface adhesion properties and hardness (Whitehouse, 2011).

In conclusion, these measurement techniques enable the quantitative evaluation of the effectiveness of surface preparation methods used and contribute to a better understanding of the relationship between surface properties and adhesion performance.

1.4.2 Chemical Surface Preparation Methods

Chemical methods aim to increase polarity by altering the chemical composition of the surface and improve wettability by raising surface energy.

1.4.2.1 Solvent Cleaning

Solvent cleaning is a preparatory step in adhesion. Surface cleaning consists of dissolving and removing oil, grease, and fingerprint contaminants from the surface. Solvents used to clean metals and rubber include acetone, isopropyl alcohol, and

methyl ethyl ketone. Although this procedure does not directly increase mechanical strength, it does give the zero-point cleanliness essential for thermodynamic wetting to occur. Solvent selection is critical for rubber surfaces; fast-evaporating solvents that do not penetrate into the polymer matrix and cause swelling or structural damage should be used. Solvent cleaning is commonly used before (to prevent contaminants from adhering into the surface) and after mechanical procedures (to remove any generated dust) (Packham, 2003).

1.4.2.2 Acid Etching

Acid etching for metals involves the complete dissolution of natural oxides on the surface using sulfuric acid and chromate mixtures, followed by the formation of a stable oxide layer with controlled, microscopic pores. This porous structure allows for nano-level penetration of the adhesive. For rubbers, the most common method is acid-based halogenation (especially chlorination). In this method, using solutions such as trichloroisocyanuric acid (TCI), unsaturated carbon-carbon double bonds (C=C) on the rubber surface are broken and Chlorine (Cl) atoms are added to the structure. Additionally, a sulfuric acid bath (cyclization) prevents cohesion breaks by forming a hard crust on the rubber surface (Romero-Sánchez et al., 2001).

1.4.2.3 Surface Cleanliness Measurement Methods

Cleanliness verification of the metal surfaces is very essential in quality assurance before bonding. Several physical and chemical test methods are available for measuring cleanliness.

The contact angle measurement is a common method to determine wettability of the surface and hence its suitability for bonding. In this technique, a controlled drop of liquid (usually water) is placed on the metal surface and angle of contact of liquid with surface is measured. Low contact angle indicates high surface energy and good cleanliness of the surface (Owens & Wendt, 1969).

Fluorescence-based contaminant measurement instruments such as SITA Cleanospector provide fast and non-contact evaluation. This device detects organic contaminants on the surface under UV lighting and makes quantitative evaluation of the surface cleanliness. SITA Cleanospector detects hydrocarbon-based oils, greases, process oils, protective film residues, and other organic contaminants on surfaces (SITA Messtechnik GmbH, 2021).

Surface analysis techniques such as XPS (X-ray Photoelectron Spectroscopy) and SEM-EDX (Scanning Electron Microscopy with Energy Dispersive X-Ray Spectroscopy) can determine the elemental composition of the surface and show residual contaminants at the atomic level. Both surface techniques are so sensitive that they can detect carbon deposits or silicate traces on the surface easily (Briggs & Grant, 2003).

1.4.3 Physicochemical Surface Preparation Methods

Physicochemical methods encompass high-tech processes that alter the molecular structure of a surface without producing chemical waste.

1.4.3.1 Plasma Treatment

Plasma is a state of high-energy excitement of atoms, ions, and electrons in the gas phase. Plasma treatment (usually argon or oxygen plasma) on metal surfaces provides an ultra-clean surface by breaking down organic contaminants on the surface through atomic bombardment. The interaction of plasma with the rubber surface is a more complex phenomenon. The polymer chains on the rubber surface are broken by the plasma, resulting in free radicals on the surface. These free radicals react with the oxygen or nitrogen present on the surface, resulting in the formation of hydroxyl, carbonyl, and carboxyl functional groups on the surface. This process maximizes the surface energy, thereby maximizing the potential for chemical interaction between the adhesive and the rubber by altering the surface properties of

the rubber, i.e., the top few nanometers, while the properties of the bulk rubber remain unaffected. These functional groups on the surface of the rubber have the potential to create covalent bonds, thereby enhancing the weak boundary layer by increasing the density of cross-linking on the surface of the rubber (Hegemann et al., 2003; Friedrich, 2012).

1.5 Aim and Motivation of The Study

Elastomer-metal bonding systems play a critical role in applications requiring high reliability, such as solid propellant rocket motors used in the defense industry. These systems operate under challenging conditions throughout their service life, including high mechanical loads, thermal cycling, vibration, and environmental influences. Therefore, maintaining the long-term mechanical integrity of the adhesive bond formed between the elastomer and metal components is critical for system safety and structural continuity. EPDM rubber, commonly used in rocket engine insulation systems, is preferred due to its elastic properties and environmental resistance. However, its low surface energy and chemically inert structure present significant challenges in forming a strong and repeatable bond with adhesives. This can lead to interface-related weaknesses and a risk of premature failure during service in EPDM-metal bonding systems.

A large part of the literature on metal-rubber bonding focuses on vulcanization-based or primer-based bonding methods. In contrast, the quantitative effects of surface preparation parameters on bond behavior in adhesive-based EPDM-metal bonding systems have been addressed in a limited number of studies. The role of metal surface cleanliness on bond strength has often been considered a secondary parameter in most studies or has not been systematically investigated. Furthermore, the specific interfaces that limit bond strength in elastomer-metal bonding systems and the relative effects of surface preparation processes on these interfaces have not been clearly and comprehensively established in the literature.

The aim of this study is to systematically and quantitatively investigate the critical interfaces and surface preparation parameters that determine the bond behavior in EPDM-metal adhesion systems. In this context, metal-adhesive and EPDM-adhesive interfaces were considered separately; the effect of each interface on bond strength was isolated and evaluated comparatively. The effect of metal surface roughness and surface cleanliness parameters on the metal-adhesive interface was investigated using a metal-metal bonding configuration, while the bond behavior at the EPDM-adhesive interface was improved by mechanical roughening methods and atmospheric plasma applications. The obtained bond performance was evaluated by tensile and shear tests; the bonding mechanisms were clarified through damage type analyses and microstructural observations.

In conclusion, this study presents an interface-oriented and reproducible surface preparation approach applicable in engineering applications and contributes to the mechanical reliability of EPDM-metal sealing and insulation systems used in the defense industry.

CHAPTER 2

LITERATURE REVIEW

2.1 The Effect of Surface Roughness of Materials on Adhesion Strength

In the study by Ghumatkar et al., the effects of different roughness levels of aluminum AA6063 and mild steel AISI 1045 surfaces on the shear strength of single strap joints created with epoxy-based Araldite® 2015 adhesive were examined in detail. In the research, the roughness of the specimens' surface was generated by means of mechanical abrading with the use of P50, P80, and P120 grit sandpaper. The average roughness values (Ra), which varied from 1.55 µm (unsanded specimens) to 3.46 µm (P50 grit specimens), with variations in aluminum from 1.63 µm to 3.24 µm for the steel specimens, were used. Wettability tests showed that with increasing surface roughness, the contact angle increased from 88° to 112° (for aluminum) and from 85° to 107° (for steel), thereby reducing wettability. Shear tests showed that the maximum bond strength in aluminum was achieved at Ra ≈ 2.05 µm (P120), increasing strength by 40% from 3.54 N/mm² to 4.97 N/mm². Similarly, in steel samples, the optimum strength was achieved at Ra ≈ 1.98 µm (P120), and the strength increased by 60% from 4.24 N/mm² to 6.78 N/mm². At higher roughness levels (P80–P50), the strength tended to decrease (Ghumatkar et al., 2016).

Table 2.1 Shear Strength with respect to Surface Roughness Value of Aluminum Adherends Joints (Ghumatkar et al., 2016)

Surface treatment	Roughness, R_a (µm)	Shear strength (N/mm^2)	Increase in shear strength
Non abraded	1.55± 0.15	3.54	
Abraded by P120	2.05± 0.19	4.97	40.39
Abraded by P80	2.92±0.20	3.95	11.58
Abraded by P50	3.46±0.17	3.70	4.52

Table 2.2 Shear Strength with respect to Surface Roughness Value of Mild Steel Adherends Joints (Ghumatkar et al., 2016)

Surface treatment	Roughness, R_a (µm)	Shear strength (N/mm^2)	Increase in shear strength
Non abraded	1.63± 0.12	4.24	
Abraded by P120	1.98± 0.10	6.78	59.90
Abraded by P80	2.60±0.16	6.15	45.04
Abraded by P50	3.24±0.19	6.03	42.21

In all samples, the failure mode was predominantly of the adhesive–adherend interface type. The authors emphasize that changes in bond strength cannot be explained solely by mechanical interlocking or increased surface area; roughness, surface energy, wettability, and chemical bond character must be evaluated together. As a result, it was stated that maximum adhesion strength for both aluminum and steel is achieved at medium levels of roughness (Ra ≈ 2 µm), while excessive roughness reduces adhesion quality (Ghumatkar et al., 2016).

In the study by Khan et al., the effects of surface roughness and oxidation on adhesion strength were studied in detail with experiments involving the AA6061 and AA7075 aluminum alloys and AISI 1080 steel. Two types of epoxy adhesives were used in the study: A1 (polyamideepoxy) and A2 (epichlorohydrin-epoxy). The surface roughness was investigated by using 60, 120, 240, and 320 grit SiC abrasives, and measurements were made by using an optical interferometer. The specimens were then heat-treated at 100, 200, and 300 °C for 1 hour before bonding to investigate the effects of oxidation. All tests were conducted on single-lap specimens in compliance with ASTM D1002 standard. Results showed that shear strength increased with increasing roughness value up to a certain value, beyond which the strength decreased when an optimal roughness value is reached. For adhesive A1, this maximum strength was determined at Ra = 0.83 µm (240 grit) for aluminum and Ra = 0.62 µm for steel. Beyond a further increase in roughness values, for instance

Ra > 1 μm, a significantly reduced strength could be developed. In the case of adhesive A2, again, the optimal roughness was found at 0.83 μm for aluminum, whereas for steel, this was at 0.47 μm (320 grit). Thus, each alloy and adhesive has an optimal roughness value. In general, the steel specimens resulted in higher shear strength compared to those of aluminum; for instance, for A1, the strength of steel was roughly double that of aluminum. In conclusion, the authors noted that the optimal surface roughness value depends on the type of material as well as the applied adhesive type (Khan et al., 2016).

Uehara and Sakurai systematically investigated the relationship between surface roughness and bond strength under tensile, shear, and peel loading using five adhesives with different chemical structures (epoxy, cyanoacrylate, synthetic rubber, vinyl chloride, and cellulosic). They demonstrated that a "strength increases with roughness" approach is not valid. The study identified a distinct "optimum roughness range" for all adhesives in terms of tensile strength, reporting that maximum bond strength was achieved in the range of Ra ≈ 3–6 μm. Furthermore, the observation of a second strength increases at low roughness levels (Ra < 2 μm) in some systems revealed that film thickness and micro-anchoring effects, along with increased surface area, are also critical. In contrast, no significant correlation was found between roughness and peel strength, while the shear strength trend remained between tensile and peel behaviors in terms of magnitude and slope. The authors explain these different curves with three main effects: (i) theoretical strength depending on film thickness according to adhesion theory (change in effective thickness and stress state as roughness increases), (ii) the positive contribution of the actual contact area increasing with roughness, and (iii) the negative contribution resulting from the notch effect and stress concentration created by increasing roughness. Therefore, this study supports the concept of optimum surface roughness in the literature with a theoretical framework, emphasizing that a single "more roughness, the better" rule does not apply in adhesive-surface systems, and that the optimum roughness value varies depending on both the type of loading

(tensile/peel/shear) and the mechanical/viscoelastic properties of the adhesive (Uehara and Sakurai, 2002).

Sługocka et al. researched the effect of surface topography created by different abrasive processing parameters on the shear strength of single lap joints formed with epoxy adhesive on the surface of S355 low carbon steel. Samples were subjected to mechanical surface preparation (abrasive blasting) using $Al_2 O_3$ abrasive under varying pressure and distance conditions; surface characterization was evaluated using 2D roughness parameters such as Ra and Rz, as well as 3D topographic parameters such as Sa, Sz, and Sdr. SikaFast-555Lx acrylic adhesive was used as the adhesive, and the joints were loaded according to ASTM standards with single-lap shear (SLS) testing. The resulting surface roughness varied between 1.00 and 2.50 μm in terms of Ra; it was reported that the strength showed a nonlinear relationship with roughness. In this study, the highest shear strength was obtained at a surface with Ra ≈ 1.10 μm, reaching 23.6 MPa; as Ra increased to 1.50 μm, the strength decreased to 14.2 MPa, but it increased again to 19.3 MPa at a coarser surface with Ra ≈ 2.50 μm. The researchers emphasized that optimum adhesion is not only dependent on Ra, but is shaped by multiple parameters such as micro-anchoring capacity, peak-valley ratios, surface heterogeneity, and wettability of the surface; therefore, the "more roughness = higher strength" approach is not valid. In conclusion, this study showed that controlled application of mechanical surface preparation maximizes adhesion strength on surfaces with moderate roughness (≈1.0–1.5 μm) and regular micro-topography (Sługocka et al., 2024).

Spaggiari and Dragoni utilized a comprehensive experimental design to investigate the effect of various mechanical surface preparation processes—namely, the as-received condition, P20 SiC sandpapering, alumina sandblasting, and knurling—applied to AISI 1010 steel and 2011-T3 aluminum substrates on the strength of single- and double-lap adhesively bonded joints. Table 2.3 shows the surface

roughness of steel and aluminum which was obtained with different mechanical treatment techniques (Spaggiari and Dragoni, 2013).

Table 2.3 Experimental Surface Roughness Ra and Rz Depending on the Mechanical Treatment (Spaggiari and Dragoni, 2013).

		Steel	Aluminum	Steel	Aluminum
Level	Joint treatment	Ra (μm)		Rz (μm)	
↓↓	As-received	0.81 ± 0.07	0.24 ± 0.02	6.025 ± 0.79	3.17 ± 0.95
↓	Sandblasting	1.95 ± 0.11	2.42 ± 0.04	14.385 ± 1.84	13.525 ± 1.19
↑	Sandpaper	1.99 ± 0.25	4.56 ± 0.19	14.24 ± 1.32	21.595 ± 1.44
↑↑	Knurling	3.85 ± 0.15	9.45 ± 0.11	26.55 ± 1.15	64.16 ± 1.96

The average shear strength values obtained from joints bonded with epoxy (Hysol 9466) and acrylic (Multibond 330) adhesives were highly dependent on surface roughness. For single-lap steel-epoxy joints, the average shear strength was reported to be 21.0 MPa for as-received surfaces, increasing to 23.8 MPa after sandblasting and 28.0 MPa after sandpapering, while decreasing to 17.8 MPa for knurled surfaces. Similarly, in aluminum-epoxy single-lap joints, shear strength improved from 5.7 MPa for as-received surfaces to 12.7 MPa for sandblasted surfaces, and 18.1 MPa for sandpapered surfaces (Spaggiari and Dragoni, 2013).

The results demonstrated that adhesive joint strength depends not only on the magnitude of surface roughness but also on the presence of a homogeneous micro-topography distributed over the entire bonding surface. Although the knurling process produced the highest Ra values (3.85 μm for steel and 9.45 μm for aluminum) the corresponding joint strengths remained relatively low. This behavior was attributed to excessively coarse surface features that promote local void formation and crack initiation, leading to stress concentration at the adhesive–substrate interface. Overall, the study concluded that sandpapering and sandblasting provide the highest joint strengths for both steel and aluminum substrates, with an optimum surface roughness range of approximately Ra ≈ 1.9–2.5 μm, within which cohesive failure was observed in the majority of the tested samples (Spaggiari and Dragoni, 2013).

In the study by Hamdi et al., the effects of mechanical (2–6 bar grit blasting, Scotch-Brite), chemical (methanol solvent cleaning, primer coating) and energetic (UV/ozone – 3 and 10 min, atmospheric plasma) treatments applied to EPDM, PVC and ABS surfaces on the adhesion strength obtained with three different adhesives (silicone, polyurethane and silane-modified – MS) were quantitatively compared. The study shows that EPDM is the least optimized system due to its low surface energy and chemical stability: for example, although surface roughness Rq ≈ 4.1 µm to 5.6 µm is increased by grit blasting, the T-peel strength achieved with silicone-based adhesives in EPDM is significantly reduced, while only limited increases, which can be classified as insignificant slight (approximately in the range of 0.5–5 times), are reported with polyurethane (Ad-PU) and MS-based adhesives; moreover, the failure mode persistently remains adhesive under all these conditions. In contrast, in PVC, particularly after 2 bar grit blasting with silicone-based adhesive, the T-peel strength increased approximately 19-fold, from 0.34 kPa to 6.47 kPa. High-pressure grit blasting (6 bar), priming, and UV/ozone treatments resulted in significant, and in some cases highly significant (>20-fold) improvements, with the failure mode shifting from adhesive to mixed/cohesive. In ABS, both mechanical roughening and active treatments such as priming and UV/ozone resulted in increases of up to 5-10 times in lap-shear strength and predominantly cohesive failure. SEM observations after UV/ozone treatment showed a significant increase in mechanical interlocking with a micro-porous structure of ≈0.1 µm diameter. The authors suggest that, specifically for EPDM, significant improvement cannot be achieved with a single process and therefore propose exposing the fresh surface layer with high-pressure grit blasting and applying it in combination with UV/ozone or a suitable primer as a possible optimization method. For PVC and ABS, they emphasize that combinations of UV/ozone + high-pressure grit blasting / Scotch-Brite are the most effective strategy for converting adhesive failure to cohesive failure. Thus, the study reveals that adhesion on polymer surfaces should be optimized not only by roughness level but also by surface chemistry activation, micromorphology (micro-pits, pores, wrinkled structure), and the chemistry of the chosen adhesive, and that "optimum

surface preparation" in elastomers like EPDM has a very limited improvement window (Hamdi et al.,2020).

In the research by Bakkal et al., the effect of roughness obtained by different surface preparation methods on the interfacial strength of epoxy hybrid joints bonded with PA66 composite (Hysol EA 9394) of Al 2024-T6, AISI 304 and Ti-6Al-4V metals were systematically investigated. In the study, sandblasting, sandblasting and sandblasting+laser treatments were applied to the metal surfaces, and as a result of these treatments, the roughness values ranged from Ra ≈ 1 μm to 15 μm. The experimental results showed that the bond strength remained limited at low roughness levels, only ≈2 MPa shear strength was obtained for Ra ≈ 1 μm on the Al 2024 surface; increasing the roughness to Ra ≈ 9 μm increased the strength to ≈8 MPa; The study shows that the strength increases to approximately 15 MPa when Ra ≈ 15 μm with sandblasting + laser. Similarly, on AISI 304 surfaces, the strength is around 2 MPa at low roughness, while it reaches the order of 9–10 MPa with high roughness. On Ti-6Al-4V surfaces, after sanding, the strength is limited to around ≈2.7 MPa due to Ra < 1 μm, but at high roughness values such as Ra = 13.4 μm, the strength increases to ≈7.5 MPa. Surface morphology and wettability values were evaluated, and it was noted that the contact angle is not always inversely proportional to roughness; in particular, the contact angle increased despite the increase in roughness on sandblasted surfaces, indicating that different mechanical abrasion mechanisms have a strong effect on wettability. Failure analyses showed that excessive roughening of the metal surface significantly increased mechanical interlocking at the interface, shifting failure from the metal/adhesive interface to the composite side. Overall, the study concludes that high adhesion strength in metal-composite hybrid joints can be achieved not only by chemical cleaning but also by optimizing the combined effect of controlled increase in surface roughness, surface energy, and micro-anchoring; and that the highest performance is achieved with combined surface preparations such as sandblasting + laser (Bakkal et al., 2022).

2.2 Effect of Surface Contamination of Materials on Adhesion Strength

In the study by Kostyuk et al., the effects of surface oil contamination on adhesion strength and long-term durability at the interface of stainless steel–PIB (polyisobutylene) pressure-sensitive adhesive (PSA) were investigated. In the study, steel surfaces were contaminated with sunflower oil and naphthenic mineral oil, and then the 90° peel and static shear strengths were compared on clean and contaminated surfaces. According to the findings, contamination with sunflower oil reduced the peel strength in fresh samples by approximately 10 times compared to the clean surface (initial strength of the surface contaminated with sunflower oil ~1–2 N/cm, clean surface ~10–12 N/cm), while naphthenic oil reduced the strength by approximately half (~5–6 N/cm). However, as the oils were absorbed by the PIB over time, the strengths increased again; in the naphthenic oil sample, the adhesion approached the clean surface level after only 30 minutes, while in the sunflower oil sample, this recovery took approximately 24 hours. In static shear tests, sunflower oil initially reduced the strength by an order of magnitude (~100–200 min), while naphthenic oil showed almost no adverse effect (~10^4 min). The study also showed that the contamination effect is directly related to viscoelastic behavior, with sunflower oil forming a weak, plasticized layer near the surface because it is only 7–10% volume soluble in PIB; however, naphthenic oil, being completely miscible with PIB, diffuses faster and the weak layer disappears quickly. Furthermore, it was reported that nanoclay-filled PSAs offered higher strength on both clean and contaminated surfaces, and especially on surfaces contaminated with sunflower oil, the strength exceeded even the clean surface value after 20 minutes (~15 N/cm). These results show that surface cleanliness is critical in PSA-metal bonding, especially in cases of contamination with polar vegetable oils, while in mineral oil contamination, effective adhesion can be quickly restored depending on the adhesive's ability to absorb the contaminant (Kostyuk et al., 2019).

Moreira et al. investigated the effect of surfactant contamination (0, 10, and 20 sprays) on the peel strength of silicone-based adhesives on Al 6082-T6 aluminum surfaces and showed that bond strength decreased significantly as contamination increased. According to the failure toughness values obtained from peel tests, on the uncontaminated surface, G ≈ 3.0–3.2 N/mm and failure occurred entirely cohesionally (Figure 2.1). When the surface was contaminated with 10 sprays, the failure mode became mixed and the failure toughness decreased to ≈2.0–2.3 N/mm. (Figure 2.2) In the most severe contamination condition, 20 sprays, failure became almost entirely adhesive/interfacial and the failure toughness decreased to approximately half of the initial value, i.e., ≈1.4–1.5 N/mm (Figure 2.3). The authors emphasized that the surfactant film layer prevents the adhesive from wetting the surface and chemical bonding, creating a weak interface layer; therefore, on contaminated surfaces, not only is the strength reduced, but failure shifts entirely to the interface. Overall, the study shows that even small deteriorations in surface cleanliness in aluminum-adhesive bonds can result in up to 50% strength loss and a transition to adhesive failure (Moreira et al., 2022).



Figure 2.1 Uncontaminated Peel Test (Cohesive Failure) (Moreira et al., 2022)



Figure 2.2 Peel Test with 10 Sprays (Mixed Failure) (Moreira et al., 2022)



Figure 2.3 Peel Test with 10 sprays (Mixed Failure) (Moreira et al., 2022)

In their study, Zhao et al. researched the effect of surface cleaning on the final mechanical performance of 316H stainless steels joined by additive forging and showed that the level of cleanliness directly determined the bond strength. In cleaned samples(T1), the water contact angle was ≈58–65° and the cleanliness indicator RFU value was ≈2–3 RFU, while in uncleaned samples(T2), the contact angle increased to ≈69–81° and the RFU to ≈9–29 RFU; this indicates that oil/particle contamination significantly lowers the energy of the surface. In mechanical tests, cleaned samples(T1) exhibited a yield-tensile strength of 435–439 MPa and an elongation of 52–54%, while in uncleaned samples(T2), the strength decreased to 420–426 MPa and the elongation to 48% (Zhao et al., 2021).

Table 2.4 Stress-Strain Values of Tensile Specimens (T1→Cleaned Surface, T2 →Uncleaned Surface) (Zhao et al., 2021)

	T1-1	T1-2	T1-3	T2-1	T2-2	T2-3
Stress (MPa)	434.76	435.83	439.45	419.68	425.82	419.22
Strain	0.5444	0.5434	0.5173	0.4796	0.4830	0.4799

This approximately 10–15 MPa strength loss and 7–10% ductility reduction resulted from the formation of discontinuous, weak bonding zones at high temperatures by the residual oil film, chips, and particles at the interface; microscopic examinations showed a continuous interface line and inclusions 8–30 μm deep on contaminated surfaces, while the interface was largely or completely disappeared on clean surfaces (Zhao et al., 2021).

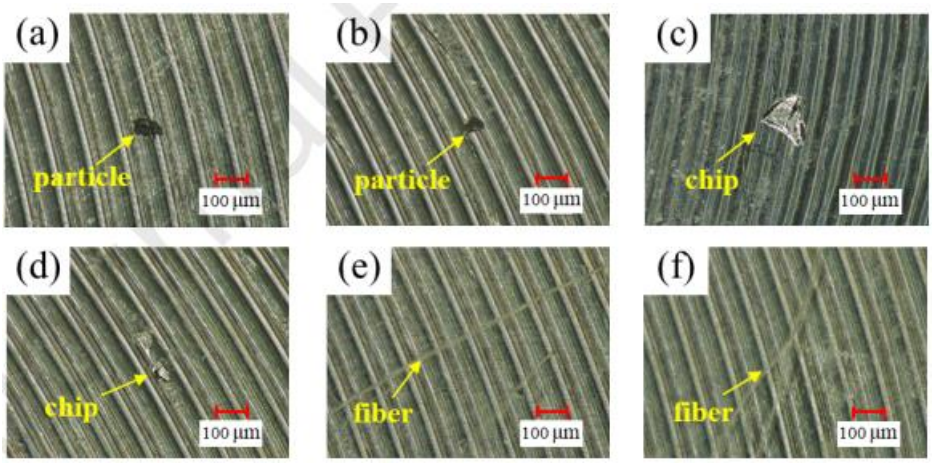


Figure 2.4 Microscopic Morphology of Uncleaned Surfaces, (a)(b) particles, (c)(d) chips, (e)(f) fibers (Zhao et al., 2021)

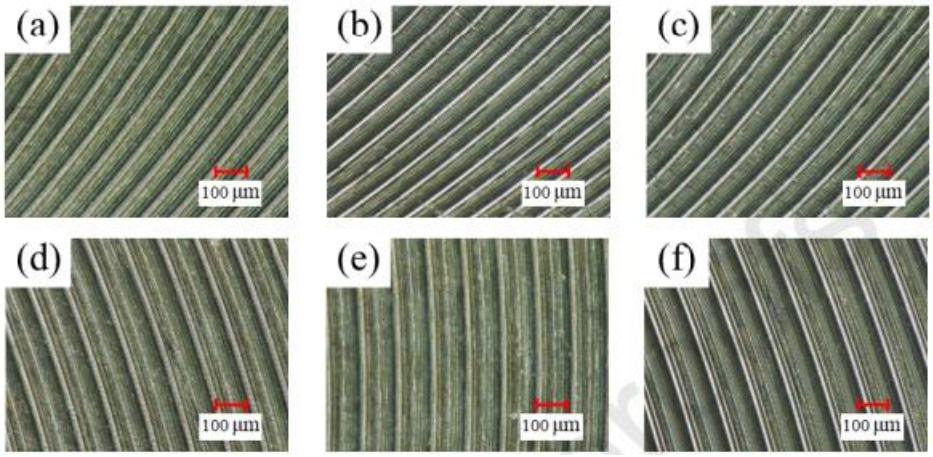


Figure 2.5 Microscopic Morphology of Cleaned Substrate Surfaces (Zhao et al., 2021)

Overall, the study demonstrates that when surface cleanliness is not ensured, atomic contact and grain boundary coupling are prevented during forging, leading to a measurable and critical reduction in ultimate mechanical performance.

2.3 Effect of Surface Activation of Materials on Adhesion Strength

Moraes et al. investigated the effect of N_2 /Ar and N_2 /H_2 /Ar RF plasma treatments on the surface properties and adhesion strength of EPDM rubber, which can be used as a thermal protection material in solid propellant rocket motors, to improve its poor adhesion behavior due to its low surface energy. After plasma treatment, a reduction of approximately 70% in the water contact angle of the EPDM surface was observed; XPS analyses revealed the formation of polar functional groups (C–O, C=O, C–N) containing approximately 25% oxygen and 6% nitrogen on the surface (Moraes et al., 2007).

Table 2.5 Element Content in Atomic Percent of the Untreated and Plasma Treated NBR and EPDM Rubbers (Moraes et al., 2007)

Element content (%)	Untreated NBR	Untreated EPDM	EPDM N_2/Ar plasma treated	EPDM N_2/H_2/Ar plasma treated
C1s	88.4	91.1	69.2	67.6
O1s	8.2	8.9	25.6	25.8
N1s	3.4	—	5.2	6.6

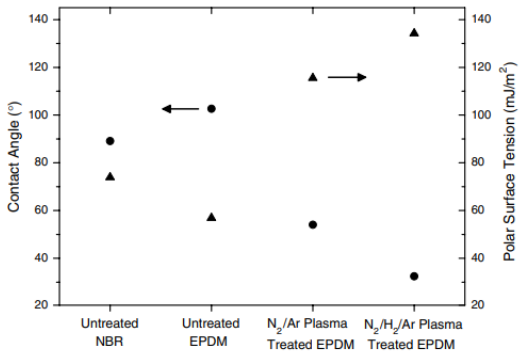


Figure 2.6 Contact Angle and Polar Surface Tension (mJ/m^2) of Untreated NBR and EPDM Rubber and Plasma Treated EPDM Rubber (Moraes et al., 2007)

AFM measurements showed that the RMS surface roughness, which was 113 nm before plasma treatment, decreased to ≈76–77 nm after plasma treatment, indicating

that the increase in adhesion was mainly due to chemical surface activation. In mechanical tests, it was reported that the adhesion strength at the EPDM–polyurethane liner interface increased by approximately 30% with plasma application, reaching levels comparable to untreated NBR–liner systems. A more significant improvement was observed at the EPDM–epoxy interface; the adhesion strength on plasma-treated EPDM surfaces increased by more than 110%, approximately twofold, compared to untreated EPDM–epoxy bonds. The study demonstrates that the polar chemical groups and increased surface energy created by plasma on the EPDM surface significantly improve the bond strength, especially with epoxy-based adhesives, and that EPDM, with appropriate surface treatments, can be used as an alternative rocket motor insulation material to NBR (Moraes et al., 2007).

In the study by Kovács et al., the effect of different surface preparations and plasma activation on the tensile strength of 90MnCrV8 tool steel bonded with high-strength epoxy adhesive (Loctite EA9514) was investigated through three surface conditions: only lathe-turned and alcohol-cleaned surface (A), lathe-turned + sandblasted with quartz grains + alcohol-cleaned surface (B), and lathe-turned + sandblasted + alcohol-cleaned surface followed by atmospheric pressure cold plasma activation surface (C). The optimal curing regime was determined to be 90 min–165 °C for all samples; under this condition, the average tensile strength of the A-type surface was only 21.17 MPa, while the strength of the B-type surface after sandblasting increased to 56.16 MPa, and the C-type surface, which also underwent plasma activation, increased to 67.63 MPa. Interestingly, the roughness of the turned surface decreased from Ra = 3.0 μm to Ra = 2.2 μm with sandblasting, and to Ra = 2.1 μm with sandblasting + plasma treatment; thus, the highest strength was obtained not on the roughest surface, but on the more homogeneous and finer micro structured surface. Wettability and surface energy results support this picture: the water contact angle was 73.1° and the total surface energy was 31.9 mN/m on the turned surface, while these values were 47.6° and 53.3 mN/m on the sandblasted surface, respectively; and

in the sandblasting + plasma treatment, the water contact angle increased to 7.4°, the ethylene glycol contact angle to 0°, and the total surface energy to 86.6 mN/m. EDX analyses showed that the carbon content on the C-type surface decreased from 44–45% to 24.85%, while the oxygen content increased to 75.15%; The increased O content and the change in the C/O ratio revealed that plasma treatment enriched the surface with oxygenated functional groups, creating a higher surface energy and hydrophilic character for adhesion. The authors emphasize that the combination of more homogeneous micro-roughness obtained by sandblasting and high surface energy + oxygenated surface chemistry provided by plasma treatment increased the tensile strength by approximately three times to 67.63 MPa compared to the turned condition, and that optimizing surface roughness, wettability, and surface chemistry together is critical in steel-epoxy bonded joints (Kovács et al., 2023).

Santos et al. systematically examined the effect of Ar and N_2 microwave plasmas on EPDM–PU bond strength, demonstrating that the adhesion performance of vulcanized EPDM surfaces is directly related to surface cleaning and surface activation. The high contact angles of untreated EPDM surfaces revealed low surface energy and limited adhesive wetting; the contact angle was measured as 122.4° for Nordel IP 3430 and 117.9° for Nordel IP 4520. Following 300 s Ar plasma treatment, the contact angle was reduced to 52.2° for IP 3430 and 44.5° for IP 4520, indicating a substantial increase in surface wettability. As a result of this treatment, the surface energy increased by approximately threefold; for instance, the surface energy of IP 3430 increased from 33.8 mN/m to 117.4 mN/m. This surface activation was directly reflected in T-peel tests. Peel strengths of only 0.07–0.09 N/mm² in untreated EPDM/PU joints increased to 0.18 N/mm² for IP 3430 and 0.28 N/mm² for IP 4520 after Ar/300 s treatment, and bond strength increased by over 100% and 300%, respectively. The authors stated that the improvement was due to both the increased chemical bonding of polar oxygen groups such as C–O, C=O, and O–C=O formed by plasma on the surface and the improvement of adhesive wettability by slight surface roughening; they warned that excessive duration or aggressive plasma

conditions could lead to surface degradation in EPDM, reducing this gain. The study clearly demonstrates that surface cleaning and plasma activation are critical processes that can increase adhesion strength several-fold in low surface energy elastomers such as EPDM (Santos et al., 2013).

Grythe and Hansen investigated the surface modification of pure and filler-free EPDM films prepared by solution casting technique with Ar, N_2 , and O_2 plasmas to overcome adhesion problems caused by the low surface energy of EPDM rubber used as insulation in solid rocket motors. Initially, it was shown that the EPDM surface is completely nonpolar and has a very low surface energy (total surface energy ≈24–25 mN/m; polar component ≈0 mN/m), and therefore sufficient thermodynamic adhesion could not be achieved with propellant and primer systems. It was emphasized that even with very short plasma times, the water contact angle decreased rapidly and the total surface energy increased to approximately 60–70 mN/m; According to multi-liquid analysis, after 2 minutes of O_2 plasma treatment, the dispersive component remained constant at approximately ≈23 mN/m, while the polar component increased to ≈35 mN/m, meaning that the thermodynamic adhesion energy, considered "proportional to strength," increased by more than twofold. XPS analyses showed that oxygen could be easily introduced into the post-plasma surface layer, up to 20% atomic oxygen; that the oxygen was predominantly in the form of hydroxyl groups (COH), with smaller proportions of carbonyl (C=O) and carboxyl (COOH) groups; and that these polar functional groups significantly strengthened the initially very weak acid-base interactions of EPDM. In the roughness analysis performed with AFM, it was shown that the RMS roughness of the EPDM surface, which was very smooth before plasma treatment, was approximately 0.26 nm, but increased to the range of 0.3–0.7 nm with short treatment times, and to ≈2.0 nm after 6 minutes of treatment in O_2 plasma; however, it was shown that in very long treatment times (≥4–6 min), the contact angle measurements became unstable due to increasing roughness and chemical heterogeneity, and the gain in surface energy could be partially lost. Although the authors did not directly measure tensile/peel strength, they state that increasing the surface energy of EPDM from ≈25 mN/m to

≈60–70 mN/m and the polar component from ≈0 to ≈35 mN/m significantly increases the adhesion strength achievable with metal/propellant/liner systems within the framework of the Fowkes approach. Therefore, short-duration (0.5–2 min) plasma treatments offer an effective surface preparation strategy for improving adhesion at EPDM–metal and EPDM–propellant interfaces (Grythe and Hansen, 2006).

CHAPTER 3

EXPERIMENTAL WORK

This experimental study was conducted in four main stages following a step-by-step approach. In the first stage, metal surfaces were prepared at different surface roughness and cleanliness levels and bonded to EPDM rubber surfaces using two different structural adhesives. The adhesion performance of the resulting rubber-metal bonds was evaluated using tensile and shear tests. However, it was observed that the types of failure observed in this stage mainly occurred within the rubber or at the rubber-adhesive interface, and the metal-adhesive interface did not emerge as a limiting factor in bond strength.

Based on this observation, the second stage aimed to isolate the effect of metal surface properties on adhesion performance. In this context, only metal-metal test specimens were prepared using the same surface roughness and cleanliness variables, and shear tests were performed for both adhesives. This approach allowed the determination of the surface roughness and cleanliness range that provides the highest adhesion strength at the metal-adhesive interface.

In the third stage, the studies focused on improving the rubber-adhesive interface. Different surface preparation methods, such as roughening with sandpapering and peel ply, were applied to the EPDM surfaces; Tensile and shear tests were then performed. The surface roughening method that provided the highest bond strength was selected for further studies.

In the final stage, surface activation was achieved by applying plasma treatment to the EPDM surfaces for different durations after the selected roughening method. The plasma application time was evaluated in line with the results obtained from the tensile and shear tests, and the optimum time that provided the highest bond strength was determined.

3.1 Materials

3.1.1 AISI 4140 Steel

In this study, AISI 4140 steel was chosen because it represents the metal substrates used in solid propellant rocket motors and allows for the investigation of rubber-metal bonding systems under realistic industrial conditions. AISI 4140 steel is a medium-carbon alloy structural steel that is frequently employed in defense and aerospace applications because of its excellent toughness, high mechanical strength, and heat-treatable qualities (ASM International, 1990). This material is preferred in solid propellant rocket motors for load-bearing structural elements like motor casings because it can sustain structural integrity under high internal pressures and mechanical loads while in operation. Furthermore, AISI 4140 steel is suitable to produce complex geometries such as cylindrical motor casings due to its good machinability, and its suitability for mechanical surface preparation processes such as sandblasting and grinding provides a significant advantage in rocket motor applications where rubber-based insulation systems are bonded to the metal surface. In such systems, the metal surface acts both as a substrate supporting structural loads and as an interface ensuring the rubber insulation layer adheres securely via adhesive (Sutton & Biblarz, 2017).

3.1.2 Ethylene Propylene Diene Monomer (EPDM)

The EPDM material reinforced with aramid fiber and silica powder used in this study was selected to represent rubber-based insulation materials used in solid-fuel rocket motors. The EPDM compound was supplied in the form of 2 mm thick vulcanized sheets. EPDM rubber reinforced with aramid fiber and silica powder is among the widely preferred elastomeric materials in solid-fuel rocket motor applications due to its properties such as high temperature resistance, good elasticity, and resistance to environmental effects.

In rocket motor applications, these types of EPDM-based rubbers are used in insulation and liner systems located between the metal motor case and the solid fuel, and play a critical role in protecting the internal structure against thermal and mechanical loads generated during engine operation (Sutton & Biblarz, 2017). Aramid fiber reinforcement contributes to the preservation of structural integrity by increasing the tensile strength and tear resistance of the rubber, while silica powder filler improves the mechanical strength and thermal stability of the EPDM matrix. Thanks to this multiphase structure, the elastomer exhibits high deformation capability while maintaining its dimensional and mechanical stability under long-term service conditions (Shirazi & Noordermeer, 2011).

3.1.3 Araldite® 2011

Araldite 2011 adhesive used in this study has an anhydride-based hardener system in addition to the epoxy resin system. The anhydride curing system occurs through the reaction of epoxide groups and anhydride groups. The anhydride curing system has a slow rate of curing in comparison to the epoxy resin system. This generally results in the formation of a polymer network structure with a lower cross-linking density and a relatively more flexible structure.

The cured polymer structure of Araldite 2011 shows low elastic modulus and high deformation capability compared to DP490. This results in the adhesive bond showing more ductile properties when subjected to impact and vibration loading conditions. On the other hand, the increased flexibility of the polymer network may limit load transfer efficiency in applications where high interfacial strength is required, especially in structurally demanding bonding systems (Henkel, 2023).

Due to its anhydride-based curing chemistry, Araldite 2011 is more sensitive to interfacial conditions and surface preparation parameters. Consequently, the adhesion performance of this adhesive is strongly affected by surface energy, wetting

behavior, and the continuity of the adhesive–substrate interface. These aspects were taken into account when evaluating and interpreting the adhesion behavior of the samples bonded with Araldite 2011 in this study.



Figure 3.1 Araldite® 2011 Adhesive (Henkel, 2023)

3.1.4 3M™ Scotch-Weld™ DP490

The 3M™ Scotch-Weld™ DP490 used in this study is a two-component, structural epoxy adhesive. DP490 is formulated using an epoxy resin and an amine-based hardener system, forming a three-dimensional, cross-linked thermoset network structure during curing by opening the epoxy rings with amine groups. Amine-cured epoxy systems are generally characterized by high cross-linking density and a rigid polymer network. This dense network structure in DP490 provides the adhesive with a high elastic modulus, high shear strength, and good thermal stability. These properties make DP490 a preferred choice, especially in structural bonding systems operating under high mechanical loads. Furthermore, thanks to the toughness enhancing components in the DP490 formulation, completely brittle fracture behavior is prevented, and more controlled cohesive failure can occur. The amine-based curing mechanism enables DP490 to effectively interact with metal surfaces, and with proper surface preparation, the interfacial strength is limited only by the adhesive's own cohesive strength (3M, 2022). In this study, DP490 was used to

evaluate the effect of higher-rigidity epoxy systems on rubber-to-metal bonding performance and to conduct a comparative analysis with Araldite 2011.



Figure 3.2 3M™ Scotch-Weld™ DP490 (3M, 2022)

3.2 Preparation and Characterization Instruments

3.2.1 Sandblasting Equipment

In this study, a closed-cabin type manual sandblasting system was used for the mechanical roughening of metal surfaces. This system is a closed-loop sandblasting unit that allows the operator to manually guide the samples inside the cabin using protective gloves located on the front panel. During the sandblasting process, abrasive particles are directed to the metal surface with the help of compressed air, aiming to create a controlled roughness on the surface. 180-grit and 16-grit sand were used depending on the desired degree of roughness. 180-grit sand was used to achieve roughness between 1-2 microns, and 16-grit sand was used to achieve roughness above 2 microns. The possibility of manual control allowed for homogeneous roughening of the surface, especially on small and geometrically sensitive samples, and made it possible to obtain different roughness levels in a controlled manner.

3.2.2 Universal Testing Machine

In this study, the mechanical properties of the bonded samples were tested using a universal testing machine (Instron). The advantage of using this testing equipment lies in the fact that the servo control system facilitates the testing of the samples under tensile and shear conditions. During the test, the samples are fixed to the testing equipment using fixtures, and the uniaxial force is applied to the sample at a constant speed. The applied force and displacement are recorded continuously during the test. The mechanical properties of the bonded samples are determined based on the recorded data. The high precision load cell and the rigid frame of the universal testing equipment enable the reliable testing of the adhesive bonds under tensile and shear conditions.



Figure 3.3 Universal Testing Machine

3.2.3 Surface Cleanliness Measurement Device (SITA Cleanospector)

In this research, the SITA Cleanospector was used to measure the cleanliness level of metal surfaces. The SITA Cleanospector is a non-contact measuring device that applies the fluorescence principle to detect organic contaminants on surfaces like oil, grease, fingerprint residues, and other low molecular weight organic substances. When the surface that contains the organic contaminants is exposed to UV light of a specific wavelength, the organic contaminants on the surface fluoresce, and the

device measures the intensity of the emitted light in Relative Fluorescence Units (RFU). The obtained values allow a comparison of the relative cleanliness level of the surface. In this research, the device was used to determine the influence of the cleanliness level of metal surfaces on the adhesion strength, and metal surfaces were categorized based on the measured values of the RFU. Therefore, the influence of surface cleanliness on the mechanical bond strength could be explored (SITA Messtechnik GmbH, 2021).



Figure 3.4 SITA Cleanospector (SITA Messtechnik GmbH, 2021)

3.2.4 Surface Roughness Measurement Device (MAHR Marsurf PS10)

In this study, the characterization of the roughness of metal surfaces was carried out by using a MAHR MarSurf PS10 contact surface roughness measurement device. The device is based on a contact measurement principle where a diamond-tipped probe is scanned over a surface. The device can record a profile of the surface topography with high accuracy. The arithmetic mean roughness value and maximum height difference are the parameters that can be calculated based on the profile information obtained from the measurement device. The device is also a widely

preferred measurement system due to its features for investigating the effect of mechanical locking and surface morphology on bond strength. In this study, the device is used for quantitatively measuring the level of roughness achieved on metal surfaces after sandblasting and other mechanical processes (Mahr GmbH, 2021).



Figure 3.5 MAHR MarSurf PS10 (Mahr GmbH, 2021)

3.2.5 Cold Plasma Treatment Device (PiezoBrush® PZ3)

In the present study, a cold plasma system, i.e., PiezoBrush® PZ3, working at atmospheric pressure was used to enhance the surface energy of EPDM rubber surfaces for adhesive purposes. PiezoBrush® PZ3 is a portable surface treatment device working on the piezoelectric principle, and it has the capability to create a plasma atmosphere in ambient air without the need for any other vacuum system. The application of cold plasma to the surface also provides surface chemical activation, leading to the elimination of low molecular weight substances and the creation of polar groups on the surface. During the application of cold plasma, the EPDM surfaces were exposed to the plasma source for specific periods of time, thus attempting to enhance the surface energy of the EPDM surfaces. The device has the advantage of working at atmospheric pressure and low temperature, thus providing a potential surface treatment tool for heat-sensitive polymeric surfaces. The device

was used to improve the interaction at the EPDM adhesive interface and to enhance the adhesive bond strength, and the effect of different periods of application was investigated on the adhesive bond strength (Relyon Plasma, 2022; Hegemann et al., 2003; Friedrich, 2012).



Figure 3.6 PiezoBrush® PZ3 (Relyon Plasma, 2022)

3.2.6 Scanning Electron Microscopy (Thermo Scientific Phenom XL)

In this study, scanning electron microscopy (SEM) was used to examine the surface morphology of EPDM surfaces after different surface roughening methods (smooth, peel-paper roughened, and sand-paper roughened surfaces). Since EPDM rubber is an electrically insulating material, a gold-plating process was applied to make the surfaces conductive before SEM examination. The gold-plating process was carried out using the sputter coating method. In this method, atoms detached from the gold target material in a plasma environment created under vacuum are deposited on the sample surface as a thin and homogeneous layer. Thanks to the sputter coating process, the electrical conductivity of EPDM surfaces was increased, charge accumulation on the surface was prevented, and the clarity and contrast of the SEM images were improved. This process is a commonly used sample preparation technique in preparing polymer-based and insulating materials for SEM analysis

(Goldstein et al., 2018; Newbury & Ritchie, 2015). The surface morphology of the samples after gold plating was examined using a Thermo Scientific Phenom XL scanning electron microscope. Phenom XL, thanks to its high-resolution imaging capabilities, allows for detailed observation of surface topography and surface properties resulting from roughening methods (Thermo Fisher Scientific, 2021). SEM analyses were performed to comparatively evaluate the morphological changes caused by different surface preparation methods on the EPDM surface; the obtained images were used to qualitatively reveal the effects of mechanical roughening methods on the surface structure.

The elemental composition of the EPDM surfaces was examined using energy-dispersive X-ray spectroscopy (EDS), which was integrated into the SEM equipment, in addition to SEM images. The existence and relative distribution of constituent elements on the surface were determined by EDS studies, which complemented morphological observations. By integrating surface morphology with elemental composition after various surface roughening treatments, the combined SEM–EDS technique allowed for a more thorough characterization of the EPDM surfaces.

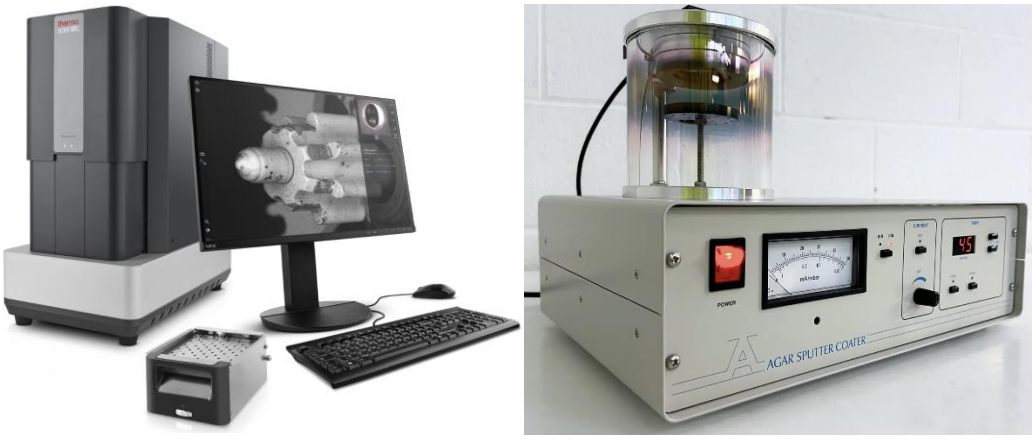


Figure 3.7 Thermo Scientific Phenom XL (Thermo Fisher Scientific, 2021) and Agar Sputter Coater

3.3 Investigation of the Effect of Metal Surface Preparation Parameters on EPDM-Metal Bond Strength

This stage focuses on a systematic evaluation of how metal surface roughness and surface cleanliness influence EPDM–metal bonding performance. For this purpose, metal surfaces were prepared with different levels of roughness and contamination, bonded to EPDM, and the mechanical response of the joints was examined through tensile and shear tests. In this way, the contribution of metal surface preparation parameters to bond strength was evaluated, and the interface that controls the overall bonding behavior was identified for the subsequent stages of the study.

To ensure reliable and reproducible results, five specimens were prepared for each parameter set for both tensile and shear test configurations. Metal surfaces were sandblasted using a manual sandblasting device. To achieve a roughness of 1-2 micrometers, 180-grit Al_2O_3 sand was used, while to achieve a roughness value above 2 micrometers, 16-grit Al_2O_3 sand was used. Surface roughness measurements were taken with a Marsurf PS10 device. Surface roughness levels were classified based on the measured Ra values. Metal surfaces without sandblasting exhibited Ra values below 1 µm. Low, medium, and high roughness levels were defined by Ra ranges of 1–2 µm, 2–4 µm, and 4–8 µm, respectively.



Figure 3.8 Surface Roughness Measurements with Marsurf PS10



Figure 3.9 Non-sandblasted Surfaces (<1 μm)



Figure 3.10 Samples with Low Surface Roughness (1-2 μm)



Figure 3.11 Samples with Moderate Surface Roughness (2-4 µm)



Figure 3.12 Samples with High Surface Roughness (4-8 µm)

Before and after sandblasting, the metal surfaces were cleaned with MEK using the immersion method.



Figure 3.13 Cleaning of Samples with MEK by Using the Immersion Method

Subsequently, Artificial contamination was created using Mobil Vactra Oil No. 2.



Figure 3.14 Surface Contamination Process with Mobil Vactra Oil No. 2

Contamination values were measured with a SITA Cleanospector device. Surface cleanliness levels were determined according to the relative fluorescence unit (RFU) values obtained using the SITA Cleanospector. Surfaces with RFU values between 0 and 50 were considered clean, while values in the range of 50–200 indicated

moderately contaminated surfaces. RFU values between 300 and 750 were used to define highly contaminated surfaces.

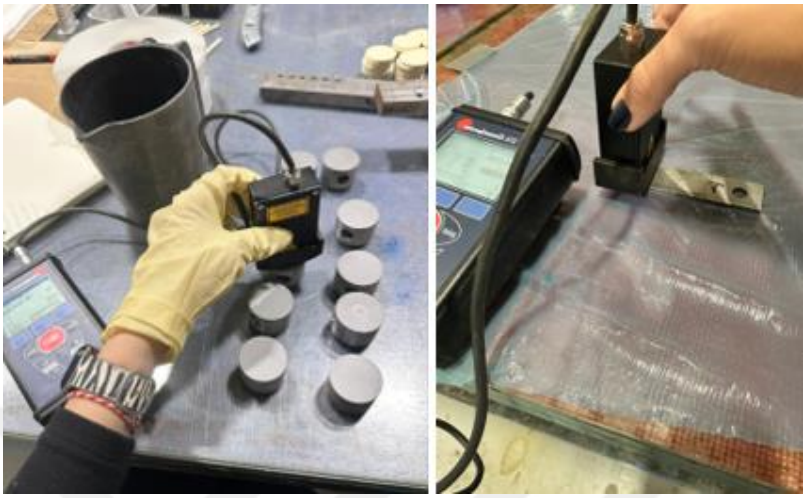


Figure 3.15 Surface Cleaning Measurement with Sita Cleanospector

Rubber–metal adhesive bonding experiments were conducted according to the surface preparation matrix presented in Table 3.1, in which metal surface roughness and cleanliness levels were systematically varied while EPDM roughened with peel ply and two different structural adhesives were used.

Table 3.1 Surface Preparation Matrix for Rubber-Metal Bonding

Sample Group	Ra Range (μm)	RFU Range	Adhesive	Rubber
RM–R0–C0–A1	<1	0–50	DP-490	EPDM
RM-R0–C1–A1	<1	50–200	DP-490	EPDM
RM-R0–C2–A1	<1	300–750	DP-490	EPDM
RM-R1–C0–A1	1–2	0–50	DP-490	EPDM
RM-R1–C1–A1	1–2	50–200	DP-490	EPDM
RM-R1–C2–A1	1–2	300–750	DP-490	EPDM
RM-R2–C0–A1	2–4	0–50	DP-490	EPDM
RM-R2–C1–A1	2–4	50–200	DP-490	EPDM
RM-R2–C2–A1	2–4	300–750	DP-490	EPDM
RM-R3–C0–A1	4–8	0–50	DP-490	EPDM
RM-R3–C1–A1	4–8	50–200	DP-490	EPDM
RM-R3–C2–A1	4–8	300–750	DP-490	EPDM
RM-R0–C0–A2	<1	0–50	Araldite 2011	EPDM
RM-R0–C1–A2	<1	50–200	Araldite 2011	EPDM
RM-R0–C2–A2	<1	300–750	Araldite 2011	EPDM
RM-R1–C0–A2	1–2	0–50	Araldite 2011	EPDM
RM-R1–C1–A2	1–2	50–200	Araldite 2011	EPDM
RM-R1–C2–A2	1–2	300–750	Araldite 2011	EPDM
RM-R2–C0–A2	2–4	0–50	Araldite 2011	EPDM
RM-R2–C1–A2	2–4	50–200	Araldite 2011	EPDM
RM-R2–C2–A2	2–4	300–750	Araldite 2011	EPDM
RM-R3–C0–A2	4–8	0–50	Araldite 2011	EPDM
RM-R3–C1–A2	4–8	50–200	Araldite 2011	EPDM
RM-R3–C2–A2	4–8	300–750	Araldite 2011	EPDM

RM → rubber-metal bonding

R0–R3 → roughness level

C0–C2 → cleanliness level

A1 / A2 → adhesive (A1: DP-490, A2: Araldite 2011)

Samples using Araldite 2011 adhesive were kept under pressure at room temperature for 24 hours. Samples using DP490 adhesive were kept under pressure at room temperature for 24 hours and then placed in an oven at 80°C for 1 hour.

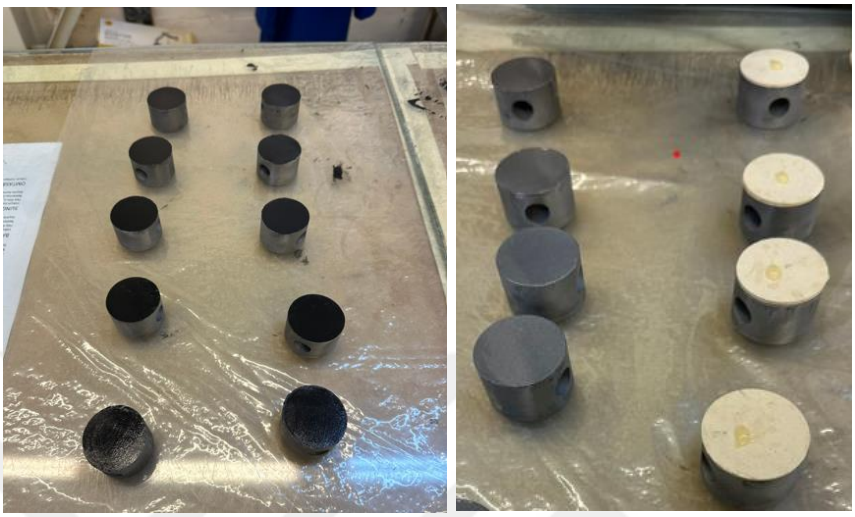


Figure 3.16 Preparing a Tensile Test Specimens with DP490 and Araldite 2011



Figure 3.17 Tensile Test Specimens Curing Under Pressure



Figure 3.18 Shear Test Specimens Curing Under Pressure

Tensile tests and shear tests were conducted on INSTRON Universal Test Machine under room conditions. Tensile tests were performed at a constant traverse speed of 5 mm/min. Due to the viscoelastic nature of EPDM, the test speed was kept constant for all tensile specimens to ensure comparability between conditions. The specimen geometry and loading principle were based on the butt-joint approach defined in ASTM D897. Lap shear tests were performed at a constant traverse speed of 1.3 mm/min, and the test approach was based on ASTM D1002. The geometries and dimensions of the tensile and shear test specimens are illustrated in Figure 3.19.

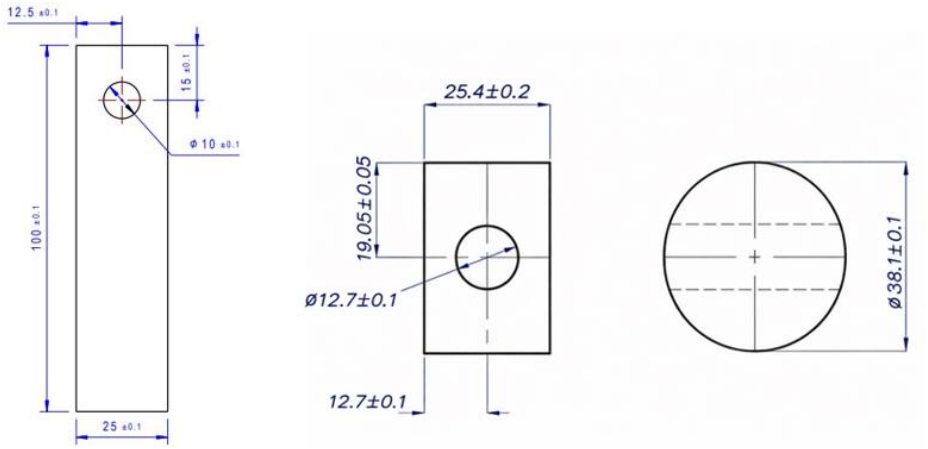


Figure 3.19 Geometrical Details and Dimensions of the Tensile and Shear Test Specimens

3.4 Evaluation of Metal-Adhesive Interface Through Metal-Metal Bonding Experiments

The aim of this stage is to evaluate the effect of metal surface roughness and cleanliness levels on bond strength, independently of the limiting effects arising from the elastomeric structure of EPDM. Accordingly, the metal-adhesive interface was isolated using a metal-to-metal bonding configuration, and the direct investigation of the effect of different surface preparation conditions on bond performance was targeted.

In this context, only metal-metal test specimens were prepared using the same surface roughness and cleanliness variables, and shear tests were performed for both adhesives. To ensure verifiability and repeatability, four samples were prepared for each parameter. Metal surfaces were sandblasted again using a manual sandblasting device to the same roughness levels as the previous section.

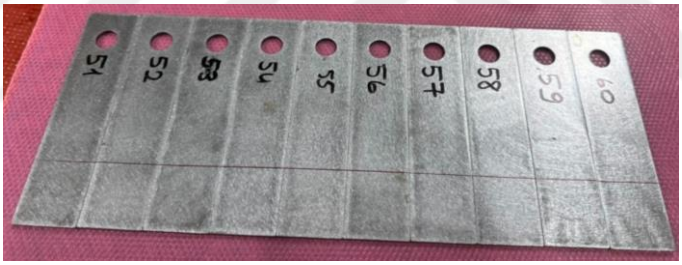


Figure 3.20 Non-sandblasted Surfaces (<1 µm)



Figure 3.21 Samples with Low Surface Roughness (1-2 µm)



Figure 3.22 Samples with Moderate Surface Roughness (2-4 µm)



Figure 3.23 Samples with High Surface Roughness (4-8 µm)

Surface cleaning procedures were performed before and after sandblasting using the same surface cleaning technique as in the previous section. Roughness and cleanliness measurements were performed again. Scanning electron microscopy (SEM) combined with energy dispersive X-ray spectroscopy (EDS) analyses were performed on selected metal surface samples to examine surface morphology and to identify possible surface contaminants and embedded abrasive residues resulting from different surface preparation conditions.

Artificial contamination was created using Mobil Vactra Oil No. 2.



Figure 3.24 Shear Test Coupons for Clean Surface → 40, Modaretely Contaminated Surface → 51, Highly Contaminated Surface →41

The prepared surfaces were bonded using DP490 and Araldite 2011 adhesives. Metal-metal adhesive bonding experiments were conducted according to the surface preparation matrix presented in Appendix A. Adhesives were cured in the same curing cycles as in the previous section. Shear tests were performed at a speed of 1.3 mm/min on an INSTRON Universal Test Machine under room conditions.

3.5 Investigation of the Effects of Different EPDM Surface Roughening Methods on the EPDM-Adhesive Interface

After determination of the optimum surface roughness and cleanliness range for the metal surface in the previous stage, it was assessed that the main interface limiting the bond strength was the EPDM–adhesive interface. Accordingly, additional experimental studies were conducted to investigate the effect of different EPDM surface roughening methods on improving the interaction of the EPDM surface with the adhesive. In this context, EPDM surfaces were prepared under three different surface conditions: smooth EPDM without any surface treatment, EPDM roughened using peel ply to create surface morphology during curing, and mechanically sandpapering EPDM surfaces.

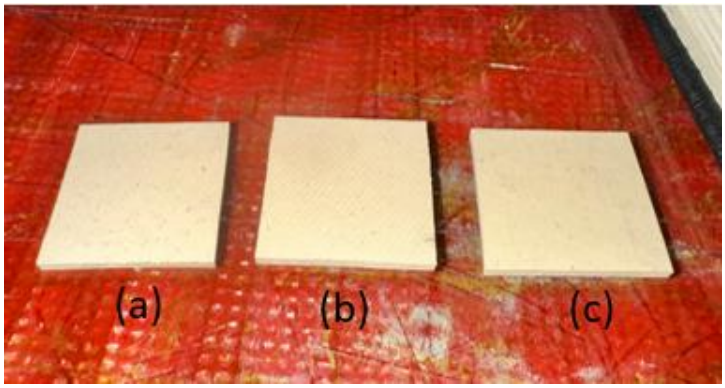


Figure 3.25 a) Smooth Surface b) Roughened with Peel Ply c) Roughened with Sandpaper

The metal coupons to which the EPDM surfaces were bonded were sandblasted to achieve a surface roughness of 4–8 μm and surface cleanliness levels were brought to the range of 0–50 RFU, in accordance with the conditions determined in the previous stage. The prepared EPDM surfaces were bonded with Araldite 2011 and DP490 adhesives while keeping the metal surface conditions constant, and the resulting samples were prepared for tensile and shear tests. Scanning electron microscopy (SEM) combined with energy dispersive X-ray spectroscopy (EDS) analyses were performed to selected samples to investigate the surface morphology and chemical composition of EPDM. The distribution and relative proportions of elements present on the EPDM surface were determined using EDS analysis.

3.6 Investigation of EPDM Surface Activation and Time Effect via Plasma Application

In the final stage of the study, since it was determined that the EPDM-adhesive interface was the main interface limiting bond strength despite the optimization of metal surface preparation parameters in previous experiments, atmospheric plasma application was performed to activate the EPDM surface. The low surface energy, nonpolar character of EPDM rubber, and the presence of low molecular weight components on the surface make it difficult for the adhesive to adequately wet the

surface and create a strong interface interaction. Therefore, plasma applications were preferred to improve interface properties by providing chemical and physical activation on the EPDM surface. The aim of the atmospheric plasma treatment was to increase the surface energy by forming oxygen-containing polar functional groups on the EPDM surface and to remove weak boundary layers on the surface. Thus, the aim was to increase the wettability of the adhesive on the EPDM surface, strengthen the interface bonds, and obtain a bond behavior where the failure mode is removed from the interface and limited by the cohesive strength of the rubber. In this stage, bonding processes were carried out using Araldite 2011 and DP490 adhesives. To isolate the effect of plasma application, all other parameters were kept constant. Accordingly, metal coupons were sandblasted to achieve a surface roughness of 4–8 µm, and surface cleanliness levels were maintained in the range of 0–50 RFU; for EPDM surfaces, the sandpaper roughening method, which was observed to provide the best strength in the previous stage, was used.

Plasma application was performed using a PiezoBrush PZ3 atmospheric plasma device. For tensile test specimens, plasma application times of 0 s, 30 s, and 60 s were selected; for shear test specimens, plasma application times of 0 s, 15 s, and 30 s were selected. After the plasma treatment, EPDM surfaces were bonded to coupons with the specified metal surface conditions using Araldite 2011 and DP490 adhesives under the same bonding and curing conditions, and the specimens were prepared for tensile and shear tests.



Figure 3.26 EPDM Plasma Treatment

CHAPTER 4

RESULTS AND DISCUSSION

This chapter presents the results obtained from multi-stage bonding experiments conducted in the experimental part of the study and discusses them in light of the relevant literature. Experimental studies were carried out in four main stages to systematically investigate the fundamental parameters affecting bond strength. In the first stage, the effect of metal surface roughness and surface cleanliness level on EPDM-metal bond strength was evaluated. In the second stage, the metal-adhesive interface was isolated using a metal-metal bonding configuration to eliminate the limiting effects arising from the elastomeric structure of EPDM, and the effect of surface preparation parameters on bond behavior was investigated. In the third stage, the effect of different EPDM surface roughening methods on improving the EPDM-adhesive interface, which was determined as the main interface limiting bond strength, was investigated. In the final stage, the effect of surface activation achieved by atmospheric plasma treatment applied to the EPDM surface and the plasma application time on bond performance were evaluated. By considering the mechanical test results, failure mode analyses, and surface characterization findings obtained within the scope of these stages, the critical mechanisms determining bond strength in the rubber-metal bonding system were revealed.

4.1 The Effect of Metal Surface Roughness and Cleanliness Level on EPDM-Metal Bond Strength

At this stage, EPDM-metal bonds were created by preparing the metal surface roughness at four levels (R0: no sandblasting; R1: 1–2 μm; R2: 2–4 μm; R3: 4–8 μm) and the surface cleanliness level under three different conditions (clean/moderately contaminated/highly contaminated), and both tensile and shear

tests were applied with two different epoxy-based adhesives (DP490 and Araldite 2011). In general, the graphs show that the change in metal surface roughness and contamination level does not produce a uniform and linear trend in bond strength; even if certain increases are observed under some conditions, this is not consistently repeated across all roughness levels and with both adhesives. This suggests that the metal-adhesive interface is not a critical limiting component in the examined range; the system performance is significantly limited by the EPDM-adhesive interface and/or the cohesive behavior of EPDM.

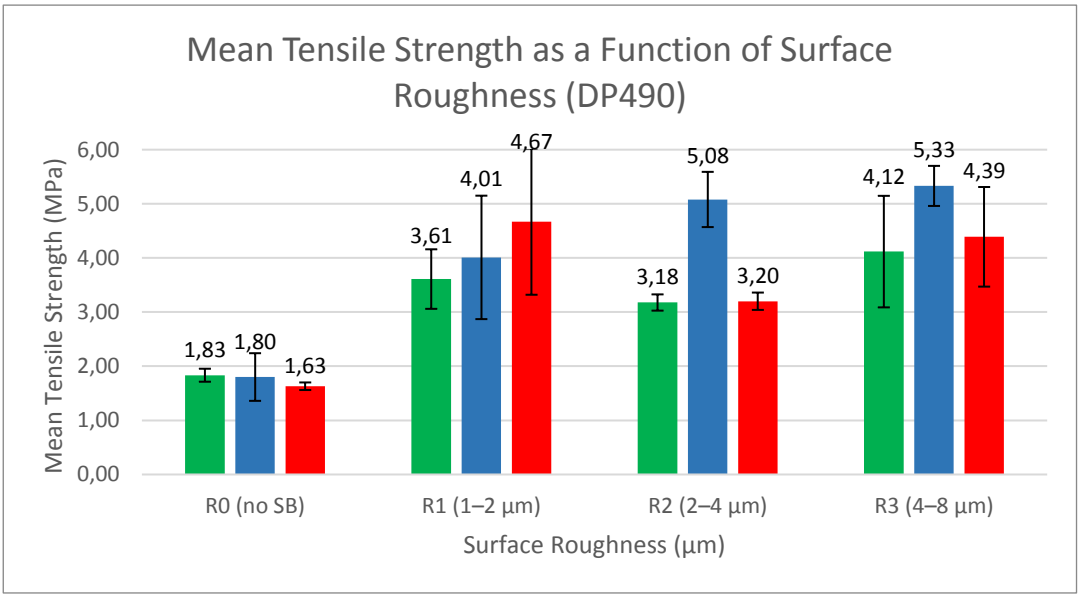


Figure 4.1 The Mean Tensile Strength as a Function of Surface Roughness for DP490

Green column → Clean Surface

Blue column → Moderately Contaminated Surface

Red column → Highly Contaminated Surface

In tensile tests with DP490, the average strengths at the R0 level are low, approximately 1.83 / 1.80 / 1.63 MPa for clean/medium/high contamination, respectively. When sandblasting reaches the R1 range, the averages increase significantly (3.61 / 4.01 / 4.67 MPa), but this increase does not continue uniformly

at the R2 and R3 levels. For example, at R2, while the clean and highly contaminated conditions remain around ~3.18–3.20 MPa, the moderately contaminated condition rises to ~5.08 MPa; at R3, the values increase again (4.12 / 5.33 / 4.39 MPa). Particularly noteworthy here is that the moderately contaminated condition yields the highest average at certain roughness levels, and the expected monotonic decrease in strength as contamination increases does not occur. This table indicates that the contamination level, represented by RFU on the metal surface, is not the sole determining parameter in the DP490 system; factors such as test scattering/local interface heterogeneity or the initiation of failure in another region may be more dominant.

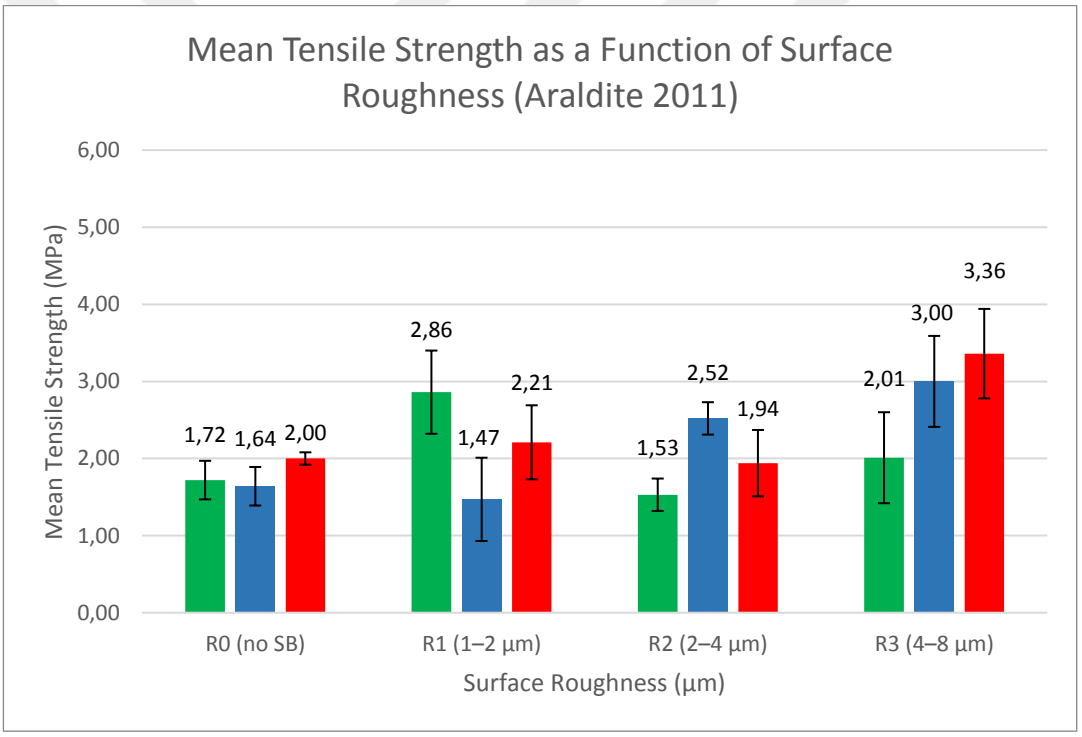


Figure 4.2 The Mean Tensile Strength as a Function of Surface Roughness for Araldite 2011

In tensile tests with Araldite 2011, average strengths generally remained in a lower range compared to DP490. While values of approximately 1.72, 1.64, and 2.00 MPa were found in R0, the clean condition at R1 showed an increase of approximately

~2.86 MPa, while the moderately contaminated condition showed a fall to around 1.47 MPa. The clean state in R2 stayed at around ~1.53 MPa, whereas the moderately contaminated condition was comparatively high at about ~2.52 MPa. In R3, an increasing trend is particularly noticeable in the moderately and highly contaminated conditions (~3.00 and 3.36 MPa). This distribution shows that for Araldite 2011, there is no clear relationship between the metal surface contamination level and the strength, such as "strength decreases as contamination increases". In addition, the relatively large error bars in some groups create an ambiguity, suggesting that failure in the tensile test may have been initiated by local weaknesses of the interface rather than a metal parameter.

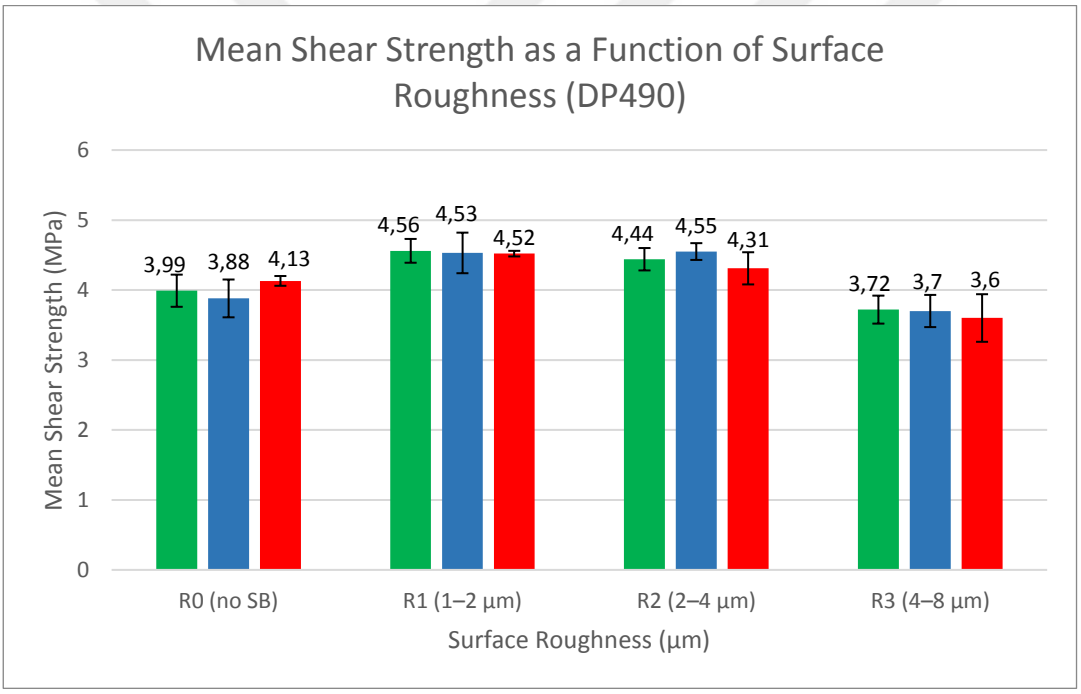


Figure 4.3 The Mean Shear Strength as a Function of Surface Roughness for DP490

In shear tests with DP490, the average shear strengths obtained in the R0–R2 range are quite similar, varying between approximately 3.9–4.6 MPa. No significant difference was observed in this range between clean, moderately contaminated, and

highly contaminated surfaces. At the R3 (4–8 µm) level, however, the average shear strength decreased to approximately 3.6–3.7 MPa under all cleanliness conditions.

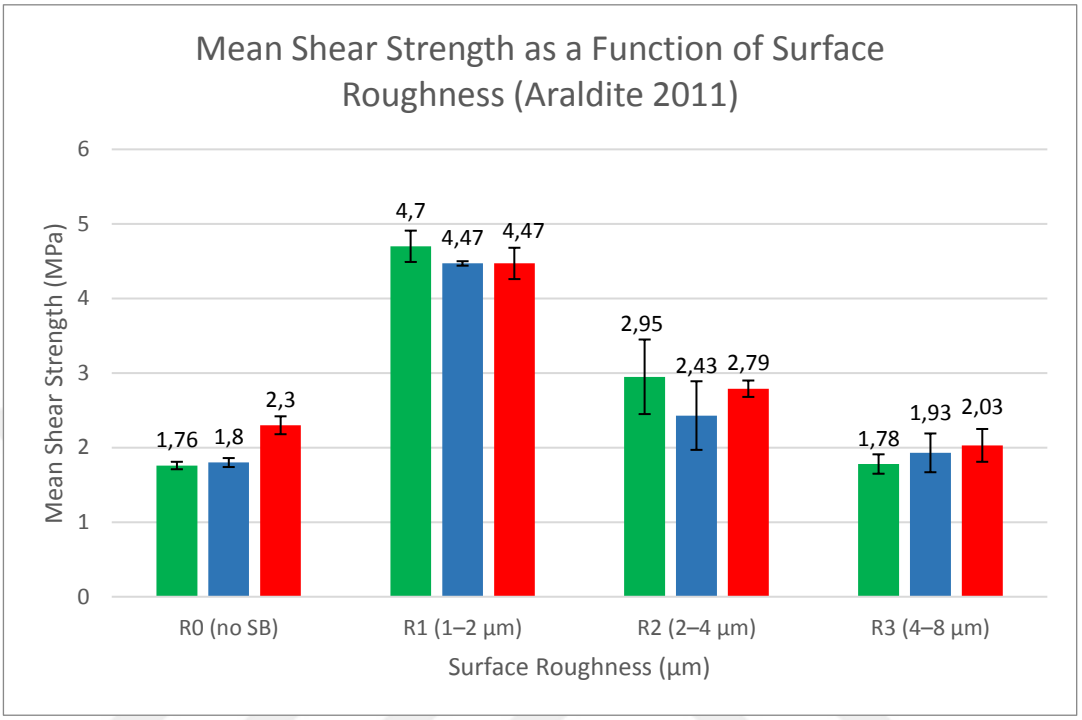


Figure 4.4 The Mean Shear Strength as a Function of Surface Roughness for Araldite 2011

In shear tests with Araldite 2011, more significant changes were observed depending on the roughness level. While average strengths remained in the range of approximately 1.76–2.30 MPa at the R0 level, the highest values were obtained at the R1 (1–2 µm) level with approximately 4.47–4.70 MPa for all cleanliness conditions. At the R2 and R3 levels, the average shear strengths decreased again and were measured in the range of approximately 1.78–2.95 MPa. This indicates that in the Araldite 2011 system, more pronounced differences in bonding behavior occur depending on the metal surface roughness; however, these differences cannot be directly attributed to the metal interface in the EPDM–metal configuration.

Failure mode analyses showed that in tensile test specimens, failure mostly occurred at the EPDM-adhesive interface, while in shear tests, cohesive failure frequently

occurred within the rubber itself. The absence of significant adhesive failure at the metal-adhesive interface suggests that the surface preparation treatments applied on the metal side ensured sufficient bonding. Therefore, it was concluded that the strength differences obtained depending on the metal surface roughness and cleanliness level are not the fundamental parameters limiting the ultimate strength of the system. Images of the samples are provided in Figure 4.5, 4.6, 4.7, and 4.8.

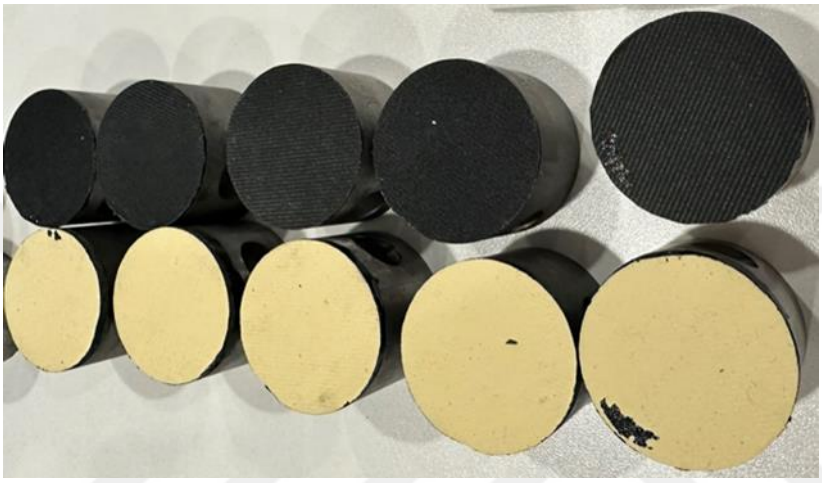


Figure 4.5 2-4 µm, 0-50 RFU, DP490, Adhesive Failure

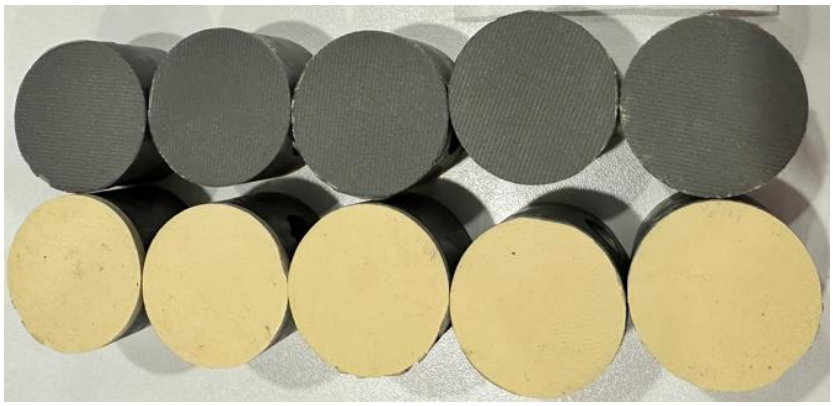


Figure 4.6 2-4 µm, 0-50 RFU, Araldite 2011, Adhesive Failure

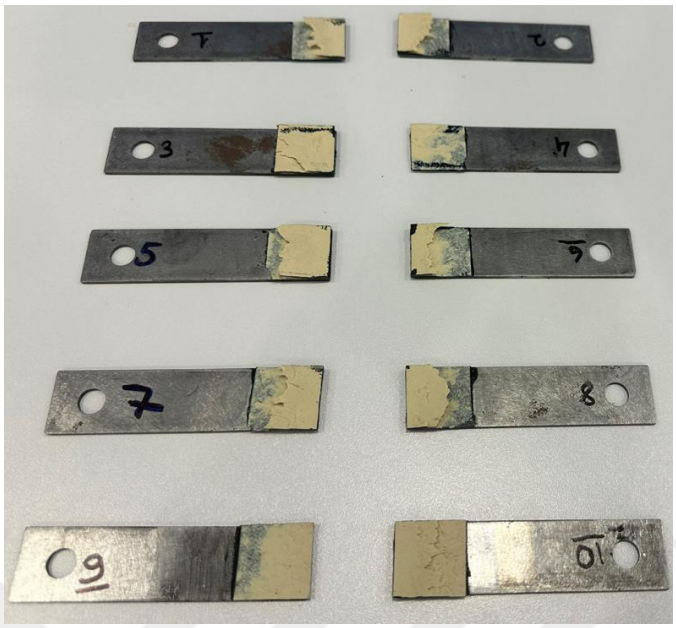


Figure 4.7 1-2 µm, 0-50 RFU, DP490, Cohesive Failure in EPDM, DP490

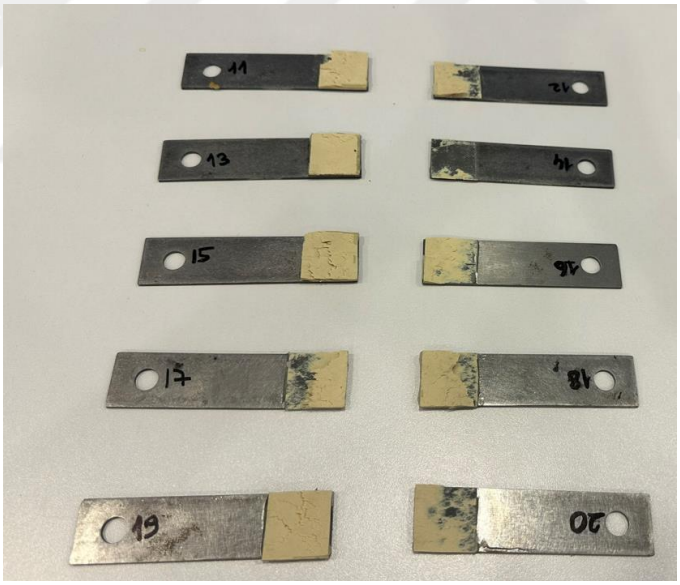


Figure 4.8 1-2 µm, 0-50 RFU, DP490, Cohesive Failure in EPDM, Araldite 2011

When the numerical results obtained at this stage are evaluated together, it is seen that metal surface roughness and cleanliness level lead to certain variations in bond strength in EPDM-metal bonds; however, these variations do not form a generalizable and unidirectional trend. The fact that failure modes predominantly

occur on the EPDM side indicates that the effect of metal surface parameters is masked at this stage. Therefore, in order to more clearly reveal the true effect of metal surface roughness and cleanliness level on bond behavior, a metal-to-metal bonding configuration that eliminates the effect of EPDM was used in the next stage.

4.2 Evaluation of Metal-Adhesive Interface with Metal-Metal Shear Tests

In this stage, a metal-to-metal bonding configuration was used to evaluate the effect of metal surface roughness and cleanliness level on bond strength independently of the elastomeric behavior of EPDM. Metal surfaces were prepared at four different roughness levels (R0: no sandblasting, R1: 1–2 µm, R2: 2–4 µm, and R3: 4–8 µm) and three different cleanliness conditions (clean, moderately contaminated, and highly contaminated); shear strength tests were performed using DP490 and Araldite 2011 adhesives. Thanks to this configuration, the metal-adhesive interface was isolated, and the actual effect of metal surface preparation parameters on bond behavior could be directly investigated.

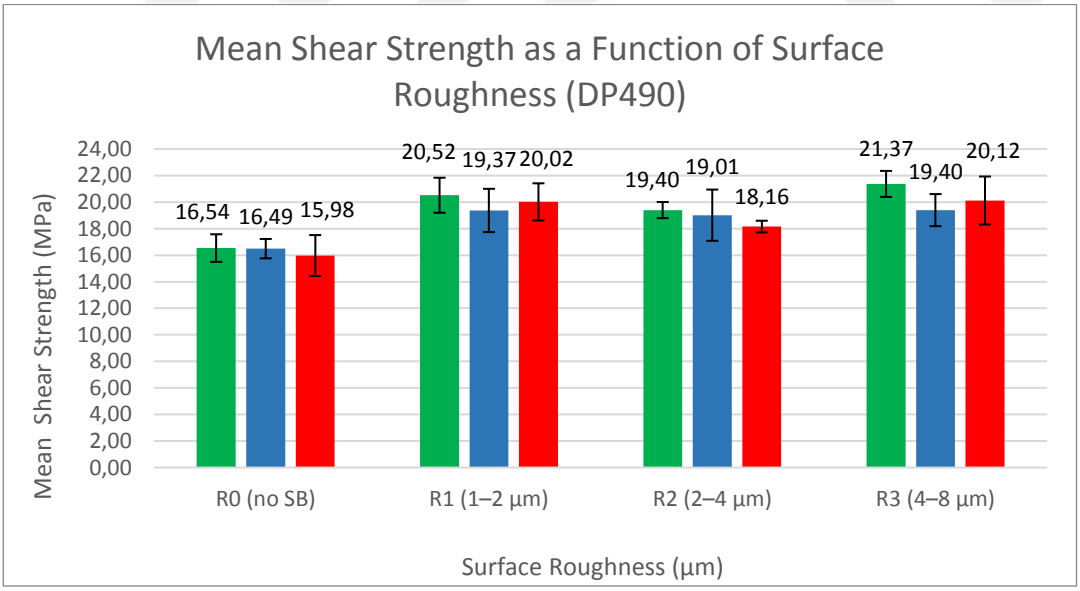


Figure 4.9 The Mean Shear Strength as a Function of Surface Roughness for DP490 (Metal-Metal Bonding)

Metal-to-metal shear strength results obtained using DP490 showed a relatively high and narrow range depending on the metal surface roughness and cleanliness level. In R0 samples without sandblasting, the average shear strengths were measured as 16.54 MPa, 16.49 MPa, and 15.98 MPa for clean, moderately contaminated, and highly contaminated surfaces, respectively. When the roughness level of R1 (1–2 μm) was reached, the strengths increased significantly under all cleanliness conditions, reaching a range of 19.37–20.52 MPa.

At the R2 (2–4 μm) level, the average shear strengths were measured in the range of 18.16–19.40 MPa; a limited decrease was observed compared to R1. At the R3 (4–8 μm) level, the strengths increased again, reaching 21.37 MPa, 19.40 MPa, and 20.12 MPa for clean, moderately contaminated, and highly contaminated surfaces, respectively. These results demonstrate that metal surface roughness has a certain effect on bond strength in metal-to-metal bonds with DP490, but this effect is largely independent of the cleanliness level. The fact that the average values obtained among clean, moderately contaminated, and highly contaminated surfaces are quite close suggests that DP490 exhibits tolerant bonding behavior towards limited contamination on the metal surface.

When failure mode observations were examined, it was seen that in the vast majority of DP490 samples, failure occurred cohesively within the adhesive layer. This indicates that the metal-adhesive interface provides sufficient bonding and that the ultimate strength of the system is largely limited by the cohesive strength of the adhesive itself. Therefore, it is considered that the strength increases obtained for DP490 depending on the metal surface roughness are related to approaching the load-carrying capacity of the adhesive rather than interface improvement.



Figure 4.10 Metal-Metal Bonding, Shear Test, DP490, 2-4 µm, 0-50 RFU, Cohesive Failure in Adhesive

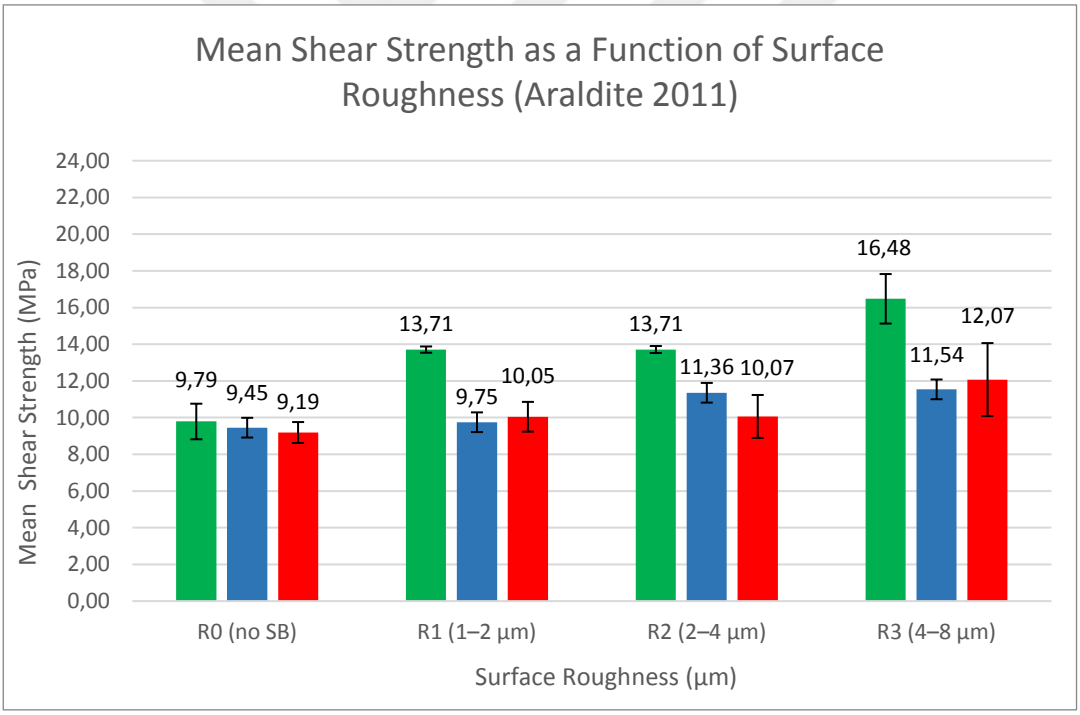


Figure 4.11 The Mean Shear Strength as a Function of Surface Roughness for Araldite 2011 (Metal-Metal Bonding)

Metal-to-metal shear strength results obtained using Araldite 2011 showed a more sensitive behavior to metal surface roughness and cleanliness level compared to

DP490. At the R0 level, average shear strengths were measured as 9.79 MPa, 9.45 MPa, and 9.19 MPa, indicating a lower initial level compared to DP490. At the R1 (1–2 µm) roughness level, the strength increased to 13.71 MPa on clean surfaces, while on moderately and highly contaminated surfaces, the values were measured as 9.75 MPa and 10.05 MPa, respectively.

At the R2 (2–4 µm) level, the average shear strength remained similar to the R1 level at 13.71 MPa on clean surfaces, while on moderately and highly contaminated surfaces, the values were 11.36 MPa and 10.07 MPa, respectively. At the R3 level (4–8 µm), a significant increase was observed, especially on clean surfaces, and the average shear strength reached 16.48 MPa. The upward trend at the R3 level continued on moderately and highly contaminated surfaces (11.54 MPa and 12.07 MPa). These results demonstrate that metal surface roughness plays a decisive role in bond strength for Araldite 2011, with the highest strengths obtained in the 4–8 µm roughness range.

Failure mode analyses revealed that failures in Araldite 2011 samples largely occurred adhesively at the metal-adhesive interface. This indicates that, unlike DP490, the metal-adhesive interface is the primary region limiting bond behavior in the Araldite 2011 system. Therefore, variations in metal surface roughness and cleanliness level directly impact bond strength for Araldite 2011, as observed results.

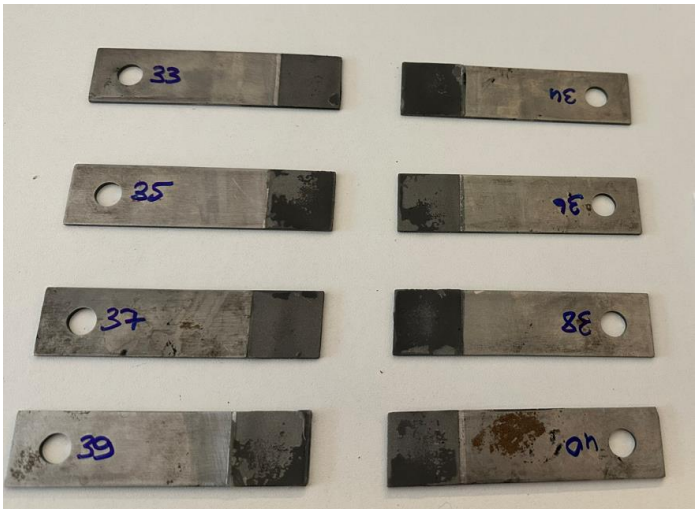


Figure 4.12 4-8 µm, 0-50 RFU, Adhesive Failure, Araldite 2011

When both adhesives are evaluated together, it is noteworthy that a limited decrease in strength is observed in the R1 → R2 transition under certain conditions, depending on the metal surface roughness, while an increase is observed again in the R2 → R3 transition. This behavior is a typical trend reported in the literature and indicates that the roughness-strength relationship is not always monotonic.

When the effect of surface roughness (Ra) on shear strength was investigated, a general increase in strength was observed on roughened surfaces compared to smooth surfaces (R0) for both DP490 and Araldite 2011 adhesives. However, this increase did not exhibit a linear trend. Metal-to-metal shear tests revealed that the effect of surface roughness on bond strength did not show a linear trend. For DP490, as the Ra value increased to the 1–2 μm range, the average shear strength increased by approximately 24%, reaching 20.52 MPa; however, a limited decrease in strength was observed with increasing roughness to the 2–4 μm range, and the average value was measured as 19.40 MPa. This decrease can be attributed to the rounded and coarse particle-like structures observed locally on surfaces with a roughness level of 2–4 μm in SEM analyses. The predominant detection of aluminum and oxygen elements in EDS analyses taken from these regions indicates that these structures are aluminum oxide ($Al_2 O_3$) particles embedded in the surface during the sandblasting process. Such embedded or semi-embedded hard particles disrupt the continuity of the metal surface, limiting direct contact of the adhesive with the metal matrix and thus partially hindering the expected chemical bonding mechanisms at the metal-adhesive interface. In addition, microscopic air bubbles can form around the particles due to the adhesive's inability to fully wet the surface; these voids both reduce the effective bonding area and cause stress concentrations under load, creating early damage initiation zones and cracks. It was observed that increasing the roughness to 4–8 μm resulted in an increase in the average shear strength of DP490 to 21.37 MPa. This behavior can be explained by the fact that more aggressive surface preparation conditions more effectively remove weak oxide or contamination layers from the metal surface, exposing a fresher, chemically active metal surface. Furthermore, the

more continuous micro-anchoring structure formed at higher roughness levels may have increased mechanical interlocking, making crack propagation more difficult.

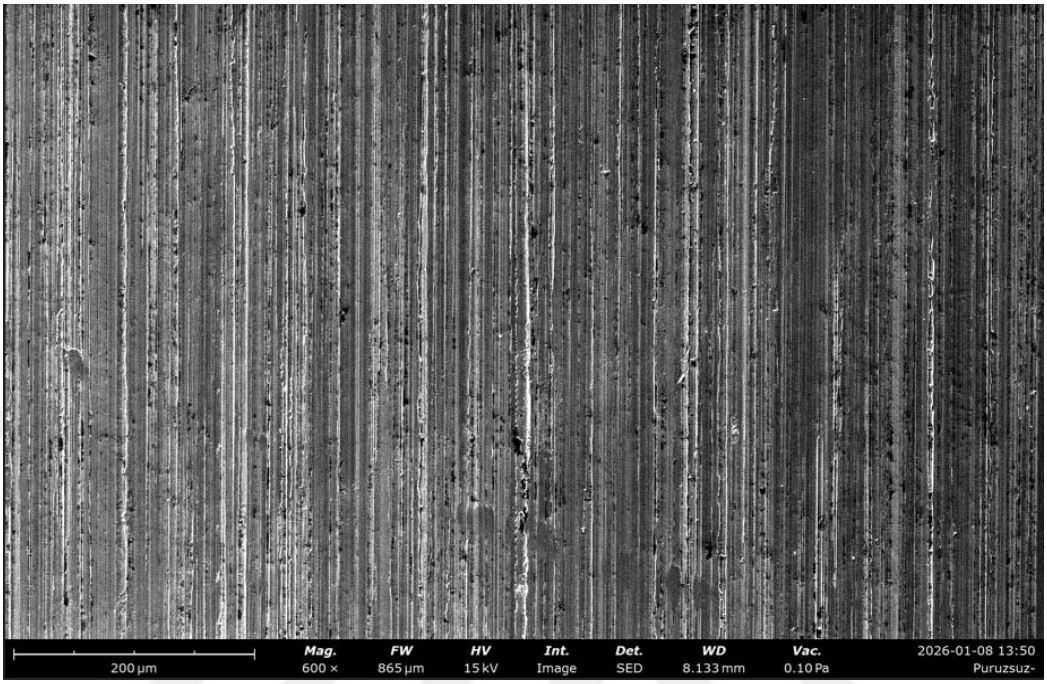


Figure 4.13 SEM Image of Smooth Metal Surface (<1 µm)

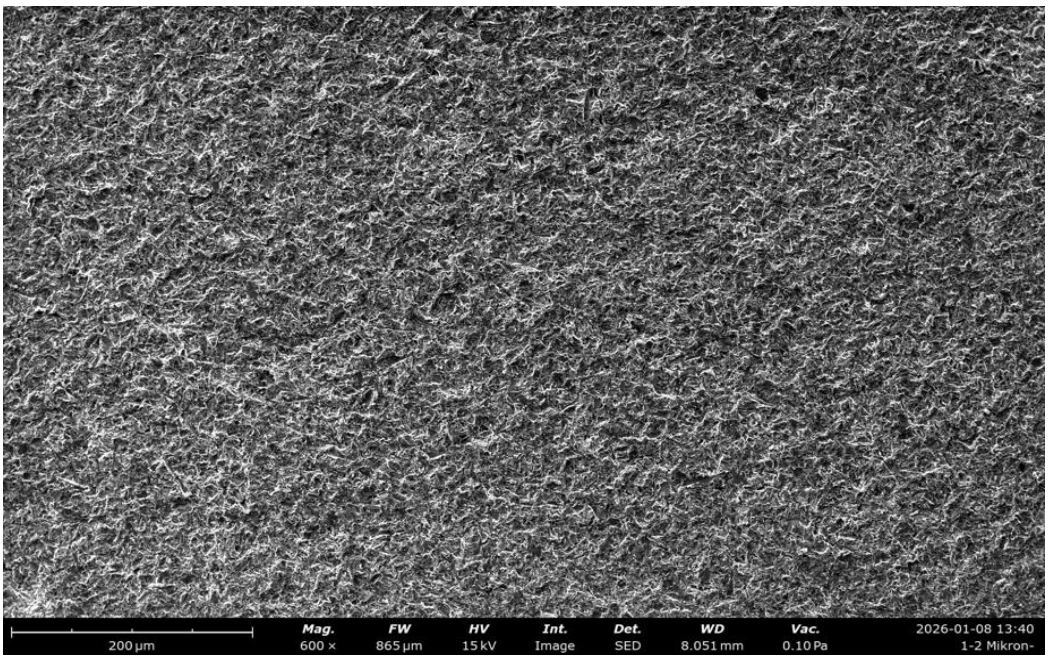


Figure 4.14 SEM Image of Metal with Low Roughness (1-2 µm)

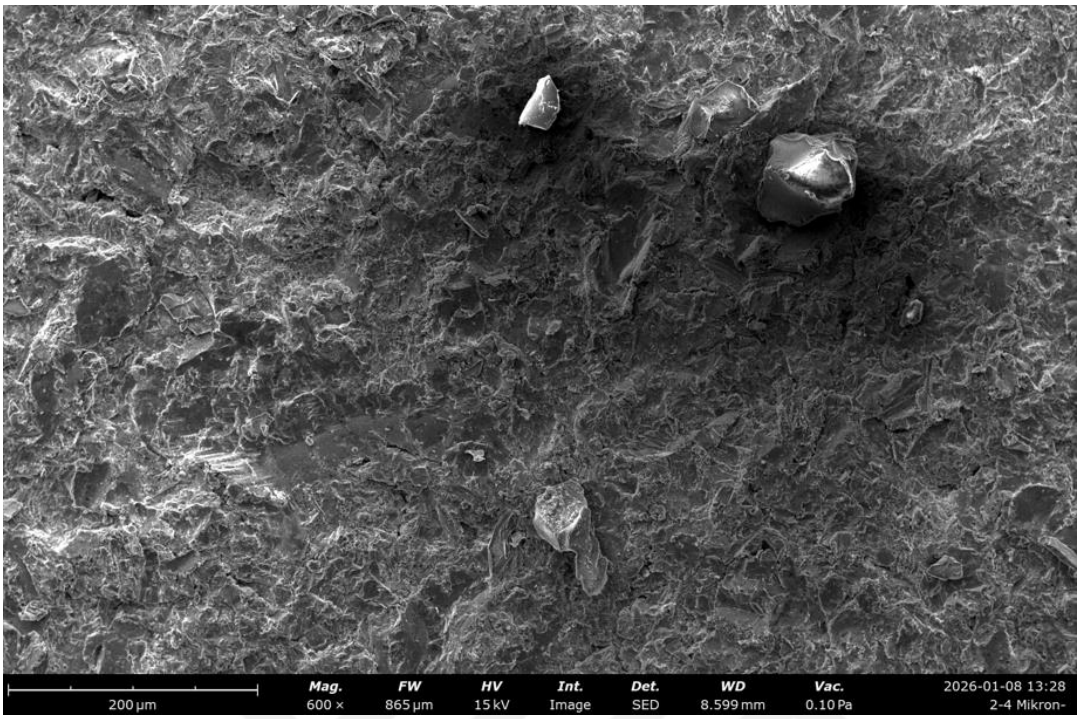


Figure 4.15 SEM Image of Metal with Medium Roughness (2-4 µm)

Table 4.1 EDS Analysis of Metal with Medium Roughness (2-4 µm)

Element Number	Element Symbol	Element Name	Atomic Conc. [%]	Weight Conc. [%]
8	O	Oxygen	57.53	43.20
13	Al	Aluminum	39.10	49.50
14	Si	Silicon	0.91	1.20
22	Ti	Titanium	0.93	2.10
26	Fe	Iron	1.53	4.00

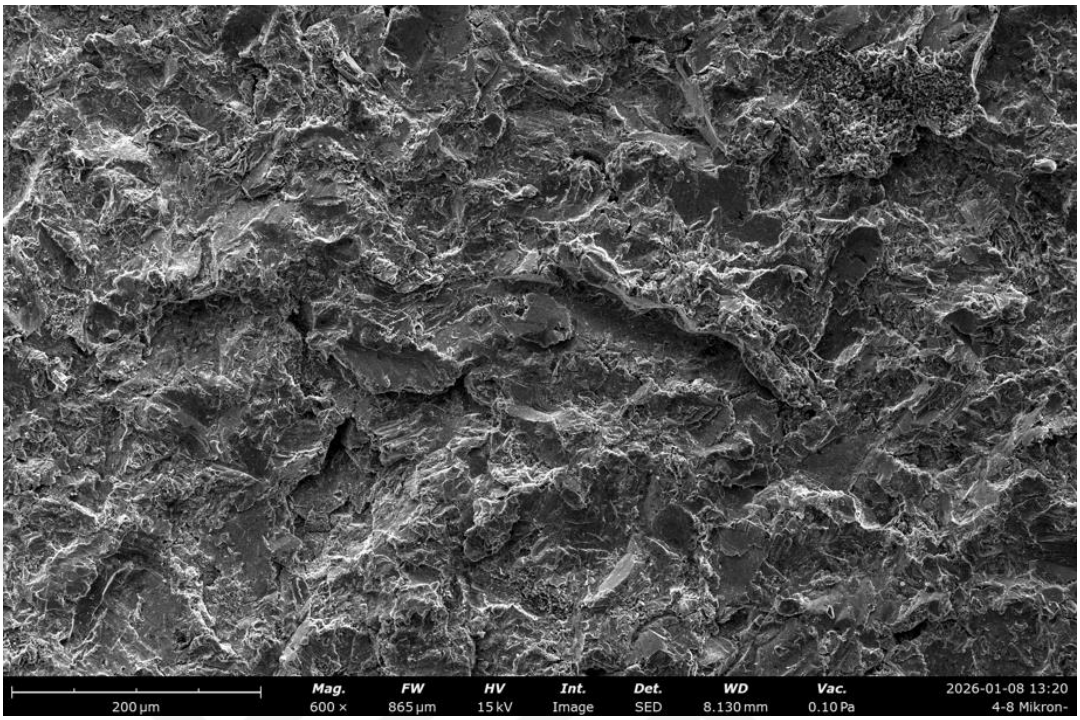


Figure 4.16 SEM Image of Metal with High Roughness (4-8 µm)

Table 4.2 EDS Analysis of Metal with High Roughness (4-8 µm)

Element Number	Element Symbol	Element Name	Atomic Conc. [%]	Weight Conc. [%]
8	O	Oxygen	10.87	3.50
13	Al	Aluminum	6.27	3.40
26	Fe	Iron	82.86	93.10

For Araldite 2011, a more balanced behavior was observed against increasing roughness due to the advantage provided by lower viscosity; nevertheless, the highest strength values were still obtained at the 4–8 µm roughness level. These results demonstrate that the bond strength at the metal-adhesive interface is strongly dependent not only on the magnitude of the roughness but also on the morphology of the roughness and the presence of secondary phases formed on the surface.

When these results are evaluated together, it is clear that for the Araldite 2011 system, the metal-adhesive interface is the key region limiting the bond behavior,

and therefore, metal surface roughness and cleanliness level play a decisive role in bond strength. Specifically, surface roughness of 4–8 μm and cleanliness levels of 0–50 RFU were identified as the conditions under which the highest and most reproducible shear strengths were obtained for Araldite 2011.

In contrast, in joints using DP490, failure occurs predominantly cohesively within the adhesive layer, indicating that the metal-adhesive interface is not the main factor limiting the bond behavior in this system. Therefore, it is not possible to definitively define a single "optimum" point for DP490 depending on metal surface roughness and cleanliness level. However, results from metal-to-metal shear tests revealed that a surface roughness of 4–8 μm and a cleanliness level of 0–50 RFU provided a safe operating range with high bond strength for both adhesives.

Accordingly, in the later stages of EPDM–metal bonding experiments, the metal surface parameters of 4–8 μm surface roughness and 0–50 RFU cleanliness level were kept constant for Araldite 2011, as they clearly represent optimum conditions and provide a reference state for DP490 where interface effects are minimized.

4.3 The Effect of EPDM Surface Roughening Methods on the EPDM-Adhesive Interface

In previous experimental stages, it was determined that the metal-adhesive interface was not the primary region limiting the bonding behavior for either adhesive, or that the EPDM-adhesive interface was the main factor determining bond strength, especially in EPDM-metal bonds. Therefore, in this stage, while keeping the metal surface parameters constant (4–8 μm surface roughness and 0–50 RFU cleanliness level), the effect of modifying the EPDM surface with different mechanical roughening methods on bonding performance was investigated. In this context, EPDM surfaces were prepared as unroughened (smooth), roughened with sandpaper, and roughened with peel ply ; tensile and shear tests were performed using DP490 and Araldite 2011 adhesives.

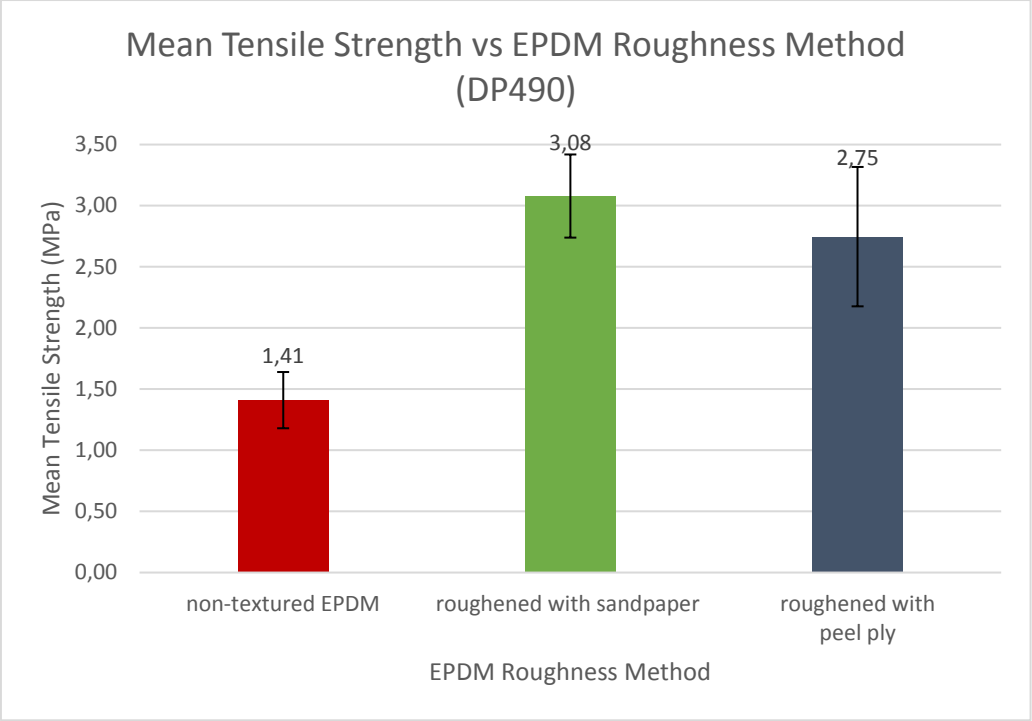


Figure 4.17 The Mean Tensile Strength vs EPDM Roughness Method for DP490

In EPDM-metal tensile test specimens prepared with DP490, the average tensile strength on unroughened EPDM surfaces was measured as 1.41 MPa. When the EPDM surface was roughened with sandpaper, the average tensile strength increased to 3.08 MPa, representing an increase of approximately 118%. On EPDM surfaces roughened with peel ply, the average tensile strength was measured as 2.75 MPa; although this value showed a significant increase compared to the unroughened case, it remained lower compared to sand-paper roughened surfaces.

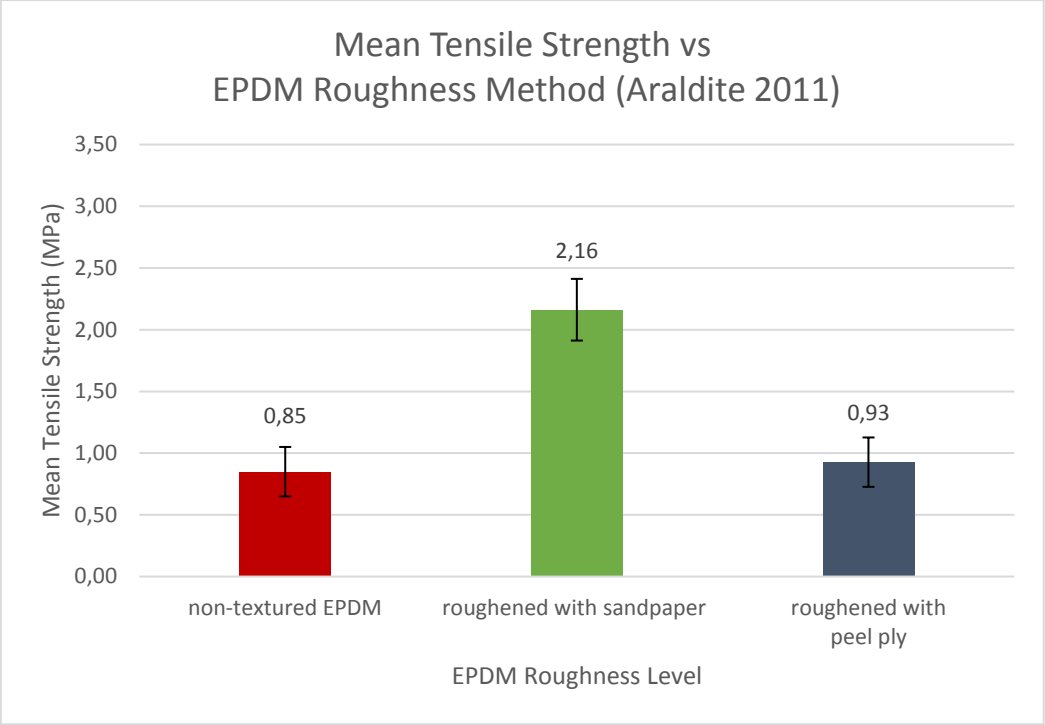


Figure 4.18 The Mean Tensile Strength vs EPDM Roughness Method for Araldite 2011

In tensile test specimens prepared with Araldite 2011, the average tensile strength on unroughened EPDM surfaces was measured as 0.85 MPa. When the EPDM surface was roughened with sandpaper, this value increased to 2.16 MPa, representing an increase of approximately 154% compared to the unroughened surface. On EPDM surfaces roughened with peel ply, the average tensile strength was measured as 0.93 MPa, showing only a limited increase of approximately 9% compared to unroughened surfaces. These results demonstrate that the EPDM surface roughening method is highly decisive for bond strength for Araldite 2011, with sandpaper being by far the most effective method.

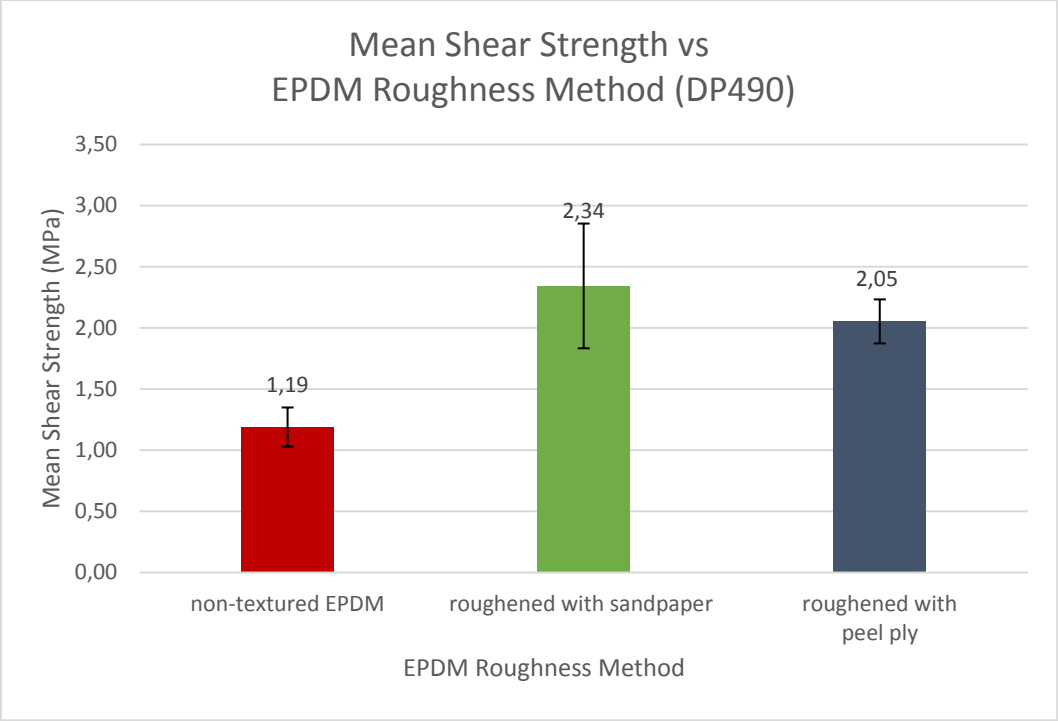


Figure 4.19 The Mean Shear Strength vs EPDM Roughness Method for DP490

Shear tests provide results that complement tensile tests in terms of evaluating load transfer at the EPDM-adhesive interface. In samples prepared with DP490, the average shear strength on unroughened EPDM surfaces was measured as 1.19 MPa. When the EPDM surface was roughened with sandpaper, the average shear strength increased to 2.34 MPa, resulting in an increase of approximately 97%. On EPDM surfaces roughened with peel ply, the average shear strength was measured as 2.05 MPa, a lower value compared to surfaces roughened with sandpaper.

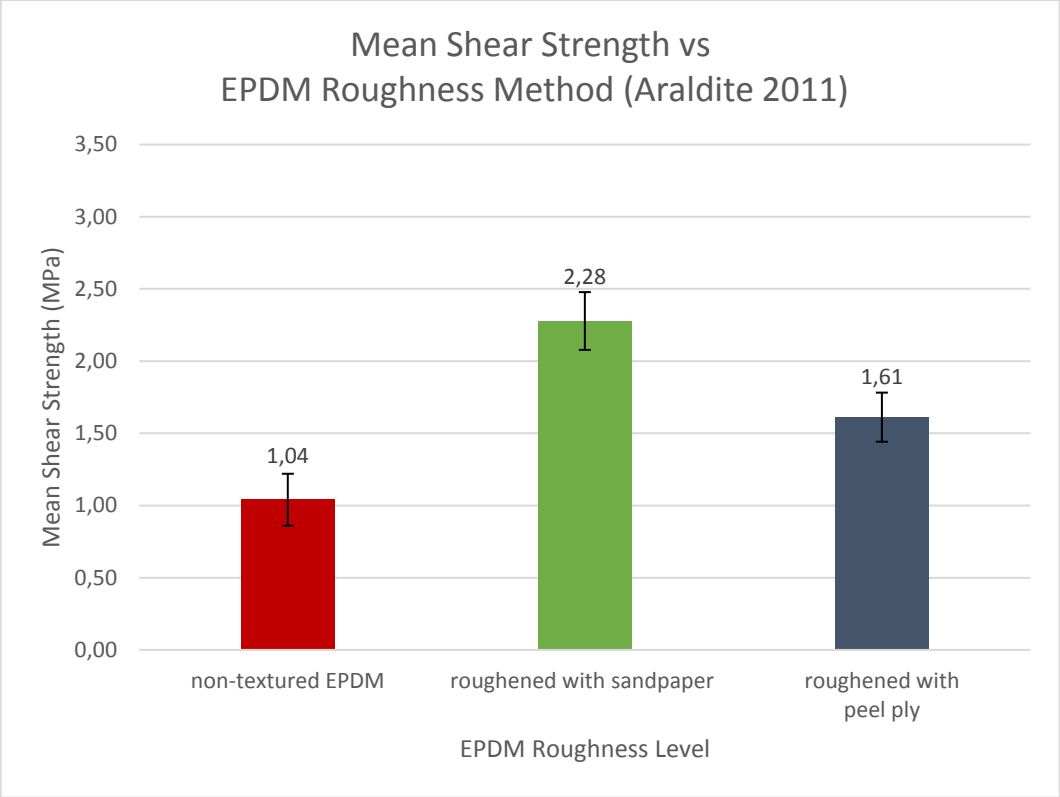


Figure 4.20 The Mean Shear Strength vs EPDM Roughness Method for Araldite 2011

A similar trend was observed in shear tests performed with Araldite 2011. While the average shear strength on unroughened EPDM surfaces was 1.04 MPa, this value increased to 2.28 MPa on EPDM surfaces roughened with sandpaper, resulting in an increase of approximately 119%. On EPDM surfaces roughened with peel ply, the average shear strength was measured as 1.61 MPa; although this value shows an increase of approximately 55% compared to unroughened surfaces, it remains below that of surfaces roughened with sandpaper. This reveals that for Araldite 2011, not only the presence of roughness created on the EPDM surface but also the morphology and continuity of the roughness determine the bonding behavior.

When all tensile and shear test results are evaluated together, it is seen that roughening the EPDM surface with sandpaper provides the highest bond strengths for both adhesives. Surface roughness measurements were performed on the selected

EPDM samples to observe the difference in roughness created by the roughening methods. The roughness values were found to be Ra ≈ 0.6 μm-1 μm on average for unroughened EPDM surfaces, Ra ≈ 5.5 μm-7 μm for EPDM surfaces roughened with sandpaper, and Ra ≈ 9 μm-12.5 μm for EPDM surfaces roughened with peel ply. These results show that the bond strength does not increase linearly with EPDM surface roughness; on the contrary, it reaches its maximum within a certain roughness range.

The moderate and more homogeneous roughness obtained by sandpapering allowed the adhesive to effectively penetrate the EPDM surface and establish a continuous mechanical locking mechanism. In contrast, the higher roughness values (Ra ≈ 12.5 μm) measured on EPDM surfaces roughened with peel ply may have led to the formation of excessive and irregular topographic structures on the surface. The inability of the adhesive to fully penetrate deep grooves on such surfaces, the formation of local air voids, and the reduction of the effective contact area along the interface explain the lower bond strength compared to sandpaper roughened surfaces. Therefore, these findings demonstrate that not only the roughness level but also an optimum roughness range and the continuity of surface morphology are critical for bond behavior at the EPDM-adhesive interface.

Failure mode analyses revealed that in all sample groups, failure predominantly occurred at the EPDM-adhesive interface with an adhesive character, and no significant cohesive failure occurred within the EPDM's own volume. However, rubber particles transfer onto the adhesive after failure was observed only on EPDM surfaces roughened with sandpaper. This indicates that sandpaper increased EPDM-adhesive adhesion compared to unroughened and peel-ply roughened surfaces; however, the system is still not at a level to achieve complete cohesive EPDM failure. The partial removal of the weak boundary layer on the EPDM surface by sandpaper, revealing a fresher and more active elastomer surface, and the increase in mechanical interlocking are considered the main mechanisms explaining this behavior.

To better understand the effect of different EPDM surface roughening methods on bonding behavior, unroughened, peel-ply roughened, and sandpaper-roughened EPDM surfaces were examined using scanning electron microscopy (SEM) and energy dispersive X-ray spectroscopy (EDS). SEM images of unroughened EPDM surfaces generally exhibited a relatively smooth surface structure but showed local particle formations and heterogeneous regions. EDS analyses revealed the presence of silicon (Si) and calcium (Ca) elements, in addition to carbon and oxygen. While the Si element is attributed to the silica filler present in the EPDM formulation, the absence of the Ca element among the EPDM components indicates the presence of impurities or contamination on the surface. Such calcium-based surface residues can negatively affect EPDM–adhesive interaction by forming a weak boundary layer for bonding.

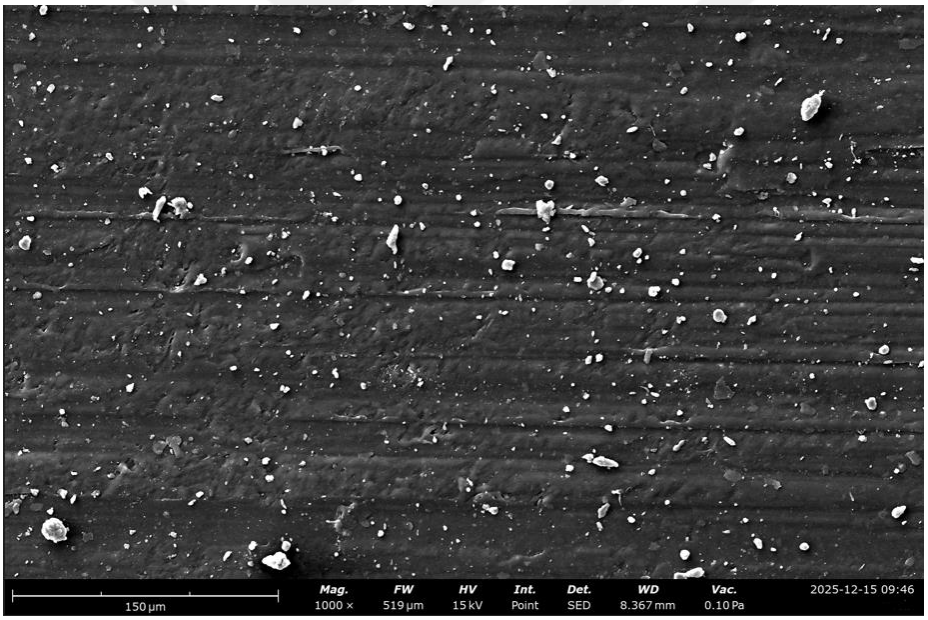


Figure 4.21 SEM Image of Unroughened EPDM

Table 4.3 EDS Analysis of Unroughened EPDM

Element Number	Element Symbol	Element Name	Atomic Conc. [%]	Weight Conc. [%]
6	C	Carbon	44.45	29.40
8	O	Oxygen	35.30	31.10
11	Na	Sodium	0.55	0.70
13	Al	Aluminum	1.48	2.20
14	Si	Silicon	5.17	8.00
17	Cl	Chlorine	0.56	1.10
19	K	Potassium	0.79	1.70
20	Ca	Calcium	11.69	25.80

SEM images of peel-ply roughened EPDM surfaces show a coarser surface topography compared to the unroughened state; however, this roughness exhibits a distinct orientation and irregularity. EDS results revealed that the presence of the Si element, corresponding to the silica filler, persists, while the Ca element shows a heterogeneous distribution across the surface. This indicates that the peel-ply method partially removes some weak boundary layers on the surface but does not completely eliminate Ca-related surface contaminations. It is thought that the resulting irregular and oriented surface morphology limits the homogeneous penetration of the adhesive into the EPDM surface, leading to local contact losses.

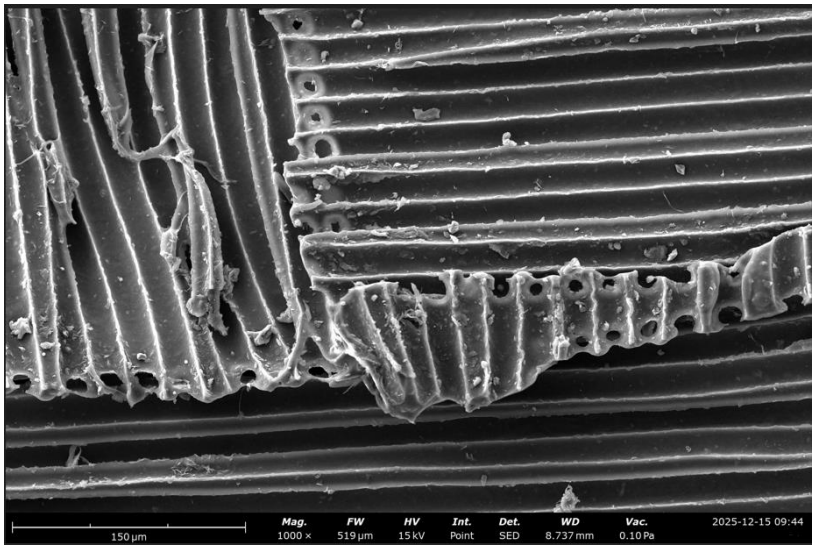


Figure 4.22 SEM Image of EPDM Roughened with Peel Ply

Table 4.4 EDS Analysis of EPDM Roughened with Peel Ply

Element Number	Element Symbol	Element Name	Atomic Conc. [%]	Weight Conc. [%]
6	C	Carbon	82.23	69.70
8	O	Oxygen	7.17	8.10
14	Si	Silicon	9.18	18.20
20	Ca	Calcium	1.41	4.00

In contrast, SEM images of EPDM surfaces roughened with sandpaper revealed a significantly different morphology. Sandpaper resulted in a more homogeneous, controlled, and continuous roughness on the surface; furthermore, it was observed that the aramid fibers within the EPDM matrix were partially exposed to the surface. EDS analysis revealed the presence of silicon (Si) and nitrogen (N) elements, along with carbon and oxygen, respectively, confirming the presence of silica filler and aramid fibers on the surface.

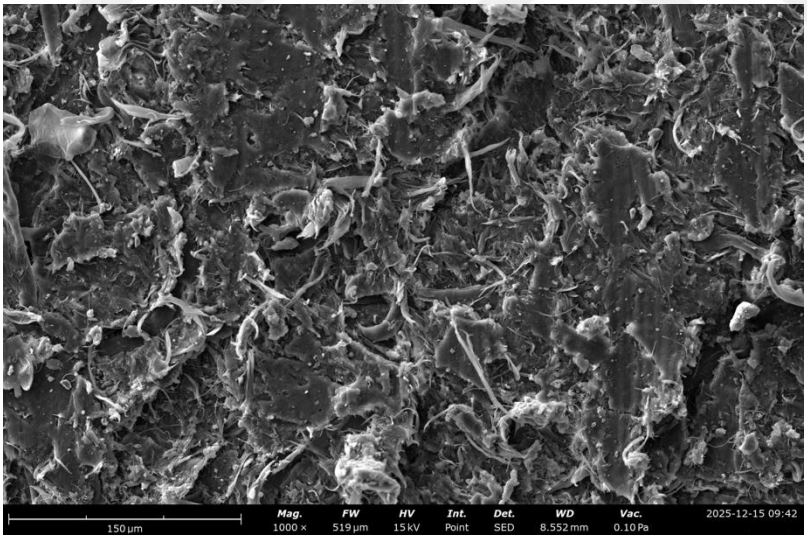


Figure 4.23 SEM Image of EPDM Roughened with Sandpaper

Table 4.5 EDS Analysis of EPDM Roughened with Sandpaper

Element Number	Element Symbol	Element Name	Atomic Conc. [%]	Weight Conc. [%]
6	C	Carbon	74.97	66.70
7	N	Nitrogen	4.24	4.40
8	O	Oxygen	16.03	19.00
14	Si	Silicon	4.76	9.90

Fiber-like structures, evident in SEM analysis of sandpaper roughened EPDM samples, constitute one of the most critical morphological findings obtained in this study. The exposure of aramid or polyamide-derived synthetic reinforcement elements, present as strength enhancers within the EPDM matrix, by aggressive mechanical abrasion (sandpaper) tear off the passive polymer layer on the surface, one fundamental mechanism directly affecting adhesion performance. Firstly, in a process described as micro-anchoring and mechanical interlocking, viscosity-optimized structural adhesives (especially DP490) penetrate the microscopic voids of these fibers, which emerge perpendicularly or at an angle to the surface, hardening and forming a root-like adhesion system at the interface. This fiber effect maximizes load transfer capacity by creating a physical bridge between the adhesive phase and the elastomeric matrix. Secondly, from a failure mechanics perspective, the propagation of microscopic cracks initiated at the interface under both tensile and shear loading is inhibited by these high-strength fiber barriers. According to this phenomenon, referred to in the literature as crack pinning or crack blunting, when the crack tip encounters these stiff fibers, it requires much higher energy to progress or is forced to change direction. Consequently, the fact that the sandpaper roughening method exceeds other surface preparation techniques by providing the highest tensile and shear strength values can be justified by both the static mechanical interlocking and dynamic crack resistance provided by these exposed fibers. In contrast, signals for the Ca element were significantly reduced on sandpaper roughened surfaces compared to unroughened and peel-fabric-roughened surfaces. This indicates that the roughening with sandpaper process partially removes calcium-based impurities

and the weak boundary layer on the surface, resulting in a fresher and more active elastomer surface.

When SEM and EDS findings are considered together, the more homogeneous roughness obtained on sandpaper roughened EPDM surfaces, the exposure of aramid fibers to the surface, and the reduction of Ca-related surface contaminants can be directly correlated with the higher tensile and shear strengths observed in mechanical tests. Conversely, the irregular morphology and surface contaminants observed on unroughened and peel-ply roughened EPDM surfaces are considered the primary microstructural factors explaining the lower bond strengths obtained on these surfaces.

4.4 Investigation of EPDM Surface Activation and Time Effect with Plasma Application

In the previous stage, the aim was to improve the EPDM-adhesive interface by roughening the EPDM surface using mechanical methods (roughening with sandpaper and peel ply application). In this stage, atmospheric plasma application, a physicochemical surface modification method, was used to further enhance the bond performance of mechanically activated EPDM surfaces. The aim of atmospheric plasma treatment was to alter the chemical structure and surface energy of the EPDM surface, thereby strengthening the interaction with the adhesive. In this context, the effect of different plasma application times on the bond strength at the EPDM-adhesive interface was evaluated using tensile and shear tests.

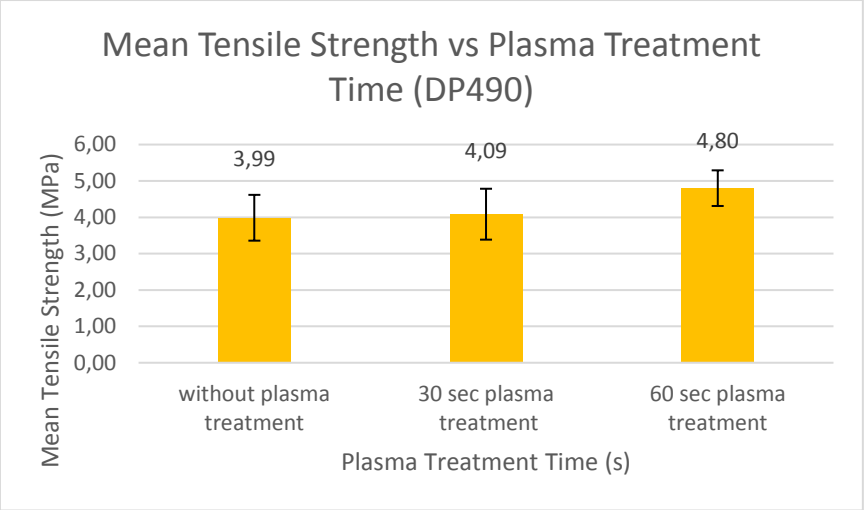


Figure 4.24 The Mean Tensile Strength vs Plasma Treatment Time for DP490

In tensile test specimens produced using DP490, the average tensile strength for EPDM surfaces without plasma application was measured as 3.99 MPa, while this value increased to 4.09 MPa after 30 seconds of plasma application and reached 4.80 MPa after 60 seconds of plasma application. Accordingly, a 60 second plasma application resulted in approximately a 20% increase in tensile strength for DP490 compared to the plasma-free condition.

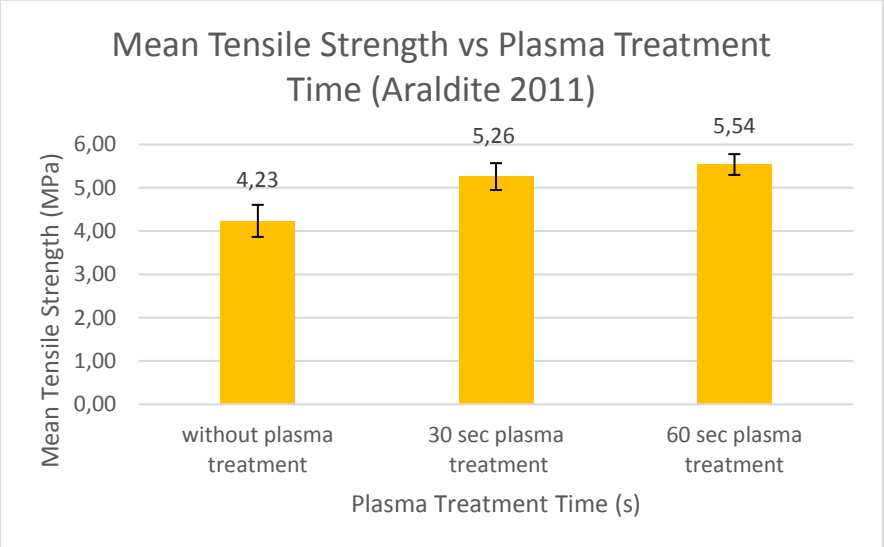


Figure 4.25 The Mean Tensile Strength vs Plasma Treatment Time for Araldite 2011

In tensile test specimens using Araldite 2011, the plasma effect was even more pronounced, with the average tensile strength measured on plasma-free EPDM surfaces increasing from 4.23 MPa to 5.26 MPa after 30 seconds of plasma treatment, and to 5.54 MPa after 60 seconds of plasma treatment. These results correspond to an approximately 31% increase in tensile strength at the maximum plasma duration for Araldite 2011 compared to the plasma-free condition.

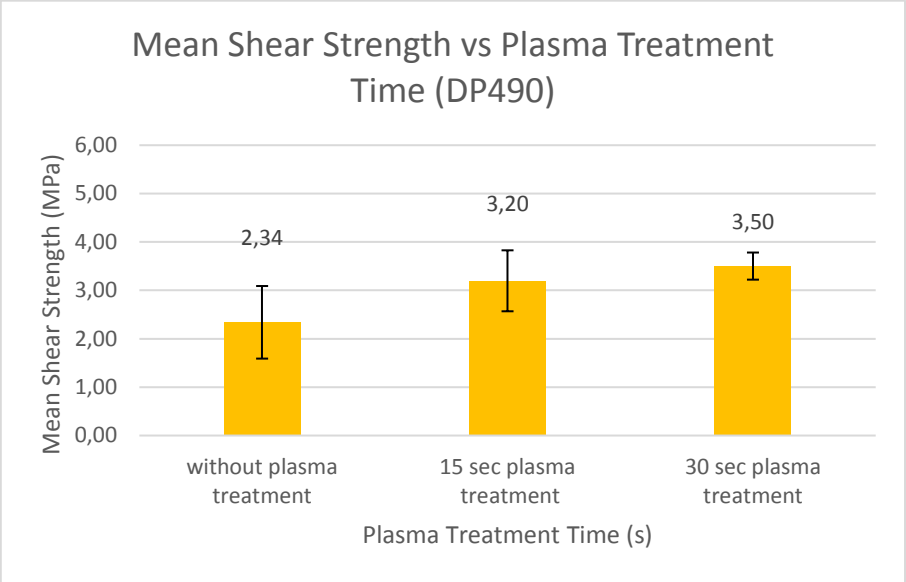


Figure 4.26 The Mean Shear Strength vs Plasma Treatment Time for DP490

When shear tests were examined, the effect of plasma application was even more pronounced compared to tensile tests. In shear test specimens prepared with DP490, the average shear strength on EPDM surfaces without plasma application was measured as 2.34 MPa; After 15 seconds of plasma application, this value increased to 3.20 MPa, and after 30 seconds of plasma application, it increased to 3.50 MPa. This increase corresponds to an improvement of approximately 50% for the maximum plasma time compared to the plasma-free case.

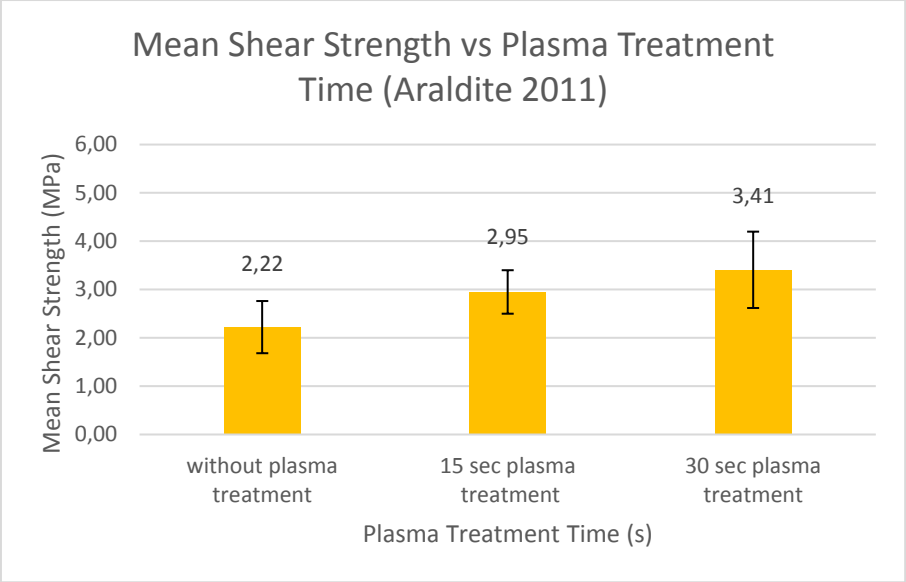


Figure 4.27 The Mean Shear Strength vs Plasma Treatment Time for Araldite 2011

Similarly, in shear tests using Araldite 2011, the average strength of 2.22 MPa measured for plasma-free EPDM surfaces increased to 2.95 MPa with 15 seconds of plasma application and to 3.41 MPa with 30 seconds of plasma application, indicating an increase of approximately 54%.

The increase in bond strength observed on the EPDM surface with atmospheric plasma application can primarily be explained by the chemical and physical activation of the surface. During plasma treatment, the EPDM surface is exposed to high-energy ions, radicals, and UV photons; as a result of this interaction, low-energy weak boundary layers (e.g., processing residues, low molecular weight chain ends, and contaminants) on the surface are removed, and the surface energy is significantly increased. Furthermore, limited chain breaks occur in the surface regions of the EPDM chains, making it possible for oxygen-containing polar functional groups (such as –OH, –C=O, –COOH) to form. These functional groups contribute to better wetting of the EPDM surface by the adhesive and increase physical and chemical interactions at the interface. The fact that this activation effect becomes more pronounced with increasing plasma time explains the trend of increasing bond strength; however, since there is a risk of excessive oxidation or

chain breakdown of the surface in excessive plasma applications, it is understood that application time is a critical parameter.

The fact that plasma application yields more effective results on EPDM surfaces roughened by sandpaper can be explained by considering the morphological and chemical changes on the surface together. The sandpapering process causes the aramid fibers within the EPDM matrix to be partially exposed to the surface; the nitrogen containing amide groups in the chemical structure of these fibers can participate in stronger secondary bond interactions (especially hydrogen bonds and dipole-dipole interactions) with adhesive systems under plasma-activated surface conditions. Although direct chemical covalent bond formation cannot be claimed, the exposure of aramid fibers to the surface and the increase in plasma-activated polar functional groups may have created a stronger and more stable interaction environment at the EPDM-adhesive interface. This situation is considered as a possible mechanism explaining why bond strength reaches its highest values, especially on sandpaper roughened and plasma-applied EPDM surfaces, and why failure moves away from the interface, evolving towards a more resistant bond structure.

4.5 Evaluation of Adhesion Behaviors Based on Wetting and Mechanical Interlocking Mechanisms

The experimental results obtained in this study reveal that in EPDM-metal adhesion systems, bond strength cannot be explained only by the mechanical properties of the adhesive or the polymeric or metallic nature of the bonded materials; it is primarily determined by the effective contact conditions achieved at the interface. These contact conditions, which play a role in the formation of the adhesion mechanism, can be evaluated through two main complementary processes: the wetting mechanism, which enables the adhesive to establish molecular-level contact with the substrate surface, and the mechanical interlocking mechanism, which contributes to maintaining this contact under mechanical loads. Experimental findings show that

these two mechanisms are not independent but hierarchical and collaborative processes.

Wetting is the most fundamental and prerequisite step in adhesion formation. Sufficient spreading of the adhesive on the substrate surface and its ability to establish close molecular contact with the surface makes it possible to create a continuous and flawless contact area along the interface. This process is directly controlled by the relationship between the surface energy of the substrate material and the surface tension of the adhesive. On surfaces with high surface energy, the adhesive exhibits a lower contact angle, spreading across the surface and penetrating microscopic surface irregularities.

Metal surfaces are naturally well-wetted by epoxy-based adhesives due to their high surface energy and polar surface oxides. In this study, mechanical roughening treatments applied to metal surfaces not only altered the surface topography but also indirectly improved the wetting behavior of the adhesive. The micro-scale asperities created by roughening prevented the adhesive from bridging the surface, allowing for a wider contact area with the surface; thus, the formation of discontinuous voids at the interface was minimized. The cohesive failure within adhesive which was observed in metal-to-metal bonding experiments, especially in samples using DP490, clearly shows that effective wetting was achieved at the metal-adhesive interface and that the bond strength was limited by the adhesive's own cohesive strength rather than the interface. This indicates that the metal surface preparation reached a sufficient level in terms of both wetting and mechanical bonding.

In contrast, EPDM surfaces cannot be effectively wetted by epoxy-based adhesives due to their low surface energy, nonpolar chemical structure, and limited surface reactivity. At the EPDM-adhesive interface, adhesive diffusion is limited, the contact angle is high, and this significantly reduces the effective molecular contact area established with the surface. As a result, the adhesive cannot sufficiently penetrate the surface asperities, leading to the formation of weak boundary layers and discontinuous contact zones at the interface. These insufficient wetting conditions

constitute the primary reason for the low adhesion strengths and predominant adhesion damage observed at the EPDM-adhesive interface. In this context, the higher adhesion performance exhibited on metal surfaces, despite both the adhesive and EPDM being polymeric in structure, can be explained not by the chemical similarity of the materials, but by the wetting conditions achieved at the interface.

In systems where wetting conditions are provided or improved, the mechanical interlocking mechanism comes into play as a second and complementary process supporting bond strength. Roughening treatments applied to metal surfaces have allowed the adhesive to penetrate into the surface asperities and mechanically interlock; this has contributed to increased bond strength, especially under shear loads. Similarly, mechanical roughening methods (sandpaper, peel-ply applications) applied to EPDM surfaces have increased the mechanical interlocking potential by altering the surface topography. However, experimental results clearly show that mechanical interlocking alone is not a determinant of bond strength on EPDM surfaces where sufficient wetting is not achieved; mechanical interlocking only makes a significant contribution when combined with effective wetting.

Therefore, atmospheric plasma treatment applied to EPDM surfaces should be evaluated in conjunction with mechanical roughening. Plasma application has increased the surface energy by introducing polar functional groups to the EPDM surface, enabling the adhesive to wet the surface more effectively. This improvement in wetting conditions also increased the effectiveness of asperities created by mechanical roughening; thus, the mechanical interlocking mechanism became more effective at the interface. As a result of the combined action of these two mechanisms, it was observed that the bond strength at the EPDM-adhesive interface increased significantly, and the failure modes evolved from adhesive failure to mixed or cohesive failure.

In conclusion, this study reveals that wetting is a fundamental and decisive prerequisite for achieving high bond strength in EPDM-metal adhesion systems, while mechanical interlocking acts as a complementary mechanism that comes into

play after this condition is met. While naturally occurring favorable wetting conditions on metal surfaces, supported by mechanical roughening, make it possible to achieve high and stable bond strengths; similar performance on EPDM surfaces requires both an increase in surface energy and the activation of mechanical interlocking. In this context, the surface preparation and optimization strategy followed in this study offers a mechanism-based approach consistent with experimental findings.

4.6 Mechanical and Interfacial Evaluation of the Difference Between Tensile and Shear Test Results in EPDM-Metal Bonding Systems

This study found that shear testing on EPDM-metal bond systems yielded much greater strength levels than tensile tests. This variation is not due to test geometry or sample dimensions; rather, it is directly related to the stress state formed at the interface because of the type of loading applied and how the bonding mechanisms are engaged. Tensile and shear tests should be considered as complementary evaluation methods that represent various mechanical and interfacial characteristics of the EPDM-metal bond system.

In tensile testing, the load is applied mainly perpendicular to the bond interface, resulting in opening-type stresses at the interface. Under this loading scenario, discontinuous contact regions, weak boundary layers, and insufficiently wetted areas along the interface are directly stressed, making them ideal locations for crack initiation. These weak regions, particularly those formed at the EPDM-adhesive interface due to low surface energy and restricted wetting, are crucial in determining bond strength under tensile loads. Tensile tests provide a highly sensitive evaluation of interface quality and wetting continuity in EPDM-metal bond systems.

In shear testing, the applied force acts parallel to the bond interface, distributing stresses over a larger area of the interface. Instead of a sudden opening, friction, shear, and deformation mechanisms are activated, allowing the bond to withstand

higher stress. Mechanical roughening treatments performed to the EPDM surface provide micro-scale irregularities that allow the adhesive to mechanically lock into these regions under shear loads, hence improving the effectiveness of the mechanical interlocking mechanism. This is one of the main reasons why the strength values measured in shear tests are higher compared to tensile tests.

The strength difference between tensile and shear tests became more obvious after mechanical roughening and atmospheric plasma treatments were applied to the EPDM surface. While the wetting conditions improved by plasma application contribute to bond strength by increasing interface integrity under tensile loads, mechanical roughening forms surface irregularities that make the mechanical locking mechanism more efficient, particularly under shear loads. The combination of these two factors has resulted in greater increases in shear strength than tensile strength in EPDM-metal bonding systems.

As a result, shear tests in EPDM-metal bonding systems yield higher strength values due to better mechanical interlocking and load distribution. Tensile tests, on the other hand, are crucial for determining limiting mechanisms, especially wetting and interface continuity at the EPDM-adhesive interface. When these two test methods are combined, the behavior of EPDM-metal bonding systems under mechanical loads can be examined more comprehensively and reliably.

CHAPTER 5

CONCLUSION

In this thesis, the surface preparation parameters determining the bond strength in EPDM-metal bonding systems were investigated with a holistic approach, and the experimental program was designed in a stepwise manner to systematically isolate and improve the adhesion-limiting interfaces within the EPDM–metal bonding system. Metal surface roughness and cleanliness level, EPDM surface roughening methods, and atmospheric plasma application were evaluated in complementary stages; thus, the mechanical and physicochemical foundations of bond behavior in EPDM-metal bonding systems were clarified. Figure 5.1 schematically summarizes the experimental strategy adopted in this study.

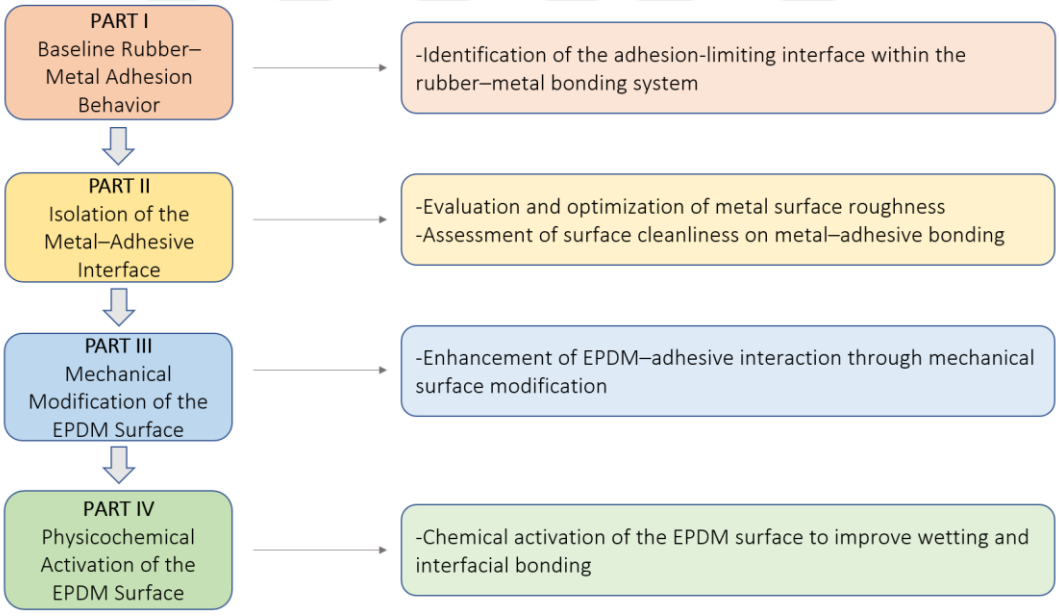


Figure 5.1 Schematic Illustration of the Experimental Strategy Adopted in the Study to Investigate and Optimize Rubber–Metal Adhesion

In the first stage, where the effect of metal surface roughness and cleanliness level on EPDM-metal bond strength was examined, it was shown that these parameters did not create a significant, consistent, and unidirectional correlation on bond strength. Failure mode analyses, especially in tensile tests, revealed that failure occurred predominantly at the EPDM-adhesive interface, experimentally proving that the main factor limiting bond performance in this system is not the metal-adhesive interface, but the EPDM-adhesive interface. This finding was the fundamental conclusion that determined the direction of the subsequent stages of the study.

In metal-to-metal bonding experiments, different bonding behaviors were observed depending on the type of adhesive used when the metal-adhesive interface was isolated. The predominance of cohesive failure within adhesive in samples using DP490 indicates that metal surface preparation parameters are not a limiting factor in bond strength. In contrast, in samples using Araldite 2011, it was determined that bond strength was sensitive to metal surface roughness, and the highest shear strength was obtained in the Ra 4–8 μm roughness range and 0–50 RFU cleanliness level. This result clearly shows that metal surface optimization only becomes meaningful in systems where the metal-adhesive interface is the limiting factor.

In mechanical roughening studies which was conducted to improve the EPDM-adhesive interface, remarkable increases in bond strength were obtained. Compared to smooth EPDM surfaces, bond strength on sandpaper-roughened EPDM surfaces increased by approximately 118% in tensile tests and 97% in shear tests for DP490. In systems using Araldite 2011, these increases were determined to be 154% and 119%, respectively. These increases demonstrate that in EPDM-metal bonding systems, bond strength is strongly related not only to surface energy but also to the continuity of surface morphology and effective mechanical interlocking. Surface roughness measurements and SEM-EDS analyses revealed that a moderate and homogeneous roughness (Ra ≈ 5.5 μm) obtained by sanding provides more effective interface contact and maximizes bond strength compared to excessively rough EPDM surfaces (Ra ≈ 12.5 μm).

Modification of mechanically activated EPDM surfaces by sandpaper with atmospheric plasma further improved bond performance. Compared to non-plasma EPDM surfaces, for DP490, tensile strength increased by approximately 20% and shear strength by 50% at maximum plasma duration; For Araldite 2011, an additional increase of 31% in tensile strength and 54% in shear strength was achieved. These findings demonstrate that atmospheric plasma application significantly improves bond strength, especially under shear loads, by increasing surface energy on the EPDM surface, eliminating weak boundary layers, and strengthening interface interactions.

In conclusion, this thesis clearly demonstrates that the EPDM-adhesive interface is the fundamental interface determining bond strength in EPDM-metal bonding systems; the effect of metal surface preparation parameters is secondary when this interface is not limiting. Mechanically roughening the EPDM surface followed by physicochemical activation with atmospheric plasma has been identified as the most effective surface preparation strategy for progressively and consistently improving bond performance. This study provides an experimental and holistic contribution to the literature on elastomer-metal bonding mechanisms and offers important implications for the scientifically based design of surface preparation strategies in EPDM-metal bonding applications.

CHAPTER 6

FINAL REMARKS and FUTURE WORK

This study investigated metal-adhesive and polymer (EPDM)-adhesive interfaces in a solid rocket motor insulation system, as schematically shown in Figure 6.1. The figure shows the metal case, adhesive layer, polymer insulation, liner, and propellant. Important surface preparation parameters such as surface roughness, surface cleanliness, and plasma treatment are also specified for the metal and polymer interfaces.

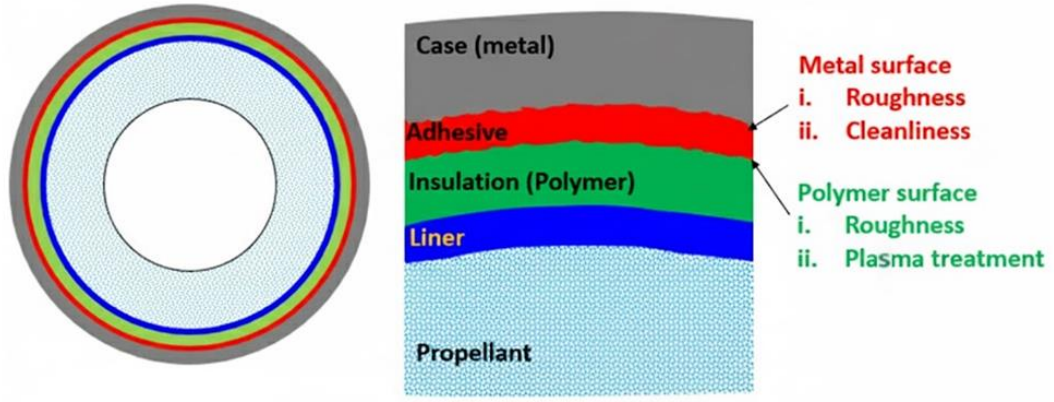


Figure 6.1 Schematic Cross-section of the Solid Rocket Motor Assembly

The results show that the DP-490 adhesive forms stronger bonds with the metal case compared to the polymer insulation. This is due to the favorable surface properties of the metal surface, such as roughness and cleanliness, as shown in the figure. To address the relatively weak polymer–adhesive interface, the polymer surface was mechanically roughened and subsequently treated with plasma, which resulted in a noticeable improvement in bond strength.

After these surface modifications, failure was no longer observed at the interface; instead, cohesive failure occurred within the EPDM. This shift in failure mode

indicates that the interfacial bond strength exceeded the intrinsic strength of the rubber. From this perspective, the results suggest that, as failure predominantly occurs within the EPDM following interfacial strengthening, future studies should focus on enhancing the mechanical performance of the adhesive system as well as increasing the cohesive strength of the EPDM material itself.

Possible optimization strategies include increasing the cohesive strength and toughness of the adhesive layer, tailoring adhesive ductility to better accommodate the viscoelastic behavior of EPDM, and improving chemical compatibility between the adhesive and EPDM phases. In addition, EPDM side modifications such as the incorporation of reinforcing fillers such as surface-modified carbon black, optimization of fiber content and orientation, and the use of suitable binders such as silane coupling agents can further enhance interfacial interactions. These approaches can improve the overall mechanical integrity and long-term reliability of the solid rocket motor insulation system by increasing tensile and shear strengths.

REFERENCES

3M Company. (2022). *3M™ Scotch-Weld™ epoxy adhesive DP-490: Technical data sheet*. 3M Industrial Adhesives and Tapes Division.

Adams, R. D., & Wake, W. C. (1984). *Structural adhesive joints in engineering*. Elsevier Applied Science Publishers.

ASM International. (1990). *Properties and selection: Irons, steels, and high-performance alloys* (Vol. 1). ASM International.

Bakkal, M., Osmanoğlu, H., & Bodur, M. S. (2022). Effect of surface treatments on the interfacial strength for metal/composite hybrid joints. *Journal of the Faculty of Engineering and Architecture of Gazi University*, *37*(2), 1033–1046.

Baldan, A. (2004). Adhesively-bonded joints in metallic alloys, polymers and composite materials: Mechanical and environmental durability performance. *Journal of Materials Science*, *39*, 4729–4797. https://doi.org/10.1023/B:JMSC.0000035317.87118.ab

Baldan, A. (2012). Adhesively-bonded joints and repairs in metallic alloys, polymers and composite materials: Adhesives, adhesion theories and surface pretreatment. *Journal of Materials Science*, *47*, 1–49. https://doi.org/10.1007/s10853-011-5884-3

Briggs, D., & Grant, J. T. (2003). *Surface analysis by Auger and X-ray photoelectron spectroscopy*. IM Publications.

Clearfield, H. M., McNamara, D. K., & Davis, G. D. (1991). Adherend surface preparation for structural adhesive bonding. In L. H. Lee (Ed.), *Adhesive bonding* (pp. 203–237). Springer. https://doi.org/10.1007/978-1-4757-9006-1_8

Critchlow, G. W., & Brewis, D. M. (1996). Review of surface pretreatments for aluminium alloys. *International Journal of Adhesion and Adhesives*, *16*(4), 255–275. https://doi.org/10.1016/S0143-7496(96)00014-0

Culick, F. E. C. (2001). Solid propellant combustion. In *Combustion of energetic materials* (pp. 43–72). Springer.

da Silva, L. F. M., Öchsner, A., & Adams, R. D. (2011). *Handbook of adhesion technology*. Springer.

Debnath, D., Jadhav, K. B., Erande, S. N., Gopale, P. T., Daware, C. R., & Vishwakarma, A. K. (2018). An innovative method for measurement of insulation thickness of fired solid rocket motor. *International Journal of Applied Engineering Research*, *13*(18), 13985–13988.

Ebnesajjad, S., & Ebnesajjad, C. (2013). *Surface treatment of materials for adhesive bonding* (2nd ed.). William Andrew Publishing. https://doi.org/10.1016/C2013-0-12914-5

Elashker, A., Zaghloul, B., Eldakhakhny, A. M., Gobara, M., & Mokhtar, M. (2023). Study of thermal protection materials in solid propellant rocket engines. In *Proceedings of the International Conference on Aerospace Sciences and Aviation Technology* (Vol. 20, pp. 1–10).

Friedrich, J. (2012). *The plasma chemistry of polymer surfaces: Advanced techniques for surface design*. Wiley.

Ghumatkar, A. K., Budhe, S., Sekhar, R., Banea, M. D., & Barros, S. (2016). Influence of adherend surface roughness on the adhesive bond strength. *Latin American Journal of Solids and Structures*, *13*(13), 2356–2370. https://doi.org/10.1590/1679-78253066

Goldstein, J. I., Newbury, D. E., Michael, J. R., Ritchie, N. W., Scott, J. H. J., & Joy, D. C. (2017). *Scanning electron microscopy and X-ray microanalysis*. Springer.

Grythe, K. F., & Hansen, F. K. (2006). Surface modification of EPDM rubber by plasma treatment. *Langmuir*, *22*(14), 6109–6124. https://doi.org/10.1021/la053471d

Guo, X., & Zhang, N. (2015). Pulsed thermographic evaluation of disbonds in the insulation of solid rocket motors made of elastomers. *Journal of Thermal Science and Engineering Applications*, *7*(4), 041004. https://doi.org/10.1016/j.polymertesting.2015.04.015

Hamdi, M., Saleh, M. N., & Poulis, J. A. (2020). Improving the adhesion strength of polymers: Effect of surface treatments. *Journal of Adhesion Science and Technology*, *34*(17), 1853–1870. https://doi.org/10.1080/01694243.2020.1732750

Hegemann, D., Brunner, H., & Oehr, C. (2003). Plasma treatment of polymers for surface and adhesion improvement. *Nuclear Instruments and Methods in Physics Research Section B*, *208*, 281–286. https://doi.org/10.1016/S0168-583X(03)00644-X

Henkel AG & Co. KGaA. (2023). *Araldite® 2011 epoxy adhesive: Technical data sheet*. Henkel Adhesive Technologies.

Humble, R. W., Henry, G. N., & Larson, W. J. (1995). *Space propulsion analysis and design*. McGraw-Hill.

Huzel, D. K., & Huang, D. H. (1992). *Modern engineering for design of liquid-propellant rocket engines* (2nd ed.). AIAA.

Kanerva, M., & Saarela, O. (2013). The peel ply surface treatment for adhesive bonding of composites: A review. *International Journal of Adhesion and Adhesives*, *43*, 60–69. https://doi.org/10.1016/j.ijadhadh.2013.01.014

Khan, M. H., Gali, O. A., Edrisy, A., & Riahi, A. R. (2016). Effect of oxidation and surface roughness on the shear strength of single-lap-joint adhesively bonded

metal specimens. *Applied Adhesion Science*, *4*, Article 21. https://doi.org/10.1186/s40563-016-0077-1

Kinloch, A. J. (1987). *Adhesion and adhesives: Science and technology*. Springer.

Kostyuk, A. V., Ignatenko, V. Y., Antonov, S. V., & Ilyin, S. O. (2019). Effect of surface contamination on the durability and strength of stainless steel–polyisobutylene pressure-sensitive adhesive bonds. *International Journal of Adhesion and Adhesives*, *95*, 102434. https://doi.org/10.1016/j.ijadhadh.2019.102434

Kovács, P., Körömi, B., Weltsch, Z., & Berczeli, M. (2023). Investigation of the tensile strength of adhesive-bonded steels using surface treatments. Materials, 16(24), 7663. https://doi.org/10.3390/ma16247663

Lee, C.-J., Lee, S.-K., Ko, D.-C., Kim, D. J., & Kim, B. M. (2009). Evaluation of surface and bonding properties of cold rolled steel sheet pretreated by Ar/O_2 atmospheric pressure plasma. *Journal of Materials Processing Technology*, *209*(10), 4769–4775. https://doi.org/10.1016/j.jmatprotec.2008.11.043

Mahr GmbH. (2021). MarSurf PS 10 surface roughness measuring instrument: Technical data sheet. Mahr GmbH.

Mittal, K. L. (Ed.). (2013). *Contact angle, wettability and adhesion*. CRC Press.

Moraes, J. H., da Silva Sobrinho, A. S., Maciel, H. S., Dutra, J. C. N., Massi, M., Mello, S. A. C., & Schreiner, W. H. (2007). Surface improvement of EPDM rubber by plasma treatment. Journal of Physics D: Applied Physics, 40(24), 7747–7754. https://doi.org/10.1088/0022-3727/40/24/022

Moreira, F., Borges, C., Marques, E., & da Silva, L. (2022). Effect of surface contamination on the peel properties of adhesive joints. Journal on Mechanics of Solids, 1(1), 3–8. https://doi.org/10.24840/2975-8262_001-001_001798

National Aeronautics and Space Administration. (1971). *Solid rocket motor igniters* (NASA Special Publication SP-8051).

https://ntrs.nasa.gov/api/citations/19710020870/downloads/19710020870.pdf

Newbury, D. E., & Ritchie, N. W. (2015). Performing elemental microanalysis with high accuracy and high precision by SEM/SDD-EDS. *Journal of Materials Science*, *50*(2), 493–518. https://doi.org/10.1007/s10853-014-8685-2

Omairey, S., Jayasree, N. & Kazilas, M. Defects and uncertainties of adhesively bonded composite joints. *SN Appl. Sci.* 3, 769 (2021). https://doi.org/10.1007/s42452-021-04753-8

Owens, D. K., & Wendt, R. C. (1969). Estimation of the surface free energy of polymers. *Journal of Applied Polymer Science*, *13*(8), 1741–1747. https://doi.org/10.1002/app.1969.070130815

Packham, D. E. (2003). Surface energy, surface topography and adhesion. *International Journal of Adhesion and Adhesives*, *23*(6), 437–448. https://doi.org/10.1016/S0143-7496(03)00068-X

Petrie, E. M. (2007). Handbook of adhesives and sealants (2nd ed.). McGraw-Hill.

Purdue University. (n.d.). *Solid propellant rocket engine schematic* [Figure]. School of Aeronautics and Astronautics. https://engineering.purdue.edu/~propulsi/propulsion/rockets/solids.html

Relyon Plasma GmbH. (2022). *PiezoBrush® PZ3 atmospheric pressure plasma device: Technical data sheet*. Relyon Plasma GmbH.

Romero-Sánchez, M. D., Pastor-Blas, M. M., & Martín-Martínez, J. M. (2001). Adhesion improvement of SBR rubber by treatment with trichloroisocyanuric acid solutions in different esters. *International Journal of Adhesion and Adhesives*, *21*(4), 325–337. https://doi.org/10.1016/S0143-7496(01)00005-7

Santos, R. P. D., Oliveira, M. S. D., Mattos, E. D. C., Diniz, M. F., & Dutra, R. D. C. L. (2013). Study by FT-IR technique and adhesive properties of vulcanized

EPDM modified with plasma. *Journal of Aerospace Technology and Management*, *5*(1), 65–74. https://doi.org/10.5028/jatm.v5i1.163

Shirazi, M., & Noordermeer, J. W. (2011). Factors influencing reinforcement of NR and EPDM rubbers with short aramid fibers. Rubber Chemistry and Technology, 84(2), 187–199. https://doi.org/10.5254/1.3570531

SITA Messtechnik GmbH. (2021). Fluorescence-based measurement of surface cleanliness. SITA Messtechnik GmbH.

Sługocka, M., Grochała, D., Kwiatkowski, K., Grzejda, R., & Zmarzły, P. (2024). Study of the impact of surface topography on selected mechanical properties of adhesive joints. *Coatings*, *14*(8), 944. https://doi.org/10.3390/coatings14080944

Spaggiari, A., & Dragoni, E. (2013). Effect of mechanical surface treatment on the static strength of adhesive lap joints. *The Journal of Adhesion*, *89*(9), 677–696. https://doi.org/10.1080/00218464.2012.751526

Sutton, G. P., & Biblarz, O. (2017). *Rocket propulsion elements* (9th ed.). Wiley.

Thermo Fisher Scientific. (2021). *Phenom XL desktop scanning electron microscope: Technical specifications*. Thermo Fisher Scientific.

Uehara, K., & Sakurai, M. (2002). Bonding strength of adhesives and surface roughness of joined parts. *Journal of Materials Processing Technology*, *127*(2), 178–181. https://doi.org/10.1016/S0924-0136(02)00122-X

Whitehouse, D. J. (2011). *Handbook of surface and nanometrology* (2nd ed.). CRC Press.

Wypych, G. (2018). *Handbook of adhesion promoters* (2nd ed.). ChemTec Publishing.

Yang, V., Brill, T. B., & Ren, W. Z. (2000). *Solid propellant chemistry, combustion, and motor interior ballistics*. AIAA.

Zhao, Y., Jin, Z., Xu, B., Wang, Q., Feng, J., Li, X., & Guo, J. (2021). Effect of surface cleaning on interface bonding performance for 316H stainless steel joints manufactured by additive forging. *Materials & Design*, *210*, 110025. https://doi.org/10.1016/j.matdes.2021.110025

Zhou, Q.-C., Xu, J.-S., Chen, X., & Zhou, C.-S. (2016). Review of the adhesively bonded interface in a solid rocket motor. *The Journal of Adhesion*, *92*(5), 504–531. https://doi.org/10.1080/00218464.2015.1040155

APPENDICES

A. Roughness and Cleanliness Measurements of Samples and Test Results

BIT Test Coupon Samples	Surface Cleanliness Values (RFU)		Roughness Values (µm)				Maximum Load (N)	Tensile Stress at Maximum Load (MPa)	Mean Tensile Stress (MPa)	Adhesive	Cleanliness Level	Roughness Level
	First Coupon	Second Coupon	First Coupon		Second Coupon							
			Ra (µm)	Rz (µm)	Ra (µm)	Rz (µm)						
BIT–RM–R0–C0–A1–1	3,70	8,10	0,21	1,37	0,33	1,79	2141,80	1,89		DP-490	Clean Surface (0-50 RFU)	without sandblasting
BIT–RM–R0–C0–A1–2	4,00	6,10	0,39	2,03	0,34	2,26	2011,40	1,77				
BIT–RM–R0–C0–A1–3	3,40	3,50	0,28	1,72	0,43	3,30	1881,70	1,66	1,83			
BIT–RM–R0–C0–A1–4	3,20	4,40	0,21	1,35	0,31	1,87	2206,00	1,95				
BIT–RM–R0–C0–A1–5	3,20	4,10	0,17	1,25	0,63	3,84	2153,70	1,90				
BIT–RM–R1–C0–A1–1	7,20	8,20	0,36	9,70	1,33	10,26	3174,40	2,80				1-2 µm
BIT–RM–R1–C0–A1–2	7,30	8,60	0,68	11,44	1,82	13,09	4723,30	4,17				
BIT–RM–R1–C0–A1–3	10,30	14,60	1,56	10,92	1,54	10,74	3804,50	3,36	3,61			
BIT–RM–R1–C0–A1–4	6,20	14,80	1,02	8,12	1,07	7,07	4243,60	3,74				
BIT–RM–R1–C0–A1–5	9,00	19,60	1,67	12,34	1,41	8,88	3386,70	3,99				
BIT–RM–R2–C0–A1–1	9,50	8,20	2,78	21,08	2,99	21,99	4182,00	3,69				2-4 µm
BIT–RM–R2–C0–A1–2	9,90	9,40	3,50	32,05	3,61	21,86	3757,70	3,31				
BIT–RM–R2–C0–A1–3	8,40	8,60	3,55	22,62	3,66	23,77	3426,00	3,02	3,28			
BIT–RM–R2–C0–A1–4	7,80	7,10	3,21	18,72	3,00	22,97	3498,10	3,08				
BIT–RM–R2–C0–A1–5	7,60	7,60	3,94	23,10	3,98	24,23	3728,50	3,29				
BIT–RM–R3–C0–A1–1	5,70	5,80	4,14	23,15	4,11	27,02	3746,80	3,30				4-8 µm
BIT–RM–R3–C0–A1–2	15,80	4,90	4,70	30,72	4,74	27,48	5957,20	5,25				
BIT–RM–R3–C0–A1–3	5,00	4,70	4,40	27,53	4,42	27,05	4348,30	3,83	4,12			
BIT–RM–R3–C0–A1–4	4,20	4,50	4,23	24,29	4,28	24,94	3446,10	3,04				
BIT–RM–R3–C0–A1–5	5,40	4,50	4,72	26,13	4,36	27,55	5845,60	5,15				
BIT–RM–R0–C1–A1–1	105,60	107,60	0,24	1,40	0,18	1,15	2585,20	2,28			Moderately Contaminated (50-200 RFU)	without sandblasting
BIT–RM–R0–C1–A1–2	109,00	112,20	0,27	1,49	0,73	4,40	1455,80	1,28				
BIT–RM–R0–C1–A1–3	137,10	106,50	0,35	2,03	0,46	2,98	1622,50	1,43	1,80			
BIT–RM–R0–C1–A1–4	136,70	109,10	0,51	3,90	0,49	3,29	2111,70	1,86				
BIT–RM–R0–C1–A1–5	119,40	149,90	0,49	2,63	0,38	2,06	2438,00	2,15				
BIT–RM–R1–C1–A1–1	180,20	162,60	1,41	8,94	1,55	9,67	5599,20	4,94				1-2 µm
BIT–RM–R1–C1–A1–2	178,40	191,60	1,37	9,13	1,41	9,35	6168,30	5,44				
BIT–RM–R1–C1–A1–3	134,50	175,20	1,79	12,09	1,85	11,68	3147,60	2,78	4,01			
BIT–RM–R1–C1–A1–4	215,30	136,10	1,06	7,23	1,61	11,09	4223,50	3,72				
BIT–RM–R1–C1–A1–5	152,20	199,60	1,81	11,26	1,99	13,60	3621,90	3,19				
BIT–RM–R2–C1–A1–1	121,60	110,00	2,81	12,95	2,95	18,10	4927,30	4,35				2-4 µm
BIT–RM–R2–C1–A1–2	128,20	212,40	3,28	18,67	3,80	23,02	2372,60	2,09				
BIT–RM–R2–C1–A1–3	188,40	180,90	2,39	13,27	2,26	13,47	6009,30	5,30	4,48			
BIT–RM–R2–C1–A1–4	167,30	201,90	2,78	16,75	2,83	22,05	6231,80	5,50				
BIT–RM–R2–C1–A1–5	239,30	228,70	3,73	27,41	3,31	18,68	5878,80	5,18				
BIT–RM–R3–C1–A1–1	138,70	117,70	4,07	23,40	4,08	25,92	6428,80	5,67				4-8 µm
BIT–RM–R3–C1–A1–2	132,30	229,20	4,68	29,84	4,61	27,46	5726,10	5,05				
BIT–RM–R3–C1–A1–3	194,10	208,10	4,18	24,41	4,20	24,50	5503,00	4,85	5,33			
BIT–RM–R3–C1–A1–4	108,40	139,60	4,80	30,13	4,94	30,80	6128,00	5,40				
BIT–RM–R3–C1–A1–5	129,30	118,00	4,08	25,12	4,08	22,77	6421,40	5,66				
BIT–RM–R0–C2–A1–1	561,80	410,50	0,21	1,38	0,27	1,49	1857,40	1,64			Highly Contaminated (300-750 RFU)	without sandblasting
BIT–RM–R0–C2–A1–2	341,60	561,70	0,24	1,37	0,81	6,75	1749,10	1,54				
BIT–RM–R0–C2–A1–3	412,00	489,00	0,41	2,51	0,26	1,85	1433,50	1,26	1,56			
BIT–RM–R0–C2–A1–4	345,10	326,70	0,44	2,26	0,21	1,13	1929,80	1,70				
BIT–RM–R0–C2–A1–5	335,70	679,80	0,40	1,97	0,48	3,08	1860,60	1,64				
BIT–RM–R1–C2–A1–1	407,80	372,10	1,07	7,56	1,21	8,88	6265,60	5,53				1-2 µm
BIT–RM–R1–C2–A1–2	390,00	491,20	1,61	9,88	1,77	11,97	2783,30	2,45				
BIT–RM–R1–C2–A1–3	324,10	433,70	1,04	7,56	1,09	7,89	4853,40	4,28	4,67			
BIT–RM–R1–C2–A1–4	382,30	303,20	1,32	9,44	1,24	9,13	6306,70	5,56				
BIT–RM–R1–C2–A1–5	337,00	410,90	1,10	7,43	1,04	7,10	6244,30	5,51				
BIT–RM–R2–C2–A1–1	560,10	650,10	3,75	25,45	2,75	19,13	3534,40	3,12				2-4 µm
BIT–RM–R2–C2–A1–2	584,90	474,80	3,85	26,36	3,72	23,40	3858,70	3,40				
BIT–RM–R2–C2–A1–3	454,90	543,00	3,23	20,64	3,15	21,70	4710,10	4,15	3,39			
BIT–RM–R2–C2–A1–4	493,20	634,00	3,92	25,74	3,83	23,64	3670,30	3,24				
BIT–RM–R2–C2–A1–5	440,20	419,20	3,59	22,92	3,57	25,16	3443,00	3,04				
BIT–RM–R3–C2–A1–1	460,70	509,40	4,15	25,24	4,23	27,85	4758,00	4,20				4-8 µm
BIT–RM–R3–C2–A1–2	590,10	347,00	4,39	26,53	4,44	26,40	5892,60	5,20				
BIT–RM–R3–C2–A1–3	520,90	331,40	4,05	21,91	4,07	22,14	4463,60	3,94	4,39			
BIT–RM–R3–C2–A1–4	342,80	489,70	4,52	30,00	4,43	24,21	3610,40	3,18				
BIT–RM–R3–C2–A1–5	470,40	511,10	4,40	24,58	4,02	24,69	6142,00	5,42				

Table A. 1 Rubber-Metal Bonding Roughness and Cleanliness Measurement and Tensile Test Results (DP490)

BIT Test Coupon Samples	Surface Cleanliness Values (RFU)		Roughness Values (µm)				Maximum Load (N)	Tensile Stress at Maximum Load (MPa)	Mean Tensile Stress (MPa)	Adhesive	Cleanliness Level	Roughness Level
	First Coupon	Second Coupon	First Coupon		Second Coupon							
			Ra (µm)	Rz (µm)	Ra (µm)	Rz (µm)						
BIT–RM–R0–C0–A2–1	5,40	7,70	0,34	2,25	0,21	1,51	1557,80	1,37		Araldite 2011	Clean Surface (0-50 RFU)	without sandblasting
BIT–RM–R0–C0–A2–2	6,70	9,40	0,20	1,30	0,40	2,61	2228,10	1,97				
BIT–RM–R0–C0–A2–3	5,60	10,30	0,84	4,01	0,36	2,53	1793,80	1,58	1,72			
BIT–RM–R0–C0–A2–4	7,20	8,30	0,27	1,45	0,27	1,87	1960,90	1,73				
BIT–RM–R0–C0–A2–5	8,40	5,80	0,52	2,89	0,35	2,04	2213,00	1,95				
BIT–RM–R1–C0–A2–1	5,60	5,50	1,91	12,41	1,98	13,45	3034,80	2,68				1-2 µm
BIT–RM–R1–C0–A2–2	5,50	5,00	1,29	8,33	1,46	10,43	3994,00	3,52				
BIT–RM–R1–C0–A2–3	5,30	6,00	1,32	9,09	1,40	8,19	2356,30	2,08	2,86			
BIT–RM–R1–C0–A2–4	5,20	5,10	1,51	12,93	1,39	9,87	3551,90	3,13				
BIT–RM–R1–C0–A2–5	7,50	7,00	1,25	8,93	1,11	7,66	3251,50	2,87				
BIT–RM–R2–C0–A2–1	7,70	7,40	3,70	21,84	3,51	20,92	1424,20	1,26				2-4 µm
BIT–RM–R2–C0–A2–2	8,20	7,50	2,98	24,31	3,19	22,54	1969,40	1,74				
BIT–RM–R2–C0–A2–3	6,50	7,80	3,73	26,25	3,72	23,12	1761,70	1,55	1,53			
BIT–RM–R2–C0–A2–4	6,60	7,20	3,28	21,70	3,24	19,69	1960,90	1,73				
BIT–RM–R2–C0–A2–5	6,60	6,60	3,70	20,58	3,56	25,41	1577,20	1,39				
BIT–RM–R3–C0–A2–1	4,40	4,50	4,05	23,94	4,21	25,55	1837,90	1,62				4-8 µm
BIT–RM–R3–C0–A2–2	4,20	4,60	4,44	27,26	4,18	25,12	2372,10	2,09				
BIT–RM–R3–C0–A2–3	5,90	4,40	5,05	28,52	4,93	31,85	2600,50	2,29	2,01			
BIT–RM–R3–C0–A2–4	4,10	4,50	4,16	28,36	4,01	25,62	1448,60	1,28				
BIT–RM–R3–C0–A2–5	4,30	3,80	4,80	29,27	4,74	26,29	3161,30	2,79				
BIT–RM–R0–C1–A2–1	109,00	144,60	0,18	1,13	0,19	1,02	1752,80	1,55			Modarately Contaminated (50-200 RFU)	without sandblasting
BIT–RM–R0–C1–A2–2	142,20	149,90	0,26	1,96	0,28	1,43	2271,90	2,00				
BIT–RM–R0–C1–A2–3	113,90	128,40	0,29	1,69	0,37	2,16	1498,30	1,32	1,64			
BIT–RM–R0–C1–A2–4	113,20	132,20	0,25	1,74	0,36	2,52	2022,10	1,78				
BIT–RM–R0–C1–A2–5	102,10	114,50	0,29	1,79	0,68	4,01	1749,00	1,54				
BIT–RM–R1–C1–A2–1	176,80	130,20	1,29	10,16	1,11	8,03	1918,14	1,69				1-2 µm
BIT–RM–R1–C1–A2–2	143,20	175,70	1,36	9,57	1,33	9,84	1711,68	1,51				
BIT–RM–R1–C1–A2–3	172,00	195,20	1,41	9,47	1,40	8,98	1352,98	1,19	1,47			
BIT–RM–R1–C1–A2–4	114,00	146,50	1,12	9,66	1,15	8,85	1447,64	1,28				
BIT–RM–R1–C1–A2–5	169,10	182,20	1,06	8,26	1,16	8,25	1929,23	1,70				
BIT–RM–R2–C1–A2–1	122,60	188,40	3,18	23,53	3,07	20,52	5845,60	5,15				2-4 µm
BIT–RM–R2–C1–A2–2	178,70	211,00	2,15	13,31	2,25	14,95	1612,30	1,42				
BIT–RM–R2–C1–A2–3	212,50	198,20	3,79	24,41	3,50	17,67	2783,30	2,45	3,05			
BIT–RM–R2–C1–A2–4	204,20	191,90	2,65	16,20	3,19	19,25	4003,60	3,53				
BIT–RM–R2–C1–A2–5	169,10	109,80	3,96	22,77	4,00	24,79	3027,80	2,67				
BIT–RM–R3–C1–A2–1	146,20	173,30	4,44	25,12	4,51	27,03	4060,30	3,58				4-8 µm
BIT–RM–R3–C1–A2–2	171,20	194,60	4,09	27,08	4,12	27,84	2848,70	2,51				
BIT–RM–R3–C1–A2–3	156,10	230,70	4,55	27,28	4,66	29,98	3639,30	3,21	3,00			
BIT–RM–R3–C1–A2–4	196,60	207,90	4,26	26,87	4,08	24,69	2534,20	2,24				
BIT–RM–R3–C1–A2–5	231,70	142,50	4,65	29,35	4,98	36,67	3952,50	3,49				
BIT–RM–R0–C2–A2–1	406,00	494,50	0,33	1,76	0,28	1,75	2227,10	1,96			Highly Contaminated (300-750 RFU)	without sandblasting
BIT–RM–R0–C2–A2–2	510,80	298,50	0,21	1,34	0,31	1,74	2281,00	2,01				
BIT–RM–R0–C2–A2–3	389,20	438,40	0,50	3,05	0,13	3,67	1922,40	1,70	1,94			
BIT–RM–R0–C2–A2–4	437,80	376,30	0,19	1,30	0,65	3,26	2394,70	2,11				
BIT–RM–R0–C2–A2–5	462,40	369,10	0,37	1,76	0,34	2,22	2170,80	1,91				
BIT–RM–R1–C2–A2–1	311,60	333,70	1,01	6,67	1,15	8,29	2652,00	2,34				1-2 µm
BIT–RM–R1–C2–A2–2	378,60	301,70	1,95	11,36	1,88	11,08	1857,90	1,64				
BIT–RM–R1–C2–A2–3	396,90	327,40	1,29	9,38	1,33	8,79	2003,90	1,77	2,21			
BIT–RM–R1–C2–A2–4	614,40	421,00	1,76	13,83	1,73	11,05	3041,10	2,68				
BIT–RM–R1–C2–A2–5	612,80	341,60	1,12	7,47	1,09	7,67	2986,10	2,63				
BIT–RM–R2–C2–A2–1	466,50	549,90	3,04	20,78	3,33	19,19	1083,40	0,96				2-4 µm
BIT–RM–R2–C2–A2–2	639,20	419,80	2,61	22,81	2,81	17,19	1878,30	1,66				
BIT–RM–R2–C2–A2–3	553,20	604,50	3,87	24,44	3,64	23,19	1989,30	1,75	1,74			
BIT–RM–R2–C2–A2–4	488,90	403,20	3,48	22,16	3,57	20,56	1999,10	1,76				
BIT–RM–R2–C2–A2–5	708,60	543,50	3,34	21,27	3,27	21,32	2926,00	2,58				
BIT–RM–R3–C2–A2–1	307,90	579,50	4,73	29,64	4,89	29,30	1658,50	1,46				4-8 µm
BIT–RM–R3–C2–A2–2	689,70	553,00	4,32	26,72	4,43	28,89	3293,30	2,90				
BIT–RM–R3–C2–A2–3	649,90	548,50	4,95	31,34	4,78	28,58	4187,90	3,69	2,98			
BIT–RM–R3–C2–A2–4	511,00	500,00	4,18	24,14	4,13	26,98	3235,00	2,85				
BIT–RM–R3–C2–A2–5	621,90	572,20	4,41	28,88	4,30	26,97	4542,90	4,01				

Table A. 2 Rubber-Metal Bonding Roughness and Cleanliness Measurement and Tensile Test Results (Araldite 2011)

Shear Test Coupon Samples	Surface Cleanliness Values (RFU)		Roughness Values (µm)				Maximum Load (N)	Tensile Stress at Maximum Load (MPa)	Mean Tensile Stress (MPa)	Adhesive	Cleanliness Level	Roughness Level
	First Coupon	Second Coupon	First Coupon		Second Coupon							
			Ra (µm)	Rz (µm)	Ra (µm)	Rz (µm)						
SH–RM–R0–C0–A1–1	2,90	0,50	0,41	3,21	0,28	2,05	2550,00	4,08		DP-490	Clean Surface (0-50 RFU)	without sandblasting
SH–RM–R0–C0–A1–2	0,60	1,20	0,30	2,68	0,41	2,80	2520,00	4,03				
SH–RM–R0–C0–A1–3	2,60	4,40	0,29	3,05	0,30	2,77	2350,00	3,78	3,99			
SH–RM–R0–C0–A1–4	1,50	0,60	0,36	2,43	0,47	3,26	2690,00	4,30				
SH–RM–R0–C0–A1–5	0,70	0,60	0,33	2,41	0,33	2,55	2350,00	3,76				
SH–RM–R1–C0–A1–1	6,40	3,40	1,34	8,53	1,59	11,37	2730,00	4,36				1-2 µm
SH–RM–R1–C0–A1–2	3,70	3,60	1,41	9,56	1,28	9,49	2960,00	4,74				
SH–RM–R1–C0–A1–3	3,60	10,20	1,41	10,57	1,37	9,48	2840,00	4,55	4,56			
SH–RM–R1–C0–A1–4	4,30	3,90	1,34	9,27	1,52	10,36	2760,00	4,41				
SH–RM–R1–C0–A1–5	3,00	4,60	1,60	10,70	1,31	8,70	2950,00	4,72				
SH–RM–R2–C0–A1–1	4,40	4,10	2,36	16,74	3,06	22,20	2780,00	4,27				2-4 µm
SH–RM–R2–C0–A1–2	4,80	5,20	2,35	19,47	2,63	19,06	2900,00	4,50				
SH–RM–R2–C0–A1–3	6,30	4,00	2,02	15,91	2,78	21,76	2730,00	4,36	4,32			
SH–RM–R2–C0–A1–4	3,70	4,20	2,37	17,14	3,09	26,10	2400,00	3,84				
SH–RM–R2–C0–A1–5	4,60	3,30	2,41	17,44	2,92	19,64	2900,00	4,64				
SH–RM–R3–C0–A1–1	2,30	3,10	4,88	30,04	4,27	27,48	2500,00	4,00				4-8 µm
SH–RM–R3–C0–A1–2	2,80	3,80	4,09	25,93	4,31	28,30	1530,00	2,45				
SH–RM–R3–C0–A1–3	2,90	1,10	4,85	29,97	4,40	25,41	2330,00	3,73	3,47			
SH–RM–R3–C0–A1–4	4,30	2,10	4,13	25,92	4,12	26,14	2260,00	3,62				
SH–RM–R3–C0–A1–5	5,20	2,30	4,44	25,41	4,15	29,68	2210,00	3,54				
SH–RM–R0–C1–A1–1	116,60	145,10	0,59	4,33	0,71	4,95	2390,00	3,82			Modarately Contaminated (50-200 RFU)	without sandblasting
SH–RM–R0–C1–A1–2	128,30	140,00	0,58	4,58	0,62	4,61	2210,00	3,54				
SH–RM–R0–C1–A1–3	150,00	126,30	0,82	5,44	0,75	5,99	2630,00	4,21	3,88			
SH–RM–R0–C1–A1–4	107,90	115,40	0,55	4,15	0,50	3,43	2340,00	3,74				
SH–RM–R0–C1–A1–5	105,10	117,90	0,45	4,20	0,41	3,18	2560,00	4,10				
SH–RM–R1–C1–A1–1	128,70	140,60	1,70	11,99	1,21	8,76	2840,00	4,54				1-2 µm
SH–RM–R1–C1–A1–2	138,60	140,10	1,42	10,50	1,13	8,51	2550,00	4,08				
SH–RM–R1–C1–A1–3	122,50	146,50	1,75	11,67	1,38	9,72	2780,00	4,45	4,53			
SH–RM–R1–C1–A1–4	144,90	125,90	1,73	13,56	1,47	9,87	2980,00	4,77				
SH–RM–R1–C1–A1–5	150,00	149,90	1,58	12,68	1,36	9,41	3000,00	4,80				
SH–RM–R2–C1–A1–1	147,90	128,60	3,86	25,70	3,36	22,82	2850,00	4,56				2-4 µm
SH–RM–R2–C1–A1–2	117,50	128,70	2,86	21,06	2,84	19,58	2920,00	4,68				
SH–RM–R2–C1–A1–3	134,20	125,70	2,34	15,89	2,26	16,43	2770,00	4,43	4,55			
SH–RM–R2–C1–A1–4	117,30	149,10	2,26	17,41	2,75	18,48	2920,00	4,67				
SH–RM–R2–C1–A1–5	104,70	115,90	3,16	23,43	2,25	18,84	2770,00	4,43				
SH–RM–R3–C1–A1–1	134,80	150,00	4,13	25,38	4,53	28,14	2480,00	3,96				4-8 µm
SH–RM–R3–C1–A1–2	140,50	149,00	4,75	30,55	4,40	25,34	2180,00	3,49				
SH–RM–R3–C1–A1–3	126,20	149,90	4,24	25,36	4,01	23,39	2220,00	3,55	3,70			
SH–RM–R3–C1–A1–4	124,20	137,30	4,04	24,84	4,01	23,08	2220,00	3,56				
SH–RM–R3–C1–A1–5	113,60	114,70	4,03	25,76	4,19	26,08	2460,00	3,94				
SH–RM–R0–C2–A1–1	409,70	345,40	0,40	2,60	0,27	2,34	2530,00	4,06			Highly Contaminated (300-750 RFU)	without sandblasting
SH–RM–R0–C2–A1–2	557,20	454,10	0,39	3,08	0,38	3,85	2620,00	4,19				
SH–RM–R0–C2–A1–3	610,00	457,90	0,32	3,24	0,44	3,03	2620,00	4,19	3,99			
SH–RM–R0–C2–A1–4	680,10	575,30	0,44	3,15	0,45	3,91	2130,00	3,42				
SH–RM–R0–C2–A1–5	470,90	530,50	0,35	3,11	0,33	2,67	2560,00	4,09				
SH–RM–R1–C2–A1–1	341,50	424,60	1,31	9,84	1,46	10,16	2890,00	4,53				1-2 µm
SH–RM–R1–C2–A1–2	382,40	472,40	1,44	11,48	1,64	12,27	3030,00	4,85				
SH–RM–R1–C2–A1–3	410,90	499,70	1,60	10,40	1,37	10,39	2840,00	4,55	4,52			
SH–RM–R1–C2–A1–4	512,10	519,90	1,29	9,53	1,57	11,51	2800,00	4,48				
SH–RM–R1–C2–A1–5	375,30	453,40	1,37	9,29	1,46	10,74	2630,00	4,21				
SH–RM–R2–C2–A1–1	697,40	567,60	2,71	20,19	2,89	23,52	2530,00	4,04				2-4 µm
SH–RM–R2–C2–A1–2	535,60	786,30	3,70	21,70	2,13	16,53	2850,00	4,57				
SH–RM–R2–C2–A1–3	448,60	336,70	2,43	18,69	2,80	20,27	2560,00	4,10	4,31			
SH–RM–R2–C2–A1–4	665,80	372,70	2,97	20,63	2,58	18,13	2750,00	4,40				
SH–RM–R2–C2–A1–5	517,30	668,30	2,09	17,05	2,05	15,57	2780,00	4,44				
SH–RM–R3–C2–A1–1	600,70	522,70	4,75	29,32	4,22	29,79	2340,00	3,75				4-8 µm
SH–RM–R3–C2–A1–2	660,30	509,20	4,18	24,47	4,61	27,34	2160,00	3,45				
SH–RM–R3–C2–A1–3	482,90	426,80	4,79	27,00	4,31	24,71	2470,00	3,96	3,60			
SH–RM–R3–C2–A1–4	618,50	482,20	4,07	25,44	4,12	25,15	1930,00	3,08				
SH–RM–R3–C2–A1–5	491,90	446,10	4,42	26,74	4,14	25,81	2350,00	3,77				

Table A. 3 Rubber-Metal Bonding Roughness and Cleanliness Measurement and Shear Test Results (DP490)

Shear Test Coupon Samples	Surface Cleanliness Values (RFU)		Roughness Values (µm)				Maximum Load (N)	Tensile Stress at Maximum Load (MPa)	Mean Tensile Stress (MPa)	Adhesive	Cleanliness Level	Roughness Level
	First Coupon	Second Coupon	First Coupon		Second Coupon							
			Ra (µm)	Rz (µm)	Ra (µm)	Rz (µm)						
SH–RM–R0–C0–A2–1	7,80	0,50	0,42	4,90	0,34	3,02	1060,00	1,70		Araldite 2011	Clean Surface (0-50 RFU)	without sandblasting
SH–RM–R0–C0–A2–2	1,80	1,80	0,34	2,82	0,48	4,17	1130,00	1,81				
SH–RM–R0–C0–A2–3	2,20	1,10	0,39	3,48	0,29	2,32	960,00	1,54	1,72			
SH–RM–R0–C0–A2–4	1,40	3,70	0,35	3,40	0,36	4,10	1100,00	1,76				
SH–RM–R0–C0–A2–5	2,20	1,60	0,43	4,34	0,36	3,12	1110,00	1,78				
SH–RM–R1–C0–A2–1	3,20	4,00	1,32	8,95	1,38	9,47	3000,00	4,80				1-2 µm
SH–RM–R1–C0–A2–2	4,50	5,00	1,28	10,39	1,32	9,76	3130,00	5,00				
SH–RM–R1–C0–A2–3	6,80	5,00	1,31	8,65	1,29	9,64	2920,00	4,67	4,70			
SH–RM–R1–C0–A2–4	7,90	3,70	1,23	8,69	1,39	9,71	2790,00	4,47				
SH–RM–R1–C0–A2–5	2,10	7,10	1,26	9,39	1,35	9,79	2840,00	4,54				
SH–RM–R2–C0–A2–1	2,60	4,60	2,71	19,89	2,85	18,25	1530,00	2,45				2-4 µm
SH–RM–R2–C0–A2–2	10,80	5,60	2,92	20,52	2,54	18,67	1990,00	3,18				
SH–RM–R2–C0–A2–3	5,30	2,80	2,79	17,60	2,50	20,82	1600,00	2,56	2,95			
SH–RM–R2–C0–A2–4	5,00	2,70	2,30	17,26	3,57	22,82	2300,00	3,69				
SH–RM–R2–C0–A2–5	10,10	3,30	2,42	16,89	2,29	15,96	1790,00	2,86				
SH–RM–R3–C0–A2–1	21,30	6,50	4,25	25,30	5,10	31,14	1050,00	1,68				4-8 µm
SH–RM–R3–C0–A2–2	3,00	19,30	4,29	23,50	4,04	28,48	1100,00	1,77				
SH–RM–R3–C0–A2–3	20,00	3,20	4,15	25,33	4,09	22,74	1200,00	1,92	1,78			
SH–RM–R3–C0–A2–4	4,90	2,00	4,25	26,61	4,37	26,51	1200,00	1,92				
SH–RM–R3–C0–A2–5	4,60	3,40	4,22	27,78	4,37	28,04	1020,00	1,63				
SH–RM–R0–C1–A2–1	117,40	131,30	0,32	2,71	0,45	3,48	1160,00	1,86			Modarately Contaminated (50-200 RFU)	without sandblasting
SH–RM–R0–C1–A2–2	140,90	143,40	0,48	4,04	0,40	3,51	1130,00	1,80				
SH–RM–R0–C1–A2–3	146,10	150,00	0,63	5,54	0,31	2,75	1130,00	1,81	1,63			
SH–RM–R0–C1–A2–4	133,60	96,10	0,45	3,26	0,54	5,28	1070,00	1,72				
SH–RM–R0–C1–A2–5	150,00	121,50	0,27	2,62	0,36	3,28	600,00	0,96				
SH–RM–R1–C1–A2–1	127,90	140,60	1,28	8,74	1,52	10,97	2230,00	3,56				1-2 µm
SH–RM–R1–C1–A2–2	150,00	127,50	1,31	9,31	1,38	10,09	2800,00	4,47				
SH–RM–R1–C1–A2–3	140,70	140,90	1,42	10,04	1,84	13,92	2820,00	4,51	4,29			
SH–RM–R1–C1–A2–4	144,80	127,40	1,57	10,63	1,29	9,25	2780,00	4,44				
SH–RM–R1–C1–A2–5	150,00	149,70	1,23	8,83	1,45	10,29	2780,00	4,45				
SH–RM–R2–C1–A2–1	131,10	150,00	3,04	18,60	2,56	21,40	1830,00	2,93				2-4 µm
SH–RM–R2–C1–A2–2	136,90	109,50	2,18	18,29	3,16	20,79	1520,00	2,43				
SH–RM–R2–C1–A2–3	117,00	126,50	2,29	16,80	2,41	18,81	1240,00	1,98	2,43			
SH–RM–R2–C1–A2–4	122,90	111,20	2,97	21,93	2,74	22,14	1770,00	2,83				
SH–RM–R2–C1–A2–5	150,00	138,60	2,89	19,08	2,50	16,04	1230,00	1,96				
SH–RM–R3–C1–A2–1	110,90	117,40	5,11	29,89	4,13	21,83	1070,00	1,71				4-8 µm
SH–RM–R3–C1–A2–2	129,20	98,70	4,17	28,87	4,31	28,41	1330,00	2,13				
SH–RM–R3–C1–A2–3	120,40	122,40	4,40	29,66	4,47	28,15	1290,00	2,07	1,93			
SH–RM–R3–C1–A2–4	150,00	131,60	4,62	28,28	4,77	27,73	1340,00	2,14				
SH–RM–R3–C1–A2–5	125,30	107,00	4,19	23,96	4,40	27,64	1000,00	1,59				
SH–RM–R0–C2–A2–1	582,80	630,00	0,37	3,21	0,36	2,64	1080,00	1,73			Highly Contaminated (300-750 RFU)	without sandblasting
SH–RM–R0–C2–A2–2	697,60	500,70	0,41	3,19	0,51	5,02	1080,00	1,73				
SH–RM–R0–C2–A2–3	574,00	517,40	0,46	3,87	0,54	4,25	1130,00	1,81	1,84			
SH–RM–R0–C2–A2–4	546,10	358,20	0,42	4,08	0,42	3,33	1190,00	1,90				
SH–RM–R0–C2–A2–5	680,30	621,50	0,56	3,94	0,67	4,91	1,26	2,01				
SH–RM–R1–C2–A2–1	484,30	541,80	1,55	10,77	1,78	12,29	2670,00	4,27				1-2 µm
SH–RM–R1–C2–A2–2	541,90	649,10	1,58	11,00	1,39	10,02	2760,00	4,41				
SH–RM–R1–C2–A2–3	465,50	406,80	1,72	12,49	1,16	9,36	2690,00	4,30	4,47			
SH–RM–R1–C2–A2–4	436,70	567,70	1,40	11,49	1,33	9,68	2940,00	4,71				
SH–RM–R1–C2–A2–5	613,20	535,30	1,57	10,34	1,19	8,50	2920,00	4,68				
SH–RM–R2–C2–A2–1	647,80	543,10	2,25	17,62	2,84	21,56	1800,00	2,89				2-4 µm
SH–RM–R2–C2–A2–2	591,50	677,30	2,33	17,58	3,30	23,15	1940,00	3,11				
SH–RM–R2–C2–A2–3	746,70	643,80	2,83	21,17	2,96	21,83	1740,00	2,78	2,85			
SH–RM–R2–C2–A2–4	695,80	584,90	2,06	15,91	2,17	15,00	1640,00	2,63				
SH–RM–R2–C2–A2–5	488,90	366,70	2,62	17,16	2,10	16,55	1770,00	2,84				
SH–RM–R3–C2–A2–1	465,20	434,50	4,04	27,12	4,90	26,47	1170,00	1,88				4-8 µm
SH–RM–R3–C2–A2–2	454,40	478,40	4,74	27,47	4,03	23,32	1240,00	1,99				
SH–RM–R3–C2–A2–3	431,60	485,70	4,04	23,77	4,55	25,83	1180,00	1,89	2,03			
SH–RM–R3–C2–A2–4	512,40	434,00	4,35	26,54	4,65	28,77	1460,00	2,34				

Table A. 4 Rubber-Metal Bonding Roughness and Cleanliness Measurement and Shear Test Results (Araldite 2011)

Shear Test Coupon Samples	Surface Cleanliness Values (RFU)		Roughness Values (µm)				Maximum Load (N)	Tensile Stress at Maximum Load (MPa)	Mean Tensile Stress (MPa)	Adhesive	Cleanliness Level	Roughness Level
	First Coupon	Second Coupon	First Coupon		Second Coupon							
			Ra (µm)	Rz (µm)	Ra (µm)	Rz (µm)						
SH–MM–R0–C0–A1–1	33,60	16,40	0,70	5,16	0,59	4,86	11290,00	17,20	16,54	DP-490	Clean Surface (0-50 RFU)	without sandblasting
SH–MM–R0–C0–A1–2	27,40	6,70	0,70	4,91	0,49	3,48	10860,00	16,71				
SH–MM–R0–C0–A1–3	22,40	10,80	0,35	2,66	0,60	4,50	11340,00	17,22				
SH–MM–R0–C0–A1–4	32,20	25,50	0,81	6,60	0,75	5,74	9890,00	15,01				
SH–MM–R1–C0–A1–1	5,10	4,20	1,88	13,37	1,76	11,94	12230,00	19,56	20,52			1-2 µm
SH–MM–R1–C0–A1–2	5,30	5,40	1,58	13,22	1,70	11,21	13930,00	22,28				
SH–MM–R1–C0–A1–3	4,80	6,50	1,77	14,33	1,53	10,40	12980,00	20,77				
SH–MM–R1–C0–A1–4	7,60	6,60	1,35	9,18	1,49	11,13	12160,00	19,45				
SH–MM–R2–C0–A1–1	3,40	3,70	2,64	19,52	2,80	26,12	11710,00	18,74	19,40			2-4 µm
SH–MM–R2–C0–A1–2	3,20	3,90	3,19	23,66	3,73	25,24	12070,00	19,32				
SH–MM–R2–C0–A1–3	3,90	3,70	3,79	28,21	2,82	21,37	12080,00	19,32				
SH–MM–R2–C0–A1–4	5,80	4,20	3,58	25,10	3,78	28,23	12630,00	20,21				
SH–MM–R3–C0–A1–1	8,50	5,80	4,96	27,29	5,59	31,73	14210,00	22,73	21,37			4-8 µm
SH–MM–R3–C0–A1–2	8,70	7,30	5,12	29,83	6,40	38,26	12830,00	20,53				
SH–MM–R3–C0–A1–3	6,90	22,80	5,11	31,50	4,91	31,11	13010,00	20,81				
SH–MM–R3–C0–A1–4	7,20	10,50	4,69	30,46	4,91	26,97	13380,00	21,41				
SH–MM–R0–C1–A1–1	150,00	128,20	0,49	3,62	0,74	4,48	11450,00	16,81	16,49		Modarately Contaminated (50-200 RFU)	without sandblasting
SH–MM–R0–C1–A1–2	137,20	127,80	0,29	2,30	0,46	3,04	11150,00	15,65				
SH–MM–R0–C1–A1–3	150,00	125,90	0,77	4,81	0,59	3,78	11620,00	16,19				
SH–MM–R0–C1–A1–4	149,50	148,70	0,71	4,92	0,37	3,72	11470,00	17,32				
SH–MM–R1–C1–A1–1	130,90	140,30	1,49	10,65	1,65	11,58	11500,00	17,40	19,37			1-2 µm
SH–MM–R1–C1–A1–2	135,70	133,80	1,52	10,23	1,30	10,93	13370,00	21,39				
SH–MM–R1–C1–A1–3	130,30	150,00	1,45	11,24	1,68	12,24	12120,00	19,39				
SH–MM–R1–C1–A1–4	115,80	146,70	1,52	10,00	1,30	10,93	12060,00	19,30				
SH–MM–R2–C1–A1–1	146,00	149,30	3,21	20,31	3,57	20,40	11520,00	18,43	19,01			2-4 µm
SH–MM–R2–C1–A1–2	134,50	140,30	3,75	28,63	3,41	25,60	10340,00	16,55				
SH–MM–R2–C1–A1–3	127,50	150,00	3,02	18,95	2,38	16,13	12990,00	20,79				
SH–MM–R2–C1–A1–4	116,20	131,70	3,22	27,13	2,77	19,07	12670,00	20,28				
SH–MM–R3–C1–A1–1	136,40	149,60	4,44	28,21	4,53	27,21	11610,00	18,57	19,40			4-8 µm
SH–MM–R3–C1–A1–2	100,30	150,00	6,24	38,22	5,75	30,30	13070,00	20,91				
SH–MM–R3–C1–A1–3	150,00	150,00	6,27	37,82	5,43	31,61	11430,00	18,28				
SH–MM–R3–C1–A1–4	128,70	149,80	5,90	34,13	5,49	33,02	12380,00	19,82				
SH–MM–R0–C2–A1–1	643,00	706,50	0,74	5,21	0,61	3,58	10550,00	15,69	15,98		Highly Contaminated (300-750 RFU)	without sandblasting
SH–MM–R0–C2–A1–2	586,10	518,90	0,60	4,04	0,54	4,81	10890,00	15,55				
SH–MM–R0–C2–A1–3	694,60	465,90	0,68	4,02	0,32	2,60	10160,00	14,52				
SH–MM–R0–C2–A1–4	666,70	457,60	0,62	4,36	0,62	4,56	12920,00	18,14				
SH–MM–R1–C2–A1–1	571,20	453,50	1,64	11,29	1,68	10,49	13090,00	20,95	20,02			1-2 µm
SH–MM–R1–C2–A1–2	584,20	464,40	1,30	9,53	1,38	9,95	12620,00	20,19				
SH–MM–R1–C2–A1–3	513,50	538,60	1,36	9,92	1,21	8,65	13080,00	20,93				
SH–MM–R1–C2–A1–4	684,60	661,20	1,37	9,41	1,27	10,25	11240,00	17,99				
SH–MM–R2–C2–A1–1	614,40	664,50	3,52	26,39	3,77	22,94	11080,00	17,73	18,16			2-4 µm
SH–MM–R2–C2–A1–2	648,50	508,70	2,99	23,72	3,32	25,57	11590,00	18,54				
SH–MM–R2–C2–A1–3	639,30	546,60	3,64	27,40	2,86	20,36	11580,00	18,53				
SH–MM–R2–C2–A1–4	451,70	624,30	3,49	26,09	3,84	24,89	11140,00	17,82				
SH–MM–R3–C2–A1–1	719,60	683,60	5,10	29,43	5,11	29,38	12120,00	19,39	20,12			4-8 µm
SH–MM–R3–C2–A1–2	598,50	639,60	5,13	32,88	4,13	29,73	13230,00	21,17				
SH–MM–R3–C2–A1–3	683,50	614,00	4,80	28,72	5,11	30,65	11210,00	17,94				
SH–MM–R3–C2–A1–4	684,40	599,20	4,31	27,89	5,75	38,29	13730,00	21,97				

Table A. 5 Metal-Metal Bonding Roughness and Cleanliness Measurement and Shear Test Results (DP490)

Shear Test Coupon Samples	Surface Cleanliness Values (RFU)		Roughness Values (µm)				Maximum Load (N)	Tensile Stress at Maximum Load (MPa)	Mean Tensile Stress (MPa)	Adhesive	Cleanliness Level	Roughness Level
	First Coupon	Second Coupon	First Coupon		Second Coupon							
			Ra (µm)	Rz (µm)	Ra (µm)	Rz (µm)						
SH–MM–R0–C0–A2–1	27,60	32,60	0,39	3,17	0,49	3,58	6860,00	10,35	9,79	Araldite 2011	Clean Surface (0-50 RFU)	without sandblasting
SH–MM–R0–C0–A2–2	17,90	10,60	0,57	3,43	0,42	3,07	6990,00	10,75				
SH–MM–R0–C0–A2–3	28,30	18,30	0,65	5,25	0,43	3,79	6250,00	9,49				
SH–MM–R0–C0–A2–4	4,10	16,30	0,36	2,96	0,69	4,53	5640,00	8,57				
SH–MM–R1–C0–A2–1	4,60	4,70	1,69	12,61	1,45	10,38	8440,00	13,50	13,71			1-2 µm
SH–MM–R1–C0–A2–2	4,90	6,50	1,75	15,94	1,96	13,61	8650,00	13,84				
SH–MM–R1–C0–A2–3	4,60	3,60	1,49	10,93	1,61	11,13	8530,00	13,64				
SH–MM–R1–C0–A2–4	4,50	3,40	1,62	10,76	1,56	11,84	8660,00	13,85				
SH–MM–R2–C0–A2–1	3,50	5,30	3,64	25,77	2,81	18,82	8460,00	13,54	13,71			2-4 µm
SH–MM–R2–C0–A2–2	4,50	3,00	3,83	25,34	3,99	29,48	8500,00	13,61				
SH–MM–R2–C0–A2–3	2,50	3,00	2,77	21,59	3,17	23,41	8730,00	13,97				
SH–MM–R2–C0–A2–4	2,50	2,40	3,63	32,03	2,67	19,15	8580,00	13,73				
SH–MM–R3–C0–A2–1	7,30	8,70	5,29	34,59	4,87	29,64	10090,00	16,15	16,48			4-8 µm
SH–MM–R3–C0–A2–2	6,30	6,10	5,08	30,29	5,31	28,99	9530,00	15,24				
SH–MM–R3–C0–A2–3	6,70	14,00	4,81	29,53	5,45	28,92	11410,00	18,26				
SH–MM–R3–C0–A2–4	16,20	17,10	5,33	31,29	4,90	30,82	10160,00	16,25				
SH–MM–R0–C1–A2–1	124,30	122,90	0,32	2,59	0,70	5,65	4910,00	7,70	9,45		Modarately Contaminated (50-200 RFU)	without sandblasting
SH–MM–R0–C1–A2–2	109,30	133,90	0,33	3,60	0,79	5,67	6770,00	10,99				
SH–MM–R0–C1–A2–3	150,00	136,60	0,66	4,26	0,38	3,03	6370,00	9,61				
SH–MM–R0–C1–A2–4	150,00	118,20	0,67	4,62	0,37	2,78	6300,00	9,51				
SH–MM–R1–C1–A2–1	96,90	149,00	1,48	10,55	1,43	9,96	6040,00	9,66	9,75			1-2 µm
SH–MM–R1–C1–A2–2	149,40	143,60	1,51	11,31	1,46	11,90	6590,00	10,54				
SH–MM–R1–C1–A2–3	141,40	150,00	1,75	12,42	1,47	11,47	5260,00	8,41				
SH–MM–R1–C1–A2–4	144,40	128,90	1,14	8,18	1,55	10,71	6490,00	10,39				
SH–MM–R2–C1–A2–1	141,20	147,00	3,15	21,76	3,39	24,88	7100,00	11,36	11,36			2-4 µm
SH–MM–R2–C1–A2–2	121,00	107,20	2,41	18,77	2,05	15,93	7010,00	11,21				
SH–MM–R2–C1–A2–3	150,00	135,60	2,60	20,17	2,55	17,21	6980,00	11,17				
SH–MM–R2–C1–A2–4	146,90	150,00	3,24	22,66	3,28	20,92	7300,00	11,68				
SH–MM–R3–C1–A2–1	143,50	111,20	4,56	25,55	5,46	31,05	6060,00	9,69	11,54			4-8 µm
SH–MM–R3–C1–A2–2	143,10	148,40	4,33	25,30	4,47	27,06	7010,00	11,20				
SH–MM–R3–C1–A2–3	150,00	135,00	4,85	27,97	4,84	29,48	7830,00	12,54				
SH–MM–R3–C1–A2–4	107,00	150,00	5,97	31,75	4,98	27,32	7960,00	12,73				
SH–MM–R0–C2–A2–1	561,70	587,50	0,43	3,38	0,56	3,52	5770,00	8,71	9,19		Highly Contaminated (300-750 RFU)	without sandblasting
SH–MM–R0–C2–A2–2	677,10	524,40	0,24	2,17	0,49	3,96	5550,00	8,53				
SH–MM–R0–C2–A2–3	555,80	520,20	0,75	5,21	0,52	3,82	6250,00	9,62				
SH–MM–R0–C2–A2–4	749,70	690,10	0,48	3,80	0,45	3,34	6310,00	9,90				
SH–MM–R1–C2–A2–1	486,50	452,70	1,60	11,52	1,45	9,93	6090,00	9,75	10,05			1-2 µm
SH–MM–R1–C2–A2–2	647,90	655,00	1,92	11,86	1,51	10,90	5730,00	9,16				
SH–MM–R1–C2–A2–3	625,00	524,40	1,41	10,58	1,35	9,60	6910,00	11,06				
SH–MM–R1–C2–A2–4	604,60	707,00	1,42	9,95	1,59	11,02	6390,00	10,22				
SH–MM–R2–C2–A2–1	483,00	642,60	3,35	24,83	3,94	25,57	6140,00	9,82	10,07			2-4 µm
SH–MM–R2–C2–A2–2	524,00	521,50	3,83	25,27	3,81	28,04	5260,00	8,41				
SH–MM–R2–C2–A2–3	559,00	718,50	2,99	24,10	3,72	29,05	6960,00	11,14				
SH–MM–R2–C2–A2–4	559,10	632,10	3,48	22,03	3,49	21,90	6810,00	10,89				
SH–MM–R3–C2–A2–1	625,40	640,80	4,74	26,86	4,79	28,46	7790,00	12,47	12,07			4-8 µm
SH–MM–R3–C2–A2–2	589,30	603,80	4,40	25,73	5,51	33,88	8330,00	13,33				
SH–MM–R3–C2–A2–3	613,90	665,20	5,20	35,16	4,72	31,99	5650,00	9,03				
SH–MM–R3–C2–A2–4	558,20	711,70	4,88	30,06	6,12	36,55	8410,00	13,46				

Table A. 6 Metal-Metal Bonding Roughness and Cleanliness Measurement and Shear Test Results (Araldite 2011)

BIT Test Coupon Samples	Surface Cleanliness Values (RFU)		Roughness Values (µm)				Maximum Load (N)	Tensile Stress at Maximum Load (MPa)	Mean Tensile Stress (MPa)	Adhesive	Cleanliness Level	Roughness Level	EPDM Roughness Level
	First Coupon	Second Coupon	First Coupon		Second Coupon								
			Ra (µm)	Rz (µm)	Ra (µm)	Rz (µm)							
BIT–RM–R0–C0–A1–E0-1	3,90	4,40	5,99	36,22	5,37	35,23	1704,80	1,50					
BIT–RM–R0–C0–A1–E0-2	6,90	6,30	5,37	33,63	6,57	41,54	1313,90	1,16					non-textured EPDM
BIT–RM–R0–C0–A1–E0-3	6,60	5,10	6,90	38,62	4,83	28,42	1333,30	1,18	1,41				
BIT–RM–R0–C0–A1–E0-4	3,90	3,40	5,47	34,00	5,10	29,31	1717,20	1,51					
BIT–RM–R0–C0–A1–E0-5	4,20	7,10	4,62	29,56	5,45	33,81	1924,60	1,70					
BIT–RM–R0–C0–A1–E1-1	5,30	5,90	5,86	34,99	5,45	33,62	3506,10	3,09					
BIT–RM–R0–C0–A1–E1-2	4,50	4,90	5,17	29,41	6,78	39,76	4007,90	3,53					EPDM textured with peel ply
BIT–RM–R0–C0–A1–E1-3	4,20	3,50	6,42	35,53	6,33	34,21	2641,30	2,33	2,75	DP-490			
BIT–RM–R0–C0–A1–E1-4	4,00	3,90	5,51	29,65	5,58	34,68	2415,60	2,13					
BIT–RM–R0–C0–A1–E1-5	2,70	7,30	5,18	29,48	5,56	35,61	3008,00	2,65					
BIT–RM–R0–C0–A1–E2-1	4,00	3,90	6,25	37,61	5,91	32,15	3288,40	2,90					
BIT–RM–R0–C0–A1–E2-2	2,30	4,40	5,89	33,27	5,84	35,81	4126,10	3,64					EPDM roughened with sandpaper
BIT–RM–R0–C0–A1–E2-3	4,00	2,90	4,98	28,91	6,79	40,94	3509,30	3,09	3,08				
BIT–RM–R0–C0–A1–E2-4	5,10	3,40	5,39	32,35	6,31	35,88	3114,10	2,75					
BIT–RM–R0–C0–A1–E2-5	14,40	3,30	5,77	38,51	6,26	39,49	3420,60	3,02			Clean Surface (0-50 RFU)	4-8 µm	
BIT–RM–R0–C0–A2–E0-1	3,60	3,20	5,78	36,59	5,76	35,69	1186,90	1,05					
BIT–RM–R0–C0–A2–E0-2	4,00	4,90	5,20	29,98	6,43	34,95	640,40	0,57					non-textured EPDM
BIT–RM–R0–C0–A2–E0-3	3,50	3,70	5,60	33,76	5,35	33,43	919,60	0,81	0,85				
BIT–RM–R0–C0–A2–E0-4	4,60	3,20	5,39	37,07	5,81	31,47	1168,40	1,03					
BIT–RM–R0–C0–A2–E0-5	6,70	4,30	4,95	31,64	4,89	30,90	902,40	0,80					
BIT–RM–R0–C0–A2–E1-1	10,60	3,90	5,11	28,83	6,09	37,47	1313,80	1,16					
BIT–RM–R0–C0–A2–E1-2	6,40	3,80	6,18	36,21	5,43	34,78	778,90	0,69					EPDM textured with peel ply
BIT–RM–R0–C0–A2–E1-3	3,80	5,20	6,99	39,81	6,29	35,69	1006,80	0,89	0,93	Araldite 2011			
BIT–RM–R0–C0–A2–E1-4	5,80	2,60	5,48	31,31	6,41	36,17	909,90	0,80					
BIT–RM–R0–C0–A2–E1-5	48,40	7,50	5,55	33,13	5,35	34,40	1247,00	1,10					
BIT–RM–R0–C0–A2–E2-1	4,60	4,00	6,88	39,41	5,35	32,88	2283,60	2,01					
BIT–RM–R0–C0–A2–E2-2	3,70	3,00	5,72	35,91	4,83	29,95	2514,30	2,22					EPDM roughened with sandpaper
BIT–RM–R0–C0–A2–E2-3	3,30	5,40	6,24	38,55	4,82	31,54	2101,20	1,85	2,16				
BIT–RM–R0–C0–A2–E2-4	13,30	5,80	5,03	30,63	5,78	33,87	2864,50	2,53					
BIT–RM–R0–C0–A2–E2-5	3,10	3,80	5,07	32,66	6,21	38,25	2493,50	2,20					

Table A. 7 Rubber-Metal Bonding with Different Roughness Methods Tensile Test Results

Shear Test Coupon Samples	Surface		Roughness Values (µm)				Maximum Load (N)	Tensile Stress at Maximum Load (MPa)	Mean Tensile Stress (MPa)	Adhesive	Cleanliness Level	Roughness Level	Method
	First Coupon	Second Coupon	First Coupon		Second Coupon								
			Ra (µm)	Rz (µm)	Ra (µm)	Rz (µm)							
SH–RM–R0–C0–A1–E0-1	3,20	3,70	7,59	48,45	6,13	43,73	897,10	1,44					
SH–RM–R0–C0–A1–E0-2	5,60	3,90	5,18	35,85	5,22	34,45	683,50	1,09					non-textured EPDM
SH–RM–R0–C0–A1–E0-3	3,60	3,20	5,38	32,86	6,98	46,65	669,95	1,07	1,19				
SH–RM–R0–C0–A1–E0-4	5,00	3,40	6,69	39,84	4,89	31,63	775,51	1,24					
SH–RM–R0–C0–A1–E0-5	3,30	4,50	6,17	39,18	5,88	34,70	695,39	1,11					
SH–RM–R0–C0–A1–E1-1	3,80	4,00	5,08	31,23	7,21	46,02	1241,48	1,99					
SH–RM–R0–C0–A1–E1-2	2,60	5,70	6,39	36,64	6,23	39,86	1403,26	2,25					EPDM textured with peel ply
SH–RM–R0–C0–A1–E1-3	7,40	2,80	6,94	44,60	7,75	44,12	1408,23	2,25	2,05	DP-490			
SH–RM–R0–C0–A1–E1-4	3,00	2,50	6,54	37,01	5,97	36,68	1187,87	1,90					
SH–RM–R0–C0–A1–E1-5	4,00	3,30	6,34	40,35	6,24	37,59	1176,04	1,88					
SH–RM–R0–C0–A1–E2-1	7,00	2,80	7,01	43,64	5,88	36,43	1292,98	2,07					
SH–RM–R0–C0–A1–E2-2	2,60	4,40	7,89	46,31	7,92	48,00	1752,68	2,80					EPDM roughened with sandpaper
SH–RM–R0–C0–A1–E2-3	2,90	4,50	6,57	39,08	5,39	37,38	994,57	1,59	2,34				
SH–RM–R0–C0–A1–E2-4	3,40	2,90	5,22	32,13	6,69	40,22	1728,17	2,77					
SH–RM–R0–C0–A1–E2-5	2,80	7,70	5,75	41,95	7,49	44,63	1558,94	2,49			Clean Surface (0-50 RFU)	4-8 µm	
SH–RM–R0–C0–A2–E0-1	3,00	3,10	5,96	36,44	4,85	32,59	686,16	1,10					
SH–RM–R0–C0–A2–E0-2	3,00	3,20	5,40	40,14	5,29	38,24	640,20	1,02					non-textured EPDM
SH–RM–R0–C0–A2–E0-3	3,30	2,60	4,75	33,18	4,85	34,33	591,15	0,95	1,04				
SH–RM–R0–C0–A2–E0-4	3,10	3,50	4,13	28,37	4,47	36,75	821,12	1,31					
SH–RM–R0–C0–A2–E0-5	3,10	6,50	4,30	34,63	4,14	26,04	510,11	0,82					
SH–RM–R0–C0–A2–E1-1	2,40	3,30	4,51	28,86	4,43	31,43	974,38	1,56					
SH–RM–R0–C0–A2–E1-2	4,90	3,40	4,46	30,21	4,43	27,15	1030,46	1,65					EPDM textured with peel ply
SH–RM–R0–C0–A2–E1-3	5,10	5,00	4,21	27,96	4,65	26,19	1138,30	1,82	1,61	Araldite 2011			
SH–RM–R0–C0–A2–E1-4	12,00	5,30	4,31	34,00	4,59	34,91	1037,41	1,66					
SH–RM–R0–C0–A2–E1-5	1,80	5,10	4,41	31,71	4,24	28,93	853,32	1,37					
SH–RM–R0–C0–A2–E2-1	2,40	2,70	7,00	43,06	7,38	42,49	1420,94	2,27					
SH–RM–R0–C0–A2–E2-2	4,30	2,90	7,36	44,43	5,87	36,66	1435,01	2,30					EPDM roughened with sandpaper
SH–RM–R0–C0–A2–E2-3	3,30	6,90	7,58	40,55	7,37	43,09	1441,10	2,31	2,28				
SH–RM–R0–C0–A2–E2-4	3,50	7,60	6,55	36,74	5,49	34,23	1237,97	1,98					
SH–RM–R0–C0–A2–E2-5	5,70	3,40	7,14	46,16	6,28	41,21	1580,45	2,53					

Table A. 8 Rubber-Metal Bonding with Different Roughness Methods Shear Test Results

BIT Test Coupon Samples	Surface		Roughness Values (µm)				Maximum Load (N)	Tensile Stress at Maximum Load (MPa)	Mean Tensile Stress (MPa)	Adhesive	Cleanliness Level	Roughness Level	EPDM Roughening Method	Duration of Plasma Treatment
	First Coupon	Second Coupon	First Coupon		Second Coupon									
			Ra (µm)	Rz (µm)	Ra (µm)	Rz (µm)								
BIT–RM–R0–C0–A1–E0-P0-1	3,70	1,60	5,47	35,95	5,22	30,54	4820,00	4,25						
BIT–RM–R0–C0–A1–E0-P0-2	3,50	1,20	5,12	32,69	5,54	35,46	5363,40	4,73						without plasma treatment
BIT–RM–R0–C0–A1–E0-P0-3	1,30	1,40	5,33	34,19	5,73	34,15	4408,10	3,89	3,99					
BIT–RM–R0–C0–A1–E0-P0-4	1,60	2,00	5,01	26,50	5,92	32,96	3413,50	3,01						
BIT–RM–R0–C0–A1–E0-P0-5	1,50	1,60	5,14	32,59	5,34	33,34	4606,10	4,06						
BIT–RM–R0–C0–A1–E0-P30-1	1,30	1,50	5,26	36,04	4,69	30,82	4315,30	3,81						
BIT–RM–R0–C0–A1–E0-P30-2	1,80	1,00	5,34	28,98	5,19	33,40	4003,60	3,53						30 seconds plasma-treated EPDM
BIT–RM–R0–C0–A1–E0-P30-3	1,70	0,80	5,95	41,46	4,85	28,81	5647,50	4,98	4,09	DP-490				
BIT–RM–R0–C0–A1–E0-P30-4	0,90	1,20	4,66	27,09	5,52	33,22	5303,70	4,68						
BIT–RM–R0–C0–A1–E0-P30-5	0,70	0,50	5,92	38,48	5,25	31,51	3896,80	3,44						
BIT–RM–R0–C0–A1–E0-P60-1	2,70	1,70	5,65	30,97	5,27	29,89	5527,20	4,87						
BIT–RM–R0–C0–A1–E0-P60-2	2,20	1,90	5,84	35,36	4,99	30,26	4838,70	4,31						60 seconds plasma-treated EPDM
BIT–RM–R0–C0–A1–E0-P60-3	0,80	0,60	4,45	30,73	4,88	27,76	4890,90	4,31	4,80					
BIT–RM–R0–C0–A1–E0-P60-4	1,50	0,70	4,78	29,41	5,24	31,15	5748,90	5,07						
BIT–RM–R0–C0–A1–E0-P60-5	0,90	1,50	5,67	30,71	5,32	34,86	6170,90	5,44			Clean Surface (0-50 RFU)	4-8 µm	EPDM roughened with sandpaper	
BIT–RM–R0–C0–A2–E0-P0-1	1,20	0,30	5,16	27,47	4,88	32,71	4849,90	4,28						
BIT–RM–R0–C0–A2–E0-P0-2	3,00	1,00	5,70	31,16	4,85	30,83	5187,70	4,57						without plasma treatment
BIT–RM–R0–C0–A2–E0-P0-3	0,70	2,30	5,21	28,65	5,52	31,49	4149,50	3,66	4,23					
BIT–RM–R0–C0–A2–E0-P0-4	0,10	1,40	4,56	28,38	5,34	28,69	5148,20	4,54						
BIT–RM–R0–C0–A2–E0-P0-5	0,80	0,30	5,25	31,17	5,03	30,85	4677,30	4,12						
BIT–RM–R0–C0–A2–E0-P30-1	1,00	1,20	5,14	30,35	4,65	30,99	5550,50	4,89						
BIT–RM–R0–C0–A2–E0-P30-2	1,00	1,60	4,78	30,93	5,87	32,16	6167,50	5,44						30 seconds plasma-treated EPDM
BIT–RM–R0–C0–A2–E0-P30-3	2,60	1,50	5,02	32,10	4,45	26,77	5754,60	5,07	5,26	Araldite 2011				
BIT–RM–R0–C0–A2–E0-P30-4	2,50	1,90	4,73	28,48	4,95	30,34	6460,30	5,70						
BIT–RM–R0–C0–A2–E0-P30-5	0,90	1,60	5,19	32,48	5,99	39,56	5879,20	5,18						
BIT–RM–R0–C0–A2–E0-P60-1	2,10	4,40	5,43	33,48	4,72	30,10	6091,20	5,37						
BIT–RM–R0–C0–A2–E0-P60-2	2,10	2,10	5,29	33,93	5,72	33,68	5919,10	5,22						60 seconds plasma-treated EPDM
BIT–RM–R0–C0–A2–E0-P60-3	3,60	1,80	5,96	33,25	4,64	26,59	6426,70	5,67	5,54					
BIT–RM–R0–C0–A2–E0-P60-4	1,50	3,50	4,87	27,10	4,82	31,72	6528,20	5,76						
BIT–RM–R0–C0–A2–E0-P60-5	2,40	1,20	4,60	31,60	4,53	28,04	6422,50	5,66						

Table A. 9 Rubber-Metal Bonding with Different Plasma Treatment Time Tensile Test Results

Shear Test Coupon Samples	Surface		Roughness Values (µm)				Maximum Load (N)	Tensile Stress at Maximum Load (MPa)	Mean Tensile Stress (MPa)	Adhesive	Cleanliness Level	Roughness Level	EPDM Roughening Method	Duration of Plasma Treatment
	First Coupon	Second Coupon	First Coupon		Second Coupon									
			Ra (µm)	Rz (µm)	Ra (µm)	Rz (µm)								
SH–RM–R0–C0–A1–E0-P0-1	4,40	4,70	5,89	37,72	6,10	34,97	1260,00	2,05						
SH–RM–R0–C0–A1–E0-P0-2	8,70	6,60	5,97	35,93	5,25	31,59	1140,00	1,82						without plasma treatment
SH–RM–R0–C0–A1–E0-P0-3	19,30	6,70	6,08	35,53	6,25	36,13	1970,00	3,16	2,34					
SH–RM–R0–C0–A1–E0-P0-4	23,30	7,20	5,04	30,17	5,53	34,58	1950,00	3,12						
SH–RM–R0–C0–A1–E0-P0-5	15,80	4,50	4,94	30,36	6,48	37,92	970,00	1,55						
SH–RM–R0–C0–A1–E0-P15-1	15,50	19,60	6,49	36,31	6,05	33,30	2000,00	3,21						
SH–RM–R0–C0–A1–E0-P15-2	9,20	3,00	5,70	33,45	5,97	33,37	1350,00	2,16						15 seconds plasma-treated EPDM
SH–RM–R0–C0–A1–E0-P15-3	12,20	9,30	6,46	39,07	6,51	42,12	2220,00	3,55	3,20	DP-490				
SH–RM–R0–C0–A1–E0-P15-4	13,10	37,30	5,42	32,86	6,41	38,59	2380,00	3,81						
SH–RM–R0–C0–A1–E0-P15-5	12,70	3,30	6,41	35,57	5,45	32,60	2040,00	3,26						
SH–RM–R0–C0–A1–E0-P30-1	2,70	40,50	6,01	35,56	6,37	33,66	2250,00	3,59						
SH–RM–R0–C0–A1–E0-P30-2	12,40	11,10	5,46	31,70	6,40	35,89	1990,00	3,18						30 seconds plasma-treated EPDM
SH–RM–R0–C0–A1–E0-P30-3	7,30	7,20	5,93	33,33	5,51	32,67	2120,00	3,39	3,50					
SH–RM–R0–C0–A1–E0-P30-4	1,80	4,50	5,29	32,50	6,70	42,68	2130,00	3,41						
SH–RM–R0–C0–A1–E0-P30-5	7,40	3,20	6,45	36,17	5,24	32,40	2470,00	3,94			Clean Surface (0-50 RFU)	4-8 µm	EPDM roughened with sandpaper	
SH–RM–R0–C0–A2–E0-P0-1	3,90	7,00	6,88	39,76	5,43	31,52	1300,00	2,08						
SH–RM–R0–C0–A2–E0-P0-2	2,90	6,70	5,21	32,25	5,81	33,81	1120,00	1,79						without plasma treatment
SH–RM–R0–C0–A2–E0-P0-3	6,80	3,40	5,84	34,63	6,72	40,66	1750,00	2,80	2,22					
SH–RM–R0–C0–A2–E0-P0-4	6,30	17,40	6,66	40,74	5,60	32,07	1040,00	1,66						
SH–RM–R0–C0–A2–E0-P0-5	8,20	9,80	6,15	34,57	6,66	37,92	1740,00	2,78						
SH–RM–R0–C0–A2–E0-P15-1	30,30	14,90	6,37	39,19	6,21	38,82	1880,00	3,00						
SH–RM–R0–C0–A2–E0-P15-2	3,00	14,70	5,35	38,15	5,61	33,22	2090,00	3,34						15 seconds plasma-treated EPDM
SH–RM–R0–C0–A2–E0-P15-3	12,40	6,70	6,45	35,11	5,95	38,22	2080,00	3,33	2,95	Araldite 2011				
SH–RM–R0–C0–A2–E0-P15-4	4,70	10,70	5,30	30,59	5,42	31,62	1390,00	2,23						
SH–RM–R0–C0–A2–E0-P15-5	16,10	14,50	6,51	40,39	5,61	30,59	1780,00	2,85						
SH–RM–R0–C0–A2–E0-P30-1	37,10	7,80	5,61	32,60	5,38	33,20	2410,00	3,86						
SH–RM–R0–C0–A2–E0-P30-2	2,20	17,00	6,16	34,49	6,42	34,56	2050,00	3,29						30 seconds plasma-treated EPDM
SH–RM–R0–C0–A2–E0-P30-3	4,30	14,40	5,82	32,49	5,19	29,93	2580,00	4,12	3,41					
SH–RM–R0–C0–A2–E0-P30-4	2,50	13,60	6,04	34,97	6,28	36,25	1310,00	2,10						
SH–RM–R0–C0–A2–E0-P30-5	12,70	29,70	5,15	29,17	5,48	33,64	2290,00	3,67						

Table A. 10 Rubber-Metal Bonding with Different Plasma Treatment Time Shear Test Results

B. Tensile Test and Shear Test Coupon Images and Failure Modes

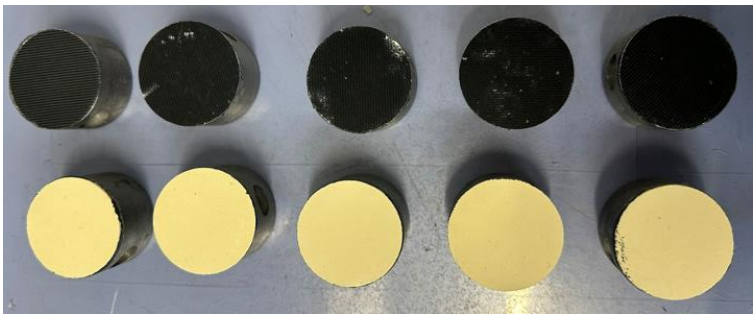


Figure B. 1 Rubber-Metal Bonding, Tensile Test, DP490, Non-blasted, 0-50 RFU, Adhesive Failure

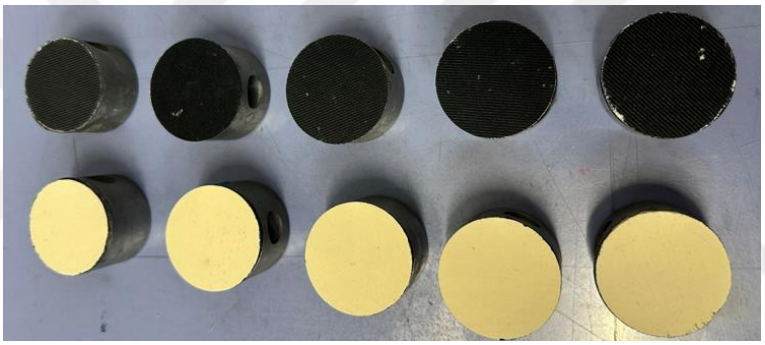


Figure B. 2 Rubber-Metal Bonding, Tensile Test, DP490, Non-blasted, 50-200 RFU, Adhesive Failure

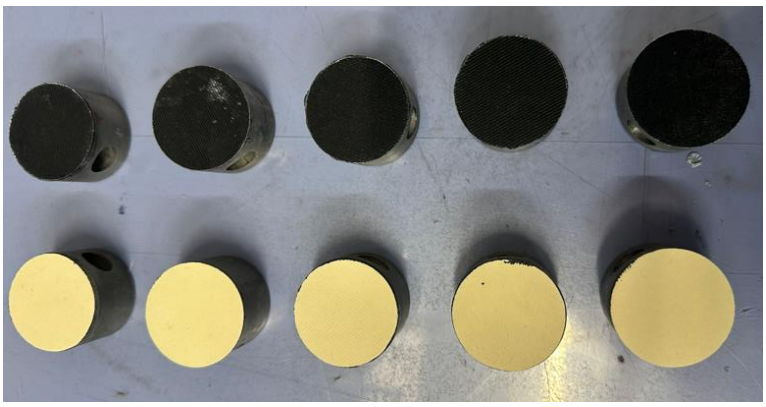


Figure B. 3 Rubber-Metal Bonding, Tensile Test, DP490, Non-blasted, 300-750 RFU, Adhesive Failure



Figure B. 4 Rubber-Metal Bonding, Tensile Test, DP490, 1-2 µm, 0-50 RFU, Adhesive Failure

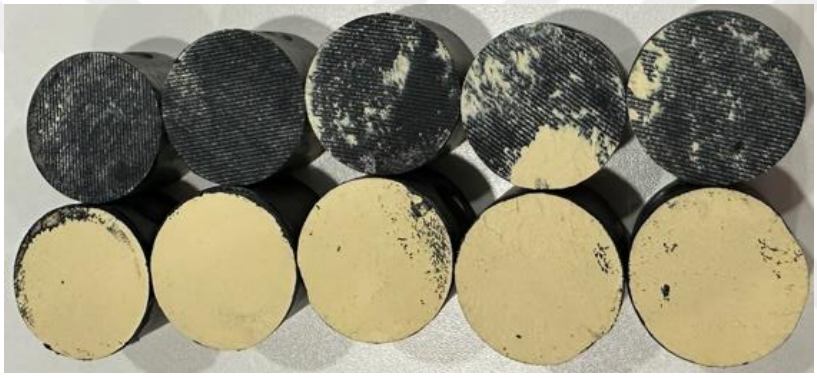


Figure B. 5 Rubber-Metal Bonding, Tensile Test, DP490, 1-2 µm, 50-200 RFU, Mixed Failure



Figure B. 6 Rubber-Metal Bonding, Tensile Test, DP490, 1-2 µm, 300-750 RFU, Mixed Failure

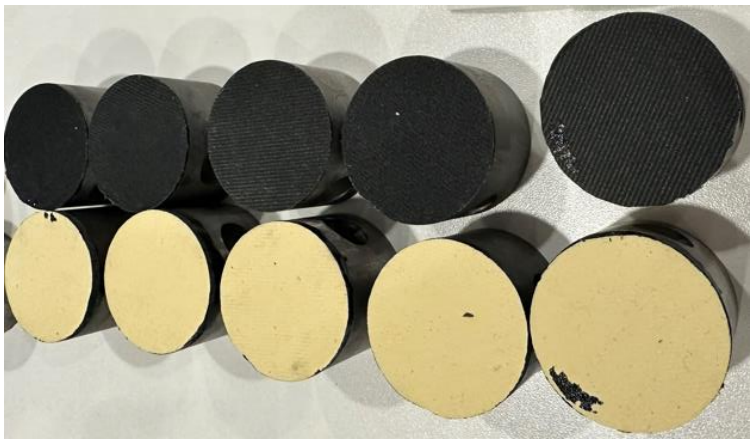


Figure B. 7 Rubber-Metal Bonding, Tensile Test, DP490, 2-4 µm, 0-50 RFU, Adhesive Failure

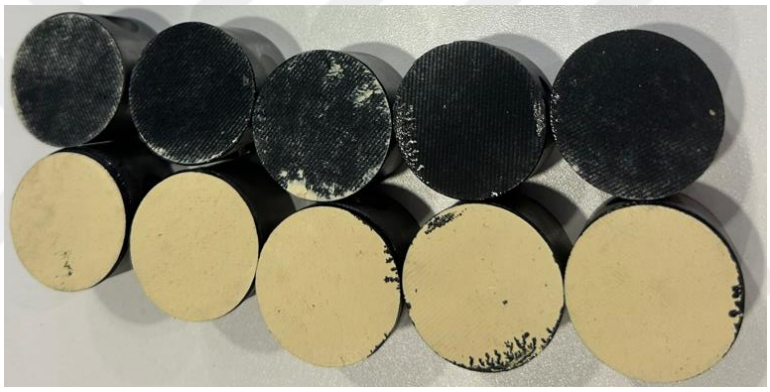


Figure B. 8 Rubber-Metal Bonding, Tensile Test, DP490, 2-4 µm, 50-200 RFU, Adhesive Failure

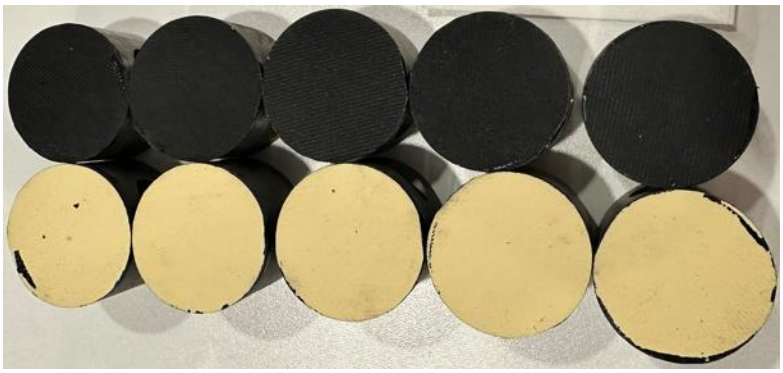


Figure B. 9 Rubber-Metal Bonding, Tensile Test, DP490, 2-4 µm, 300-750 RFU, Adhesive Failure

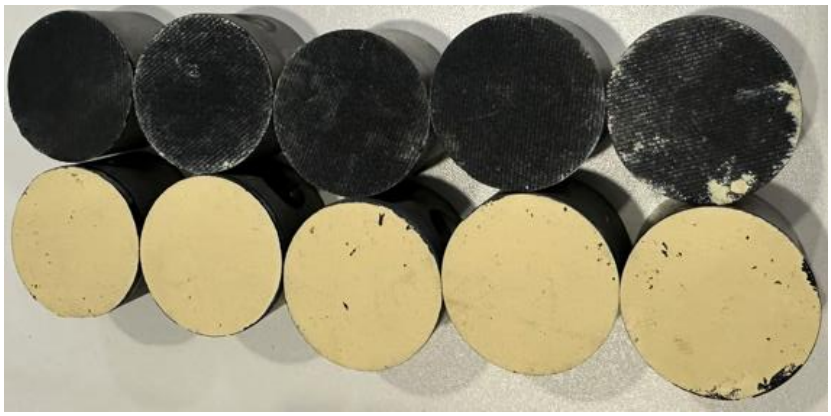


Figure B. 10 Rubber-Metal Bonding, Tensile Test, DP490, 4-8 µm, 0-50 RFU, Adhesive Failure

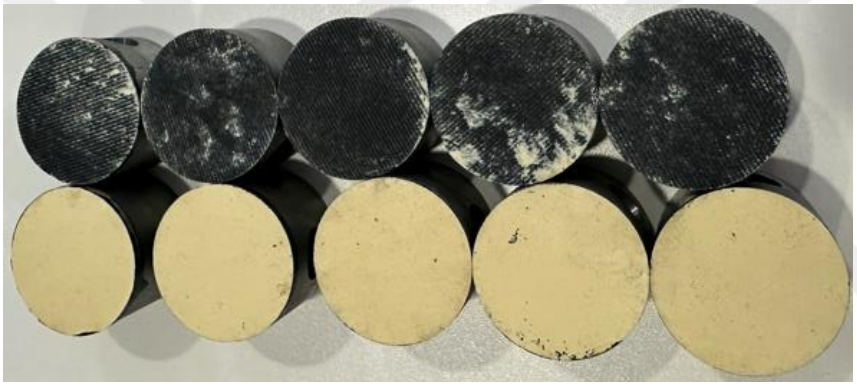


Figure B. 11 Rubber-Metal Bonding, Tensile Test, DP490, 4-8 µm, 50-200 RFU, Adhesive Failure

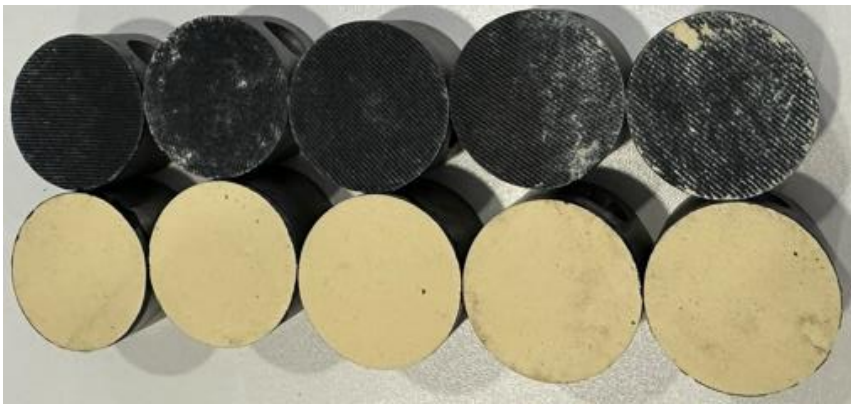


Figure B. 12 Rubber-Metal Bonding, Tensile Test, DP490, 4-8 µm, 300-750 RFU, Adhesive Failure

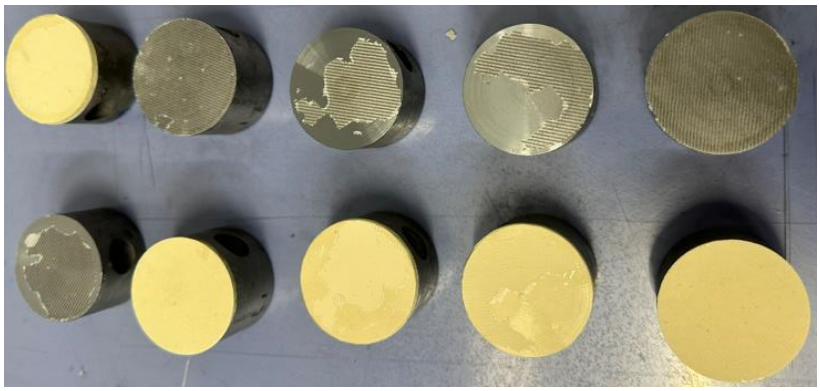


Figure B. 13 Rubber-Metal Bonding, Tensile Test, Araldite 2011, Non-blasted, 0-50 RFU, Adhesive Failure

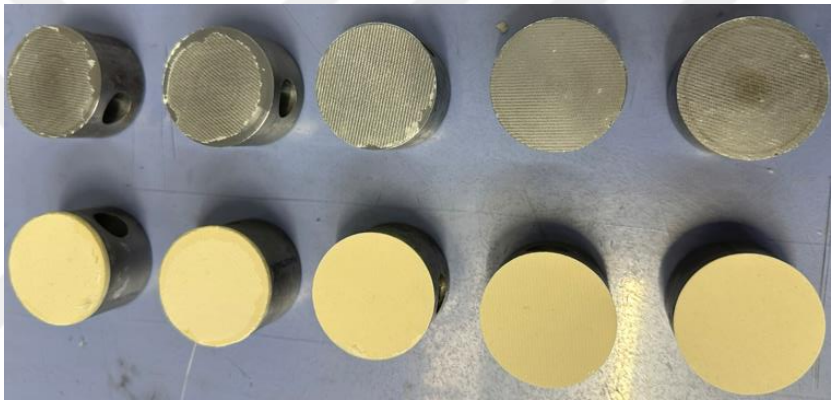


Figure B. 14 Rubber-Metal Bonding, Tensile Test, Araldite 2011, Non-blasted, 50-200 RFU, Adhesive Failure

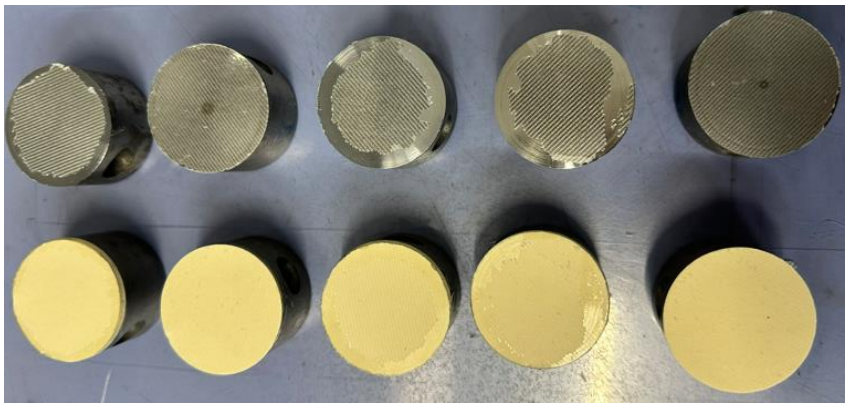


Figure B. 15 Rubber-Metal Bonding, Tensile Test, Araldite 2011, Non-blasted, 300-750 RFU, Adhesive Failure

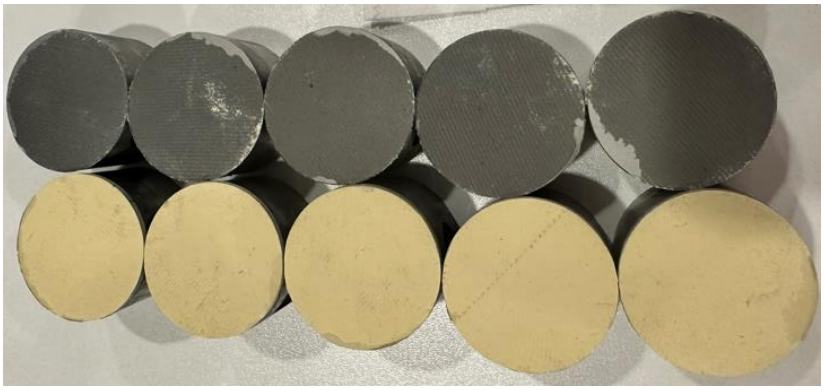


Figure B. 16 Rubber-Metal Bonding, Tensile Test, Araldite 2011, 1-2 µm, 0-50 RFU, Adhesive Failure

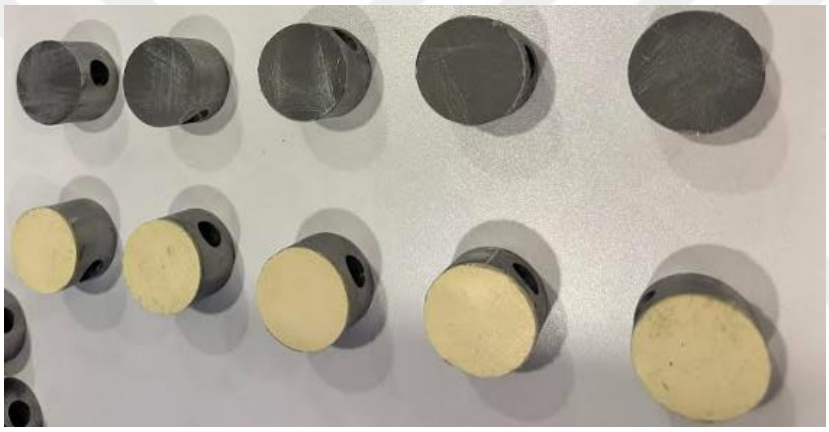


Figure B. 17 Rubber-Metal Bonding, Tensile Test, Araldite 2011, 1-2 µm, 50-200 RFU, Adhesive Failure

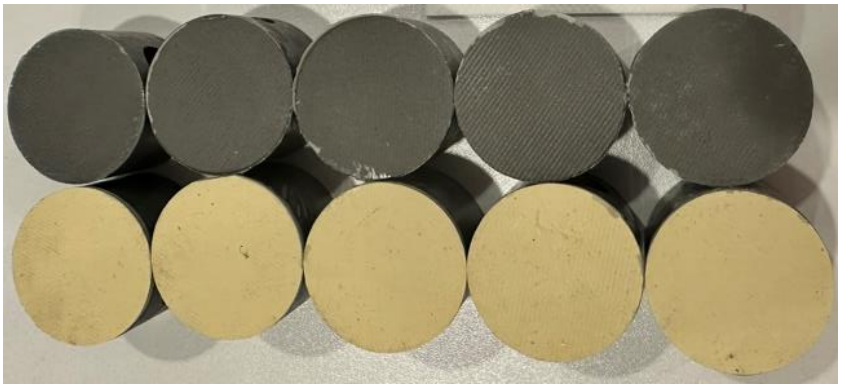


Figure B. 18 Rubber-Metal Bonding, Tensile Test, Araldite 2011, 1-2 µm, 300-750 RFU, Adhesive Failure

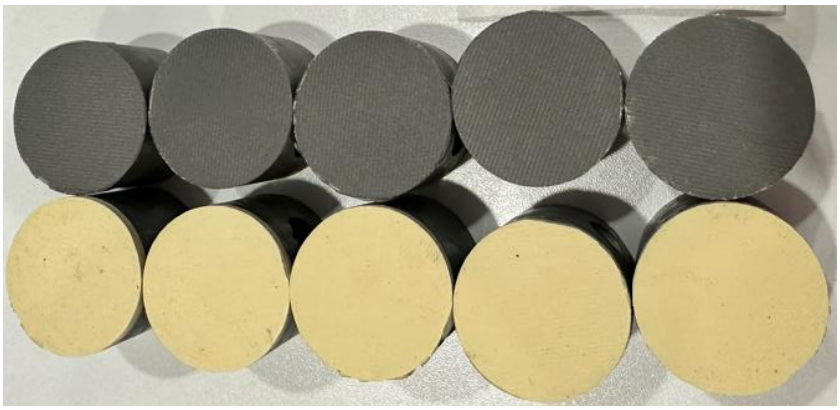


Figure B. 19 Rubber-Metal Bonding, Tensile Test, Araldite 2011, 2-4 µm, 0-50 RFU, Adhesive Failure



Figure B. 20 Rubber-Metal Bonding, Tensile Test, Araldite 2011, 2-4 µm, 50-200 RFU, Adhesive Failure



Figure B. 21 Rubber-Metal Bonding, Tensile Test, Araldite 2011, 2-4 µm, 300-750 RFU, Adhesive Failure

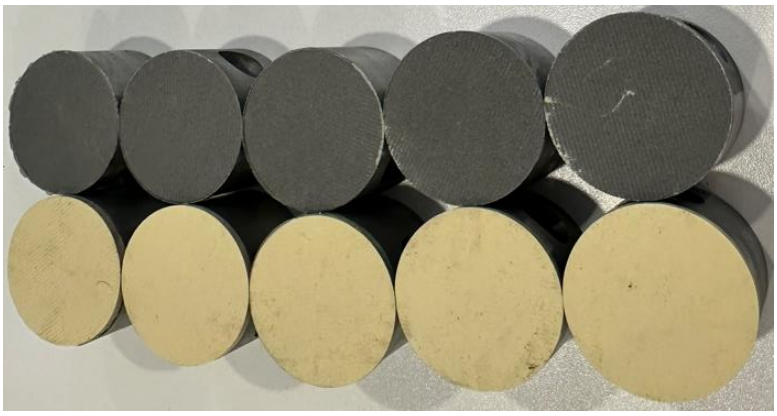


Figure B. 22 Rubber-Metal Bonding, Tensile Test, Araldite 2011, 4-8 µm, 0-50 RFU, Adhesive Failure

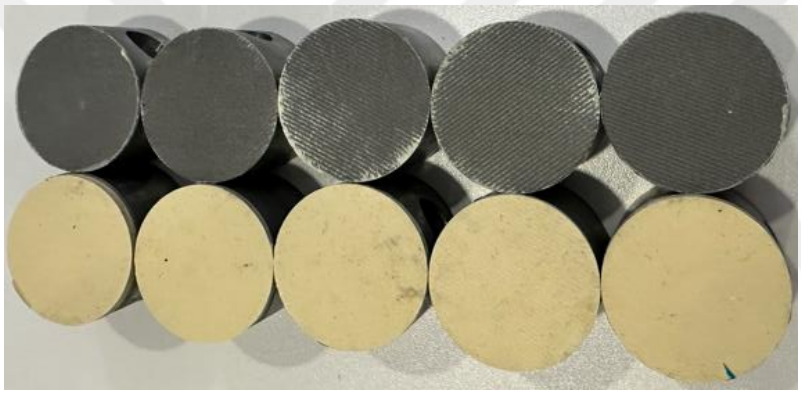


Figure B. 23 Rubber-Metal Bonding, Tensile Test, Araldite 2011, 4-8 µm, 50-200 RFU, Adhesive Failure

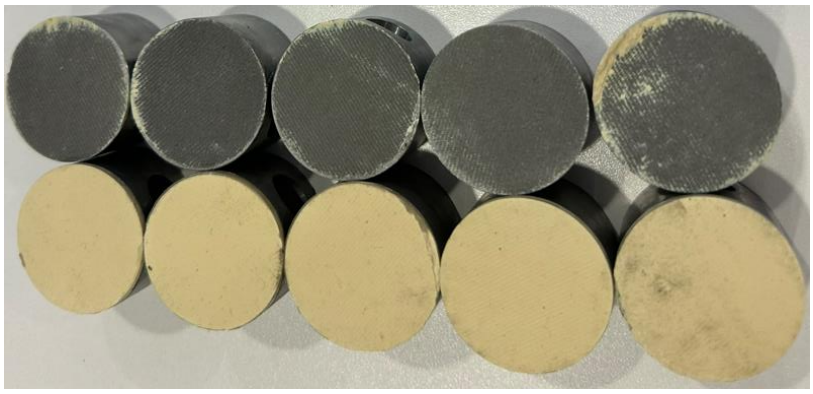


Figure B. 24 Rubber-Metal Bonding, Tensile Test, Araldite 2011, 4-8 µm, 300-750 RFU, Adhesive Failure

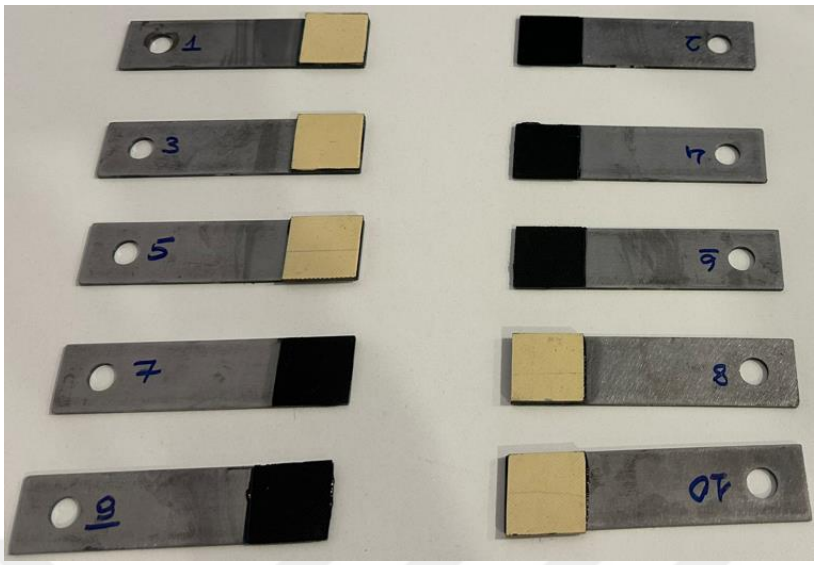


Figure B. 25 Rubber-Metal Bonding, Shear Test, DP490, Non-blasted, 0-50 RFU, Adhesive Failure

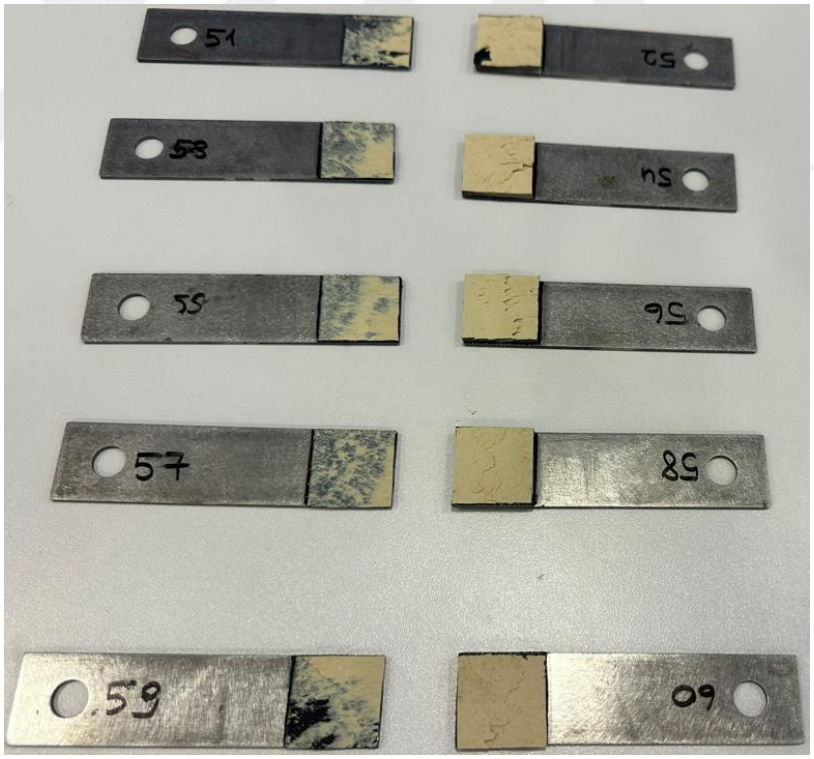


Figure B. 26 Rubber-Metal Bonding, Shear Test, DP490, Non-blasted, 50-200 RFU, Cohesive Failure in EPDM

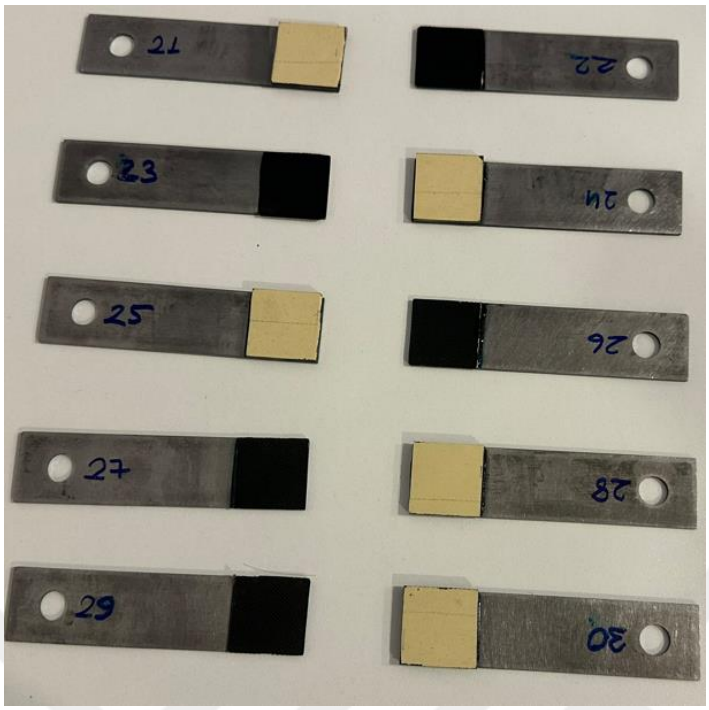


Figure B. 27 Rubber-Metal Bonding, Shear Test, DP490, Non-blasted, 300-750 RFU, Adhesive Failure

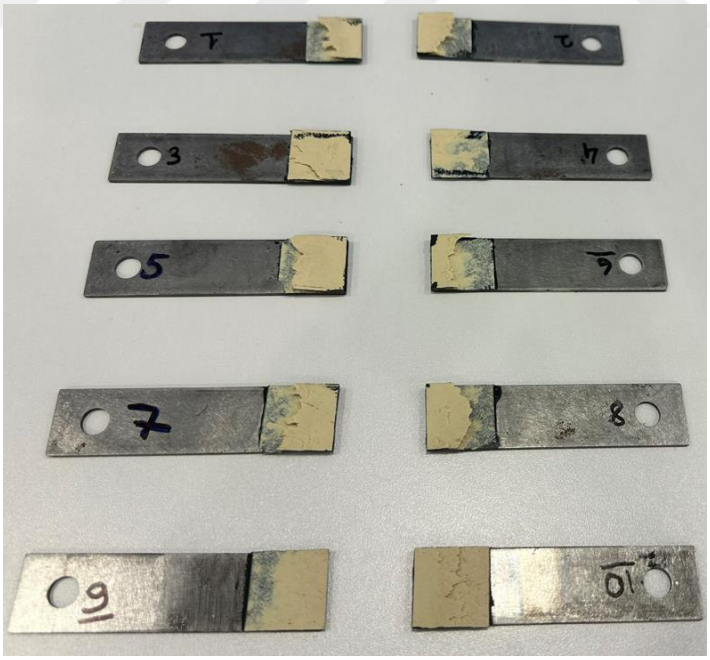


Figure B. 28 Rubber-Metal Bonding, Shear Test, DP490, 1-2 µm, 0-50 RFU, Cohesive Failure in EPDM

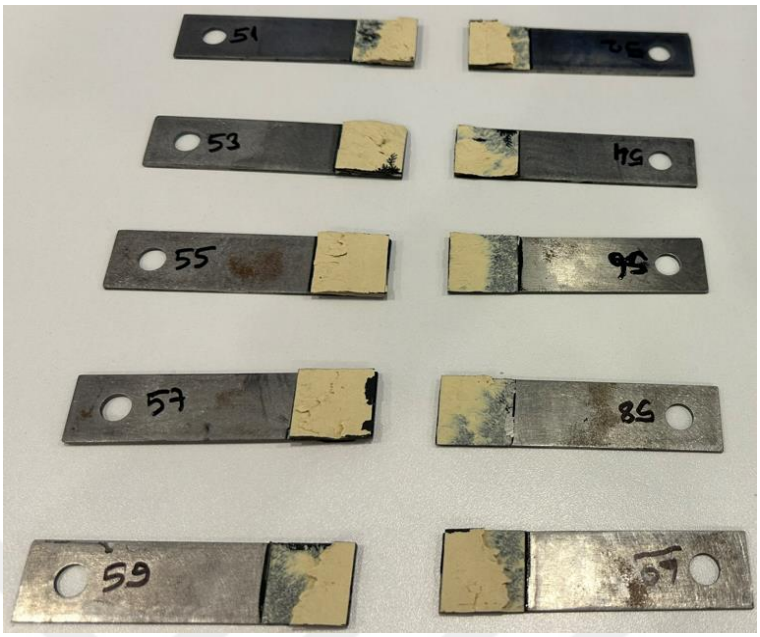


Figure B. 29 Rubber-Metal Bonding, Shear Test, DP490, 1-2 µm, 50-200 RFU, Cohesive Failure in EPDM

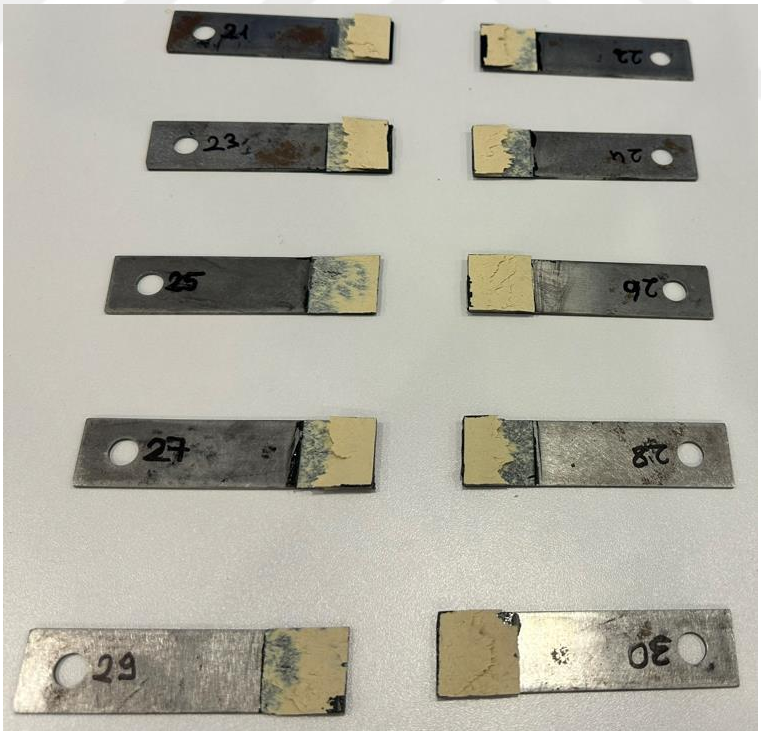


Figure B. 30 Rubber-Metal Bonding, Shear Test, DP490, 1-2 µm, 300-750 RFU, Cohesive Failure in EPDM

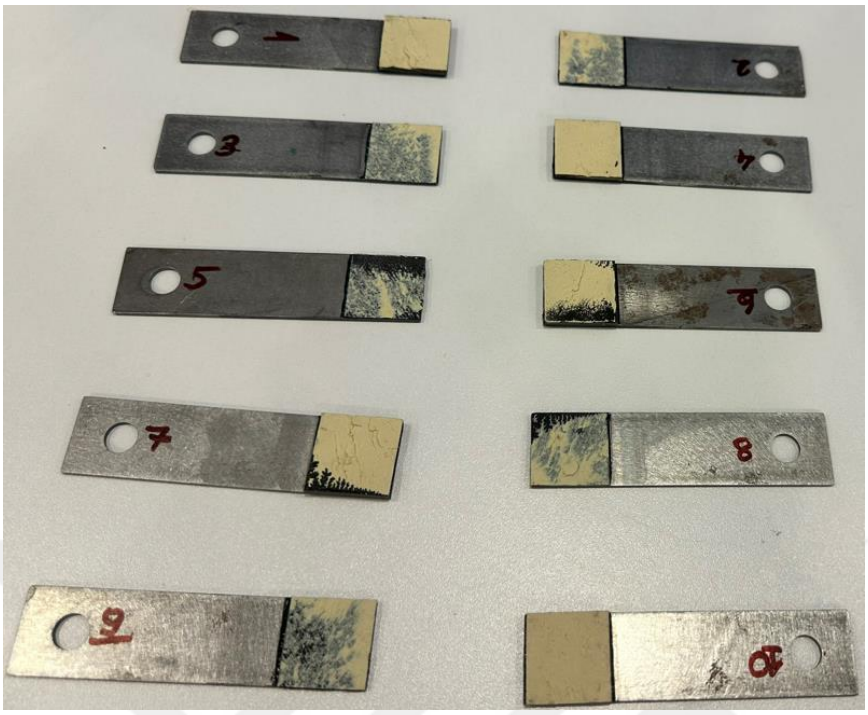


Figure B. 31 Rubber-Metal Bonding, Shear Test, DP490, 2-4 µm, 0-50 RFU, Mixed Failure

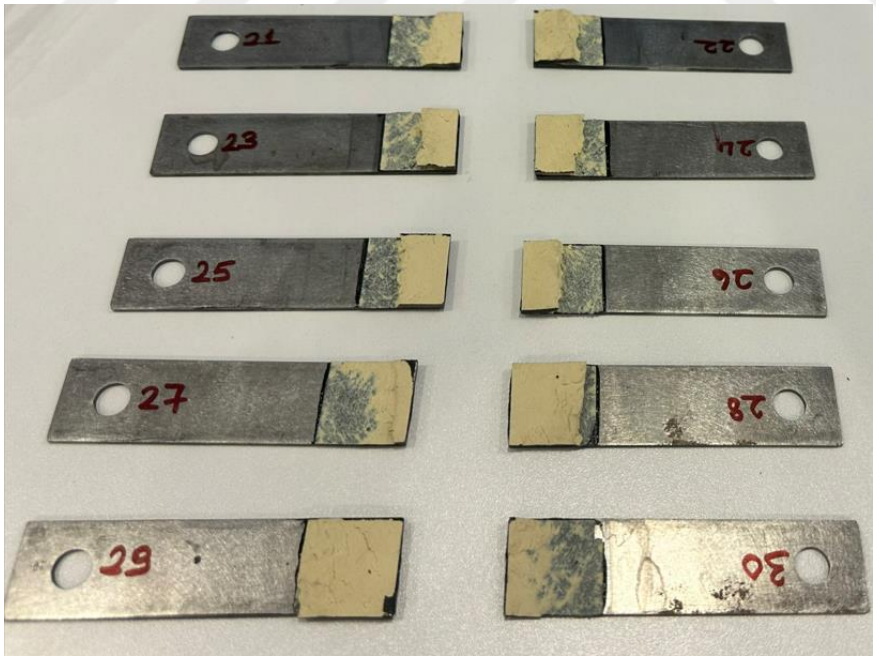


Figure B. 32 Rubber-Metal Bonding, Shear Test, DP490, 2-4 µm, 50-200 RFU, Cohesive Failure in EPDM

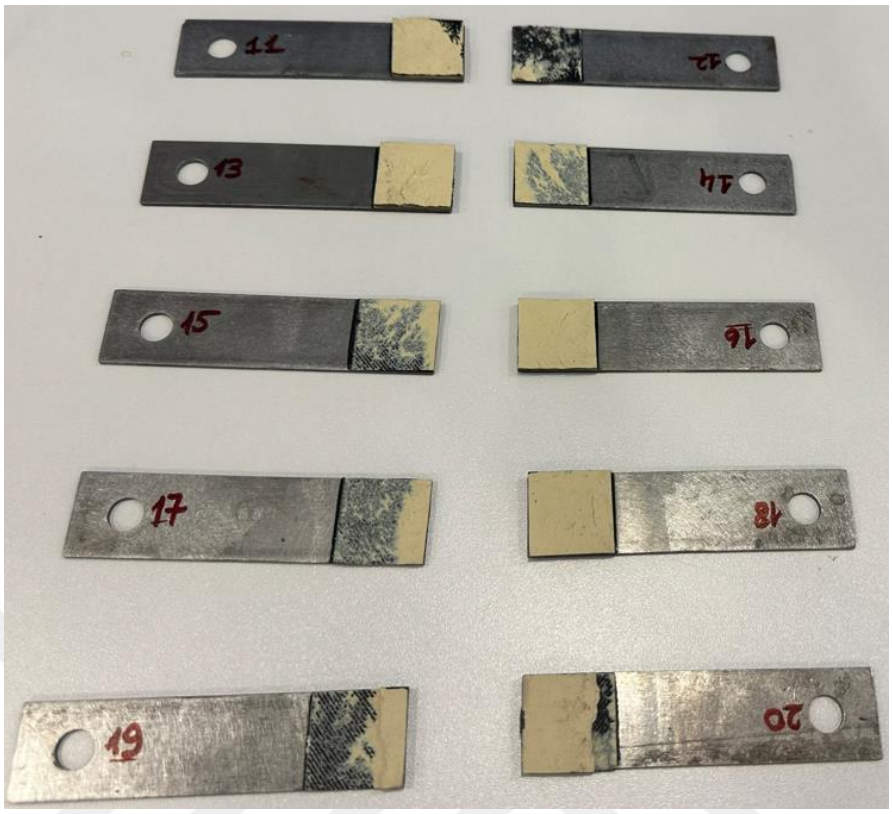


Figure B. 33 Rubber-Metal Bonding, Shear Test, DP490, 2-4 µm, 300-750 RFU, Mixed Failure

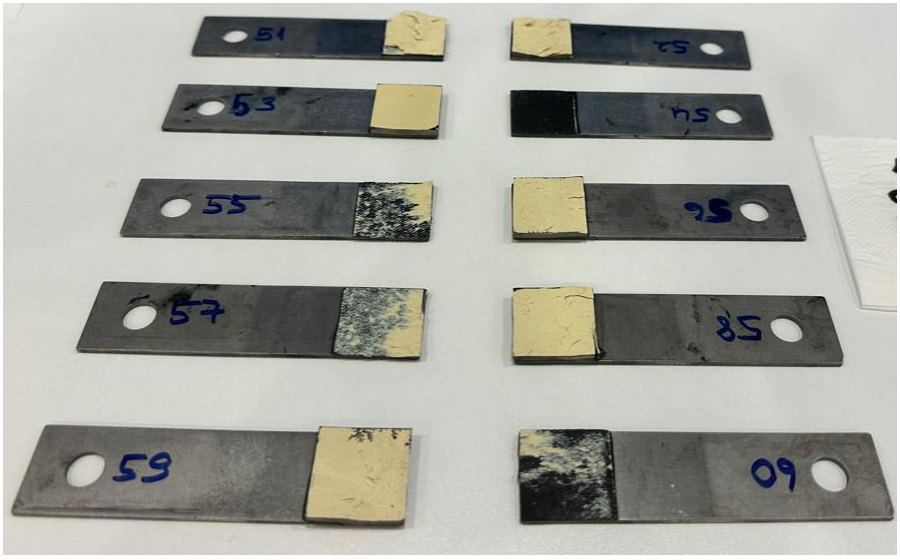


Figure B. 34 Rubber-Metal Bonding, Shear Test, DP490, 4-8 µm, 0-50 RFU, Mixed Failure

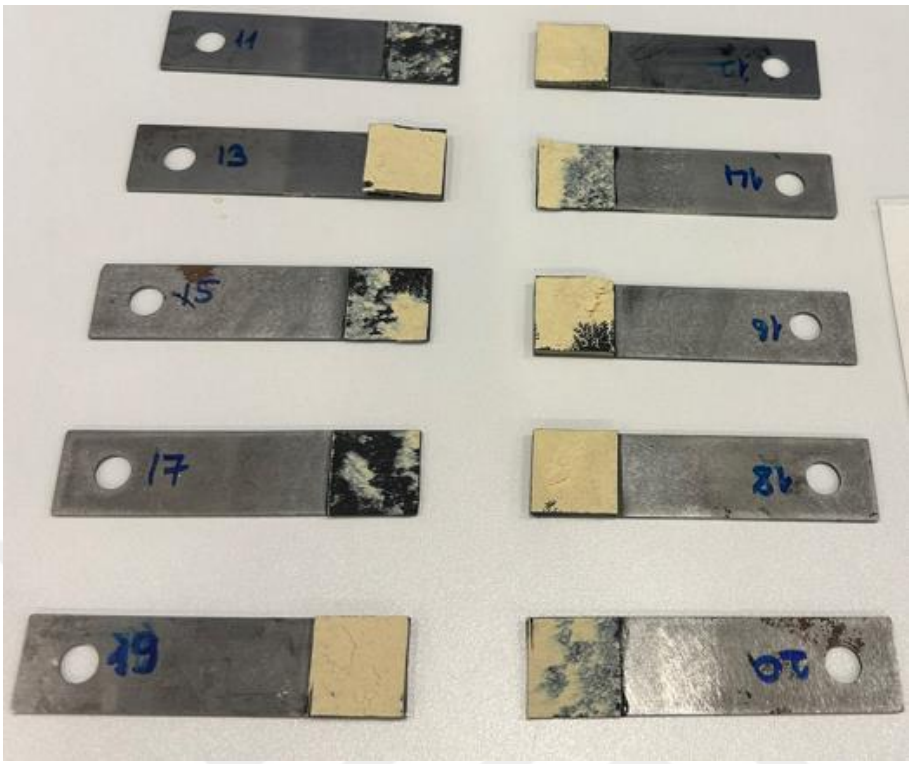


Figure B. 35 Rubber-Metal Bonding, Shear Test, DP490, 4-8 µm, 50-200 RFU, Mixed Failure

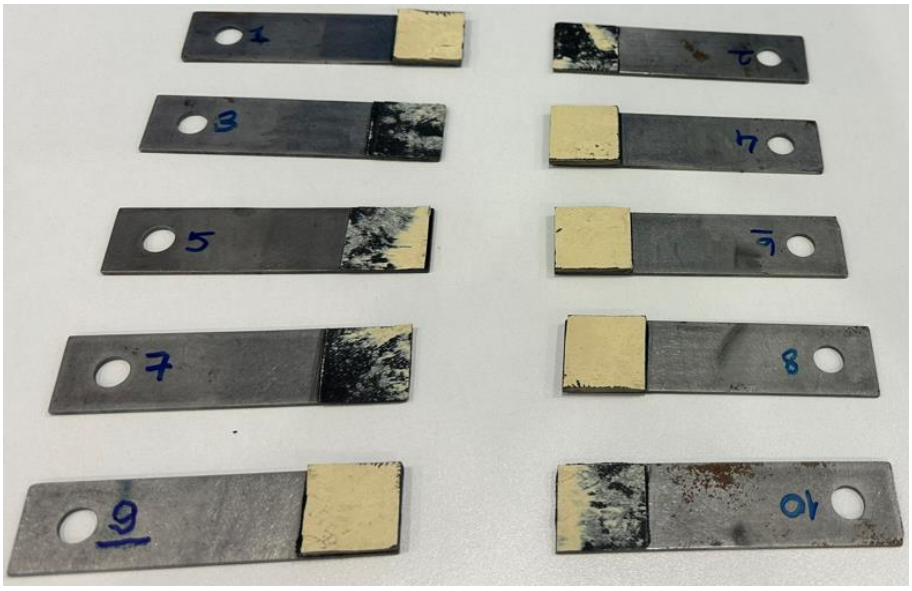


Figure B. 36 Rubber-Metal Bonding, Shear Test, DP490, 4-8 µm, 300-750 RFU, Mixed Failure

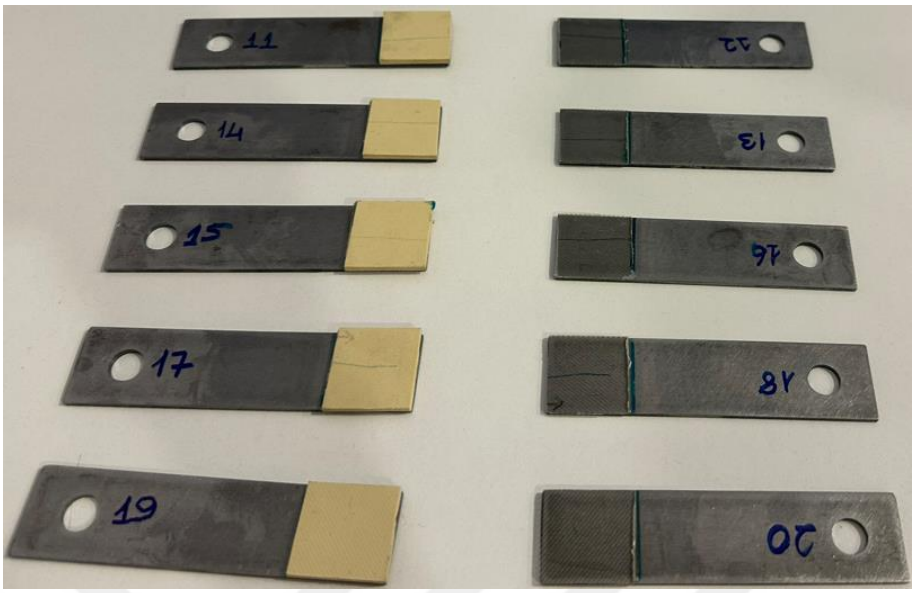


Figure B. 37 Rubber-Metal Bonding, Shear Test, Araldite 2011, Non-blasted, 0-50 RFU, Adhesive Failure

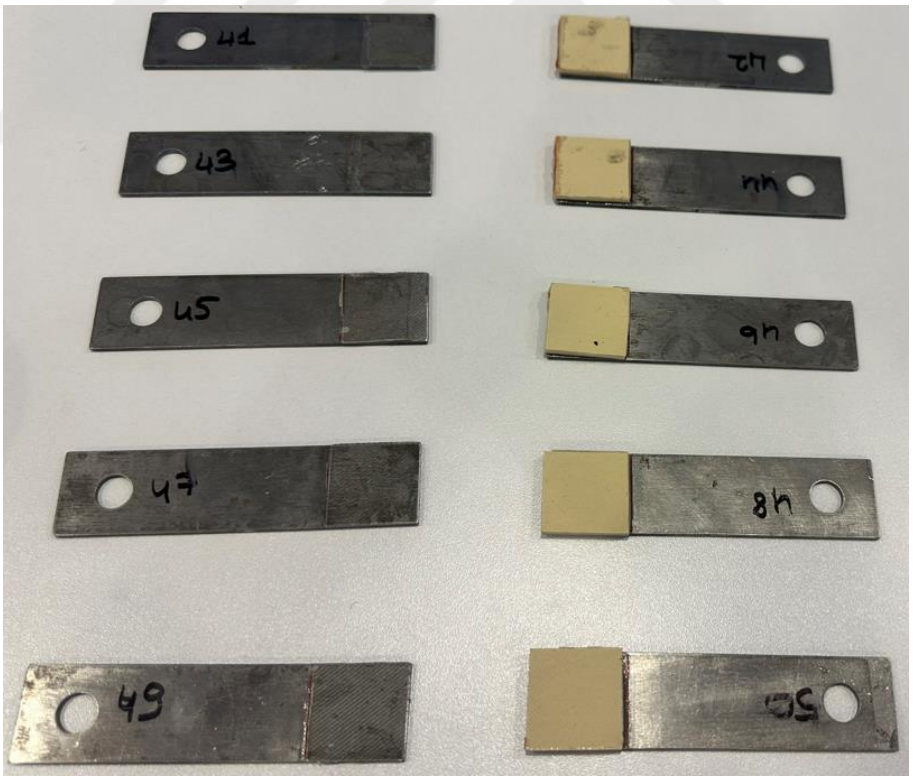


Figure B. 38 Rubber-Metal Bonding, Shear Test, Araldite 2011, Non-blasted, 50-200 RFU, Adhesive Failure

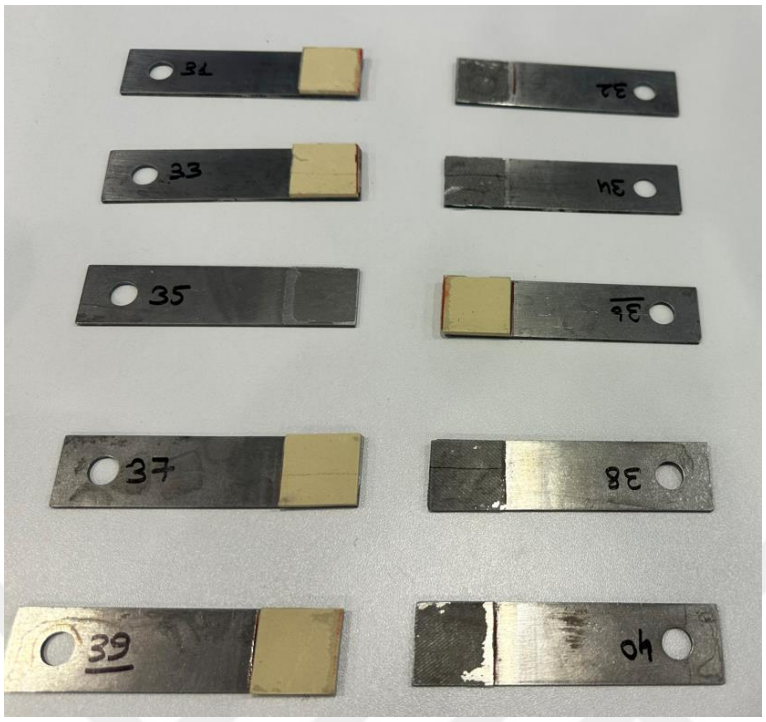


Figure B. 39 Rubber-Metal Bonding, Shear Test, Araldite 2011, Non-blasted, 300-750 RFU, Adhesive Failure

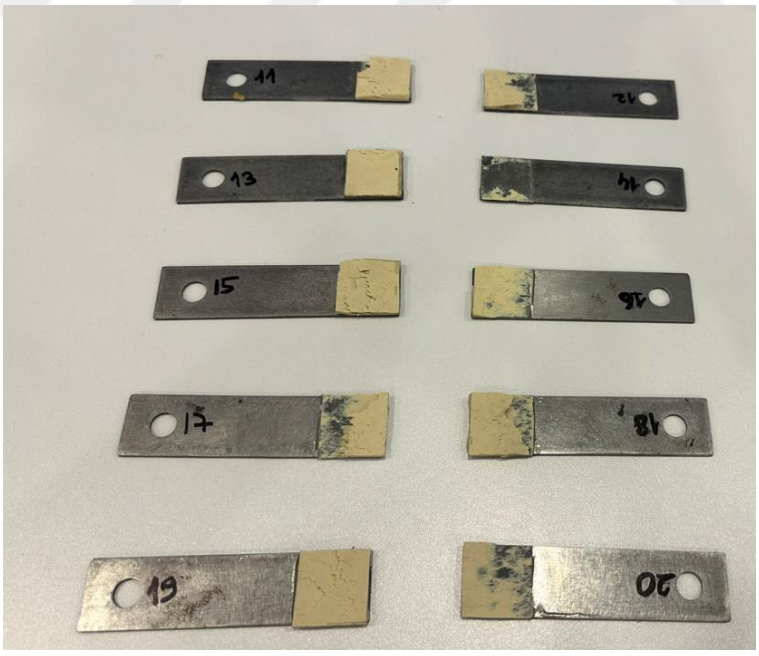


Figure B. 40 Rubber-Metal Bonding, Shear Test, Araldite 2011, 1-2 µm, 0-50 RFU, Cohesive Failure in EPDM

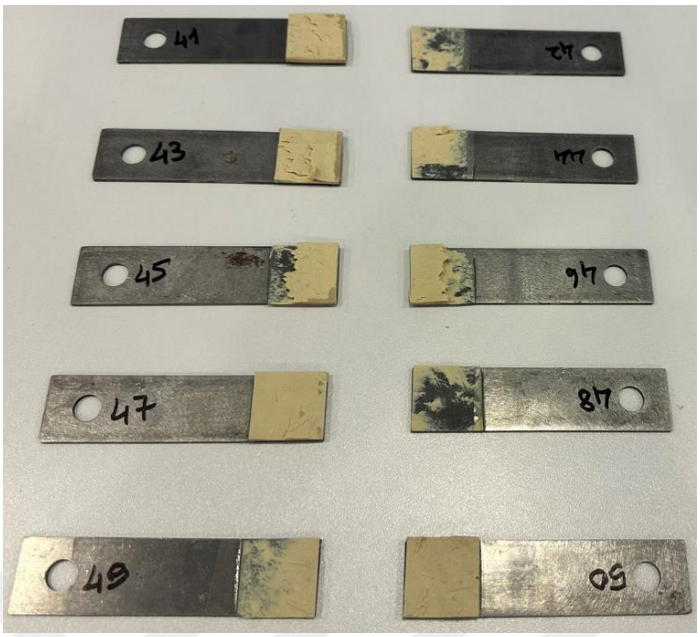


Figure B. 41 Rubber-Metal Bonding, Shear Test, Araldite 2011, 1-2 µm, 50-200 RFU, Cohesive Failure in EPDM

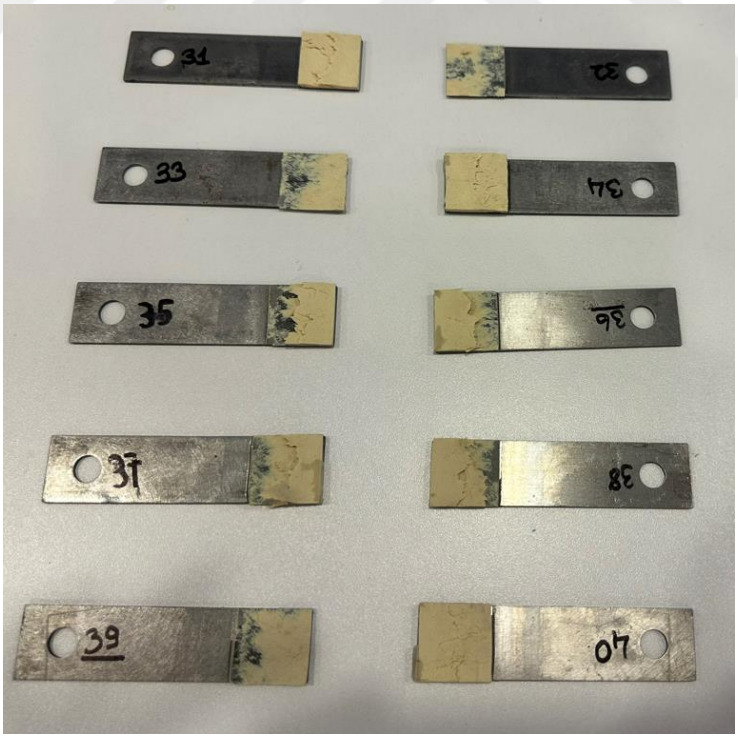


Figure B. 42 Rubber-Metal Bonding, Shear Test, Araldite 2011, 1-2 µm, 300-750 RFU, Cohesive Failure in EPDM

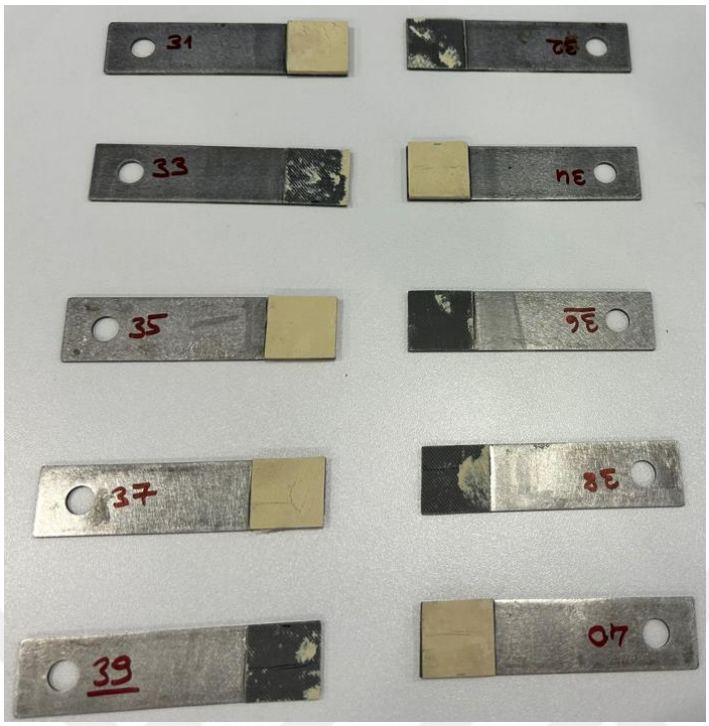


Figure B. 43 Rubber-Metal Bonding, Shear Test, Araldite 2011, 2-4 µm, 0-50 RFU, Adhesive Failure

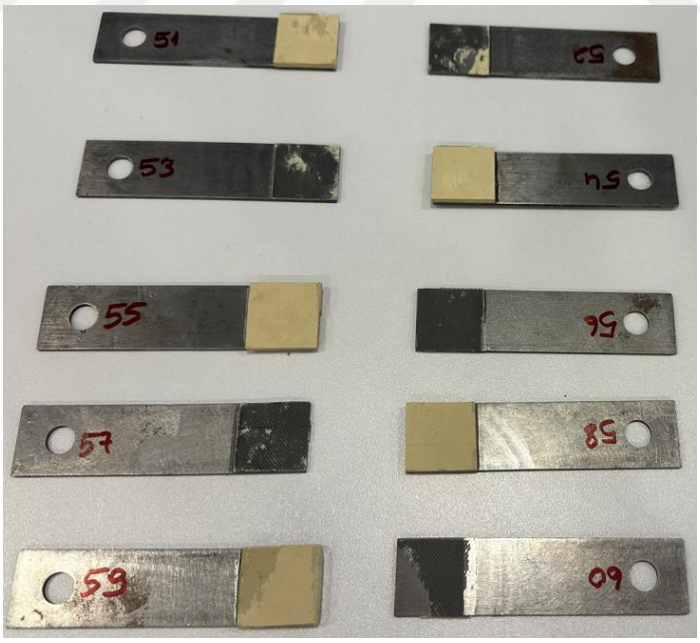


Figure B. 44 Rubber-Metal Bonding, Shear Test, Araldite 2011, 2-4 µm, 50-200 RFU, Adhesive Failure

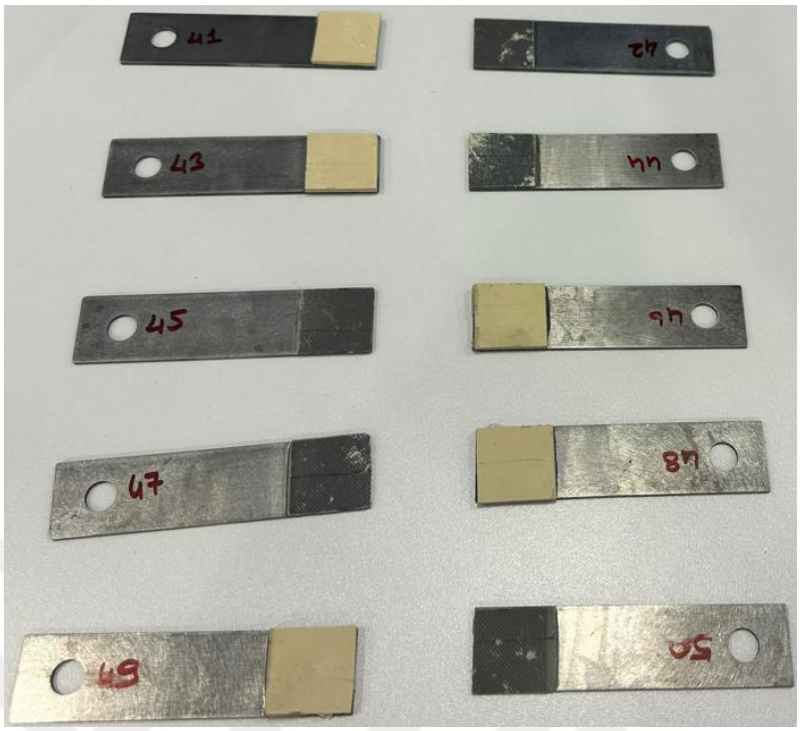


Figure B. 45 Rubber-Metal Bonding, Shear Test, Araldite 2011, 2-4 µm, 300-750 RFU, Adhesive Failure

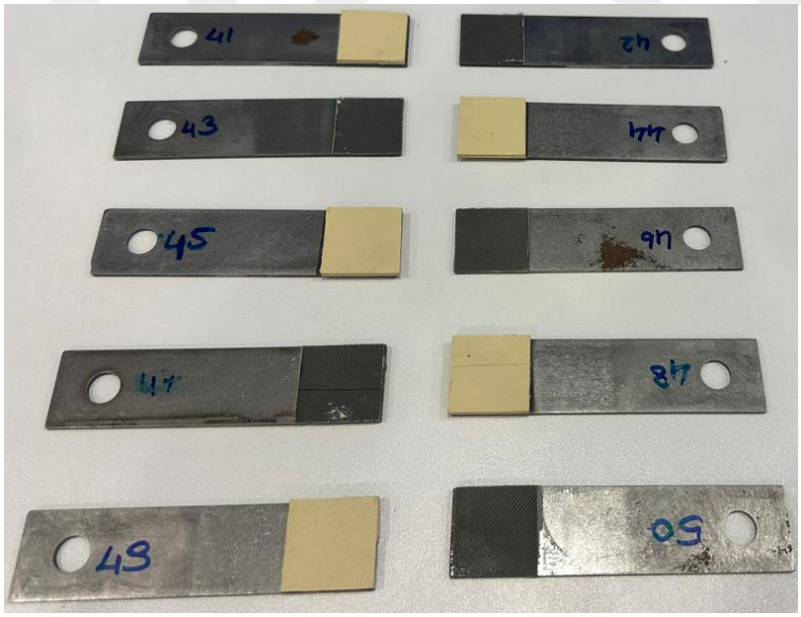


Figure B. 46 Rubber-Metal Bonding, Shear Test, Araldite 2011, 4-8 µm, 0-50 RFU, Adhesive Failure

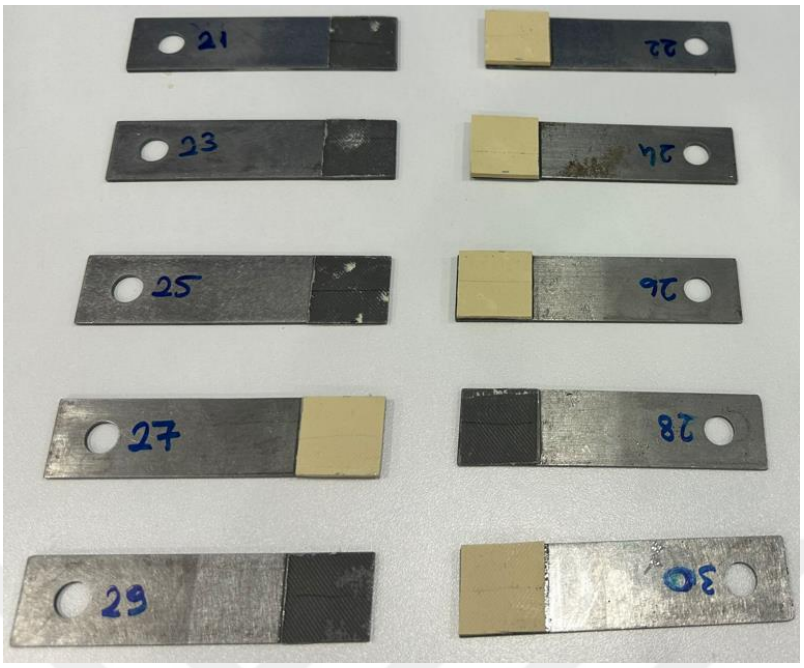


Figure B. 47 Rubber-Metal Bonding, Shear Test, Araldite 2011, 4-8 µm, 50-200 RFU, Adhesive Failure

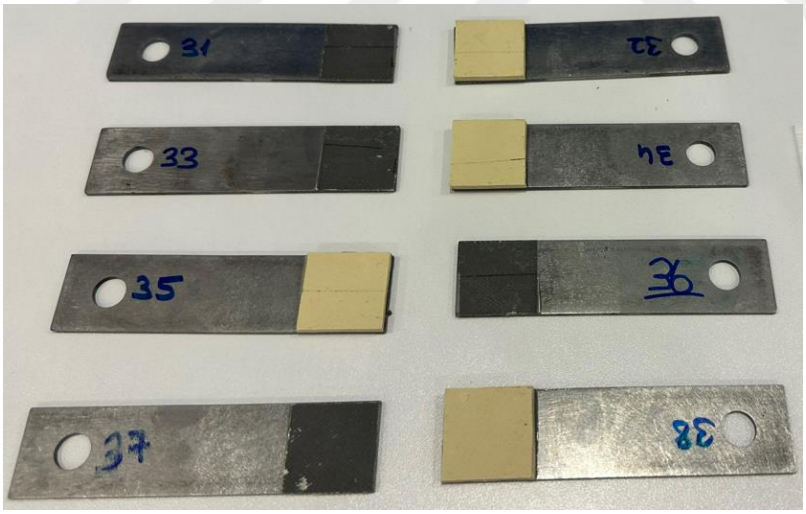


Figure B. 48 Rubber-Metal Bonding, Shear Test, Araldite 2011, 4-8 µm, 300-750 RFU, Adhesive Failure



Figure B. 49 Metal-Metal Bonding, Shear Test, DP490, Non-blasted, 0-50 RFU, Adhesive Failure



Figure B. 50 Metal-Metal Bonding, Shear Test, DP490, Non-blasted, 50-200 RFU, Adhesive Failure

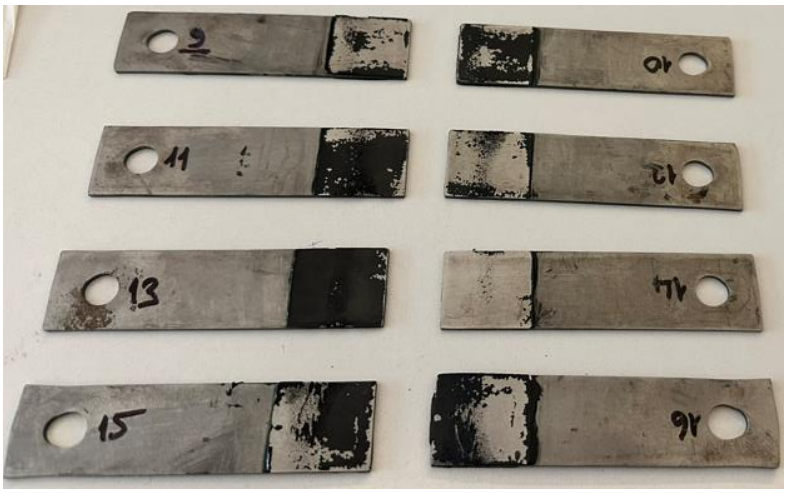


Figure B. 51 Metal-Metal Bonding, Shear Test, DP490, Non-blasted, 300-750 RFU, Adhesive Failure

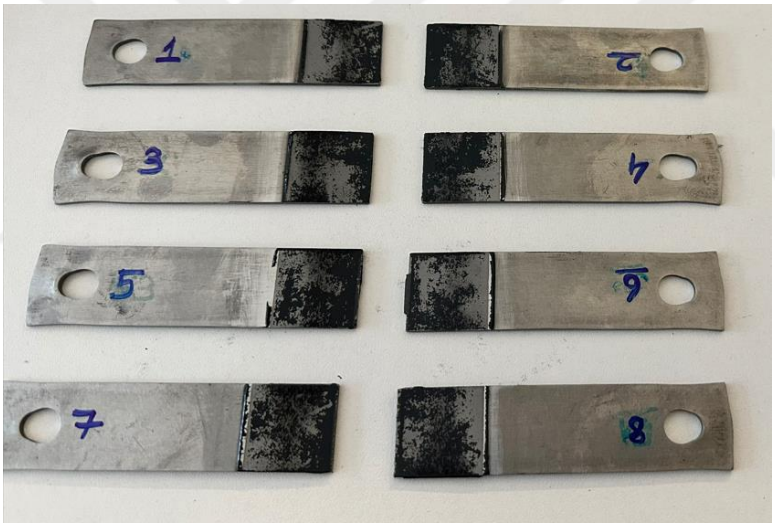


Figure B. 52 Metal-Metal Bonding, Shear Test, DP490, 1-2 µm, 0-50 RFU, Cohesive Failure in Adhesive

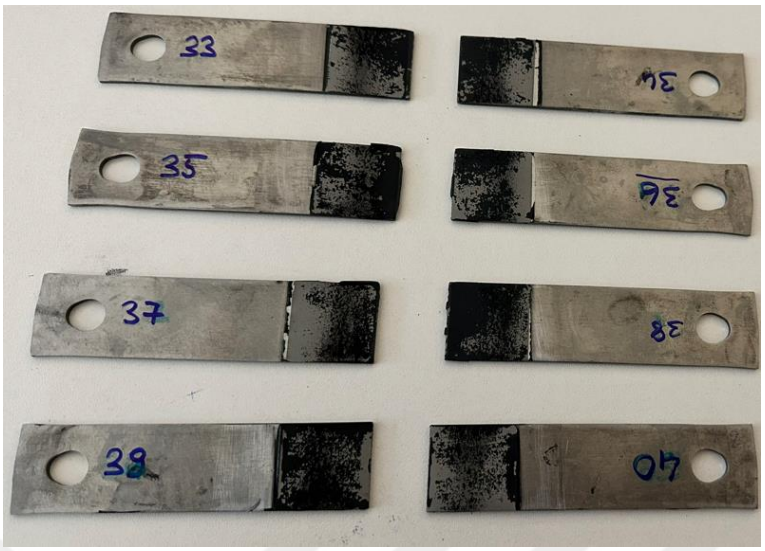


Figure B. 53 Metal-Metal Bonding, Shear Test, DP490, 1-2 µm, 50-200 RFU, Cohesive Failure in Adhesive

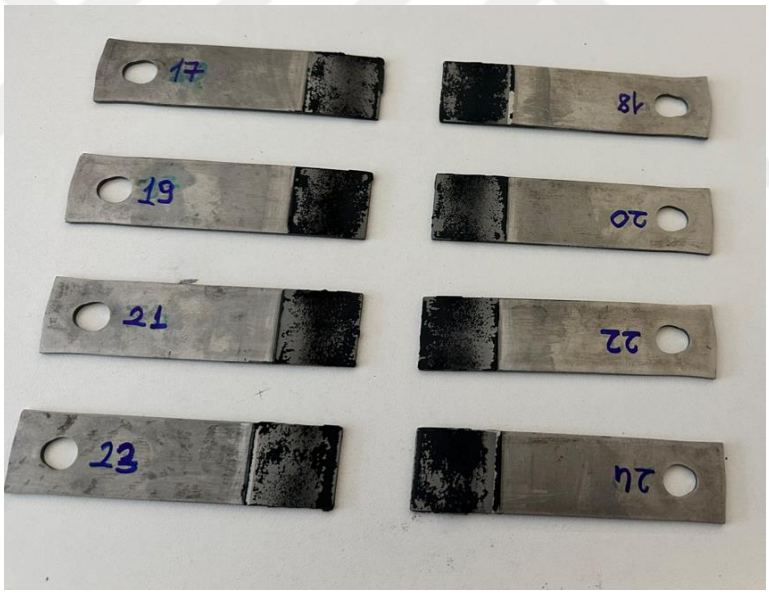


Figure B. 54 Metal-Metal Bonding, Shear Test, DP490, 1-2 µm, 300-750 RFU, Cohesive Failure in Adhesive



Figure B. 55 Metal-Metal Bonding, Shear Test, DP490, 2-4 µm, 0-50 RFU, Cohesive Failure in Adhesive

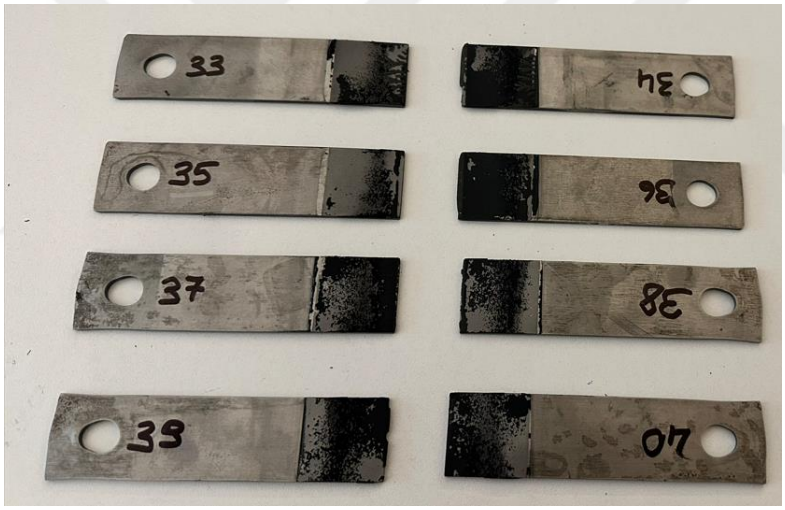


Figure B. 56 Metal-Metal Bonding, Shear Test, DP490, 2-4 µm, 50-200 RFU, Cohesive Failure in Adhesive



Figure B. 57 Metal-Metal Bonding, Shear Test, DP490, 2-4 µm, 300-750 RFU, Cohesive Failure in Adhesive

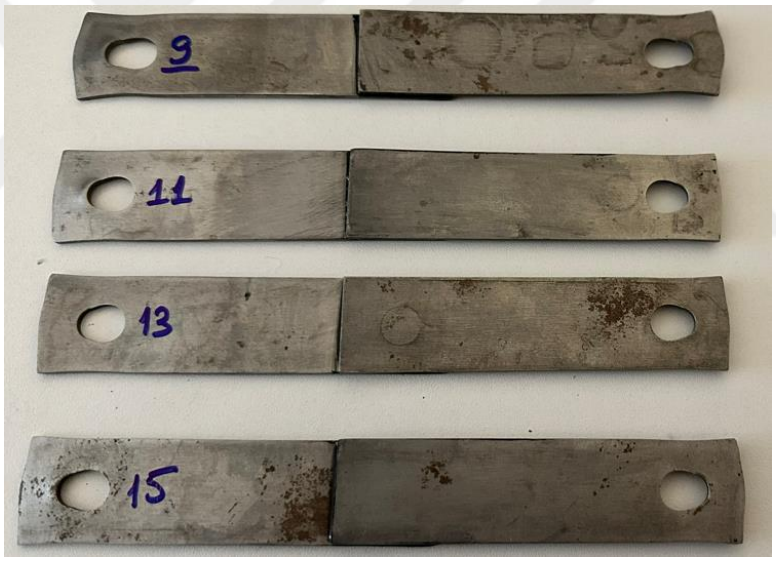


Figure B. 58 Metal-Metal Bonding, Shear Test, DP490, 4-8 µm, 0-50 RFU, Substrate Failure

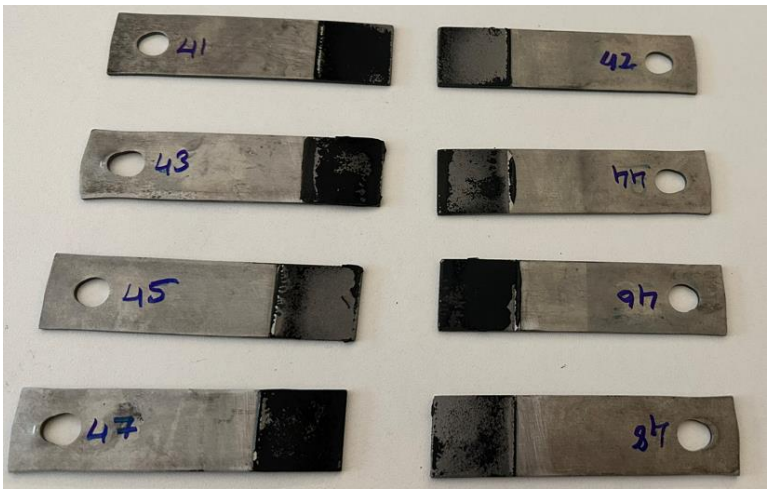


Figure B. 59 Metal-Metal Bonding, Shear Test, DP490, 4-8 µm, 50-200 RFU, Adhesive Failure

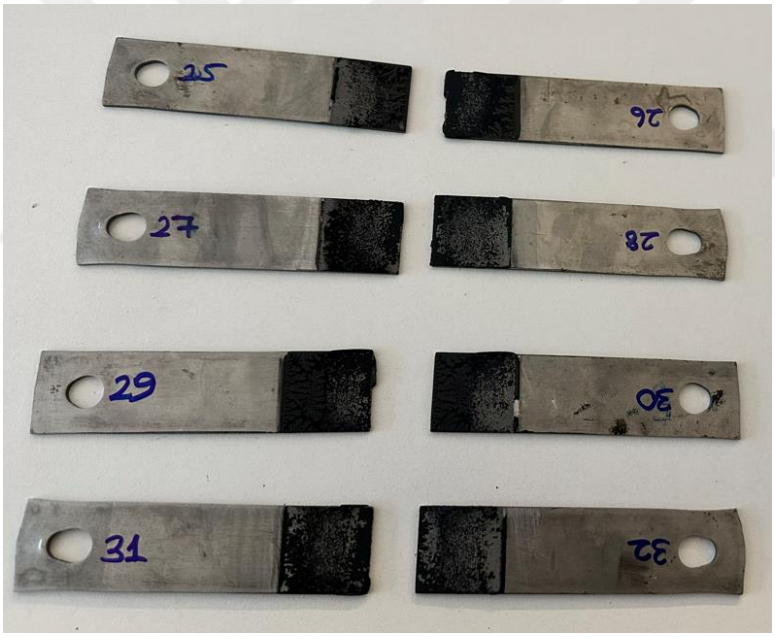


Figure B. 60 Metal-Metal Bonding, Shear Test, DP490, 4-8 µm, 300-750 RFU, Cohesive Failure in Adhesive

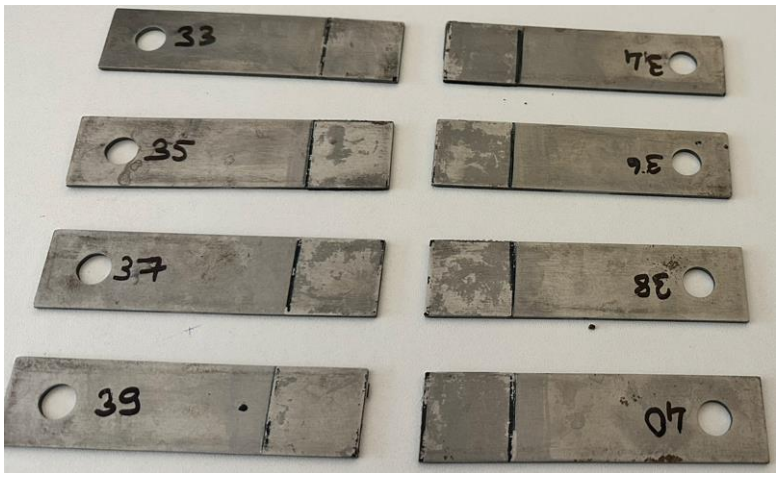


Figure B. 61 Metal-Metal Bonding, Shear Test, Araldite 2011, Non-blasted, 0-50 RFU, Adhesive Failure

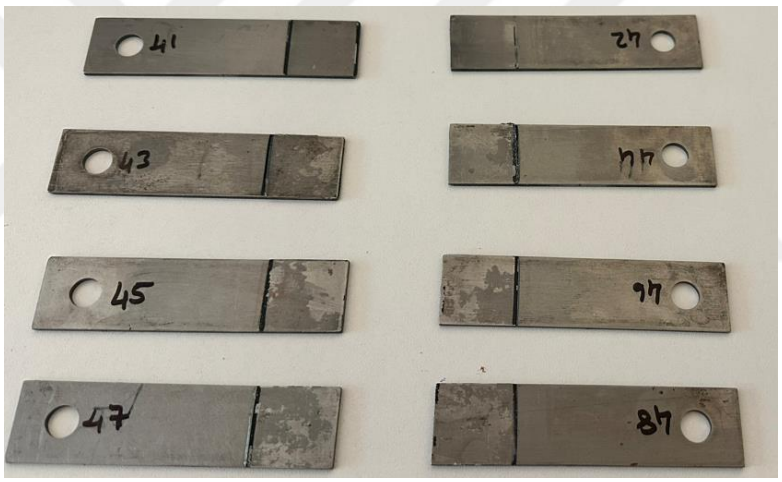


Figure B. 62 Metal-Metal Bonding, Shear Test, Araldite 2011, Non-blasted, 50-200 RFU, Adhesive Failure



Figure B. 63 Metal-Metal Bonding, Shear Test, Araldite 2011, Non-blasted, 300-750 RFU, Adhesive Failure



Figure B. 64 Metal-Metal Bonding, Shear Test, Araldite 2011, 1-2 µm, 0-50 RFU, Adhesive Failure

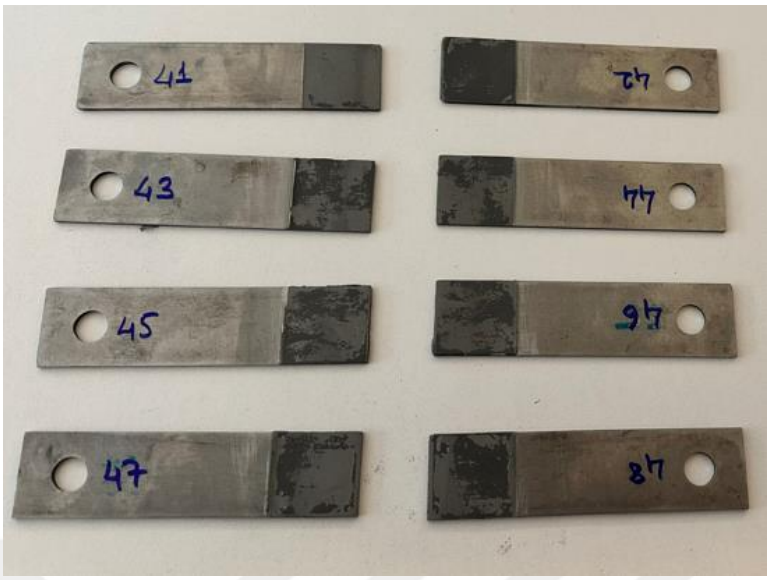


Figure B. 65 Metal-Metal Bonding, Shear Test, Araldite 2011, 1-2 µm, 50-200 RFU, Adhesive Failure

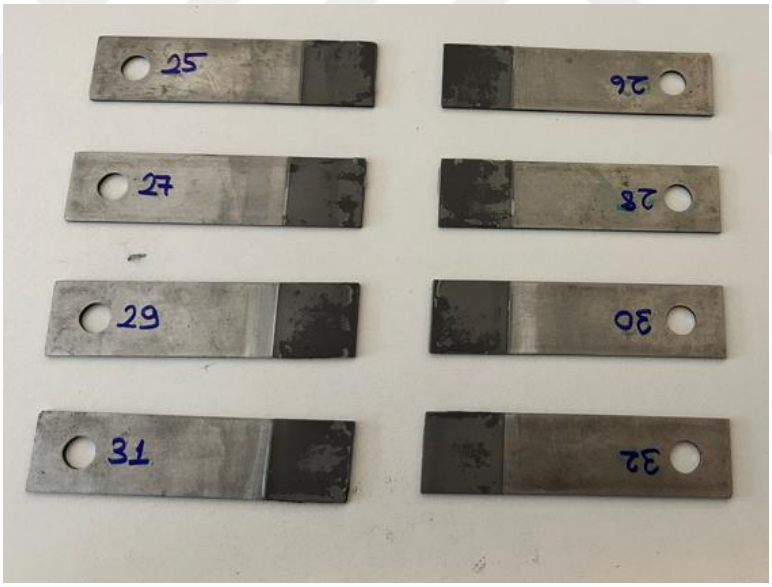


Figure B. 66 Metal-Metal Bonding, Shear Test, Araldite 2011, 1-2 µm, 300-750 RFU, Adhesive Failure

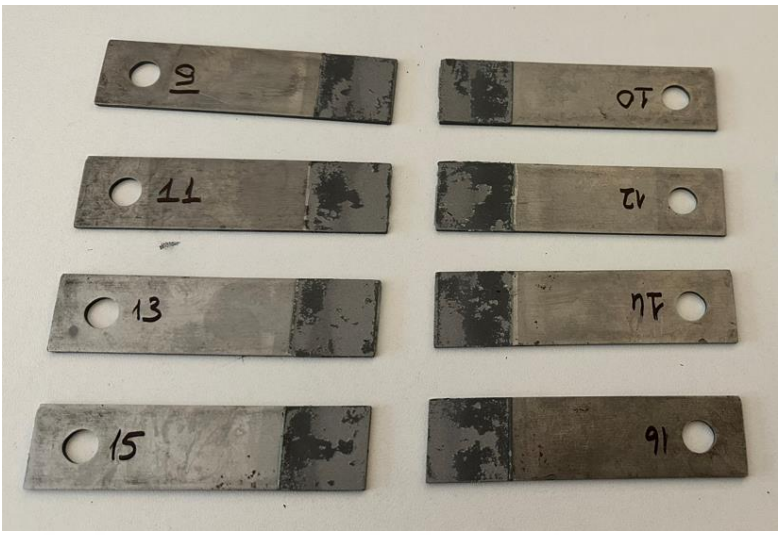


Figure B. 67 Metal-Metal Bonding, Shear Test, Araldite 2011, 2-4 µm, 0-50 RFU, Adhesive Failure



Figure B. 68 Metal-Metal Bonding, Shear Test, Araldite 2011, 2-4 µm, 50-200 RFU, Adhesive Failure

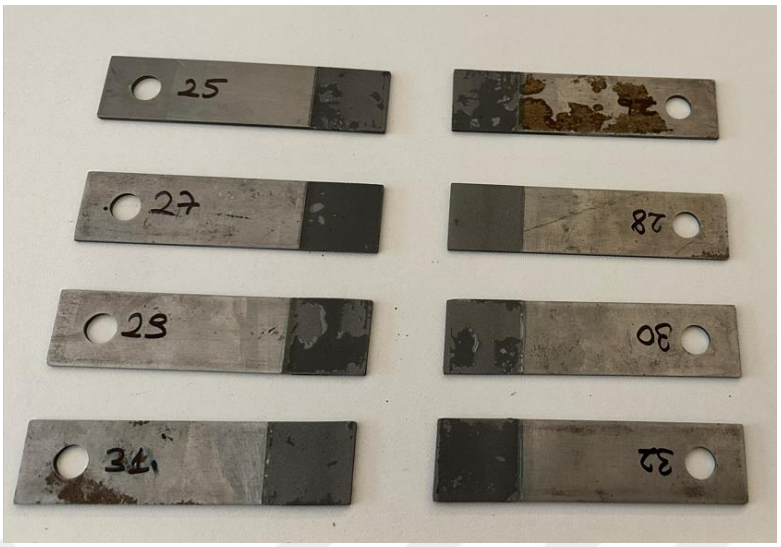


Figure B. 69 Metal-Metal Bonding, Shear Test, Araldite 2011, 2-4 µm, 300-750 RFU, Adhesive Failure

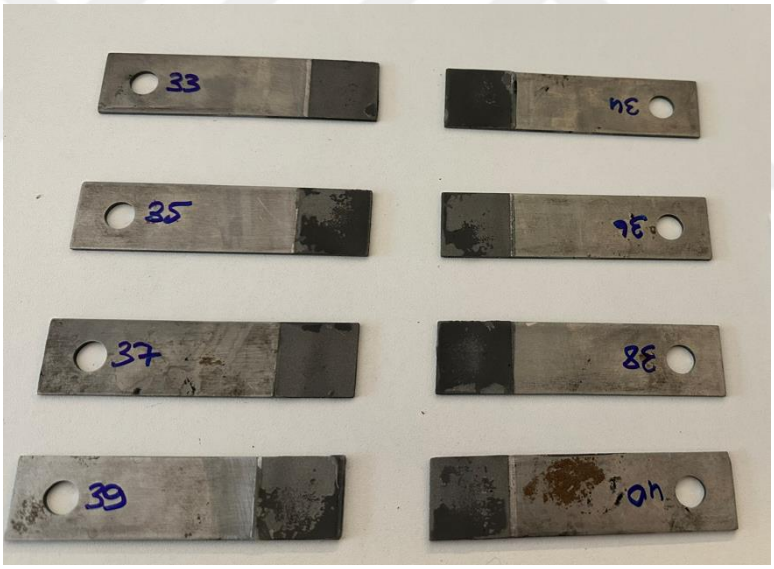


Figure B. 70 Metal-Metal Bonding, Shear Test, Araldite 2011, 4-8 µm, 0-50 RFU, Adhesive Failure

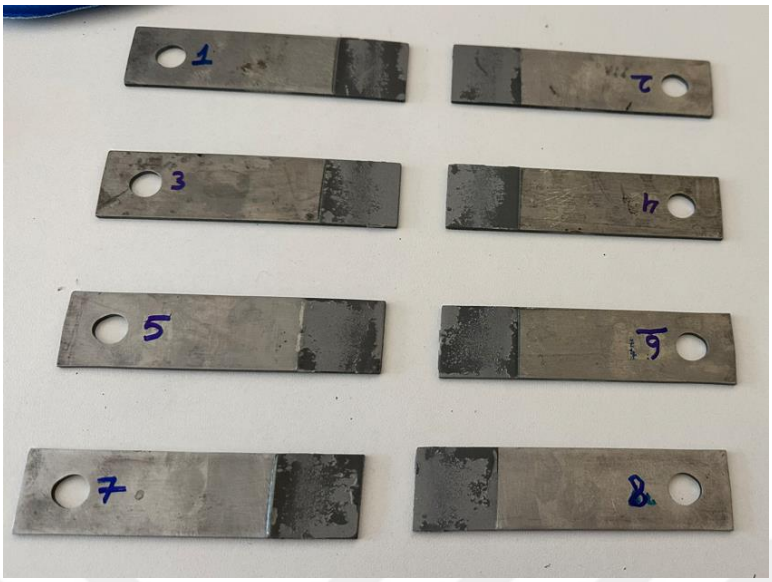


Figure B. 71 Metal-Metal Bonding, Shear Test, Araldite 2011, 4-8 µm, 50-200 RFU, Lack of Adhesive

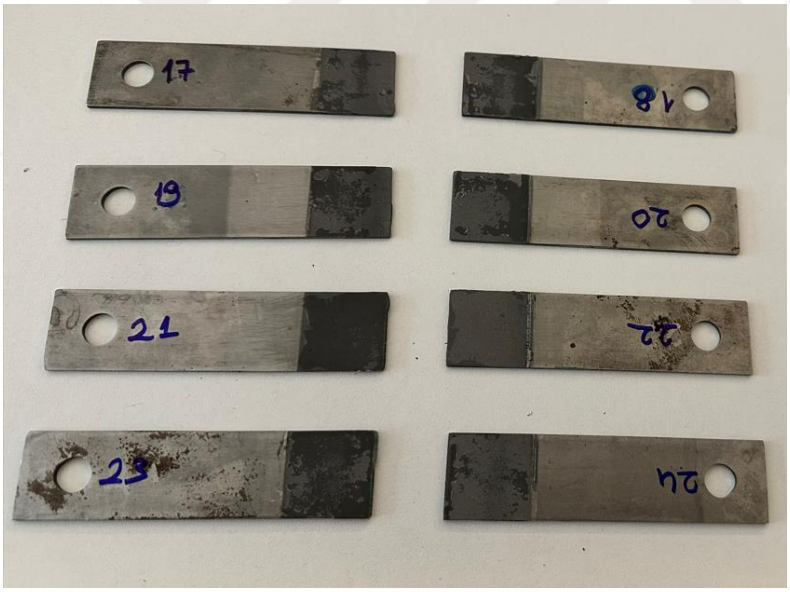


Figure B. 72 Metal-Metal Bonding, Shear Test, Araldite 2011, 4-8 µm, 300-750 RFU, Adhesive Failure

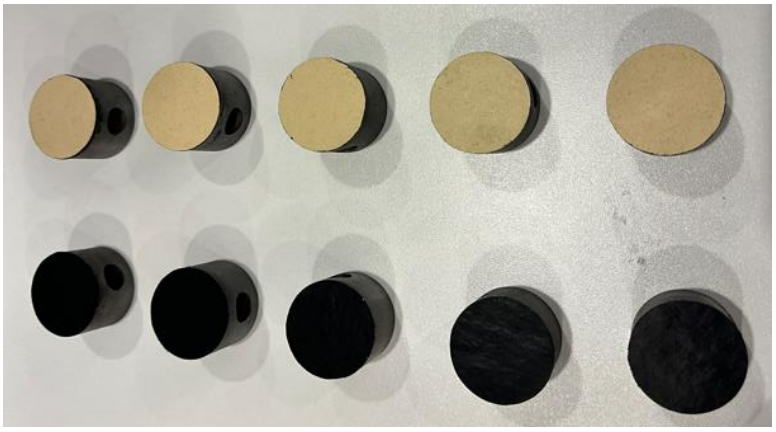


Figure B. 73 Rubber-Metal Bonding, Tensile Test, DP490, 4-8 µm, Smooth EPDM, Adhesive Failure

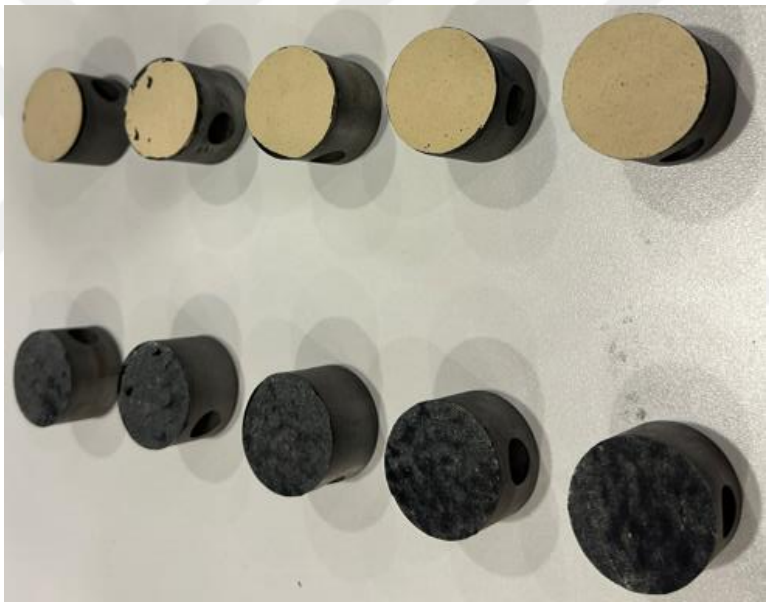


Figure B. 74 Rubber-Metal Bonding, Tensile Test, DP490, 4-8 µm, EPDM Roughened with Sandpaper, Adhesive Failure

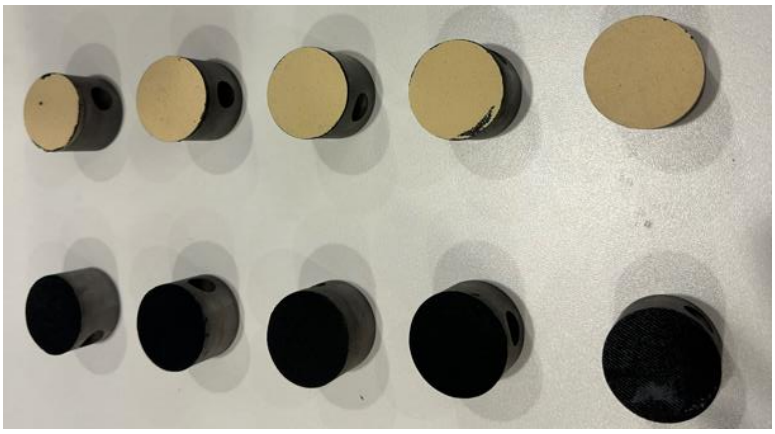


Figure B. 75 Rubber-Metal Bonding, Tensile Test, DP490, 4-8 µm, EPDM Roughened with Peel Ply, Adhesive Failure

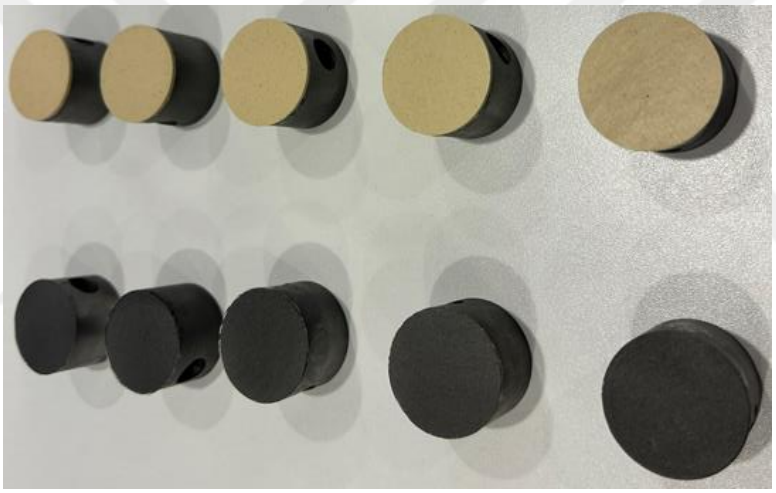


Figure B. 76 Rubber-Metal Bonding, Tensile Test, Araldite 2011, 4-8 µm, Smooth EPDM, Adhesive Failure

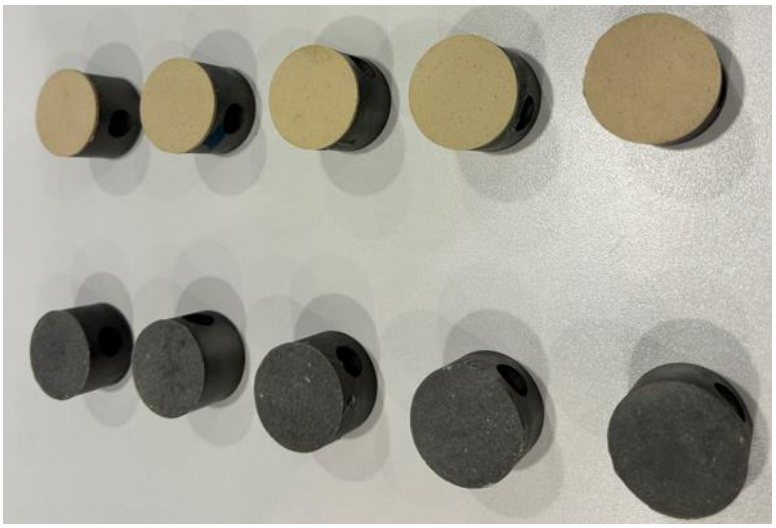


Figure B. 77 Rubber-Metal Bonding, Tensile Test, Araldite 2011, 4-8 µm, EPDM Roughened with Sandpaper, Adhesive Failure

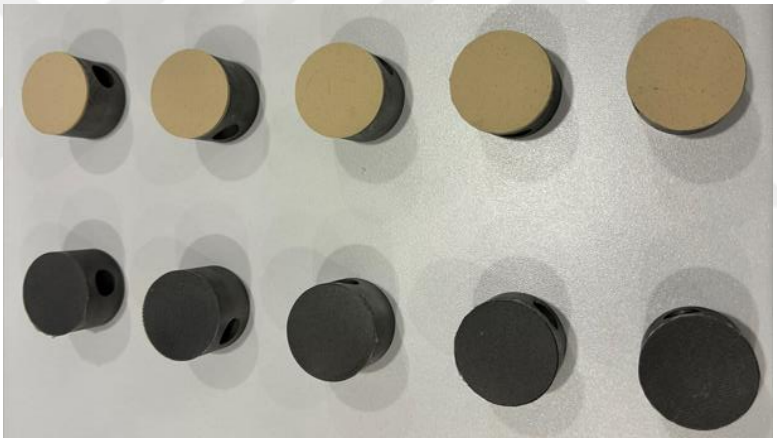


Figure B. 78 Rubber-Metal Bonding, Tensile Test, Araldite 2011, 4-8 µm, EPDM Roughened with Peel Ply, Adhesive Failure

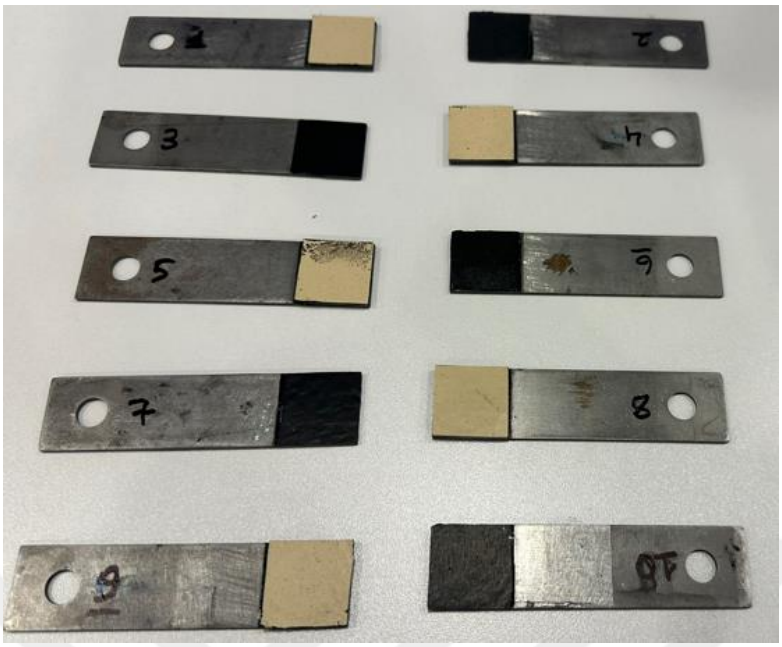


Figure B. 79 Rubber-Metal Bonding, Shear Test, DP490, 4-8 µm, Smooth EPDM, Adhesive Failure

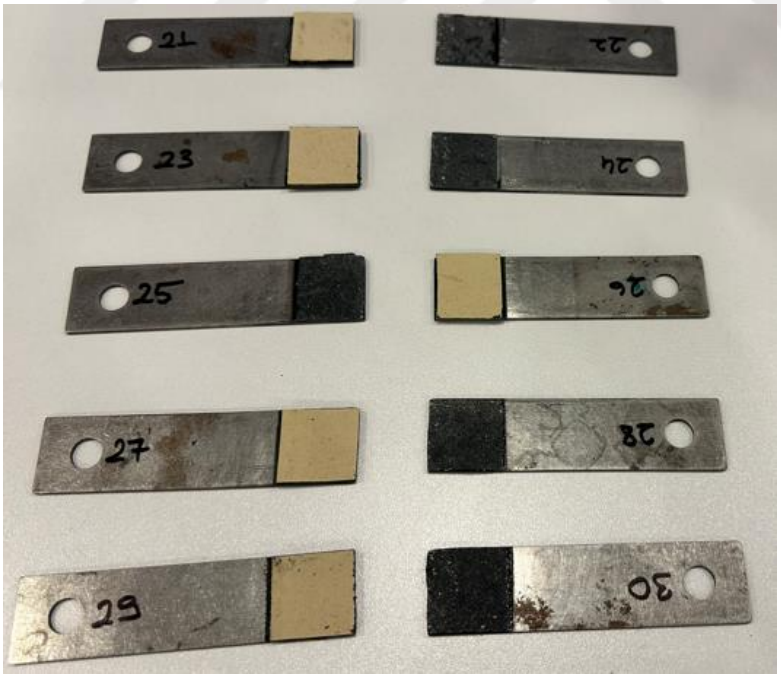


Figure B. 80 Rubber-Metal Bonding, Shear Test, DP490, 4-8 µm, EPDM Roughened with Sandpaper, Adhesive Failure

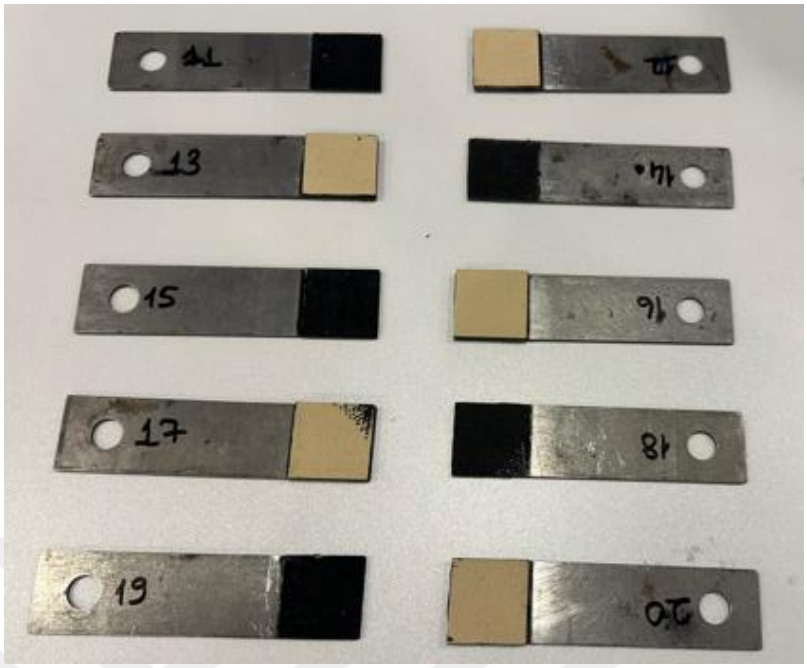


Figure B. 81 Rubber-Metal Bonding, Shear Test, DP490, 4-8 µm, EPDM Roughened with Peel Ply, Adhesive Failure

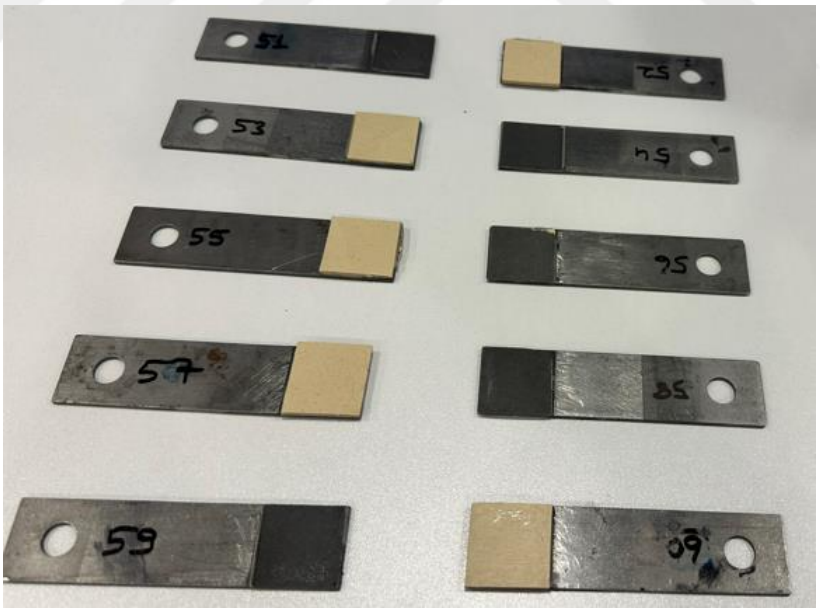


Figure B. 82 Rubber-Metal Bonding, Shear Test, Araldite 2011, 4-8 µm, Smooth EPDM, Adhesive Failure

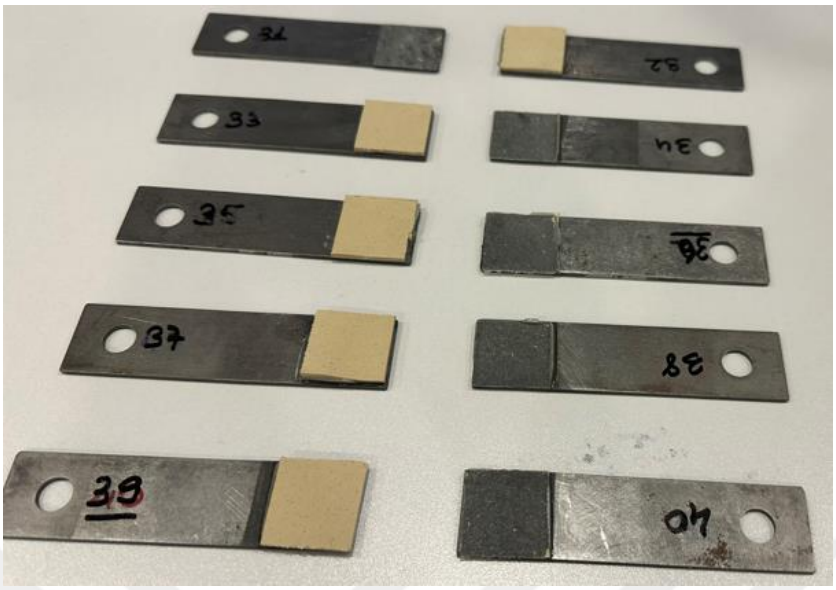


Figure B. 83 Rubber-Metal Bonding, Shear Test, Araldite 2011, 4-8 µm, EPDM Roughened with Sandpaper, Adhesive Failure



Figure B. 84 Rubber-Metal Bonding, Shear Test, Araldite 2011, 4-8 µm, EPDM Roughened with Peel Ply, Adhesive Failure

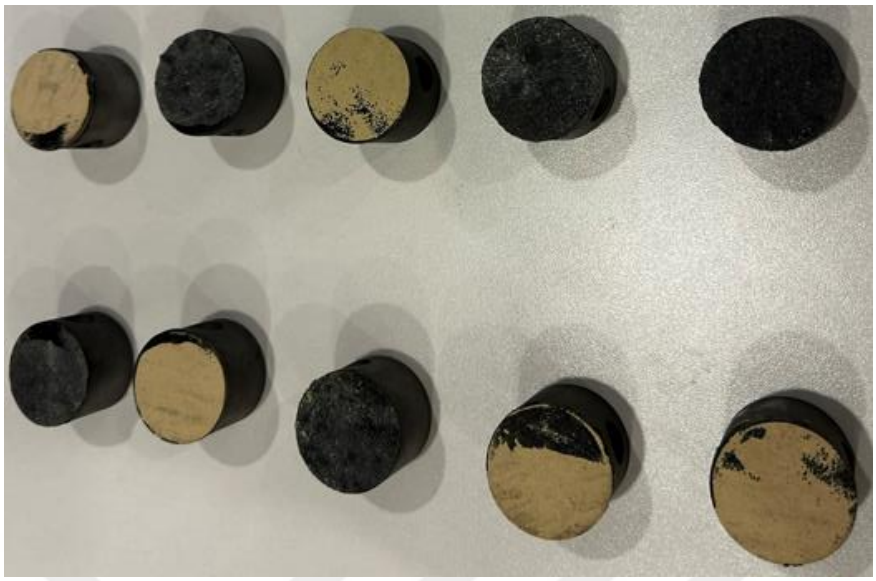


Figure B. 85 Rubber-Metal Bonding, Tensile Test, DP490, 4-8 μm, EPDM Roughened with Sandpaper, EPDM Without Plasma, Mixed Failure

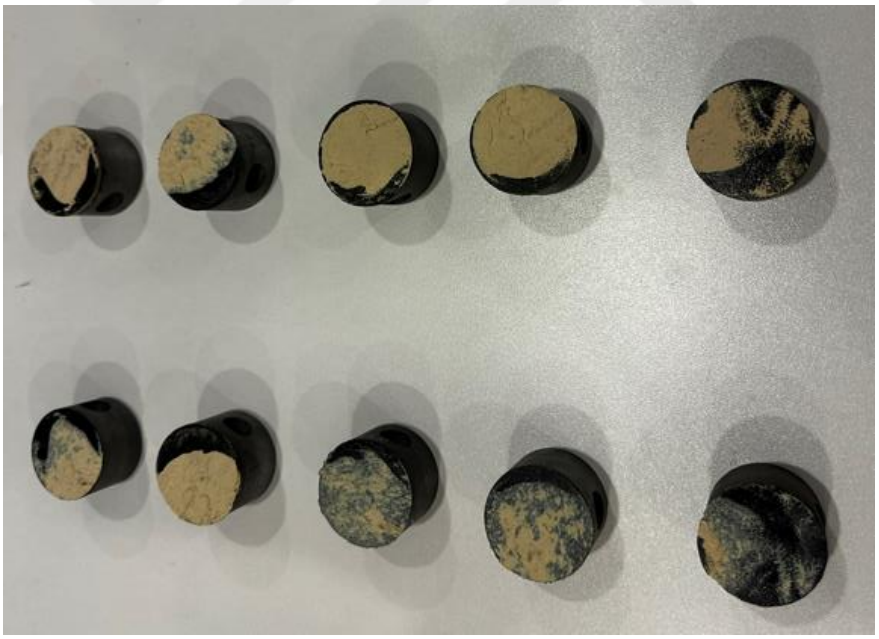


Figure B. 86 Rubber-Metal Bonding, Tensile Test, DP490, 4-8 μm, EPDM Roughened with Sandpaper, 30 s Plasma Treatment, Mixed Failure

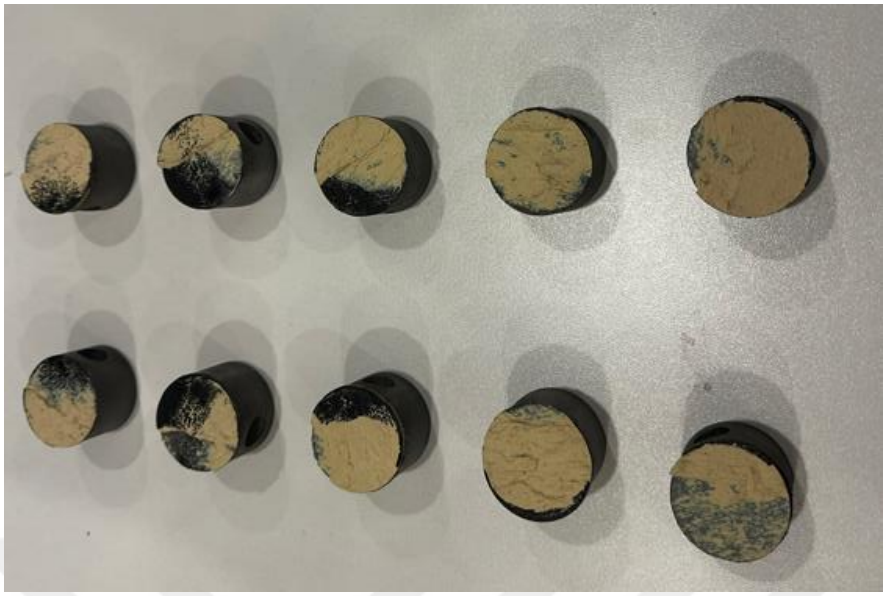


Figure B. 87 Rubber-Metal Bonding, Tensile Test, DP490, 4-8 µm, EPDM Roughened with Sandpaper, 60 s Plasma Treatment, Mixed Failure

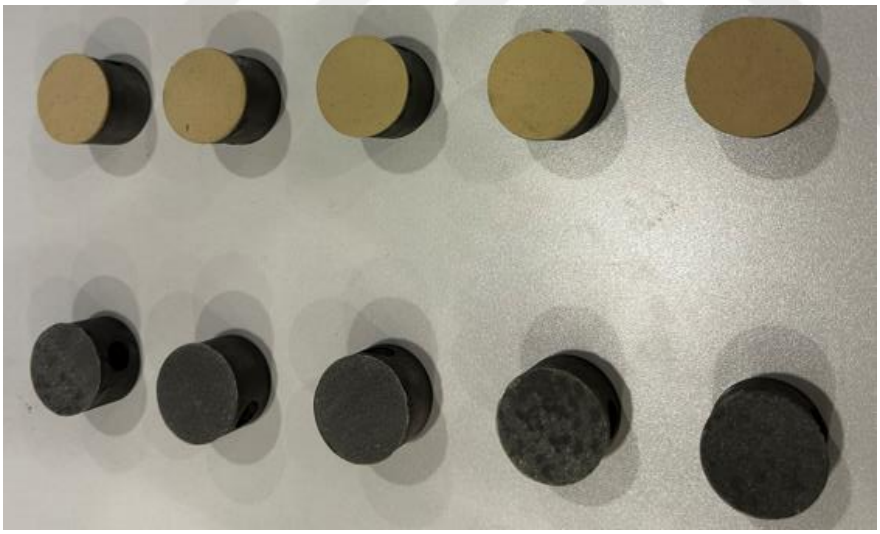


Figure B. 88 Rubber-Metal Bonding, Tensile Test, Araldite 2011, 4-8 µm, EPDM Roughened with Sandpaper, EPDM without Plasma, Adhesive Failure

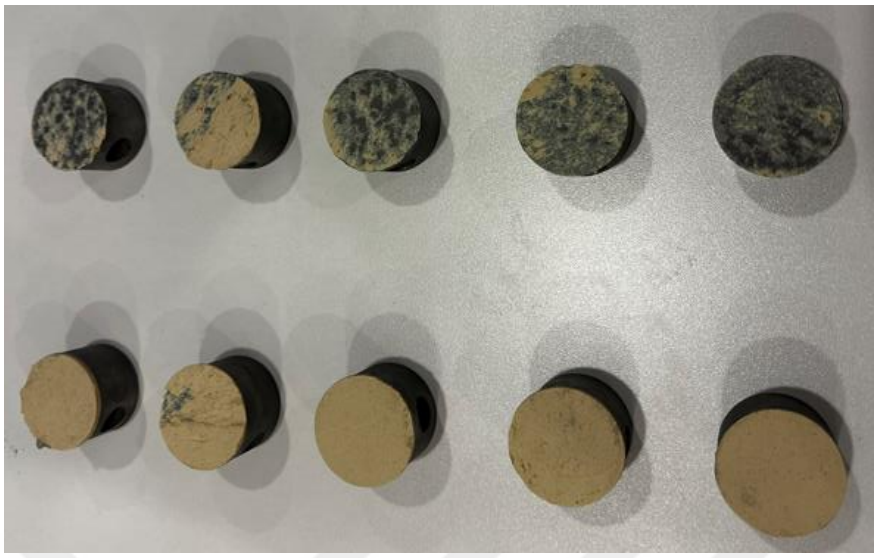


Figure B. 89 Rubber-Metal Bonding, Tensile Test, Araldite 2011, 4-8 µm, EPDM Roughened with Sandpaper, 30 s Plasma Treatment, Cohesive Failure in EPDM

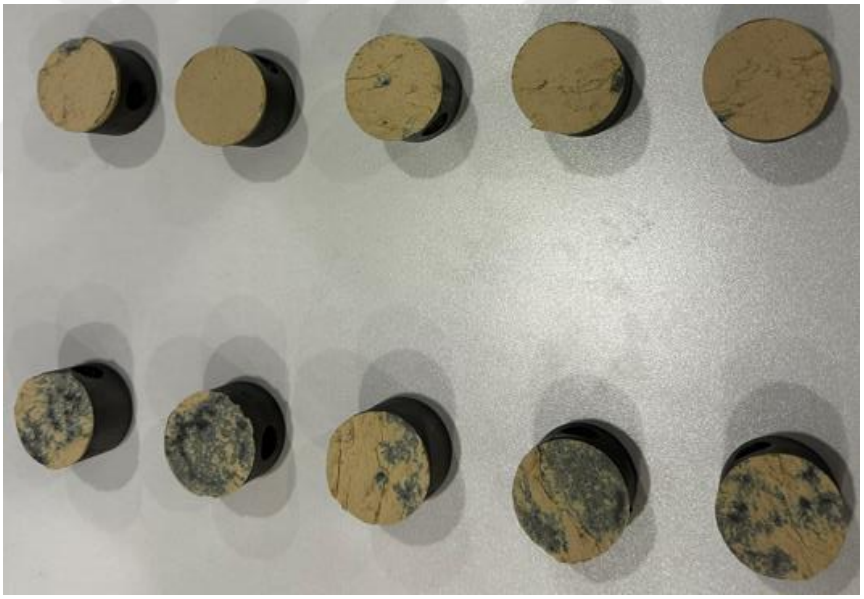


Figure B. 90 Rubber-Metal Bonding, Tensile Test, Araldite 2011, 4-8 µm, EPDM Roughened with Sandpaper, 60 s Plasma Treatment, Cohesive Failure in EPDM

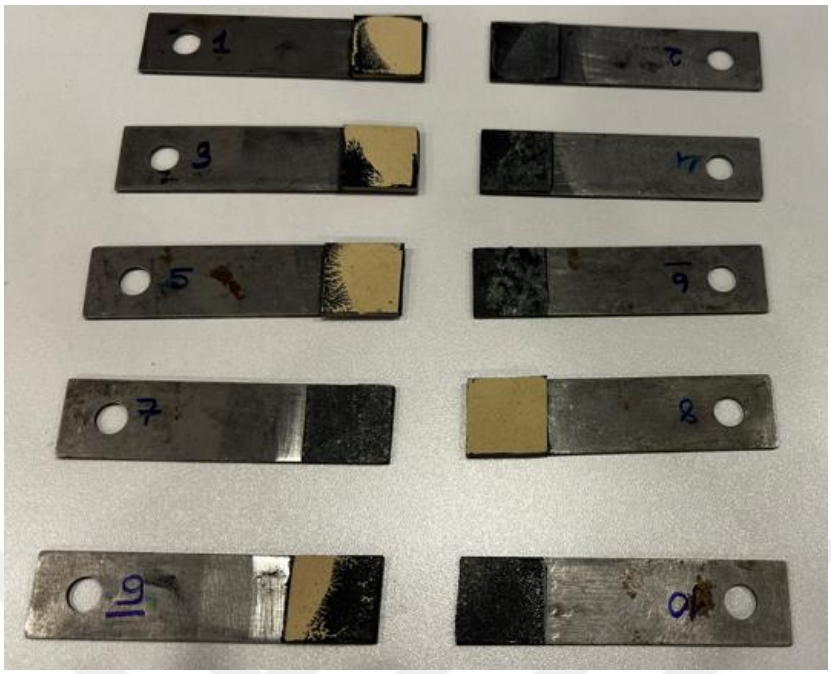


Figure B. 91 Rubber-Metal Bonding, Shear Test, DP490, 4-8 µm, EPDM Roughened with Sandpaper, EPDM Without Plasma, Mixed Failure



Figure B. 92 Rubber-Metal Bonding, Shear Test, DP490, 4-8 µm, EPDM Roughened with Sandpaper, 15 s Plasma Treatment, Mixed Failure

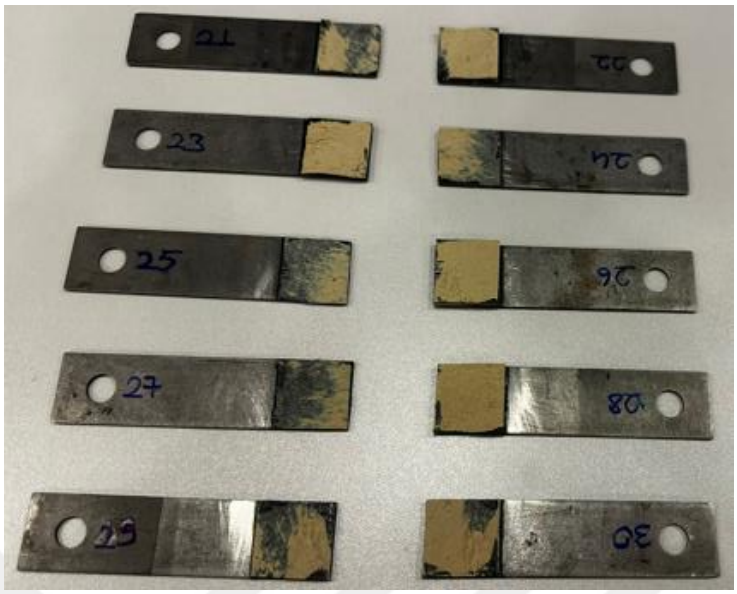


Figure B. 93 Rubber-Metal Bonding, Shear Test, DP490, 4-8 µm, EPDM Roughened with Sandpaper, 30 s Plasma Treatment, Cohesive Failure in EPDM



Figure B. 94 Rubber-Metal Bonding, Shear Test, Araldite 2011, 4-8 µm, EPDM Roughened with Sandpaper, EPDM without Plasma, Adhesive Failure



Figure B. 95 Rubber-Metal Bonding, Shear Test, Araldite 2011, 4-8 µm, EPDM Roughened with Sandpaper, 15 s Plasma Treatment, Adhesive Failure

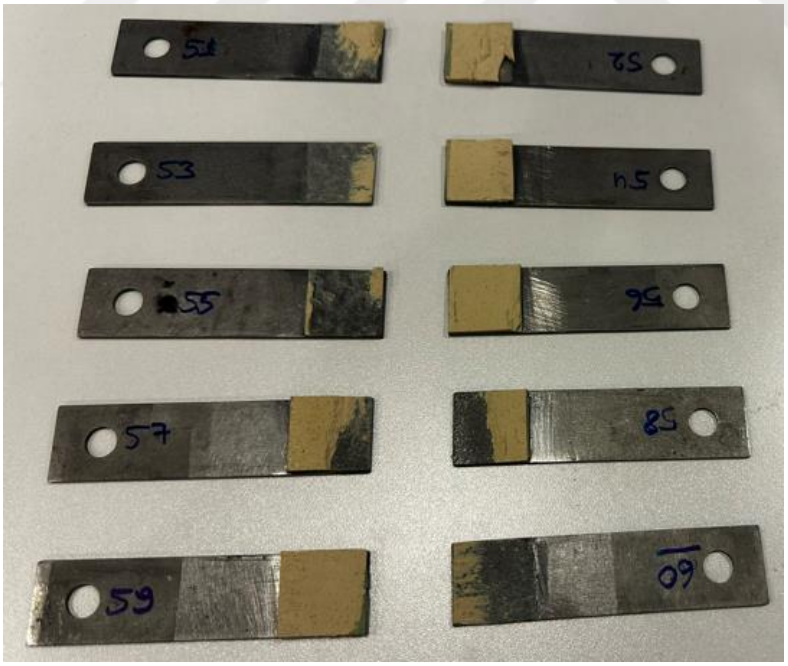


Figure B. 96 Rubber-Metal Bonding, Shear Test, DP490, 4-8 µm, EPDM Roughened with Sandpaper, 30 s Plasma Treatment, Cohesive Failure in EPDM

C. Summary of Failure Modes

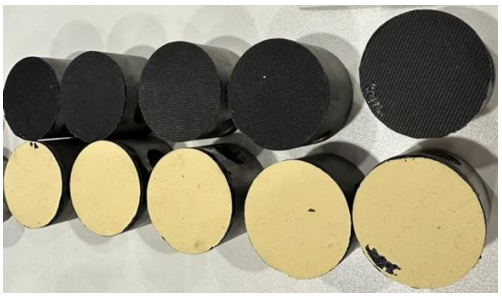
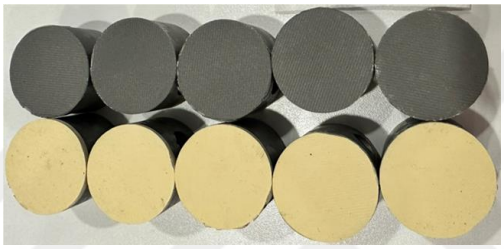
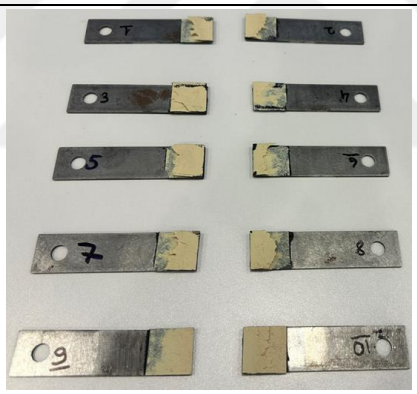
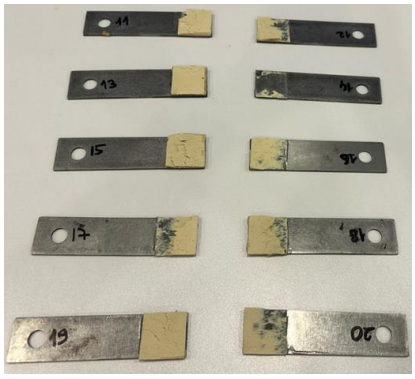
Part of the Experiment	Type of the	Type of the Test	Failure Mode	Explanation
Part I Baseline Rubber-Metal Adhesion	DP490	Tensile Test		The adhesive failure observed for both adhesives suggests that the rubber–adhesive interface represents the weakest link in the system under baseline conditions. As a result, the true influence of the adhesive type and metal surface characteristics could not be fully isolated in this part.
	Araldite 2011			
	DP490	Shear Test		In the rubber–metal shear tests, failure occurred predominantly within the rubber layer, indicating that the cohesive strength of the rubber governed the joint performance. Consequently, the effect of metal surface preparation parameters could not be clearly distinguished, as the rubber behaved as a relatively weak adherend.
	Araldite 2011			

Table C. 1 Failure Mode Analysis for Part I

Part of the Experiment	Type of the Adhesive	Type of the Test	Failure Mode	Explanation
Part II Isolation of the Metal-Adhesive Interface	DP490	Shear Test		When the metal–adhesive interface was isolated, DP490 predominantly exhibited cohesive failure within the adhesive layer, indicating a strong and tolerant interaction with the metal surface. In contrast, Araldite 2011 mainly showed adhesive failure, demonstrating that its bonding performance is more sensitive to metal surface preparation parameters.
	Araldite 2011			

Table C. 2 Failure Mode Analysis for Part II

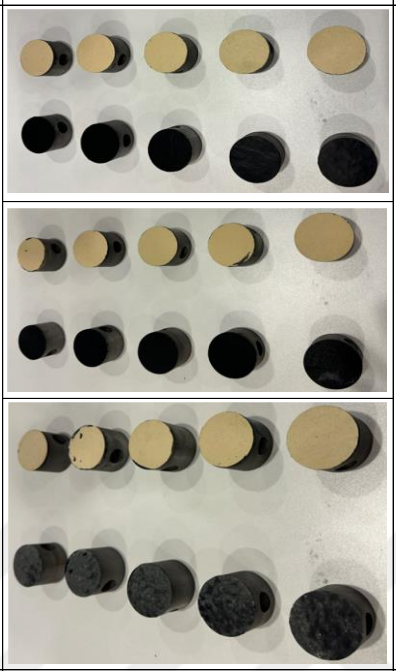
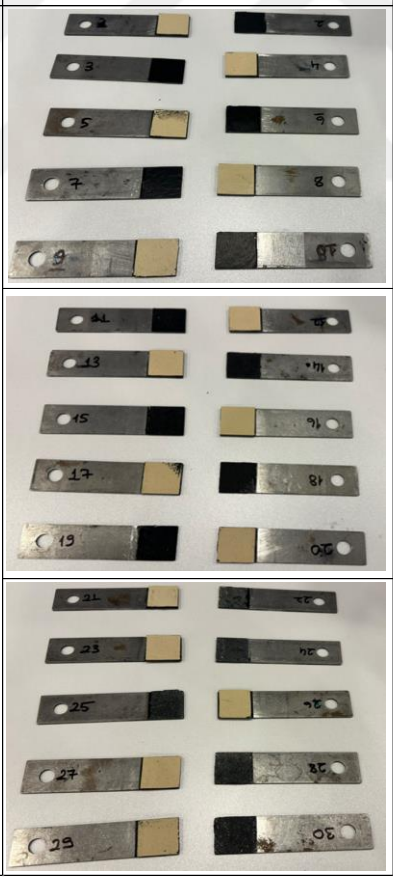
Part of the Experiment	Type of the Adhesive	Type of the Test	Failure Mode	Explanation
Part III Mechanical Modification of the EPDM Surface	DP490	Tensile Test		For the smooth EPDM surface, failure occurred predominantly at the EPDM–adhesive interface, indicating weak interfacial bonding. With increasing surface roughness through peel-ply and sandpaper treatments, EPDM residues and powder-like fragments were observed on the adhesive surface, suggesting a progressive improvement in interfacial bonding rather than purely adhesive failure. Similar failure behaviour was also observed for Araldite 2011, and therefore is not discussed separately.
		Shear Test		In shear tests, smooth EPDM surfaces showed adhesive failure at the EPDM–adhesive interface. As the EPDM surface was mechanically roughened, increasing amounts of EPDM fragments and powder were retained on the adhesive layer, indicating improved load transfer across the interface and strengthened interfacial bonding. Similar failure behaviour was also observed for Araldite 2011, and therefore is not discussed separately.

Table C. 3 Failure Mode Analysis for Part III

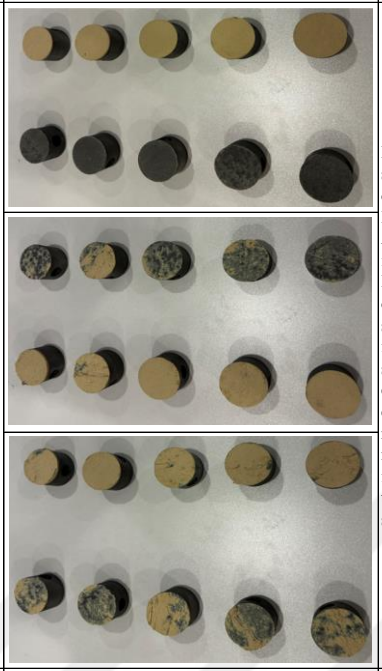
Part of the Experiment	Type of the Adhesive	Type of the Test	Failure Mode	Explanation
Part IV Physicochemical Activation of the EPDM Surface	Araldite 2011	Tensile Test		For the untreated EPDM surface, failure mainly occurred at the EPDM–adhesive interface. After plasma treatment, increasing amounts of EPDM material were observed on the adhesive surface, indicating that the failure behaviour gradually shifted from interface-controlled toward a more cohesive-dominated response. The same failure mode trends were observed for the DP490, and therefore are not shown separately.
		Shear Test		In shear tests, specimens without plasma treatment predominantly showed adhesive failure at the EPDM–adhesive interface. With plasma exposure, EPDM material transfer became more pronounced, suggesting improved interfacial bonding and a shift toward cohesive-dominated failure behaviour. The same failure mode trends were observed for the DP490, and therefore are not shown separately.

Table C. 4 Failure Mode Analysis for Part IV

D. SEM and EDS Analysis of EPDM Surface

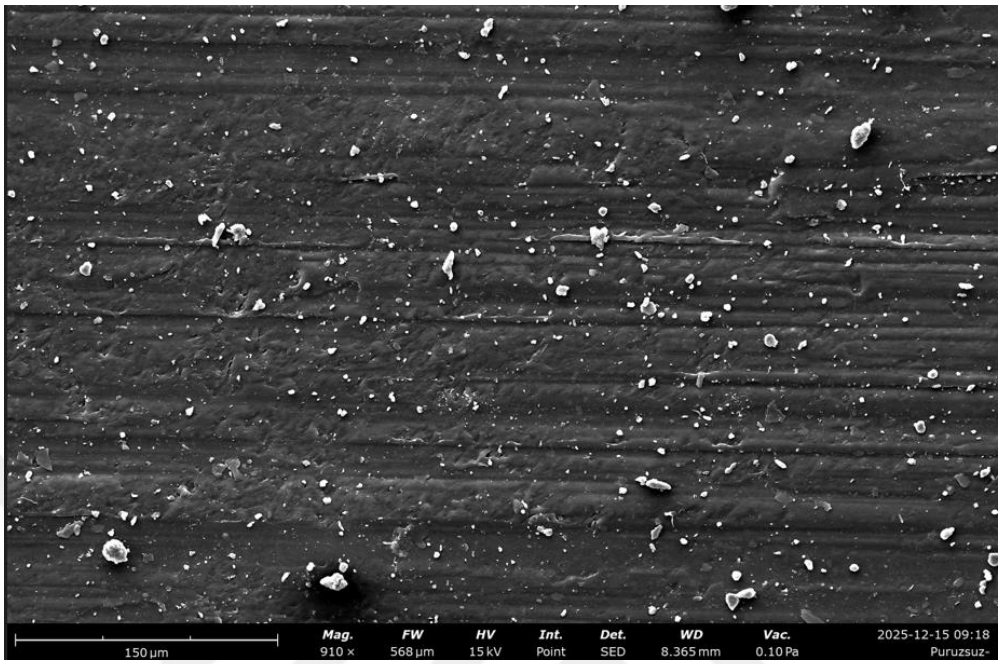


Figure D. 1 SEM Image of Smooth EPDM

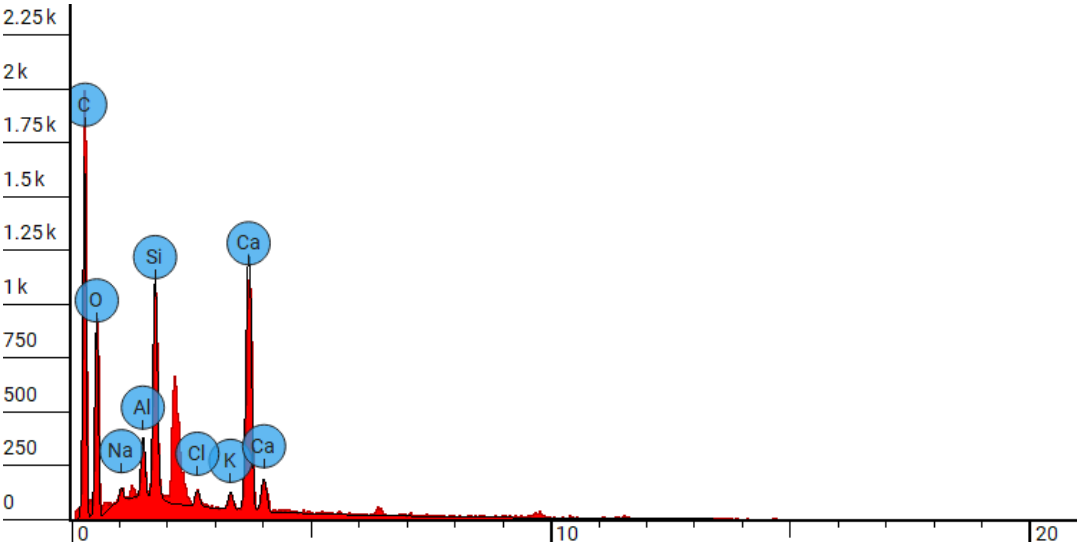


Figure D. 2 X-ray Intensity (counts) vs. X-ray Energy (keV) of Smooth EPDM Surface

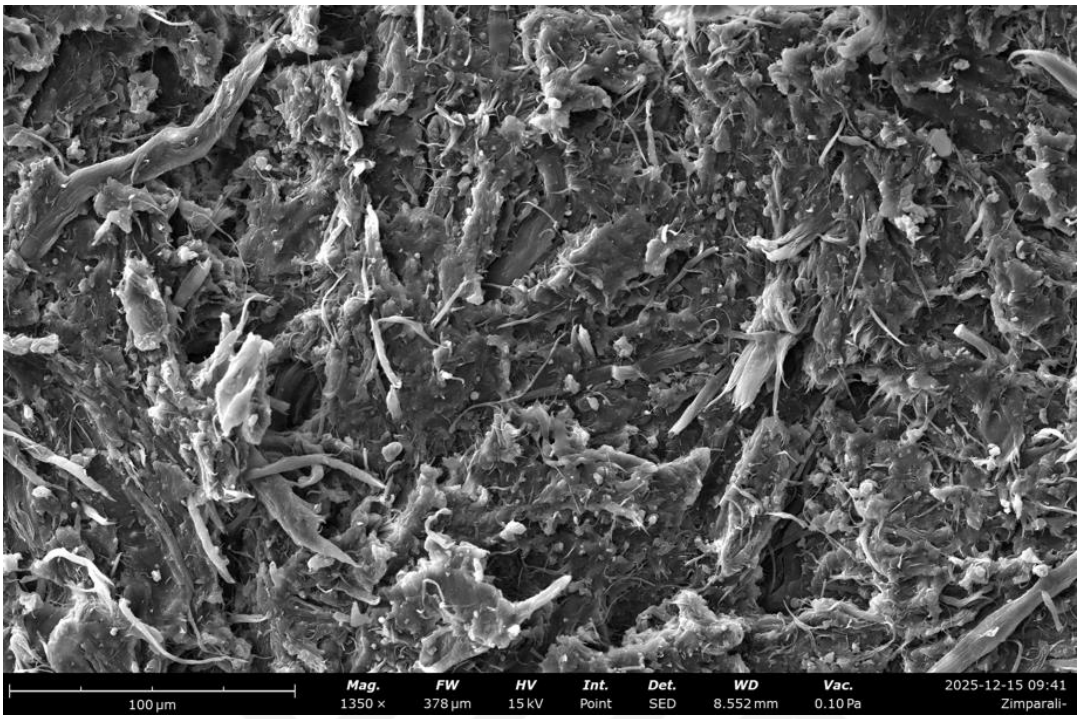


Figure D. 3 SEM Image of EPDM Roughened with Sandpaper

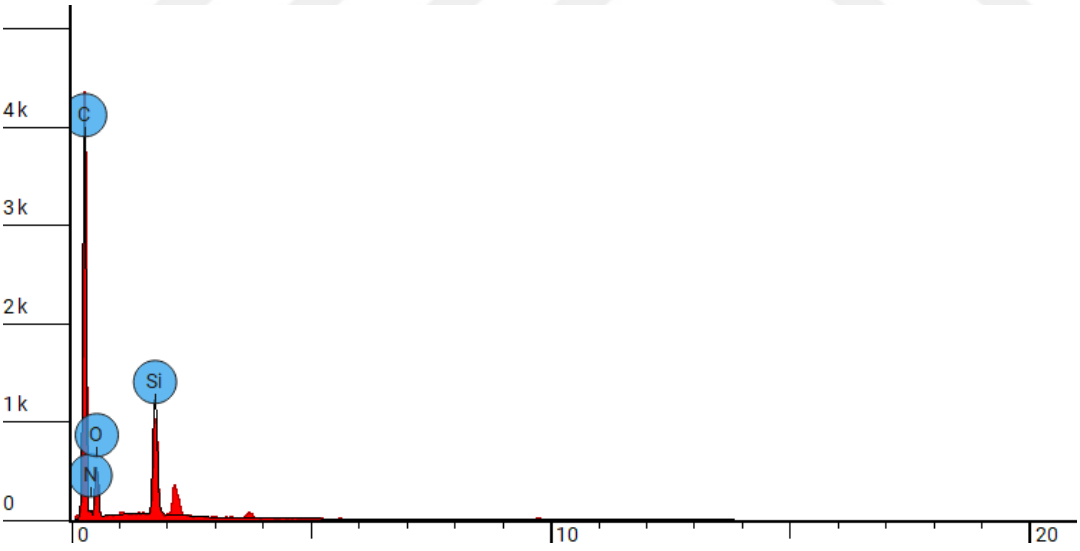


Figure D. 4 X-ray Intensity (counts) vs. X-ray Energy (keV) of EPDM Surface Roughened with Sandpaper

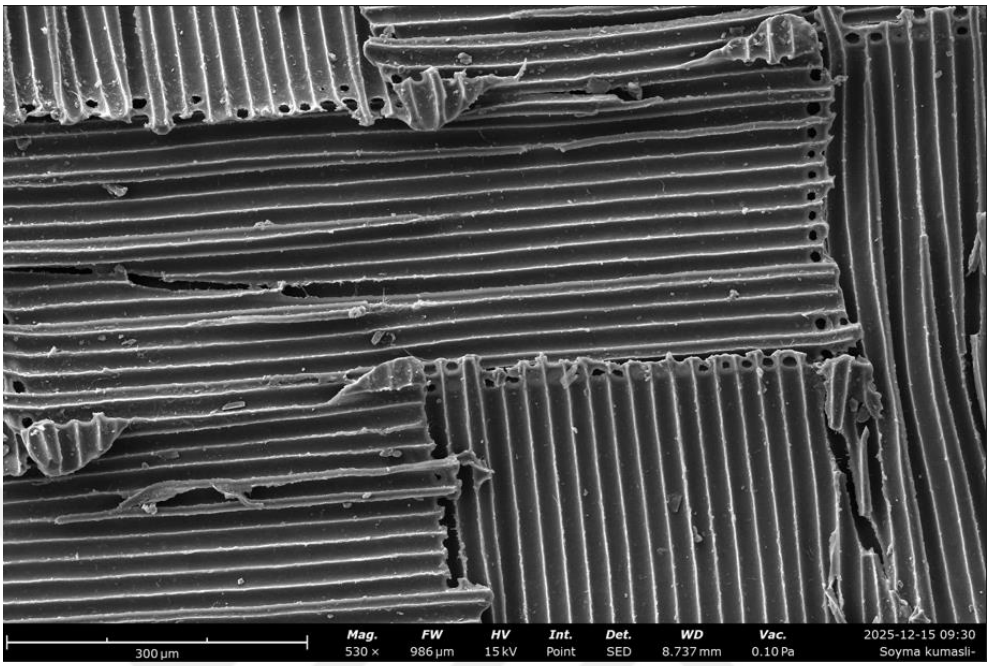


Figure D. 5 SEM Image of EPDM Roughened with Peel Ply

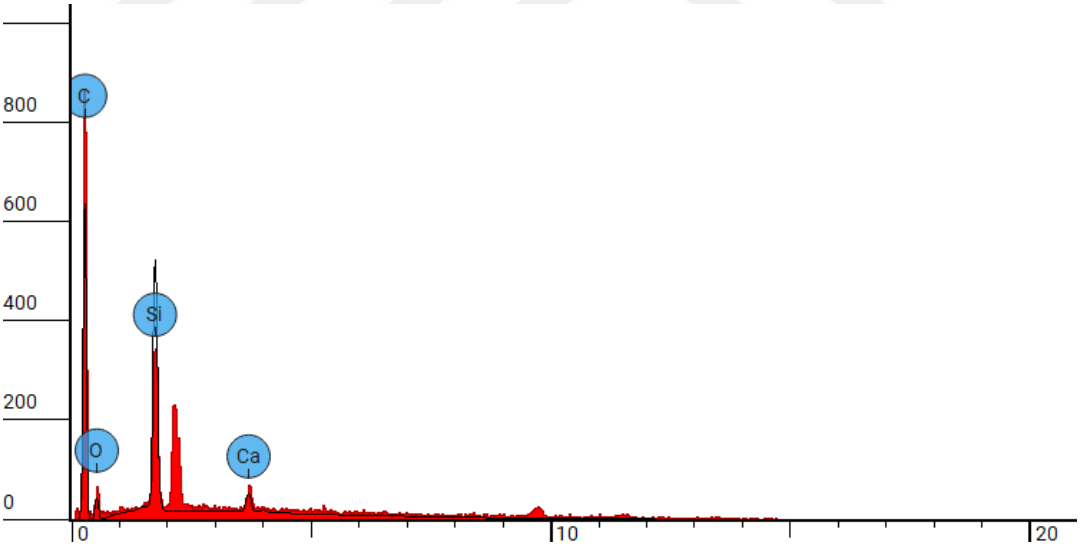


Figure D. 6 X-ray Intensity (counts) vs. X-ray Energy (keV) of EPDM Surface Roughened with Peel Ply

E. SEM and EDS Analysis of Metal Surface

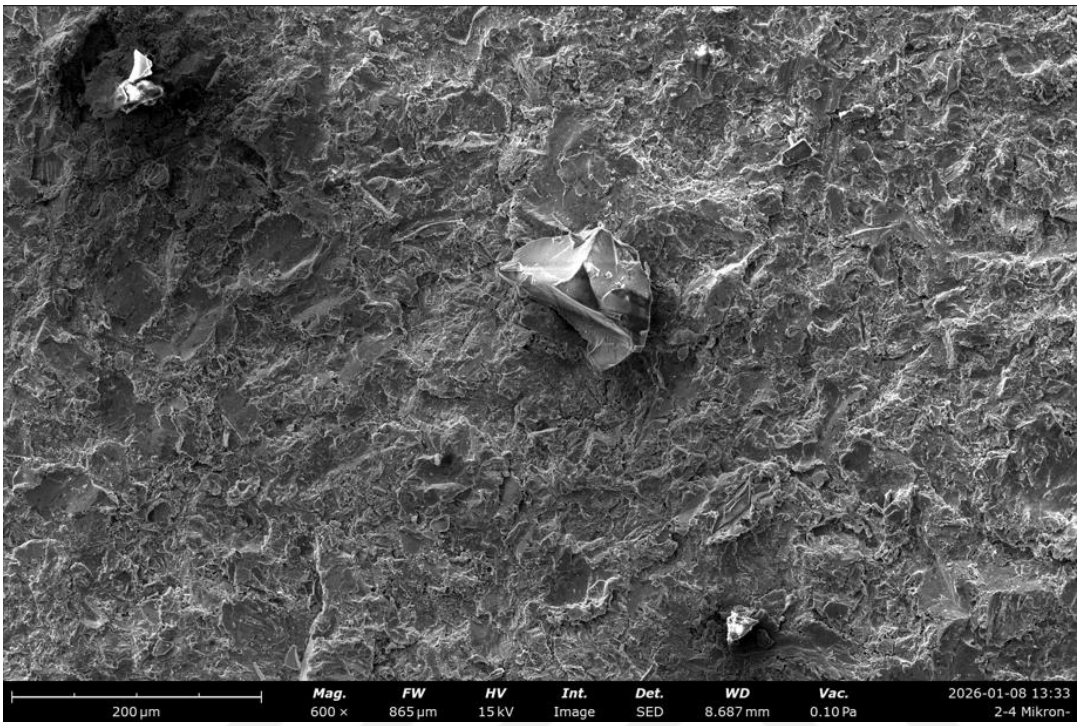


Figure E. 1 SEM Image of Metal with Medium Roughness (2-4 µm)

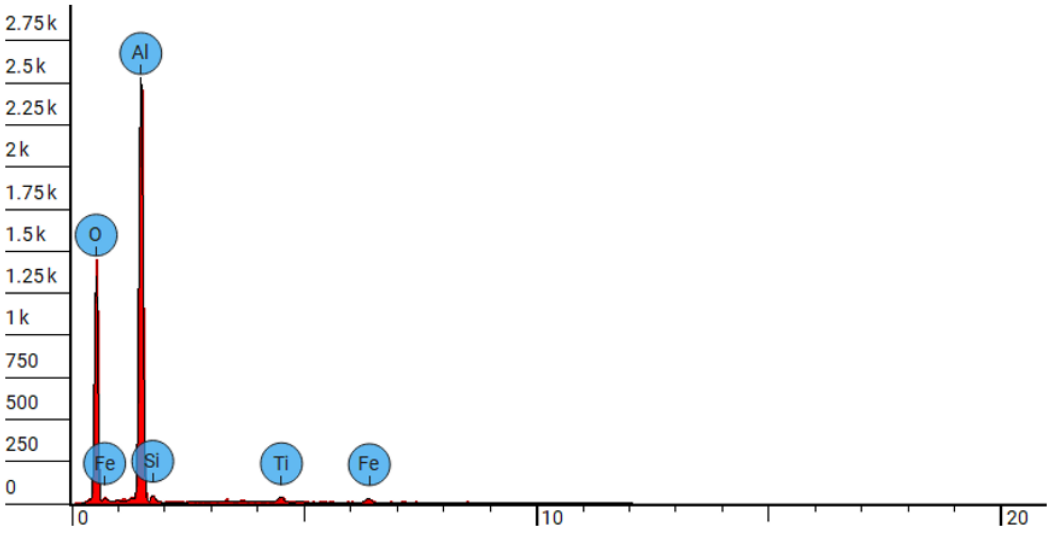


Figure E. 2 X-ray Intensity (counts) vs. X-ray Energy (keV) of Metal Surface with Medium Roughness (2-4 µm)